



Universidade de Aveiro Departamento de Química
Ano 2013

**TATIANA RIBAU
AMARANTE**

**NOVOS MATERIAIS HÍBRIDOS DE
OXOMOLIBDÉNIO(VI)**

***NEW OXOMOLYBDENUM(VI)
HYBRID MATERIALS***



**TATIANA RIBAU
AMARANTE**

**NOVOS MATERIAIS HÍBRIDOS DE
OXOMOLYBDÉNIO(VI)**

Tese apresentada à Universidade de Aveiro para cumprimento dos requisitos necessários à obtenção do grau de Doutor em Química, realizada sob a orientação científica da Doutora Isabel Maria de Sousa Gonçalves, Professora Associada do Departamento de Química da Universidade de Aveiro.

Apoio financeiro da FCT com a bolsa
de estudos SFRH/BD/64224/2009.

*Às minhas fontes de existência, conhecimento, força e inspiração:
os meus pais Preciosa e Marante, a minha irmã Lorine e
o meu tesouro Filipe.*

o júri

presidente

Prof. Doutor Fernando Joaquim Fernandes Tavares Rocha
professor catedrático do Departamento de Geociências da Universidade de Aveiro

Prof. Doutor Carlos José Rodrigues Crispim Romão
professor catedrático do Instituto de Tecnologia Química e Biológica da
Universidade Nova de Lisboa

Prof. Doutor João Carlos Matias Celestino Gomes da Rocha
professor catedrático do Departamento de Química da Universidade de Aveiro

Prof.^a Doutora Isabel de Sousa Gonçalves (orientadora)
professora associada do Departamento de Química da Universidade de Aveiro

Prof. Doutor André Duarte Lopes
professor auxiliar da Faculdade de Ciências e Tecnologia da Universidade do Algarve

Doutora Marta Ramilo Abrantes
investigadora auxiliar do Instituto Superior Técnico da Universidade Técnica de Lisboa

Doutora Anabela Tavares Aguiar Valente
investigadora auxiliar do Departamento de Química, CICECO, Universidade de Aveiro

agradecimentos

Agradeço à Professora Isabel Gonçalves por me ter proposto este desafio, por conseguinte pela sua orientação científica e apoio ao longo da realização deste doutoramento. Um muito obrigada pelos seus concelhos e incentivos à realização de outros e novos desafios.

Ao Professor João Rocha, ao Departamento de Química/CICECO e à Universidade de Aveiro pelas condições cedidas que permitiram a realização deste trabalho. Agradeço à Fundação da Ciência e Tecnologia pela bolsa SFRH/BD/64224/2009.

O meu muito obrigada à Doutora Anabela Valente, pela disponibilidade para a realização dos estudos catalíticos, um obrigada à Patrícia Neves.

Agradeço ao Doutor Martyn Pillinger pela sua colaboração nos trabalhos apresentados e, pela sua preciosa ajuda na leitura crítica desta tese. Gostaria também de prestar um agradecimento especial ao Doutor Filipe Paz pelos estudos de difracção de raios-X de pós, pelo seu apoio inigualável e pelos últimos anos de amigo/companheiro.

Quero ainda agradecer à Ana Gomes pela sua magnífica ajuda e amizade, à Rosário Soares pelas tardes de pesquisa e aquisição assim como a sua permanente disponibilidade e simpatia, à Manuela Marques pela sua amizade e realização das análises elementares, à Celeste Azevedo pela prestabilidade em todos os momentos e ao Sr. Hilário pela realização dos espectros de RMN e à Margarete pelos bocadinhos de conversa e apoio.

Agradeço a todos os amigos que, de uma forma ou outra, contribuíram para a realização deste trabalho.

palavras-chave

molibdénio(VI), óxidos de molibdénio, ligandos bidentados de azoto, materiais híbridos, polímeros, epoxidação, olefinas.

resumo

Nesta tese as moléculas 2,2'-bipiridina (bipy), di-*tert*-butil-2,2'-bipiridina (di-*t*-Bu-bipy), ácido 2,2'-bipiridina-5,5'-dicarboxílico (H₂bpdc), 2-[3(5)-pirazolil]piridina (pzpy) e 2-(1-pentil-3-pirazolil)piridina (pent-pp) foram utilizadas como ligandos bidentados de azoto para a formação de complexos do tipo [MoO₂Cl₂L], no intuito de investigar a diversidade estrutural de compostos pertencendo à família oxomolibdénio(VI). Foram estudados três métodos de aquecimento: o método hidrotérmico, de refluxo e por micro-ondas. Foi também estudada sob condições hidrotérmicas a reacção alternativa envolvendo a utilização do composto inorgânico trióxido de molibdénio (MoO₃) com os ligandos di-*t*-Bu-bipy, H₂bpdc e pzpy.

A natureza dos ligandos bidentados de azoto e/ou o método utilizado promoveram a formação de uma série de novos híbridos do tipo oxomolibdénio(VI) que claramente reflectiram a influência estruturante dos ligandos. Assim, esta tese descreve a síntese e caracterização do complexo mononuclear [MoO₂Cl₂(pent-pp)], dinuclear [Mo₂O₆(di-*t*-Bu-bipy)₂] e octanuclear [Mo₈O₂₂(OH)₄(di-*t*-Bu-bipy)₄] assim como dos materiais poliméricos {[MoO₃(bipy)][MoO₃(H₂O)]}_n, (DMA)[MoO₃(Hbpdc)]·*n*H₂O, [Mo₃O₉(pzpy)]_n and [Mo₂O₆(pent-pp)]_n (embora os detalhes estruturais deste polímero sejam ainda desconhecidos, os dados da sua caracterização remetem para um oxo-híbrido polimérico).

O comportamento catalítico dos complexos e dos compostos poliméricos foi testado na reacção de epoxidação de olefinas. Os compostos [Mo₃O₉(pzpy)]_n e [Mo₂O₆(pent-pp)]_n deram origem a espécies activas solúveis respectivamente identificadas como os complexos oxodiperoxido [MoO(O₂)₂(pzpy)] e [MoO(O₂)₂(pent-pp)].

A maioria dos compostos aqui apresentados foram caracterizados através da utilização de técnicas de caracterização do estado sólido, nomeadamente análise elementar, análise termogravimétrica, FT-IV, RMN de estado sólido, microscopia electrónica e difracção de raio-X de pós (tanto de fontes do laboratório e/ou de sincrotrão).

keywords

molybdenum(VI), molybdenum oxides, bidentate chelating N,N-donor ligands, hybrid materials, epoxidation, olefins.

abstract

In this thesis, 2,2'-bipyridine (bipy), di-*tert*-butyl-2,2'-bipyridine (di-*t*-Bu-bipy), 2,2'-bipyridine-5,5'-dicarboxylic acid (H₂bpdc), 2-[3(5)-pyrazolyl]pyridine (pzpy) and 2-(1-pentyl-3-pyrazolyl)pyridine (pent-pp) ligands were used as the *N,N*-chelate ligands in the formation of discrete [MoO₂Cl₂L]-type complexes. These complexes were employed as precursors for the preparation in aqueous media of oxomolybdenum(VI) products with a wide range of structural diversity. Three distinct heating methods were studied: hydrothermal, reflux or microwave-assisted synthesis. An alternative reaction with the inorganic molybdenum(VI) trioxide (MoO₃) and the ligands di-*t*-Bu-bipy, H₂bpdc and pzpy was also investigated under hydrothermal conditions.

The distinct nature of the *N,N*-chelate ligands and/or the heating method employed promoted the isolation of a series of new oxomolybdenum(VI) hybrid materials that clearly reflected the strong structure-directing influence of these ligands. Thus, this thesis describes the synthesis and characterization of the discrete mononuclear [MoO₂Cl₂(pent-pp)], the dinuclear [Mo₂O₆(di-*t*-Bu-bipy)₂] and the octanuclear [Mo₈O₂₂(OH)₄(di-*t*-Bu-bipy)₄] complexes as well as the highly unique polymeric materials {[MoO₃(bipy)][MoO₃(H₂O)]}_n, (DMA)[MoO₃(Hbpdc)]·*n*H₂O, [Mo₃O₉(pzpy)]_n and [Mo₂O₆(pent-pp)]_n (fine structural details of compound [Mo₂O₆(pent-pp)]_n are presently unknown; however, characterization data strongly pointed toward a polymeric oxide hybrid compound).

The catalytic behaviour of the discrete complexes and the polymeric compounds was tested in olefin epoxidation reactions. Compounds [Mo₃O₉(pzpy)]_n and [Mo₂O₆(pent-pp)]_n acted as sources of soluble active species that were identified as the oxodiperoxido complexes [MoO(O₂)₂(pzpy)] and [MoO(O₂)₂(pent-pp)], respectively.

The majority of the compounds here presented were fully characterized by using solid-state techniques, namely elemental analyses, thermogravimetry, FT-IR, solid-state NMR, electron microscopy and powder X-ray diffraction (both from laboratory and/or synchrotron sources).

articles

From the research line of the presented work the following articles were published:

T. R. Amarante, F. A. Almeida Paz, S. Gago, I. S. Gonçalves, M. Pillinger, A. E. Rodrigues, M. Abrantes, Microwave-assisted synthesis and crystal structure of oxo(diperoxo)-(4,4'-di-*tert*-butyl-2,2'-bipyridine)-molybdenum(VI), *Molecules*, **2009**, 14, 3610-3620.

M. Abrantes, T. R. Amarante, M. M. Antunes, S. Gago, F. A. Almeida Paz, I. Margiolaki, A. E. Rodrigues, M. Pillinger, A. A. Valente, I. S. Gonçalves, Synthesis, structural and catalytic performance in olefin epoxidation of a new molybdenum oxide/bipyridine hybrid material: {[MoO₃(bipy)][MoO₃(H₂O)]}_n, *Inorg. Chem.*, **2010**, 49, 6865-6873.

T. R. Amarante, P. Neves, C. Tomé, M. Abrantes, A. A. Valente, F. A. Almeida Paz, M. Pillinger, and I. S. Gonçalves, An octanuclear molybdenum(VI) complex containing coordinatively bound 4,4'-di-*tert*-butyl-2,2'-bipyridine, [Mo₈O₂₂(OH)₄(di-*t*-Bu-bipy)₄]: synthesis, structure, and catalytic epoxidation of bio-derived olefins, *Inorg. Chem.*, 51, **2012**, 3666-3676.

T. R. Amarante, P. Neves, F. A. Almeida Paz, M. Pillinger, A. A. Valente, I. S. Gonçalves, A dinuclear oxomolybdenum(VI) complex, [Mo₂O₆(4,4'-di-*tert*-butyl-2,2'-bipyridine)₂], displaying the [MoO₂(μ-O)₂MoO₂]⁰ core, and its use as a catalyst in olefin epoxidation, *Inorg. Chem. Commun.*, 20, **2012**, 147-152.

T. R. Amarante, A. C. Gomes, P. Neves, F. A. Almeida Paz, A. A. Valente, M. Pillinger, I. S. Gonçalves, A dinuclear oxo-bridged molybdenum(VI) complex containing a bidentate pyrazolylpyridine ligand: structure, characterization and catalytic performance for olefin epoxidation. *Inorg. Chem. Commun.*, 32, **2013**, 59-63.

T. R. Amarante, P. Neves, A. A. Valente, F. A. Almeida Paz, A- N. Fitch, M. Pillinger, I. S. Gonçalves, Hydrothermal synthesis, crystal structure, and catalytic potential of a one-dimensional molybdenum oxide/bipyridine-dicarboxylate hybrid, *Inorg. Chem.*, 52, **2013**, 4618-4628.

T. R. Amarante, P. Neves, F. A. Almeida Paz, A. A. Valente, M. Pillinger, I. S. Gonçalves, Investigation of a dichlorodioxomolybdenum(VI)-pyrazolylpyridine complex and a hybrid derivative as catalysts in olefin epoxidation. *J. Chem. Soc., Dalton Trans.*, **2013** (accepted)

T. R. Amarante, P. Neves, A. C. Gomes, M. M. Nolasco, P. Ribeiro Claro, A. C. Coelho, A. A. Valente, F. A. Almeida Paz, S. Smeets, L. B. McCusker, M. Pillinger, I. S. Gonçalves, Synthesis of the hybrid material $[\text{Mo}_3\text{O}_9(2\text{-}[3(5)\text{-pyrazolyl]pyridine})_n]$ by hydrolysis of a dichlorodioxomolybdenum(VI) precursor: structural elucidation and catalytic properties in olefin epoxidation, *Inorg. Chem.*, **2013** (submitted)

NEW OXOMOLYBDENUM(VI) HYBRID MATERIALS

table of contents

<i>jury presentation</i>	<i>vii</i>
<i>acknowledgments</i>	<i>ix</i>
<i>portuguese abstract</i>	<i>xi</i>
<i>english abstract</i>	<i>xiii</i>
<i>articles published</i>	<i>xv</i>

INTRODUCTION

I. ORGANIC-INORGANIC HYBRID MATERIALS

I.1. Division into classes	2
I.2. Class I examples	3
I.3. Class II examples	5
I.4. Examples of combined Class I and II materials	6

II. MOLYBDENUM(VI) CHEMISTRY

II.1. Brief overview of molybdenum(VI) oxide chemistry.....	7
II.2. Structural diversity of compounds with <i>cis</i> -MoO ₂ ²⁺ core.....	9

III. OXOMOLYBDENUM(VI) HYBRID MATERIALS with *N,N'*-CHELATING LIGANDS

III.1. Why not Metal-Organic Frameworks?	14
III.2. <i>N,N'</i> -Organic ligands	15
III.2.1. Role in the assembly of oxomolybdenum(VI) hybrid materials.....	16
III.3. Metallic precursors to the synthesis	19
III.3.1. MoO ₃	19
III.3.2. Na ₂ MoO ₄ and H ₂ MoO ₄	20
III.3.3. MoO ₂ Cl ₂	20
III.4. Preparation methods	21
III.4.1. Discrete complexes	21
III.4.2. Polymers.....	22
III.5. Oxomolybdenum(VI) with <i>N,N'</i> -organic ligands: examples	23
III.5.1. Discrete complexes	23
III.5.2. Polymers.....	28
III.6. Use of oxomolybdenum(VI) hybrid materials as catalysts.....	33
III.6.1. Olefin epoxidation.....	34

II.6.1.1. Substrates and products.....	35
II.6.1.3. Literature results	37
IV. AIM OF THIS WORK	42
CHAPTER 1	
1.1. Summary	45
1.2. {[MoO ₃ (bipy)][MoO ₃ (H ₂ O)]} _n (1.2)	46
1.2.1. Synthesis	47
1.2.2. FT-IR	47
1.2.3. Thermogravimetric analysis.....	48
1.2.4. Scanning electron microscopy.....	49
1.2.5. X-Ray diffraction: crystal structure description	50
1.2.6. Heterogeneous catalysis	55
1.3. Concluding remarks	61
CHAPTER 2	
2.1. Summary	63
2.2. [Mo ₈ O ₂₂ (OH) ₄ (di- <i>t</i> -Bu-bipy) ₃] (2.2)	64
2.2.1. Synthesis	64
2.2.2. FT-IR	66
2.2.3. Solid-state NMR	68
2.2.4. Thermogravimetric analysis.....	69
2.2.5. Scanning electron microscopy.....	69
2.2.6. X-ray diffraction: crystal structure description.....	70
2.2.7. Powder X-ray diffraction studies.....	75
2.2.8. Catalysis	
2.2.8.1. DL-Limonene (Lim)	76
2.2.8.2. Methyl oleate (Ole)	80
2.2.9. By-products of the synthesis of 2.2	82
2.3. [Mo ₂ O ₆ (di- <i>t</i> -Bu-bipy) ₂]·2H ₂ O (2.3)	82
2.3.1. Synthesis	83
2.3.2. FT-IR	83
2.3.3. Powder X-ray diffraction studies.....	84
2.3.4. Crystal structure description	85
2.3.5. Catalysis tests	89
2.3.5.1. Cis-cyclooctene (Cy8).....	90
2.3.5.2. DL-limonene (Lim), cyclododecene (Cy12)	
1-octene and <i>trans</i> -2-octene	91
2.4. Concluding remarks	92
CHAPTER 3	
3.1. Summary	95
3.2. (DMA)[MoO ₃ (HbpdC)]· <i>n</i> H ₂ O (3.1)	96
3.2.1. Synthesis	96
3.2.2. FT-IR.....	98
3.2.3. Solid-state NMR.....	100

3.2.4. Thermogravimetric analysis and variable temperature powder X-ray diffraction studies.....	102
3.2.5. Scanning electron microscopy	105
3.2.6. X-ray diffraction: crystal structure description	106
3.2.7. Catalytic studies	111
3.2.7.1. Ole epoxidation	111
3.2.7.2. Lim epoxidation	113
3.2.7.3. Ionic liquids.....	115
3.3. Concluding remarks	116

CHAPTER 4

4.1. Summary	119
4.2. [Mo ₃ O ₉ (pzpy)] (4.2).....	120
4.2.1. Synthesis	120
4.2.2. Scanning electron microscopy.....	122
4.2.3. X-ray diffraction: crystal structure description.....	122
4.2.4. Solid-state NMR.....	130
4.3. By-product [MoO(O ₂) ₂ (pzpy)] (4.4) of catalysis tests using 4.2	131
4.3.1. X-ray diffraction: crystal structure description.....	132
4.4. FT-IR comparison studies: 4.1, 4.2, 4.3 and 4.4	136
4.4.1. Discussion	137
4.5. Catalysis: Cy8 substrate.....	139
4.6. Concluding remarks.....	145

CHAPTER 5

5.1. Summary	147
5.2. Synthesis and characterization.....	148
5.2.1. pent-pp (5.1)	148
5.2.1.1. X-ray diffraction: crystal structure description.....	149
5.2.2. [MoO ₂ Cl ₂ (pent-pp)] (5.2).....	151
5.2.2.1. FT-IR.....	151
5.2.2.2. X-ray diffraction: crystal structure description.....	152
5.2.2.3. ¹ H NMR.....	154
5.2.3. [Mo ₂ O ₆ (pent-pp)] (5.3)	154
5.2.3.1. FT-IR.....	155
5.2.3.2. Thermogravimetric analysis and variable temperature powder X-ray diffraction studies.....	156
5.2.3.3. Solid-state NMR.....	158
5.2.3.4. Scanning electron microscopy	159
5.3. Catalysis	160
5.3.1. Cy8	160
5.3.2. Bio-derived olefins: Lim and Ole.....	162
5.3.3. Identification of the active species	163
5.4. Concluding remarks.....	165

EXPERIMENTAL CHAPTER

E.1. Methods	174
E.2. Materials	175
E.3. Characterization techniques	176
E.4. Experimental procedures and characterization.....	177
E.4.1. Chapter 1	
E.4.1.1. Synthesis of $\{[\text{MoO}_3(\text{bipy})][\text{MoO}_3(\text{H}_2\text{O})]\}_n$ (1.2)	177
E.4.2. Chapter 2	
E.4.2.1. Synthesis of $[\text{Mo}_8\text{O}_{22}(\text{OH})_4(\text{di-}t\text{-Bu-bipy})_4]$ (2.2)	179
E.4.2.2. Secondary product $[\text{Mo}_2\text{O}_6(\text{di-}t\text{-Bu-bipy})_2] \cdot 2\text{H}_2\text{O}$ (2.3)	181
E.4.2.3. Secondary product $(\text{H}_2\text{di-}t\text{-Bu-bipy})\text{Cl}_2$	182
E.4.2.3.1. FT-IR and PXRD	182
E.4.2.3.2. X-ray studies: structural description	184
E.4.3. Chapter 3	
E.4.3.1. Synthesis of $(\text{DMA})[\text{MoO}_3(\text{Hbpd})] \cdot n\text{H}_2\text{O}$ (3.1)	187
E.4.4. Chapter 4	
E.4.4.1. Synthesis of $[\text{Mo}_3\text{O}_9(\text{pzpy})]_n$ (4.2).....	189
E.4.4.2. Secondary product $(\text{pzpyH})_2(\text{MoCl}_4)$	191
E.4.4.2.1. Insight into the formation of the salt	191
E.4.4.2.2. Structural description.....	192
E.4.4.2.3. Data collection information	196
E.4.4.3. Secondary product $[\text{Mo}_4\text{O}_{12}(\text{pzpy})_4]$ (4.3).....	197
E.4.4.4. Synthesis of $[\text{MoO}(\text{O}_2)_2(\text{pzpy})]$ (4.4).....	197
E.4.5. Chapter 5	
E.4.5.1. Synthesis of pent-pp (5.1)	199
E.4.5.2. Synthesis of $[\text{MoO}_2\text{Cl}_2(\text{pent-pp})]$ (5.2)	200
E.4.5.3. Synthesis of $[\text{Mo}_2\text{O}_6(\text{pent-pp})]_n$ (5.3)	201
E.4.5.4. Synthesis $[\text{MoO}(\text{O}_2)_2(\text{pent-pp})]$ (5.4)	201
E.5. Catalysis studies: general considerations.....	203
E.5.1. Chapter 1	
E.5.1.1. Investigation procedures	204
E.5.1.2. Solid recovery and reusability	204
E.5.1.3. Scaled up reaction using compound 1.1	204
E.5.1.4. CatFilt experiments	204
E.5.2. Chapter 2	
E.5.2.1. Catalytic studies for 2.2	206
E.5.2.2. Preparation of TBHP/DCE and TBHP/EtOH	206
E.5.2.3. FT-IR of recovered materials in the Lim catalyst tests	207
E.5.2.4. Catalytic studies for 2.3	207
E.5.3. Chapter 3	
E.5.3.1. Catalytic studies for 3.1	208
E.5.4. Chapter 4	
E.5.4.1. Batch catalytic studies of 4.2.....	209

E.5.4.2. Catalytic stability tests	209
E.5.5. Chapter 5	
E.5.5.1. Catalytic studies for 5.2 and 5.3	211
BIBLIOGRAPHY	213



NEW OXOMOLYBDENUM(VI) HYBRID MATERIALS

I. ORGANIC-INORGANIC HYBRID MATERIALS

Current development of new materials is focused on the preparation of systems with properties that can be predicted and controlled pointing to a pre-determined technological application. This is exemplified in the case of hybrid materials (HM) where the final goal is to design a compound that joins two specific components to create a new compound with properties arising from the presence of particular atomic or molecular functional group/s from the two component groups. As shown in Figure 1, HM may range from molecular to extended structures, with the supramolecular aggregates bridging the gap.

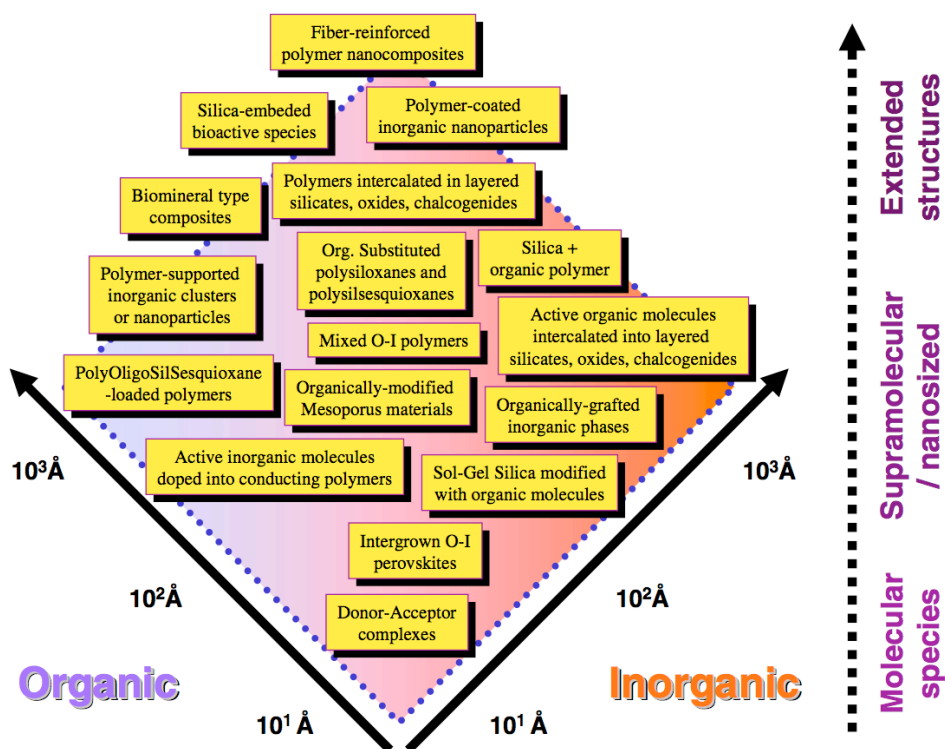


Figure 1. Examples of some known HM ranging from molecular and supramolecular structures, to clusters-polymer adducts, sol-gel hybrids, and to nanocomposite materials based on extended structures. Image reproduced from reference [1].

The interest in HM stems from the fact that they have potential applications in many fields such as optics, electronics, ionic materials, energy storage and conversion, mechanics, membranes, protective coatings, catalysis, sensors and biology. For recent reviews on applications see references [2][3][4].

Defining an organic-inorganic HM is not simple for the reason that compounds containing simultaneously organic and inorganic moieties are not necessarily included in this group. For example, physical mixtures or combinations at the micro- and macroscale level of both types of matter are not considered an organic-inorganic HM.^[1] Therefore, the main requirement for a compound to be coined as a HM is the combination, at molecular level, *i.e.*, at the nanometer scale, of the organic and inorganic parts: pure molecular systems such as the metal salts of organic anions, macromolecules containing small inorganic counter-ions of polymers or commercial polymers containing mineral charges can not, in this way, be considered HM. Some exceptions based on much bigger counter-ions like polyoxometalates, in particular the Wells-Dawson structures^[5] are, however, found in the literature. The reason for this exception stems from the fact that these systems present particular chemical and electrochemical activities that differ from those of their individual components. In fact, this is one of the requirements for a compound to be considered a HM.

I.1. DIVISION INTO CLASSES

Gómez-Romero and Sanchez refer that the classification most widely used for all sorts of hybrids relies on the nature of the interaction between the organic and inorganic components.^[1] According to these authors HM can be categorized into two main classes:

- Class I compounds comprise all the systems where no covalent or iono-covalent bonds are present between the organic and inorganic components. In these compounds the various components only exchange weak interactions such as hydrogen bonds, van der Waals contacts, π - π interactions or electrostatic forces.
- Class II compounds contain, at least, a fraction of the organic and inorganic components linked through strong chemical bonds (covalent, iono-covalent or Lewis acid-base bonds). In many Class II HMs, the organic and inorganic components can also interact *via* the same kind of weak bonds that define Class I.

In both classes the nanostructure, the degree of organization and the properties observed for the HM depend on the chemical nature of their components and on their mutual interaction. An important feature in the tailoring of HM concerns the chemical pathways used for their design. For example, because the organic components are generally “fragile”, *i.e.*, their

thermal stability is limited to less than 250 °C, high-temperature synthesis should be avoided during the hybrid formation process.^[4]

Classes I and II differ radically in the type of synthetic approaches adequate to their successful preparation. In the same way, within each class, each type of HM will also require different strategies for their synthesis (for the donor-acceptor complexes Classes see section I.3). Numerous synthetic pathways such as ion-exchange, dehydration, intercalation, redox, sol-gel, anchoring, grafting and hydrothermal, can be employed, either at ambient or at relatively mild temperatures (< 200 °C).^[2]

In sections I.2 to I.4 selected examples of HM depicted in Figure 1 will be presented. This subject has already been extensively reviewed in the literature both in journal reviews and book chapters.^{[2][6][7]}

I.2. CLASS I EXAMPLES

Active Organic Molecules Intercalated into Layered Materials

The first Class I organic-inorganic HM was the result of an intercalation process. The term “intercalation” denotes a reversible inclusion process in which a molecule or an ion (guest) is placed into a host lattice resulting in an intracrystalline insertion into the layers of a lamellar solid. The only prerequisite is the host-guest affinity based on the thermodynamic behaviour and geometrical impediments.^[1] The attention given to these materials can be attributed mainly to the fact that the host-guest interaction often changes significantly their catalytic, electronic, optical and mechanical properties.^[1]

The layered inorganic networks clay and graphite were the first hosts studied both in the academic and technological fields.^[8] The general interest in the intercalation processes increased after the preparation of other classes of layered materials such as metal(VI) phosphates and phosphonates,^[9] transition metal dichalcogenides (TMDCs),^[10] transition metal oxyhalides,^[11] alkali-transition metal oxides and the hydrotalcite-type anionic clays.^{[12][13]}

Layered metal(VI) phosphates and phosphonates are materials built up from PO_4^{3-} or C-PO_4^{2-} tetrahedral groups shared in different ways and different numbers with tetravalent metals in an octahedral configuration.^[9] As an example, Hussain *et al.* demonstrated that direct ion-exchange could be used to promote the intercalation of doxorubicin (DOX), a known drug for cancer, within a layered zirconium phosphate $[\text{Zr}(\text{HPO}_4)_2]\cdot\text{H}_2\text{O}$ inorganic material.^[14] By combining the two different organic-inorganic materials into a Class I HM (Figure 2), the drug could be successfully (at least *in vitro*) delivered to metastatic and resistant breast cancer cells.^[14]

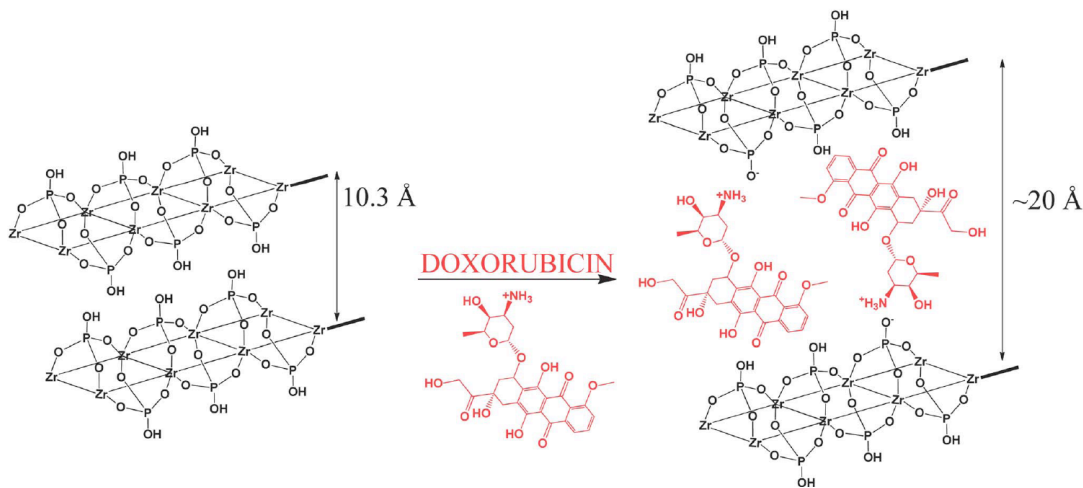


Figure 2. Schematic representation of the Class I HM resulting from the doxorubicin intercalation into zirconium phosphate layers, DOX:ZrP. Image reproduced from reference [14].

This functional HM relies on a α -type^[15] layered zirconium phosphate (α -ZrP) where the layers of metal atoms are alternately lying slightly above and below the mean plane of the layer, being bridged by tetrahedral phosphate groups (Figure 2). This purely inorganic compound is an acidic layered and cation-exchanging material with basal distance (from Zr to Zr) of *ca* 10.3 Å. After the intercalation of doxorubicin (a cationic guest) the interlayer distance expands to 20 Å. The structure of the other α -layered metal phosphates is essentially identical, although the nature of the central metal atom causes significant differences in the interlayer distance, and between adjacent phosphate groups, and also the free area available for guests.^[9]

Anionic guests may also be intercalated between inorganic host structures. For example, hydrotalcite-type anionic clays, also named layered double hydroxides (LDHs), are positively charged hosts that have the ability to intercalate negative guests, *i.e.*, contrary to the negatively charged layered metal(VI) phosphate and phosphonate materials, LDHs comprise positively charged layers that require charge-balancing anions between the layers to ensure electroneutrality. The general formula for a LDH is $[M^{II}_{(1-x)}M^{III}_x(OH)_2](A^{n-})_{x/n} \cdot zH_2O$ where M^{II} and M^{III} represent di- and trivalent cations octahedrally coordinated to hydroxyl ions, and A^{n-} is the interlayer anion. These octahedral units are connected to each other by edge-sharing to form an infinite sheet. Pillinger, Gonçalves and co-workers have prepared a Class I HM “pillared” by 2,2'-bipyridine-5,5'-dicarboxylate (Figure 3).^[16] This compound was prepared using soft chemistry of ion exchange, *i.e.*, the nitrate anions in (Zn,Al)-NO₃ were exchanged by the organic 2,2'-bipyridine-5,5'-dicarboxylate anions. Upon intercalation the interlayer distance expanded from 9 Å to 18 Å.

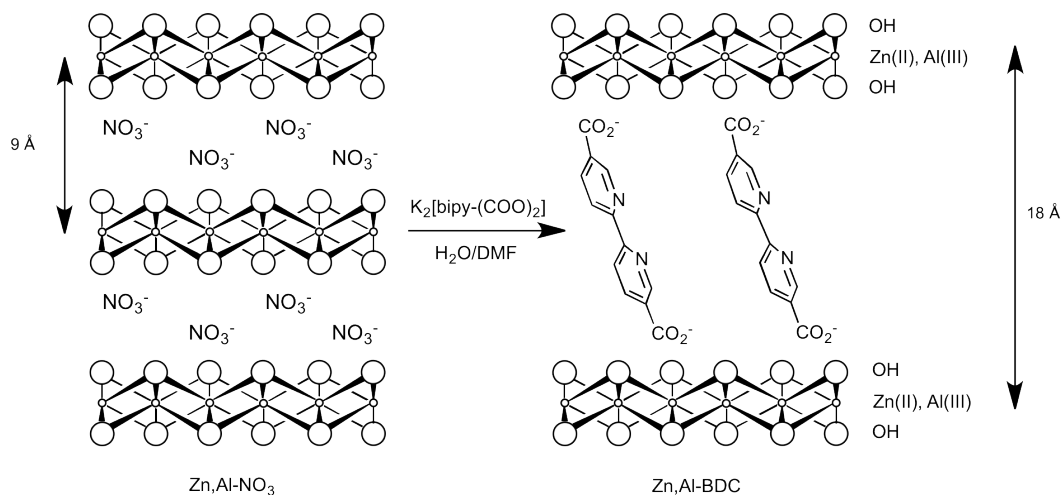


Figure 3. Schematic representation of the Class I HM resulting from the intercalation of 2,2'-bipyridine-5,5'-dicarboxylate within LDH layers. Image reproduced from reference [16].

LDHs have been used as environmental adsorbents^[17] and/or anionic exchangers,^[18] precursors in the preparation of advanced ceramics,^[19] catalysts and catalyst supports.^{[16][20][21]} The research groups of Pillinger and Gonçalves have intensively explored these layered materials as catalyst supports to improve the catalytic properties of Mo^{VI} compounds (identical to those presented in section II.4), and to promote the occurrence of selective reactions in the interlayer region of the inorganic host.

I.3. CLASS II EXAMPLES

Donor-Acceptor Complexes

Class II HM have structures in which the organic and inorganic components are joined together through strong covalent or ionic-covalent chemical bonds. Examples are typically donor-acceptor complexes (*i.e.*, ligand-to-metal). These can be of two kinds: i) discrete-based metallic complexes coordinated to an organic ligand (examples given on page 24); or ii) inorganic polymers or discrete inorganic building blocks (*e.g.*, clusters) covalently connected to the organic component (examples of polymers in page 29). In both cases materials have “durable” bonds between the organic and the solid inorganic components.

Because in these structures the organic and inorganic parts are bonded together through strong chemical bonds, the chemical strategy to prepare Class II HM depends on the stability of the employed bonds.^[1] The organic adduct employed must have, at least, one direct, non-hydrolysable heteroatom-carbon bond. This group should be either fixed by post-synthesis approaches onto the inorganic support or, alternatively, be included as an organofunctional

precursor, or prepared by combining these two approaches. Literature examples comprise adducts of transition metal cations with organic ligands. These molecules should have functional groups based on atoms that can be used to anchor the organic component to the inorganic one: for example, carboxylic acids, phosphonates, hydroxyacids, polyols, betadiketones, among others.^[22]

I.4. EXAMPLES OF COMBINED CLASS I and II MATERIALS

Because of the presence of strong and simultaneously weak bonds between organic and inorganic components, the vast majority of hybrid materials fall at the same time into both classes. Constructing on the example given for the previously described Class I HM (see Figure 4), the LDH material intercalated by the 2,2'-bipyridine-5,5'-dicarboxylate was further used by the same authors as a porous matrix to intercalate LnCl_3 ($\text{Ln} = \text{Eu}, \text{Gd}$) and improve the photoluminescence properties of Eu^{3+} .^[23] Mentioned as a Class II example, *i.e.*, donor-acceptor complexes, the coordination of the *N*-donor atoms from the organic 2,2'-bipyridine-5,5'-dicarboxylate component to the Eu^{3+} inorganic metal leads, in this way, to the formation of a Class II HM within the Class I previously existent.

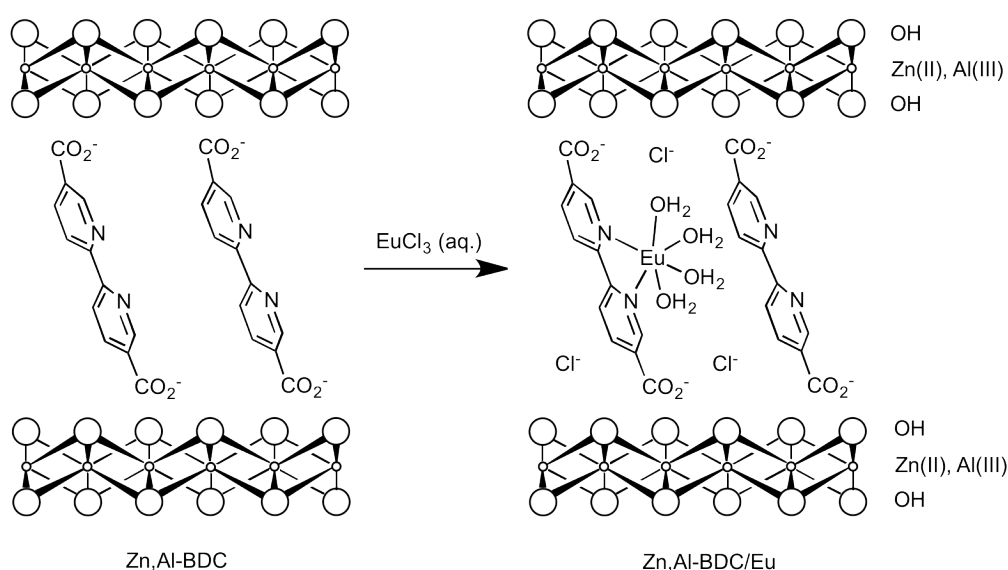


Figure 4. Schematic representation of the a Zn-Al LDH intercalated by 2,2'-bipyridine-5,5'-dicarboxylate and proposed coordination environment of Eu^{3+} ions within the interlayer region. Image taken from reference [23].

II. MOLYBDENUM(VI) CHEMISTRY

Molybdenum was “discovered” in 1778 by Carl Wilhelm Scheele and isolated for the first time in 1781 by Peter Jacob Hjelm.^[24] This metal is an essential trace element that does not occur freely in Nature. It is instead present

in several minerals such as: molybdenite (MoS_2), wulfenite (PbMoO_4) and powellite [$\text{Ca}(\text{Mo}, \text{W})\text{O}_4$]. It exists in association with organic matter and in sedimentary sulfide minerals, and in natural water as molybdate oxyanions where the dominant species are HMoO_4^- if $2 < \text{pH} < 5$, and MoO_4^- if $\text{pH} > 5$.^[24]

Molybdenum is also encountered in a wide variety of enzymes responsible for the growth and health of living organisms. The metal is required for the normal metabolism of biological systems: for example, in the nitrogen, sulfur, or carbon cycles.^{[25][26]}

In chemistry, molybdenum is a Group VI chemical element with the symbol Mo and the atomic number of 42. It has an atomic mass of 95.94 g/mol^{-1} and the ground state electronic configuration is $[\text{Kr}] 4d^5 5s^1$. Due to the large number of stable and variable oxidation states ranging from $-II$ to VI , allied with the coordination numbers ranging from four to eight, the chemistry of molybdenum is very rich. At its lowest oxidation state molybdenum is largely in the realm of organometallic chemistry, wherein it may bond directly to the carbon atom of a carbon monoxide, an organic phosphine, and/or to a variety of unsaturated carbonaceous ligands. At its highest oxidation state, molybdenum is usually characterized by binding to electronegative atoms such as oxygen and halogens.^[27]

II.1. BRIEF OVERVIEW of MOLYBDENUM(VI) OXIDE CHEMISTRY

Molybdenum oxides are the most important compounds from Mo^{VI} chemistry. In fact, this subject has become an area of great interest because the materials are important in the industrial^[28] and biochemical fields.^[29] Figure 5 depicts a search in the database Scopus using the keywords *molybdenum oxide chemistry* or (criteria search) *molybdenum oxide* and, or *oxomolybdenum*.

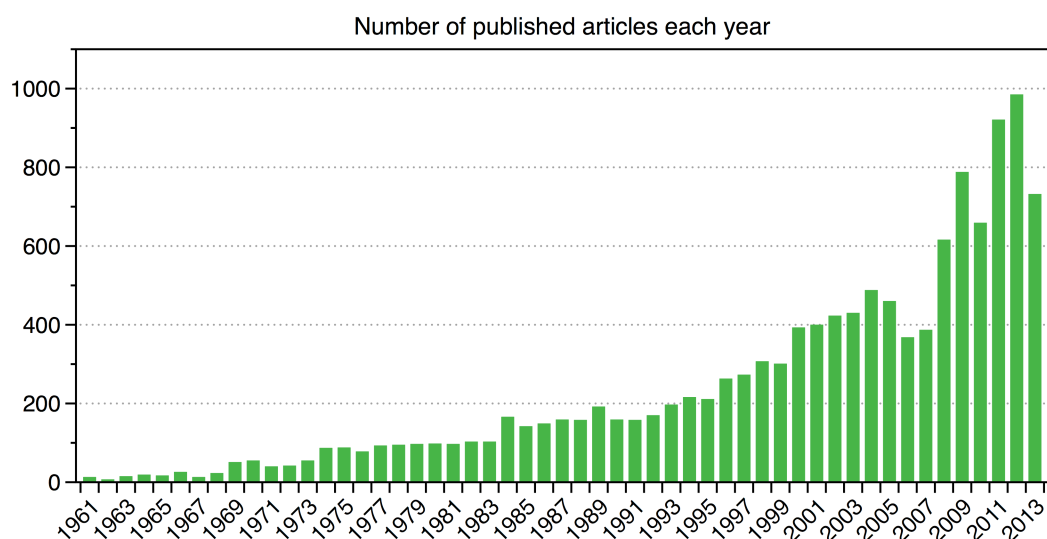


Figure 5. Number of published articles since 1961 until September 2013 about, or related to, oxo-molybdenum chemistry. The search output gave 12596 results while the integrated results since 2000 are 8050.

The search indicates that research on molybdenum oxides experienced a renaissance during the last few years having, at this date, already 7 articles published in 2014 (not shown).

Molybdenum(VI) oxide chemistry includes all molybdenum complexes to which there is attached a surrounding array of oxido (O^{2-}) ligands. See, for example, the functional cores in Figure 6. The complexes may be inorganic if no carbon is present or bonded to the metal centre, e.g., MoO_3 and MoO_2Cl_2 , organometallic if a carbon is directly bonded to the metal, or organic-inorganic if the an organic component is bonded through a coordinative covalent bond to the metal centre, e.g., $[MoO_2Cl_2(bipy)]$ where bipy stands for 2,2'-bipyridine.

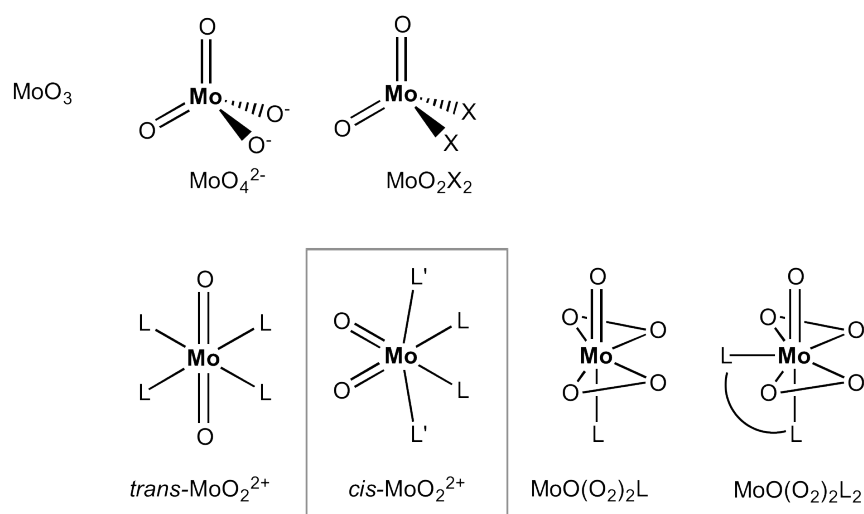


Figure 6. Structural representation of functional cores usually found in discrete complexes in Mo^{VI} oxide chemistry.

Dioxomolybdenum(VI) complexes (complexes with two O^{2-} ligands) containing the $cis-MoO_2^{2+}$ core (see Figure 6) have, by far, received the greatest attention because of their prevalence, ease of synthesis, and chemical properties that led to their extensive use as homogeneous^[30] and heterogeneous catalysts,^[31] as materials precursors^[32] as well as models for the active sites of oxo-transfer molybdenum enzymes.^{[33][34]} The dioxomolybdenum(VI) chemistry is dominated by the $cis-MoO_2^{2+}$ core but this is just one of two existent possible orientations in the distorted coordination octahedron.^[35] The cis - or $trans$ - orientations (see Figure 6) depend on the molybdenum electronic configuration d^0 or d^2 , respectively.^[35]

In the $cis-MoO_2^{2+}$ core, the geometry of the oxometal functional groups lies in a narrow range: the $Mo=O$ distances in the *ca.* 1.65-1.75 Å range, and the $O=Mo=O$ angles from *ca.* 95 to 110 °. This core can be easily identified from vibrational spectroscopy with the FT-IR spectrum presenting at *ca.* 850-950 cm^{-1} an intense two-band pattern corresponding to the symmetric and asymmetric

Mo=O stretching modes.^[35] Both the bond length and the stretching frequencies justify the multiple-bond character of the oxo-metal bond. Single bonds established by neutral and anionic oxygen donor atoms to the metal nuclei are usually 0.2-0.4 Å longer.^[35] The geometrical range of the compounds containing the *cis*-MoO₂²⁺ core coordinated to organic ligands can go from monomeric to polymeric structures, while the link between adjacent molybdenum centres is mostly established through an oxygen atom.

II.2. STRUCTURAL DIVERSITY of COMPOUNDS with a *cis*-MoO₂²⁺ CORE

In an attempt to find out more about the diversity of the known structures containing the *cis*-MoO₂²⁺ core coordinated to organic ligands, a search in the Cambridge Structural Database (CSD)^{[36][37]} version 5.34 (November 2013 with 3 updates) was performed using three criteria. First, the results should be, at least, about dimeric structures, *i.e.*, two units of *cis*-MoO₂²⁺ must be present and no monomeric discrete complex must be considered. Second, adjacent units of *cis*-MoO₂²⁺ must be bridged through oxygen single bonds established from metal-to-metal. Third, no metal other than Mo^{VI} should be present. Even though no restrictions were made about the organic ligand coordination mode (*bi*-, *tri*- or *tetradentate*), or the ligand donor atoms (O, S, N or a mix of atoms), only 133 crystal structures are known of which 96 are dimeric and 21 are tetrameric discrete complexes. Due to the high number of dimeric structures encountered, only those which have a *N,N'*-chelate ligand coordinated to the metal centre will be discussed in section III.5. Noteworthy, only two structures have an odd number of three repeating *cis*-MoO₂²⁺ units (*i.e.* trimeric), while the remaining results were all multiples of two mononuclear, *i.e.* tetranuclear, hexanuclear, octanuclear, dodecanuclear or polymeric (*i.e.*, polymeric). A relevant result is the fact that organic ligands containing oxygen donor atoms, *i.e.*, alkoxy ligands, are predominant in all types of polyoxomolybdates. An extensive review of polyoxotrialkoxometalates was compiled by Gouzerh.^[38]

TRINUCLEAR COMPLEXES

The research group of Zubieta published the largest number of structures. In fact, between 1989 and 1991 this group published all trinuclear structures found up to date. The case studies were all on branched ligands with [N,O,O,O] and [O,O,O] donor sets and, although the *cis*-MoO₂²⁺ unit was common to all structures, the trinuclear cases were only possible to isolate using the second donor set, *i.e.*, through the use of the *tris*-hydroxymethylethane ligand (H₃hmp).^{[39][40]} The trinuclear [TBA₂][Mo₃O₇(hmp)]·0.5(C₂H₅)₂O product (TBA - tetra-*n*-butylammonium) (see Figure 7, *right*) was prepared via reflux of

[TBA]₂[Mo₂O₇]^[41] in dichloromethane in the presence of excess of H₃hmp.^[42] The resulting anion, [Mo₃O₇(hmp)₂]²⁻, exhibited usual [MoO₆] *pseudo*-octahedra in an edge-sharing arrangement. Two of the Mo^{VI} centres display similar geometries: both are coordinated to two terminal oxido ligands in a *cis* configuration, with bridging and terminal alkoxy donors from the hmp³⁻ ligands completing the coordination. In contrast, the third Mo^{VI} centre displays three terminal oxido groups and an additional bonding to three bridging alkoxy oxygens. According to the author this was the first example of a solution-stable polyoxometalate coordination complex known to violate the Lipscomb's principle. This principal rationalized the inexistence of stable polyanion species containing MO₆ octahedra with more than two terminal oxido groups in terms of the strong *trans* influence of the M–O (terminal) bonds which would dissociate the *fac* [MO₃] groups attached to the structure by weaker bonds.^[43] This novel compound containing the reactive [MoO₃] moiety was later studied for its conversion to the methoxy derivative and related alkoxy species (Figure 7, *left*).^[42]

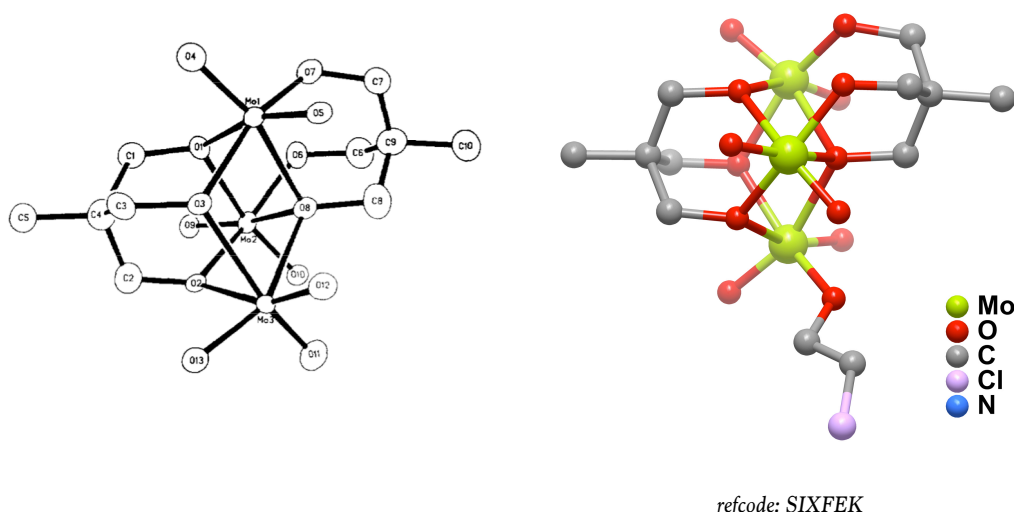


Figure 7. Right ORTEP view of the structure of the trinuclear [Mo₃O₇(hmp)₂]²⁻ anion complex. Image reproduced from reference [40] b) Trinuclear [TBA]₂[Mo₃O₇(hmp)]·0.5(C₂H₅)₂O product.

TETRANUCLEAR COMPLEXES

Tetranuclear structures have been reported by, *inter alia*, the groups of Piggott, [Mo₄O₁₂(C₁₂H₃₀N₄S₂)₂(C₃H₇ON)₂],^[44] Gouzerh [*n*-Bu₄N]₂-[Mo₄O₁₀(OMe)₄(Me₂CNHO)₂],^[45] and Zubietta who discovered structures such as [Mo₄O₆(OPr)₆Cl₄]^[46] and [*n*-Bu₄N]₂[Mo₄O₁₀(C₆H₂O₄)₂].^[47] Figure 8 depicts some examples of such complexes. A systematic structural study on the tetramers can be found on the review paper by Zubietta.^[46]

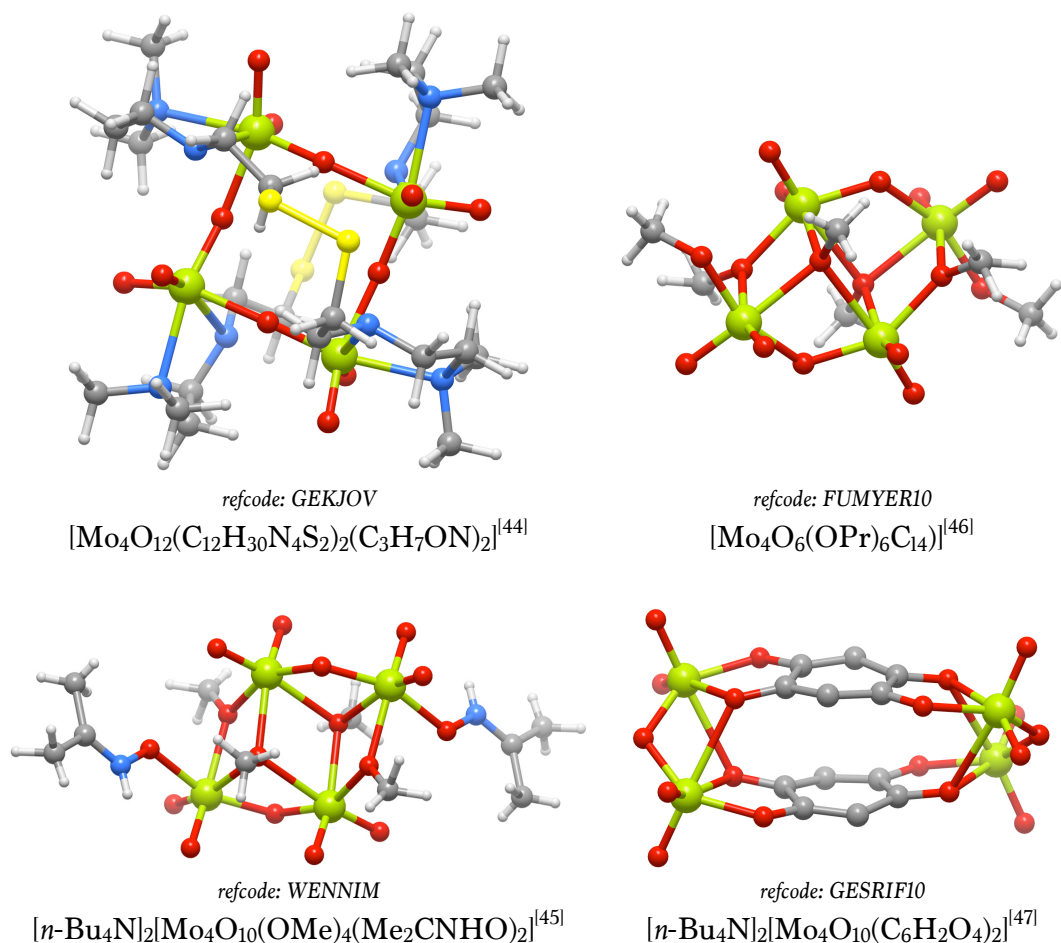
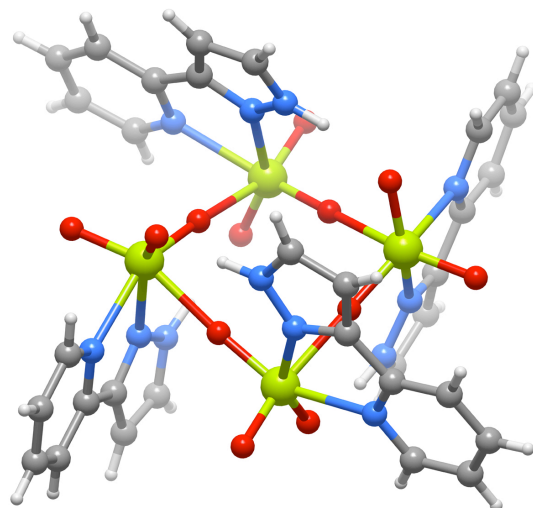


Figure 8. Tetranuclear complexes containing the *cis*- MoO_2^{2+} unit described in the literature.

Only one tetranuclear complex contains a bidentate organic ligand: $[\text{Mo}_4\text{O}_{12}(\text{pzpy})_4]$ (pzpy = 2-[3(5)-pyrazolyl]pyridine (Figure 9), which was reported by Zhang.^[48] The structure is remarkable because, contrary to the other discrete structures having four *cis*- MoO_2^{2+} units that are built via edge-sharing octahedra, the $[\text{Mo}_4\text{O}_{12}(\text{pzpy})_4]$ structure consists of a tetranuclear unit built up from single oxygen bridges, *i.e.*, corner-sharing octahedra. The complex has any three Mo^{VI} atoms defining a plane while the fourth atom lies *ca* 1.8 Å out of that plane, *i.e.*, the degree of linearity of the oxide bridges between two Mo^{VI} atoms is 175.4°. At the supramolecular level, N–H groups from the 2-[3(5)-pyrazolyl]pyridine ligands form intra-molecular hydrogen bonds (four per molecule). This structure has also been obtained using a completely different approach (the oxidative decarbonylation of the $[\text{Mo}(\text{CO})_4(\text{pzpy})]$ by reaction with excess TBHP*dec*) by the group of Gonçalves.^[49]

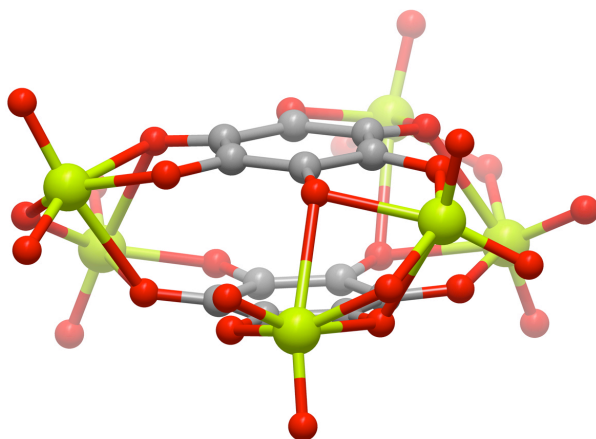


refcode: HUCGIW

Figure 9. Tetranuclear discrete $[\text{Mo}_4\text{O}_{12}(\text{C}_8\text{H}_7\text{N}_3)_4]$ complex published by Zhang.^[48] The Mo^{VI} distorted octahedra are completed by two terminal oxygen atoms, two oxygen bridges and two N atoms from 2-[3(5)-pyrazolyl]pyridine ligands.

HEXANUCLEAR COMPLEXES

An example of hexanuclear structure is $[\eta\text{-Bu}_4\text{N}]_3[\text{Mo}_6\text{O}_{15}(\text{C}_6\text{H}_6)_2]$,^[47] which consists of three $[\text{Mo}_2\text{O}_5]^{2+}$ units serving to hold two semiquinone (tetrahydroxy-1,4-benzoquinone) planes in a parallel staggered orientation with short interplanar distances (see Figure 10). The interesting feature of this compound, as for the structurally related structures published in the same article, is the significant charge delocalization as a consequence of the overlap of the ligand orbitals that facilitates redox chemistry and results in a number of readily accessible redox states.^[47] The polymolybdate crystals were prepared by addition of tetrahydroxy-1,4-benzoquinone to a solution of $[(\text{C}_4\text{H}_9)_4\text{N}]_4[\text{Mo}_8\text{O}_{26}]$ in acetonitrile, followed by overnight stirring, addition of 2-propanol and three weeks resting at 4 °C.

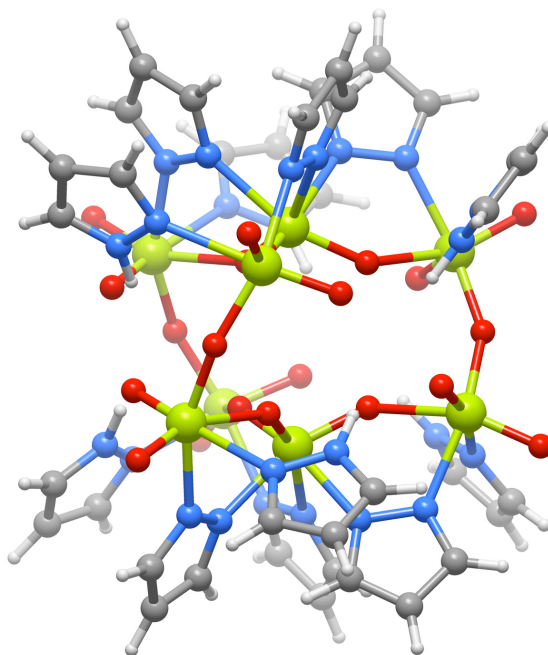


refcode: VAMYEI

Figure 10. Hexanuclear discrete structure of the $[\text{Mo}_6\text{O}_{15}(\text{C}_6\text{O}_6)_2]^{3-}$ anion published by Jubieta.^[47]

OCTANUCLEAR COMPLEXES

Considering organic ligands with N-donor atoms, only one octanuclear structure was published in which all Mo^{VI} centres have identical coordination spheres: [Mo₈O₂₁(pz)₆(pzH)₆] (pz = pyrazolate anion and pzH = pyrazole; Figure 11) reported by Thompson and Storr.^[50] The structure contains both Mo^{VI} and Mo^V centres, with the Mo^V atoms linked in pairs via metal-metal single bonds. This octanuclear structure is composed of both bridging and terminal pyrazole ligands, with an inorganic core formed by corner-linked MoO₆ octahedra.



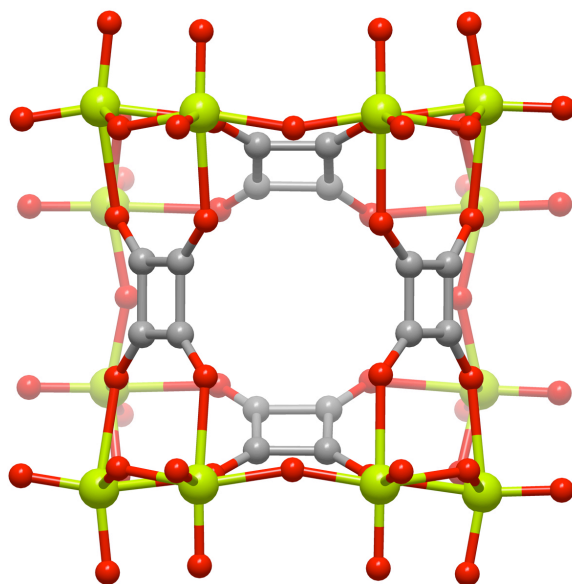
refcode: WEHMIF

Figure 11. Schematic representation of the octanuclear discrete structure of [Mo₈O₂₁(pz)₆(pzH)₆] (pzH = pyrazole) reported by Thompson and Storr.^[50]

DODECANUCLEAR COMPLEXES

With twelve *cis*-MoO₂²⁺ units only one structure is known: [(C₄H₉)₄N]₄[Mo₁₂O₃₆(C₄O₄H)₂]⁻10Et₂O.^[51] Zubietta described this compound as an unusual polyoxomolybdate because, although these complexes are generally constructed exclusively from edge-shared octahedra,^[52] this dodecameric structure has both edge- and corner-sharing octahedra. The complex encompasses a dodecanuclear cage of Mo^{VI} atoms bridged by oxido groups, producing a cyclic [Mo₁₂O₁₂] motif. Each squarate ligand bridges six Mo^{VI} sites, in such a way that two of the oxygen donors adopt bridging modes and two oxygen donors assume terminal positions. In this fashion, each Mo^{VI} centre exhibits distorted octahedral geometry through coordination to two terminal oxido groups, two bridging oxido groups, and two oxygen donors from the squarate ligands. The complex anion exhibits approximately four-fold inversion

symmetry about an axis normal to and passing through the centre of the molecule, as illustrated in Figure 12.



refcode: SEMFIZ

Figure 12. Structure of the dodecanuclear discrete anion present in the discrete compound $[(C_4H_9)_4N]_4[Mo_{12}O_{36}(C_4O_4H)_2] \cdot 10Et_2O$ reported by Zubietta.^[51]

III. OXOMOLYBDENUM(VI) HYBRID MATERIALS with *N,N'*-CHELATE LIGANDS

One class of organic ligands that have attracted particular interest in coordination chemistry is the organonitrogen class. Bipyridine derivatives, such as 2,2'-bipyridine and 4,4'-bipyridine, remain to date the most widely explored molecules in coordination chemistry.^[53] Here we focus on the former derivative units because they can be used as versatile metal chelating ligands also amenable to chemical modification. For example, they coordinate to the *cis*- MoO_2^{2+} core to form oxomolybdenum(VI) hybrid compounds, in which the organic component can be systematically varied through the inclusion of different pendant groups on the pyridyl moieties. In this section the possible roles of the *N,N*-organic ligands in these materials are presented. The precursors, synthetic strategies and representative structural examples found in the literature are summarized.

III.1. WHY NOT METAL-ORGANIC FRAMEWORKS?

The concept of hybrid materials led to a spread of an enormous diversity of coordination solids involving inorganic and organic moieties as integral parts

of new structures. With examples of organic moieties directly coordinated through a covalent bond to a metal, two subfields of hybrid organic-inorganic materials are important: the Metal-Organic Framework materials (MOFs) and the “coordination oxomolybdenum oxides with discrete or polymeric structures” (in this particular case oxomolybdenum(VI)). According to the IUPAC task group for terminology and nomenclature guidelines, the latter subgroup may be enclosed into the Coordination Polymer chemistry because the materials are coordination compounds, *i.e.*, have repeating entities in one dimension and it is sometimes possible to prove the existence of polymeric entities that can be called macromolecules.^[54] On the other hand, MOFs are defined as coordination networks (*i.e.*, coordination polymers with cross-links between two or more individual chains) containing potential voids. These materials are many times dynamic systems which change in structure and, thus, change their porosity or solvent and/or guest filled voids depending on temperature, pressure, or other external stimuli.^[54] Due to these reasons MOFs are not always crystalline materials.

A simple way to distinguish MOFs from the Coordination Polymers herein described is based on the role of the organic ligand itself. In a MOF the ligand establishes bridges between metals, metal scaffolds or discrete metallic clusters promoting the formation of open-frameworks exhibiting permanent porosity. In the coordination polymers herein presented, the bridge between metals is established only through oxygen atoms forming a pure inorganic skeleton while the ligand is a bidentate terminal chelate ligand. In opposition to MOFs these structures do not typically present voids and they are not dynamic systems.

III.2. *N,N'*-ORGANIC LIGANDS

Among all *N,N'*-chelating ligands, bipyridine is the most explored molecule due to its redox stability but also because of its simple functionalization.^[53] Bipyridines were first synthesized by Fritz Blau at the end of the nineteenth century.^[55] Since then, the synthesis has dramatically improved^[56] as well as the range of usages as starting material for new bidentate ligands.^[53]

Even though it has six structural isomers (2,2'-, 2,3'-, 2,4'-, 3,3'-, 3,4'-, 4,4'-), 2,2'-bipyridine is the most popular unit due to its structural features, *i.e.*, consists of two planar pyridyl rings connected by a covalent C-C bond and coordinates to the metal via both nitrogen atoms in such positions that yield a chelate ring where the two lone pairs of nitrogen atoms can form σ -bonds with the metal centre.^[53] During this process, the aromatic system can take part in back-bonding where the π -electron density is delocalized over the chelate ring via the metal-diimine bonding. Table 1 depicts most of the *N,N'*-organic chelating ligands found in octahedral complexes containing the *cis*-MoO₂²⁺

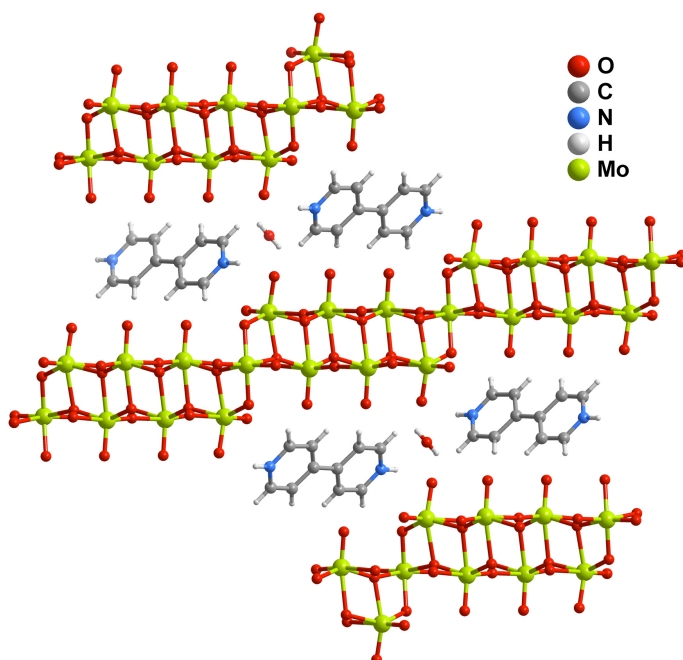
moiety. Examples of organic families found are 2,2'-bipyridine, 4,4'-bipyridine, 1,10-phenanthroline and 2-[3(5)-pyrazolyl]pyridine.

III.2.1. ROLE in the ASSEMBLY of OXOMOLYBDENUM(VI) HYBRID MATERIALS

Depending on the role of the organic moiety, Zubietta subdivided the wide field of oxomolybdenum(VI) hybrid materials into three subclasses:

Space filler and/or counter-ion

A striking example is $[4,4'\text{-H}_2\text{bpy}][\text{Mo}_7\text{O}_{22}]\cdot\text{H}_2\text{O}$ (Figure 13) for which the acidic conditions of the reaction promoted protonation^[57] of the pyridyl nitrogen atoms of 4,4'-bipyridine. In this way, *N,N*-coordination to the oxide skeleton was precluded resulting in the incorporation of the organic component in the crystal structure as the bipyridinium di-cation. As shown in Figure 13, these cationic moieties function simultaneously as charge-balancing units and space filling moieties. The inorganic subunit of $[4,4'\text{-H}_2\text{bpy}][\text{Mo}_7\text{O}_{22}]\cdot\text{H}_2\text{O}$ is both structurally and compositionally related to the layered molybdenum trioxide (section III.3.1) Indeed, reformulation of the chemical formula into $[4,4'\text{-H}_2\text{bpy}][(\text{MoO}_3)_7\text{O}]\cdot\text{H}_2\text{O}$, helps to emphasize the relationship of the inorganic component to the MoO_3 parent structure.



refcode: REFFOX

Figure 13. Class I hybrid material: $[4,4'\text{-H}_2\text{bpy}][\text{Mo}_7\text{O}_{22}]\cdot\text{H}_2\text{O}$, which consists of molybdenum oxide layers separated by an interlamellar region populated by $4,4'\text{-H}_2\text{bpy}^{2+}$ cations and H_2O molecules of crystallization.^[57]

Pillars or terminal decorating ligands

In this case the organic moiety is directly bonded to the metal site of the inorganic oxide chain. Noteworthy, the position of the bonding groups has a strong influence in the final function of the organic molecule in the structure. Indeed, if the ligand has two or more donor atoms structurally positioned in *exo* locations, connections between metal centers may be formed leading to, e.g., typical MOF structures. Alternatively, *endo* positions for the donor atoms tend to reduce polymerization by eliminating coordination sites.

As shown in Figure 14 depicting the crystal structure of $[\text{Mo}_4\text{O}_{12}(4,4'\text{-bipy})_2]_n$,^[58] 4,4'-bipyridine molecules are covalently bonded to the transition metal oxide skeleton acting as true pillars between the inorganic layers, ultimately leading to a sandwich-type compound in which the organic and inorganic components alternate in a ABAB fashion. In this case, the ligand acts as physical bridges between metal centers, leading to the formation of a typical MOF structure.

Compound $[\text{Mo}_3\text{O}_9(\text{bipy})]_n$ ^[59] is based instead on the *endo* 2,2'-bipyridine molecule which is, as mentioned above, N,N-chelated to the metallic center reducing the number of coordination sites. The crystal structure is, thus, formed by isolated 1D chains as shown in Figure 14 (*right*).

Mixed situations may also occur. A striking example concerns compound $[\text{Mo}_4\text{O}_{13}(\text{Hbpa})_2]_n$ ^[60] (Hbpa = 4-pyridyl-4'-pyridinium amine). In this case even though the parent bpa molecule could function just like 4,4'-bpy in $[\text{Mo}_4\text{O}_{12}(4,4'\text{-bipy})_2]_n$ (*i.e.*, as pillars), one pyridyl group is protonated, acting as a charge-balancing molecule and ultimately preventing further connectivity to neighbouring metallic centers (see Figure 15). As a result unidentate Hbpa molecules act as terminal ligands, decorating the 1D chains and mutually intering via weak supramolecular contacts.

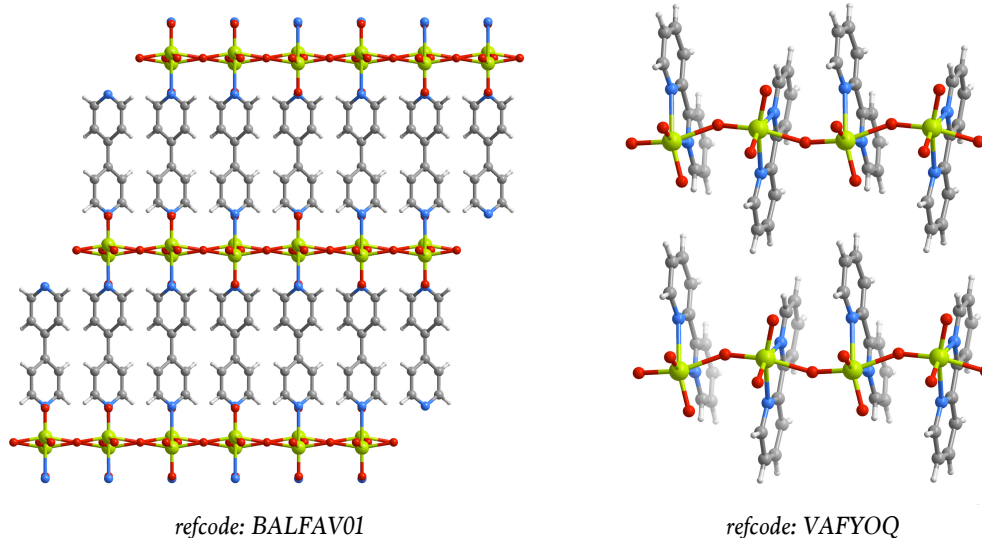
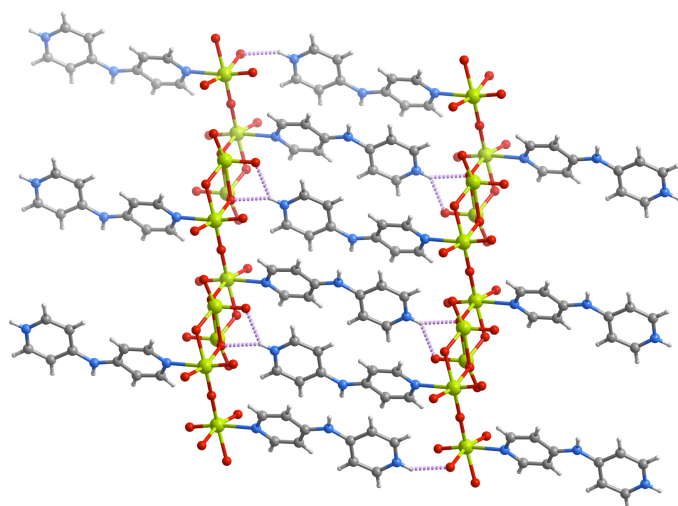


Figure 14. Examples of Class II oxomolybdenum(VI) hybrid materials where the organic ligand act as (*left*) pillars to the transition metal oxide skeleton $[\text{Mo}_4\text{O}_{12}(4,4'\text{-bipy})_2]_n$ ^[58] or (*right*) terminal groups as in $[\text{Mo}_3\text{O}_9(2,2'\text{-bipy})]_n$ ^[59]

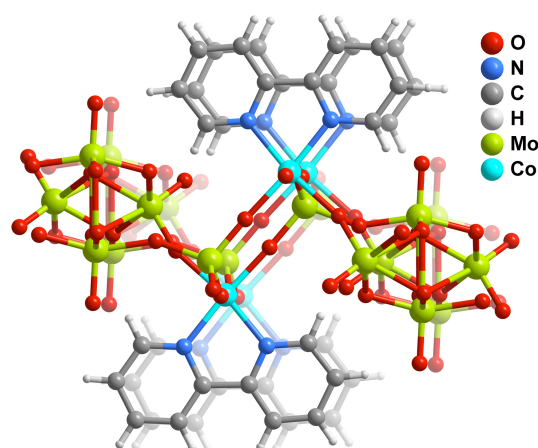


refcode: JOSNUA

Figure 15 1D chains cross-linked by ligands of give the 2D structure of $[\text{Mo}_4\text{O}_{13}(\text{Hbpa})_2]$.^[60]

Passive ligands in a heterometallic coordination polyhedron

The organic moiety may be a passive ligand bonded to a different metal centre that is incorporated into the molybdenum oxide backbone either as peripheral moieties or as complex bridging units. It is noted that in this case the molecule reduces the number of coordination sites of the other metal center, which permits to some degree to control the way the molybdenum oxide core connects to this second type of complex. For example, in $[\text{Co}(\text{bipy})\text{Mo}_3\text{O}_{10}]$ (Figure 16)^[61] 2,2'-bipyridine is chelated to Co^{2+} forming $\{\text{CoN}_2\text{O}_4\}$ octahedra. These units interconnect 1D molybdenum oxide chains (composed of molybdenum tetrahedra, octahedra and square pyramids) into a two-dimensional covalent network as shown in Figure 16.



refcode: NISZEU

Figure 16. Portion of the crystal structure of the Class II hybrid material $[\text{Co}(\text{bipy})\text{Mo}_3\text{O}_{10}]_n$,^[61] emphasizing the connections of 1D molybdenum oxide chains into 2D structures through inclusion of a second metallic center coordinated to a passive N,N' -chelated organic ligand.

III.3. METALLIC PRECURSORS to the SYNTHESIS

A literature search on the precursors used to prepare oxomolybdenum(VI) HMs containing the *cis*-MoO₂²⁺ core revealed that Mo^{VI} trioxide (MoO₃), sodium molybdate ([Na₂MoO₄]·2H₂O), molybdic acid (H₂MoO₄), polyoxomolybdenum anions ranging from ((ⁿBu₄N)₂[Mo₂O₇]) to ((ⁿBu₄N)₄[Mo₈O₂₆]), and dichlorodioxomolybdenum(VI) ([MoO₂Cl₂]) are the most common reagents. No reports were found where other polyoxomolybdenum compounds were used to prepare hybrid compounds containing *N,N'*-ligands.

III.3.1. MoO₃

Molybdenum trioxide (MoO₃) is one, if not the most important Mo^{VI} oxide. This well-known whitish solid is the molybdenum compound produced on the largest scale. It occurs in Nature as the rare mineral molybdenite but it is produced industrially by roasting molybdenum disulfide (Equation 1). Its key applications are its use as oxidation catalyst (as catalyst itself and/or precursor), and as raw material for the production of molybdenum metal.



In the gas phase the structure of MoO₃ presents three oxygen atoms double bonded to the central molybdenum atom (Figure 17, *left*). In the solid state, anhydrous MoO₃ consists of layers of linked distorted MoO₆ octahedra in an orthorhombic crystal. Their arrangement is more complex since they share edges and form chains that are cross-linked by oxygen atoms to form the layers where the octahedra have one short molybdenum-oxygen bond to a non-bridging oxygen (Figure 17, *right*).^[62] The result is a unique three-dimensional network.

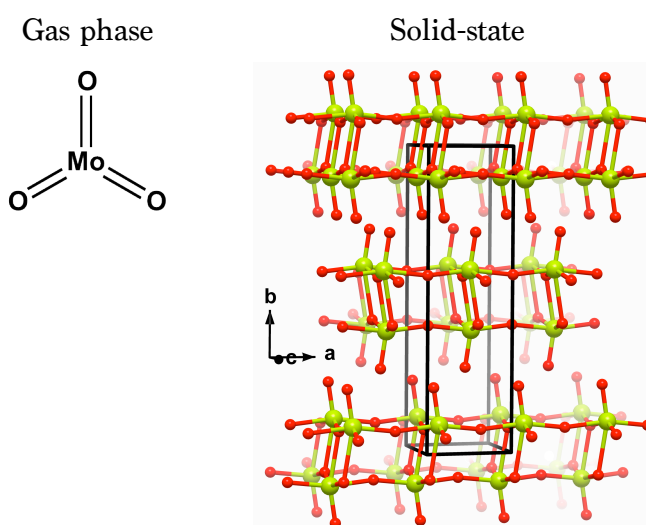


Figure 17. Representation of the gaseous and solid-state structure of MoO₃.

III.3.2. Na₂MoO₄ and H₂MoO₄

Sodium molybdate (Na₂MoO₄) and molybdic acid (H₂MoO₄) are starting materials for the synthesis of dioxomolybdenum(VI) hybrid materials containing organic ligands with N,N'-donor atoms.^[32] As for molybdenum trioxide, Na₂MoO₄ and H₂MoO₄ are commercially available precursors.

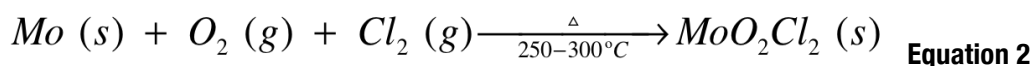
Molybdate anions (MoO₄²⁻) can be prepared by dissolution of MoO₃ in aqueous alkaline solutions. This process originates many pure inorganic salts one of which is Na₂MoO₄, being a useful starting material in oxomolybdenum chemistry.

In the pure inorganic crystalline salts, the discrete molybdenum oxoanions MoO₄²⁻ are tetrahedral and can be transformed by condensation at lower pH values into an extremely wide and complex range of homo- and heteropolyanion structures with up to hundreds of metal atoms.^{[63][64]}

The second smaller anionic structure containing Mo₂O₇²⁻ units also features tetrahedral centres. Nevertheless in this unit the two tetrahedra are sharing a corner, *i.e.*, there is a single bridge established by an oxygen atom. The structures containing the larger molybdenum anions are generally, but not exclusively, 6-coordinated and have shared edges or vertices of each distorted MoO₆ octahedra. Structures of molybdenum anions bigger than Mo₈O₂₆⁴⁻ contain octahedral and tetrahedral molybdenum environments and may also be isolated in two isomeric forms, alpha and beta.^{[65][66]}

III.3.3. MoO₂Cl₂

MoO₂Cl₂ was first synthesized by Berzelius in 1826^[67] and in 1965 Colton and Tomkins published an alternative method for its preparation.^[68] According to these authors, passing a 1:1 mixture of dry oxygen and chlorine over Mo at 250-350 °C (Equation 2) forms a white volatile product which can be purified by sublimation, to obtain MoO₂Cl₂. The final product is a pale yellow solid, which is nowadays commercially available from several suppliers including Aldrich.



The molecular structure of gaseous MoO₂Cl₂ was determined by electron diffraction studies^{[69][70]} and consists of a distorted tetrahedral arrangement of the ligands (chloride and oxygen) around the molybdenum centre (Figure 18, *left*). In the solid state the structure MoO₂Cl₂ contains -Mo-(μ₂-O)-Mo- chains in two directions forming a layered structure where a network of alternating Mo^{VI} and oxygen atoms lie on the *ab* plane perpendicular to the long axis. Two Cl⁻ end-anions approach each metal atom perpendicular to the chains, above and below the Mo^{VI} atoms, thus completing its octahedral environment (Figure 18, *right*).^[71]

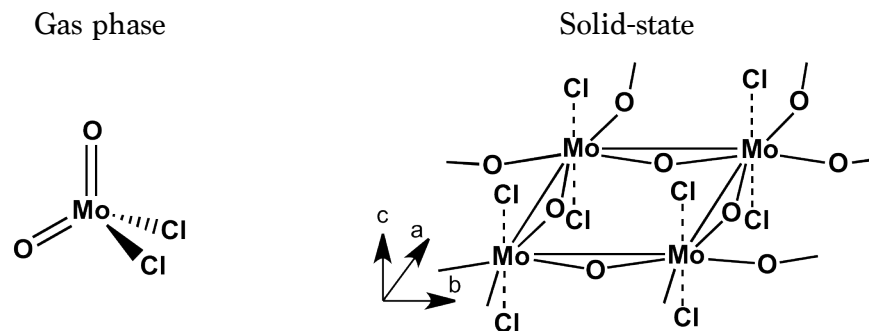


Figure 18. Representation of the gaseous and solid-state structures of MoO_2Cl_2 .

MoO_2Cl_2 can coordinate with a large array of ligands and/or solvents: molecules that will fill available coordinative positions around Mo^{VI} upon cleavage of the $-(\mu_2\text{-O})-$ linkages. This leads to hexacoordinated^[72] complexes of general formula $[\text{MoO}_2\text{Cl}_2\text{L}_n]$, where L is a mono- ($n = 2$) or bi-dentate ($n = 1$) Lewis base.

III.4. PREPARATION METHODS

A literature search on the synthetic pathways used to prepare oxomolybdenum(VI) HMs containing the *cis*- MoO_2^{2+} core coordinated to N,N' -chelate ligands revealed that the vast majority of the research groups only employ two approaches: reflux and hydrothermal synthesis. Nevertheless, the outcomes are strikingly distinct: while reflux approaches typically lead to the isolation of discrete complexes, hydrothermal synthesis promotes polymerization, producing highly insoluble 1D materials.

III.4.1. DISCRETE COMPLEXES

The vast majority of the complex-based (mostly dinuclear) structures described in section III.5 are products derived from tetrabutylammonium salts of $[\text{Mo}_8\text{O}_{26}]^{4-}$ and $[\text{Mo}_2\text{O}_7]^{2-}$. These precursors have been important starting materials because of their solubility in aprotic organic solvents. Syntheses were usually carried out by dissolution at ambient temperature, or reflux of one of the previously mentioned Mo^{VI} sources, and stirring for several hours. The resulting solutions were filtered and concentrated on a rotary evaporator. Afterwards, layers of other selected solvents were carefully added to the previous solution and several weeks later crystals were formed at the solvent's interface. This crystal growth method is known as solvent-liquid diffusion. The overall yields were always less than 30 %.

For mononuclear oxomolybdenum(VI) hybrid materials, such as the examples presented also in section III.5, the most common synthesis uses

[MoO₂Cl₂] as the starting material. It is also based in aprotic solvents and consists of a two step method.^[27] First, an *in situ* step reaction takes place typically via ligand addition and/or substitution. This step corresponds to the formation of MoO₂Cl₂(solv)₂ which, being a very electron-deficient complex, readily reacts with the Lewis base ligand to give more stable complexes (Figure 19).^[31]

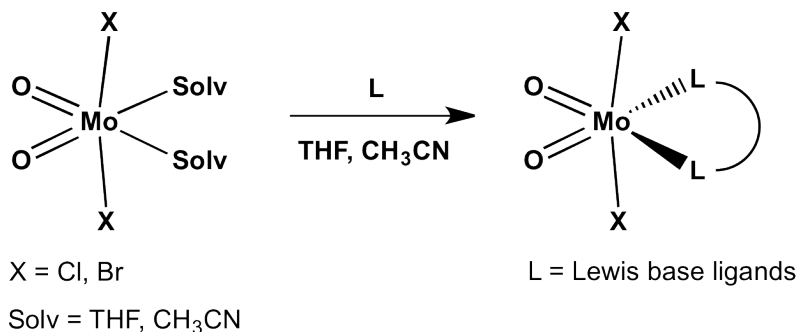


Figure 19. Schematic representation of the reaction of solvent-substituted complexes with Lewis base ligands.

The second step is the solvent substitution reaction in the [MoO₂Cl₂(solv)₂] complex, *i.e.*, the organic Lewis base ligand or ligands (if two) coordinate to the metal atom while the solvent leaves the coordination sphere. This step involves a donation to the metal centre of one or more of the ligand's electron pairs (Lewis bases).

For L = bidentate chelating *N,N'*-donor ligands the mononuclear products [MoO₂Cl₂L] are nearly quantitatively obtained at ambient temperature within a few minutes of reaction.^[73] These products display two important advantages: the two different ligand sets X and L can be easily varied in order to fine tune the coordination sphere of the Mo^{VI} centre, and the bidentate nitrogen donor ligands offer a great versatility in modifying the electron donor and acceptor properties of the ligands.^[31]

III.4.2. POLYMERS

For the preparation of polymeric oxomolybdenum(VI) HM coordinated to *N,N'*-chelating ligands (see Table 3 on section III.5.4) hydrothermal synthesis has proved to be the most well-suited method.

The hydrothermal method is typically carried out in the temperature range of 120 – 260 °C and under autogenous pressure of aqueous solutions containing the organonitrogen ligand and the molybdenum source, which can be MoO₃, Na₂MoO₄, (tBu₄N)₂Mo₆O₁₉ or (NH₄)₆Mo₇O₂₄.

The advantages of using hydrothermal synthesis are mainly focused on the quest for crystalline compounds: under autogenous pressure the water viscosity is reduced and the diffusion processes are favoured promoting crystal growth.^[74] In addition, many simple precursors such as organic compounds can be used as their solubility is improved under these conditions.^[75]

The disadvantages of the hydrothermal method are the yields that can be low, the mixtures of phases that sometimes might be obtained and which require mechanical separation. In addition small changes in one or more of the reaction parameters (time, temperature, pH value, stoichiometry) may influence the reaction outcome making the prediction of the reaction products very difficult.^[75]

III.5. OXOMOLYBDENUM(VI) with *N,N'*-ORGANIC LIGANDS: EXAMPLES

Previously in the literature search performed in section II.2 no restrictions were made on the organic ligand coordination or donor atom nature. The results were all about, at least, two octahedral *cis*-MoO₂²⁺ units bonded together though an oxido bridge.

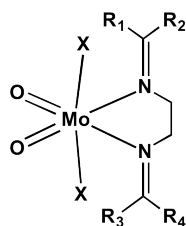
In this new section, attention is given to the dinuclear and polymeric structures especially coordinated to *N,N'*-chelating ligands. The restriction for two adjacent octahedral *cis*-MoO₂²⁺ units will be removed, allowing the introduction of a small handful of other examples such as octanuclear structures.

III.5.1. DISCRETE COMPLEXES

Monomeric hybrid compounds were the first structures reported in the literature with the *cis*-MoO₂²⁺ core. Complexes of the [MoO₂X₂L] family, with X = halide, R, OR, OSiR₃ and L = Lewis bases or donor solvents, have received great attention due to their interest as molydoenzyme models, oxo-transfer reagents or as catalysts for the epoxidation of olefins.^[32] The first characterization of an [MoO₂X₂L]-type complex was reported in 1966 (X = Br and L = bipy).^[76] Since then several other structures containing *N,N'*-chelating ligands were described, with most of the research being concentrated in the last 20 years. These complexes present distorted octahedral geometry,^[77] with the oxido ligands *cis* to each other in order to maximize the back donation into the empty *t_{2g}* set orbitals. The arrangement of the anionic X and neutral L ligands is most often *trans* and *cis*, as represented in Figure 19.^[78]

The most common examples of monomeric complexes of the [MoO₂X₂L]-type range from siloxyligated MoO₂²⁺ complexes, *i.e.* X = OSiR₃, to the dioxodichloromolybdenum complexes where X = Cl (Table 1). Over the years the groups of Gonçalves, Kühn and Romão have reported many of these complexes, mostly with halogen anions directly bonded to the metallic centre, and for which the *N,N'*-chelated molecules are *N,N'*-dibenzylidene-1,2-ethylenediamine (**1a-b**),^[79] ethyl(3-(2-pyridyl)pyrazol-1-yl)acetate (**2b**),^[80] 2-(3-pyrazole)pyridine (**2c**),^[81] 2,2'-bipyridine (**6a-d**),^{[82][83]} and 2,2'-bipyrimidine (**8a-d**).^{[83][84]}

Table 1. Monomeric complexes of the [MoO₂X₂L]-type coordinated to *N,N'*-chelating ligands.



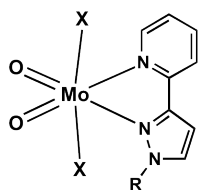
X = Cl

1a R₁=R₂=R₃=R₄= Ph ^[79]

1b R₁=R₃=H; R₂=R₄=Ph ^[79]

X = Br

1c R₁=R₂=R₃=R₄= Ph ^[79]



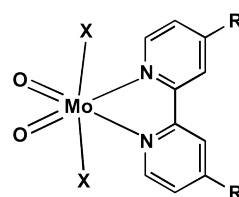
X = Cl

2a-b R= C₄H₉,
CH₂CO₂C₂H₅ ^[80]

2c R= H ^[81]

X = OSiPh₃

2d-e R=C₄H₉,
CH₂CO₂C₂H₅ ^[80]



X = Cl

3a-c R= CH₃, Br, C₆H₁₃ ^[83]

3d R= C₆H₁₃ ^[85]

3e R= *t*-Bu ^[86]

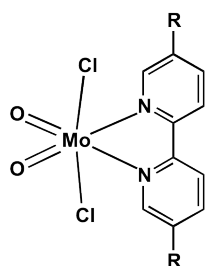
X = Br

3f R= *t*-Bu

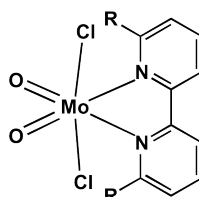
X = CH₃

3g R= C₆H₁₃ ^[85]

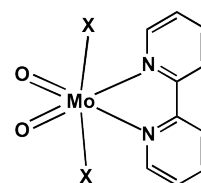
3h R= 4,4'-COOEt ^[84]



4a-e R = CH₃, Br, NH₂,
NO₂, CO₂Et ^[73]

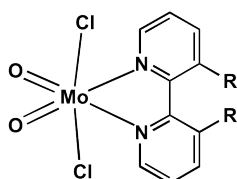


5a-d R = CH₃, Br, pyridyl,
Ph ^[73]

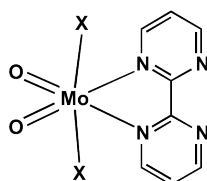


6a X = OSiR₃ ^[82]

6b-d X = Cl, Br, CH₃ ^[83]

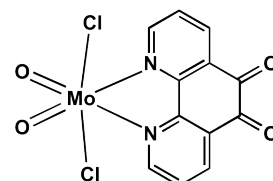


7a-b R = CH₃; Br ^[73]

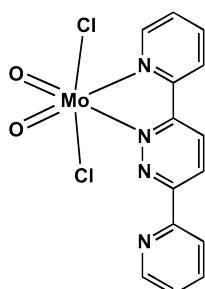


8a X = Br ^[84]

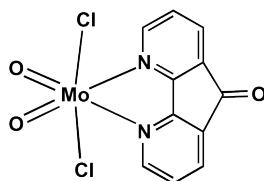
8b-d X = Cl, Br, CH₃ ^[83]



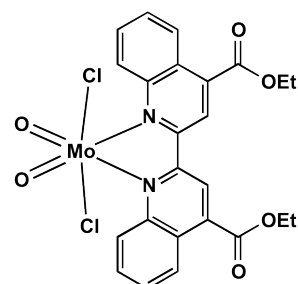
9 ^[87]



10 ^[87]



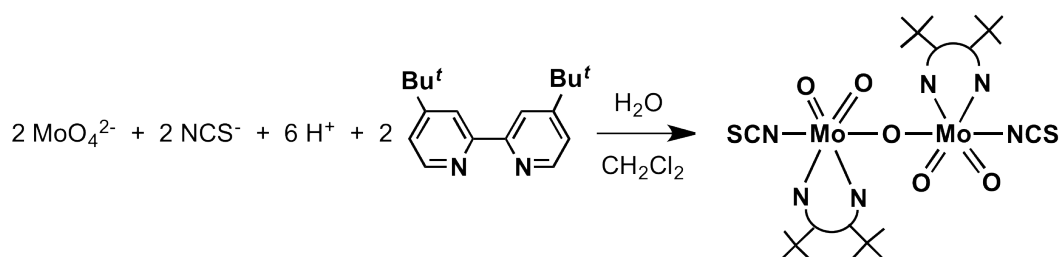
11 ^[87]



12 ^[87]

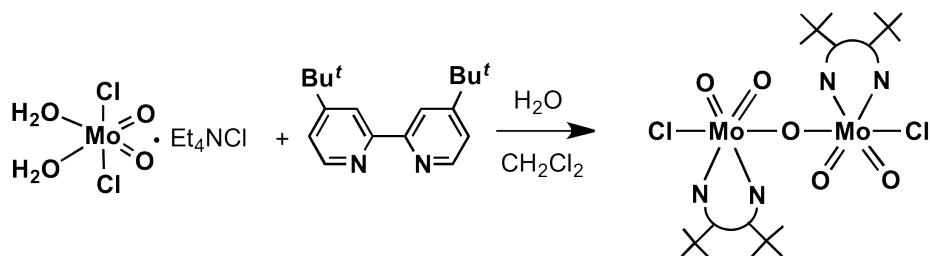
Almost all monomeric complexes depicted in Table 1 were commonly prepared by treatment of MoO_2Cl_2 with a donor solvent such as CH_3CN or THF followed by an *in situ* substitution reaction of the solvent by the N,N' -chelating ligand (Figure 19). Interested in studying the ligand impact on the catalytic performance^[83] and the complex stability^{[73][88]} the research groups of Gonçalves and Kühn concluded that bipyridines and pyrazolylpyridines appear to be optimal ligands for olefin epoxidation using *tert*-butylhydroperoxide (TBHP) as the mono-oxygen source. This occurs because they are resistant to oxidative degradation or exchange reactions under the catalytic conditions employed. Section III.6.1.2 summarizes the results of using some of these monomeric discrete complexes as catalysts for olefin epoxidation.

While a long list of monomeric structures with the cis-MoO_2^{2+} core and N,N' -chelating ligands has been reported (Table 1), the number falls dramatically when going from oligomers to polymers. Tables 2 and 3 gather the structures found based on binuclear (or higher discrete-base) and polymeric compounds. The search performed required the presence of a cis-MoO_2^{2+} core and one bidentate N,N' -chelating ligand coordinated to the metal centre. Arzoumanian reported the first dimeric structure being a thiocyanatomolybdenum(VI) dioxo- μ -oxo complex bearing a di-*t*-Bu-bipy ligand, $[\text{Mo}_2\text{O}_5(\text{NCS})_2(\text{di-}t\text{-Bu-bipy})_2]$ (**15**), as shown in Table 2. The dimer was obtained initially as a secondary product. However, in view of its potential properties as an oxygen atom transfer agent (*i.e.*, catalyst) the authors optimized its synthesis, involving addition of di-*t*-Bu-bipy dissolved in dichloromethane to an aqueous solution of molybdate and thiocyanate^[89] (see image below, route 1).

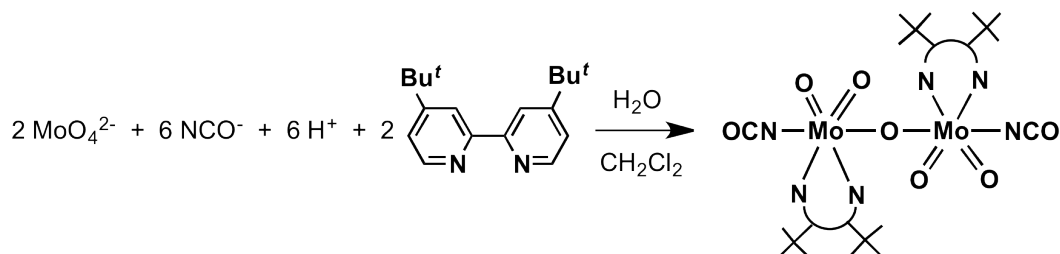


Route 1

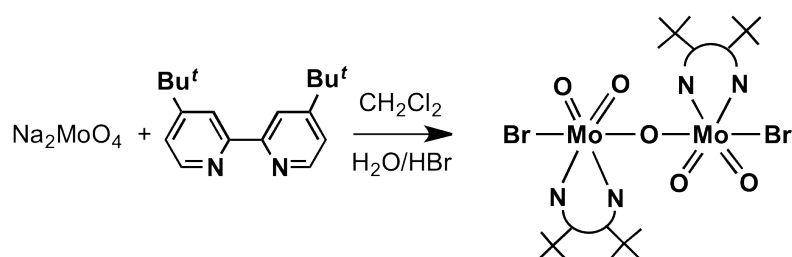
The product was obtained in 76 % yield as a light yellow crystalline solid that exhibited in the IR spectrum the characteristic bands for both terminal and bridging oxides, as well as the thiocyanato and the bipyridyl ligands.^[89] No studies were performed to identify the potential of the dimer as a catalyst. Years later the same author published three new routes to isolate, with moderate yields, different dimeric structures: two similar to **19** coordinated to both Cl or to Br atoms (no crystals were, however, isolated), and another two structures with cyanide and thiocyanide ligands^[90] such as those shown in Table 2 with the numbers **20** and **21**.



Route 2



Route 3

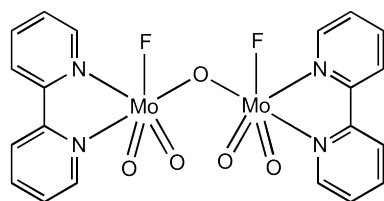


Route 4

By using route 1 proposed by Arzoumanian, Gómez prepared a dioxomolybdenum(VI) dimeric complex containing a thiocyanide ligand and a non-labile bidentate oxazolinyl-pyridine ligand, compound **18**. The latter was used to explore the nature of the asymmetric catalytic species in the epoxidation of selected olefins.^[91]

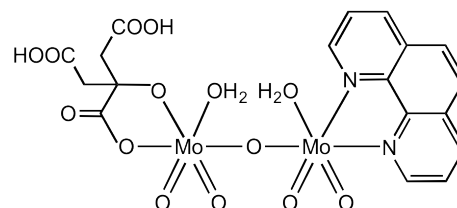
Cumbersome were the chemical syntheses performed by Gonçalves and co-workers and Zubieta and co-workers. The latter group prepared by hydrothermal synthesis (70 °C and 48 h) the dimer $[\text{Mo}_2\text{O}_4\text{F}_2(\text{bipy})]$ (compound **13**, Table 2). This product was directly obtained through the use of the reactants of MoO_3 , 2,2'-bipyridine, H_2O and HF .^[92] The research group of Gonçalves repeatedly obtained crystals of identical dimeric structures bearing the two chloro ligands. The first dimeric $[\text{Mo}_2\text{O}_4\text{Cl}_2(\text{pzpy})]$ complex **16a** was isolated from slow diffusion of diethyl ether into an acetonitrile solution containing $[\text{MoO}_2\text{Cl}_2(\text{pzpy})]$. The same structure was repeatedly obtained, depending on the re-crystallisation solvents, as a solvent-free or solvate of acetonitrile and THF.^[81] The second dimer isolated and characterised was one previously reported by Arzoumanian, $[\text{Mo}_2\text{O}_5\text{Cl}_2(\text{di-}t\text{-Bu-bipy})]$, but for which no structure was described. Gonçalves and co-workers obtained this dimeric product, $[\text{Mo}_2\text{O}_5\text{Cl}_2(\text{di-}t\text{-Bu-bipy})_2] \cdot 0.2\text{H}_2\text{O}$, by oxidation of the dicarbonyl complex $[\text{Mo}(\eta^3\text{-C}_3\text{H}_5)\text{Cl}(\text{CO})_2(\text{di-}t\text{-Bu-bipy})]$ complex with 70 % aqueous TBHP (as well as decane solution).

Table 2. Oligomeric complexes of the $[\text{MoO}_2\text{X}_2\text{L}]$ -type coordinated to N,N' -chelating ligands.



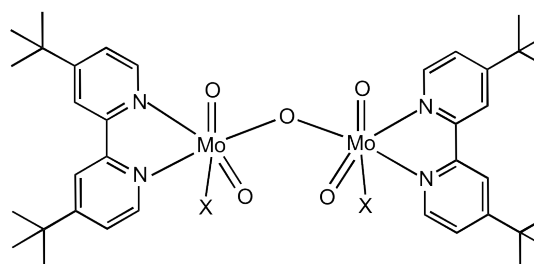
refcode: DUQZEV ^[92]

13



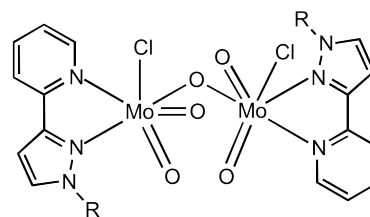
refcode: JOCGUE ^[93]

14



refcode: HOWVAQ X = SCN ^[89]

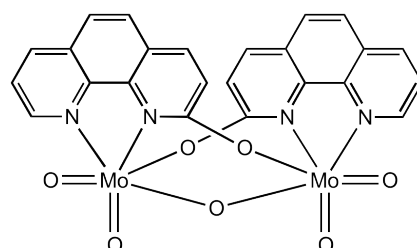
15



refcode: ZASGUX R = H ^[81]

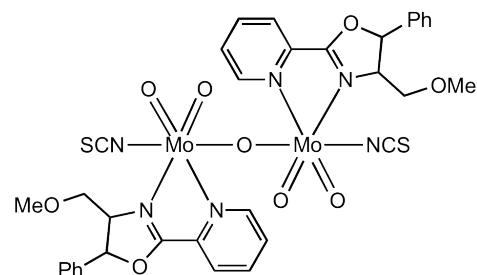
16a

R = CH₂CO₂Et ^[94] **16b**



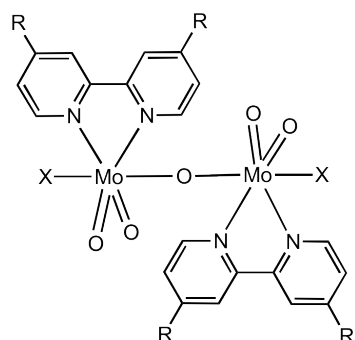
refcode: OLEPUQ ^[95]

17



refcode: OGAMAL ^[91]

18



refcode: IDECEB R = ^tBu; X = Cl; ^[96]

19

R = H; X = Cl; ^[97]

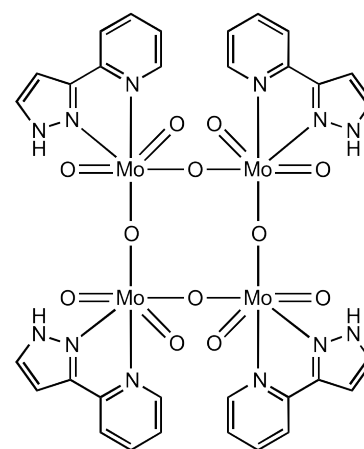
19a

refcode: GELVOJ R = ^tBu; X = NCO ^[90]

20

refcode: GELVUP R = CH₂Ph; X = NCS ^[90]

21



refcode: HUCGIW ^{[48], [49]}

22

While carrying out their research on using molybdenum tetracarbonyl complexes of the type $cis\text{-[Mo(CO)}_4\text{L]}$ as catalyst precursors for olefin epoxidation using TBHP as oxidant, Gonçalves and co-workers found that the nature of the bidentate ligand L influences not only the species formed by oxidative decarbonylation but also their catalytic performance.^{[98][97][49]} As an example, when using L = 2,2'-bipyridine, the one-dimensional polymer $[\text{MoO}_3(\text{bipy})]_n$ was obtained,^[98] and if L = 4,4'-di-*tert*-butyl-2,2'-bipyridine, the octameric complex $[\text{Mo}_8\text{O}_{24}(\text{di-}t\text{-Bu-bipy})_4]$ was isolated instead.^[98] The latter solid had a solid state structure comprising two octanuclear complexes containing a central cubane-type $\text{Mo}_4(\mu_3\text{-O})_4$ core and four peripheral $[\text{MoO}_2(\text{di-}t\text{-Bu-bipy})]^{2+}$ units capping the long edge of the Mo_4 tetrahedron of the central cubane (Figure 20). Both molybdenum oxide/bipyridine compounds give stable, selective and active catalytic systems for the epoxidation of cyclooctene with TBHP (in decane) as oxidant (see Table 5). Under the reaction conditions used (1,2-dichloroethane as co-solvent), the octanuclear complex is completely soluble in the reaction medium and is an active homogeneous catalyst, while $[\text{MoO}_3(\text{bipy})]_n$ was mostly insoluble and the reaction has both heterogeneous and homogeneous contributions.

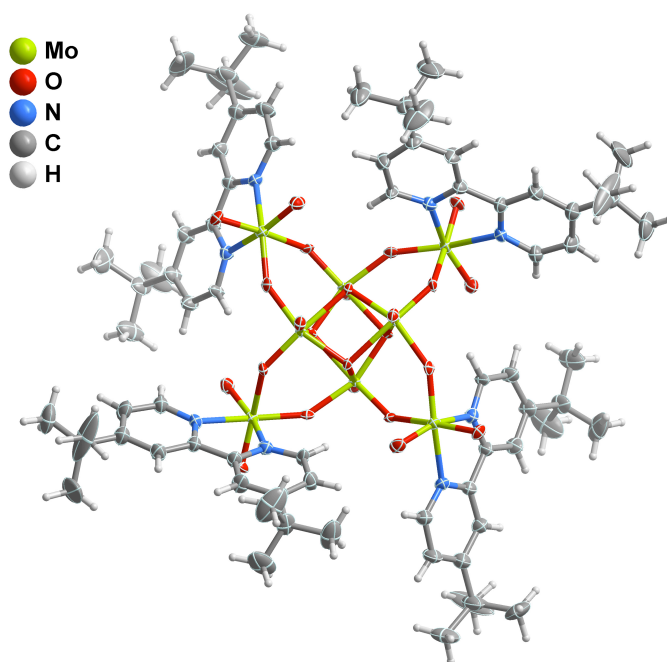


Figure 20. Schematic representation of the octameric $[\text{Mo}_8\text{O}_{24}(\text{di-}t\text{-Bu-bipy})_4]$ molecular unit. Image reproduced from reference ^[98].

III.5.2. POLYMERS

A search in the literature using ISI Web of Knowledge and the Cambridge Structural Database reveals only a handful of oxide-based molybdenum polymeric organic-inorganic hybrid structures containing organic N,N' -ligands bonded to a molybdenum oxide skeleton. Table 3 summarizes the most important features of all compounds.

Table 3: Selected structural information for the 1D structures of molybdenum organic-inorganic hybrid structures containing N,N' -organic ligands.

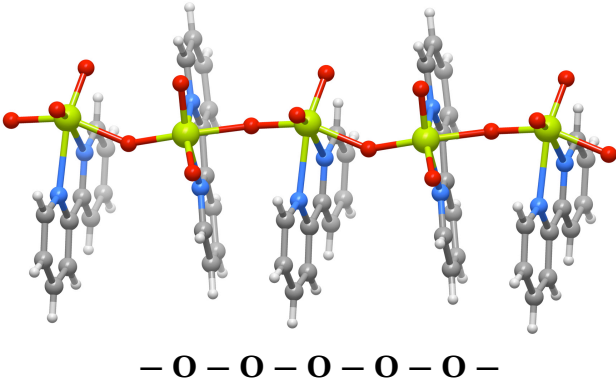
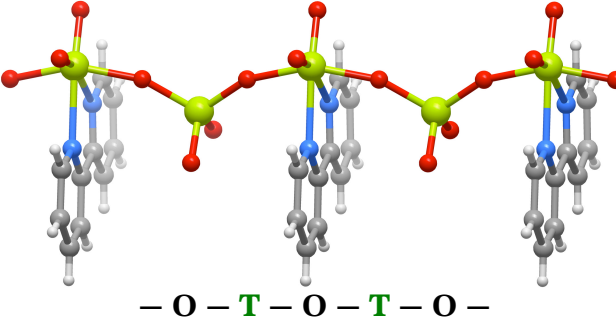
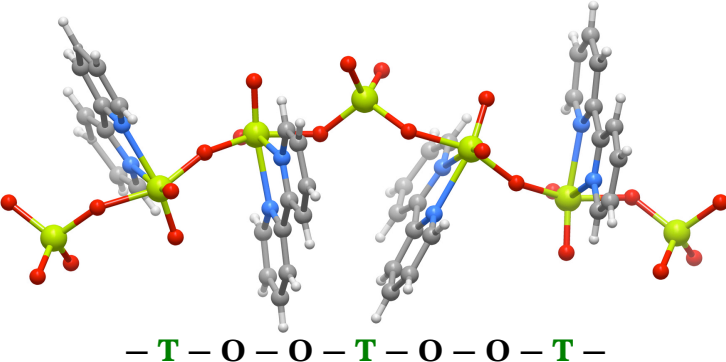
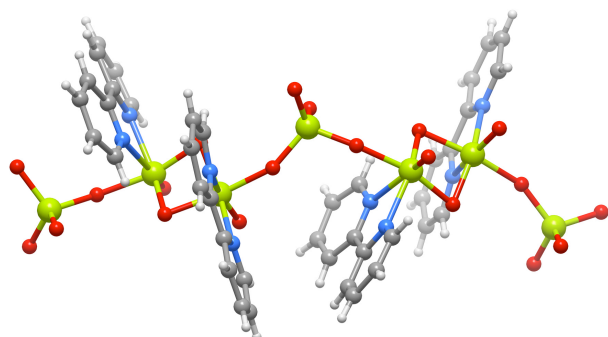
Polymeric structures	Ref.	Reaction conditions T/°C and t/days
$[\text{MoO}_3(\text{bipy})]_n$ 23 <i>refcode: VAFYOQ</i>	[59]	160 °C, 5 days MoO_3 bipy H_2O <i>or</i> 160 °C, 2 days MoO_3 bipy H_2O $\text{Na}_2\text{MoO}_4 \cdot 2\text{H}_2\text{O}$ $\text{FeCl}_2 \cdot 4\text{H}_2\text{O}$
		
$[\text{Mo}_2\text{O}_6(\text{bipy})]_n$ 24 <i>refcode: VAGDEM</i>	[59]	200 °C, 4 days MoO_3 bipy H_2O $\text{Na}_2\text{MoO}_4 \cdot 2\text{H}_2\text{O}$ $\text{MnCl}_2 \cdot 4\text{H}_2\text{O}$
		
$[\text{Mo}_3\text{O}_9(\text{bipy})_2]_n$ 25 <i>refcode: VAGDIQ</i>	[59]	160 °C, 5 d MoO_3 bipy H_2O <i>or</i> 160 °C, 5.7 days MoO_3 bipy H_2O $\text{MnCl}_2 \cdot 4\text{H}_2\text{O}$
		

Table 3 continuation

$[\text{Mo}_3\text{O}_8(\text{bipy})_2]_n$ **26**

refcode: HUXMAO

[99]



200 °C, 8 days

bipy

H₂O

Na₂MoO₄·2H₂O

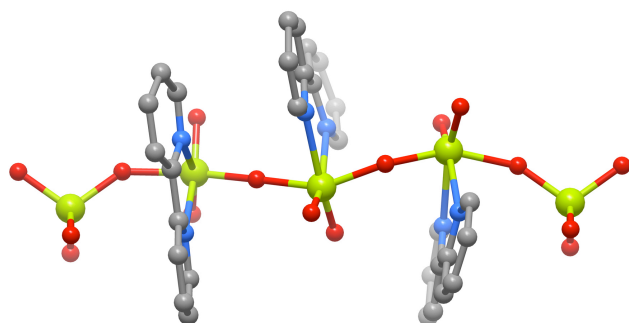
H₃PO₄

H₂C₂O₄·2H₂O

$[\text{Mo}_4\text{O}_{12}(\text{bipy})_3]_n$ **27**

refcode: DEYJAT

[100]



200 °C, 6 days

H₂O

bipy *N,N'*-dioxide

(NH₄)₆Mo₇O₂₄·4H₂O

MnCl₂·4H₂O

$[\text{Mo}_3\text{O}_9(\text{phen})_2]_n$ **28**

refcode: MAKYOM

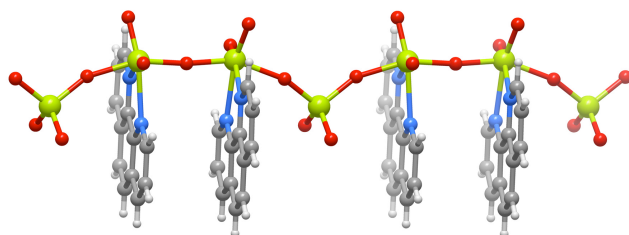
refcode: MAKYOM01

refcode: MAKYOM02

[101]

[102]

[103]



160 °C, 3 days

H₂O

phen

(^tBu₄N)₂Mo₆O₁₉

and

180 °C, 3 days

H₂O

phen

(NH₄)₆Mo₇O₂₄·4H₂O

pH control to 4

and

for ref^[103]

no article access

Legend:

T : {MoO₄} tetrahedron

O : {MoO₄N₂} octahedron

(O—O) : two edge-sharing {MoO₄N₂} octahedra

Since the mid-60's, polymeric structures based on infinite chains of oxomolybdenum(VI) polyhedra are known to be characteristic of dimolybdate $\{[\text{Mo}_2\text{O}_7]^{2-}\}$, trimolybdate $[\text{Mo}_3\text{O}_{10}]^{2-}$ and related tetramolybdate systems: for example, $[\text{H}_3\text{NCH}_2\text{CH}_2\text{NH}_3][\text{Mo}_3\text{O}_{10}]$,^[104] $[\text{H}_3\text{N}(\text{CH}_2)_6\text{NH}_3][\text{Mo}_3\text{O}_{10}]$,^[105] $[\text{Na}(\text{NH}_4)]-[\text{Mo}_3\text{O}_{10}]$,^[105] $\text{K}_2[\text{Mo}_3\text{O}_{10}]$,^[106] and $\text{Na}_2[\text{Mo}_2\text{O}_7]$.^[107] Although all polymers share in common the 1D backbone, there are marked differences in their polyhedral connectivities promoted by the templating effects of the cations. A common thread in the structural chemistry of these species is the occurrence of edge-sharing between adjacent polyhedra as part of their structural motif.^[59]

Examining the polymers in Table 3, they share the common 1D backbone to the previous salts, however, all (except polymer **26**) present structural differences between adjacent polyhedra, *i.e.*, they mostly establish corner-sharing linkages. Zubieta, the author of the first oxide based molybdenum organic-inorganic hybrid polymer, states that this can be attributed to the ligand inclusion which passivates the molybdenum oxide coordination sphere by blocking further Mo-oxo bond formation and, apparently, limits the aggregation process to mostly corner-sharing linkages.^[59] This suggests that there is a ligand control of the stepwise growth of the polymers.

Only polymeric structures comprising 2,2'-bipyridine (bipy) and 1,10-phenanthroline (phen) are found in the literature, of which five are polymers with a molybdenum backbone coordinated to bipy. Only the polymer $[\text{MoO}_3(\text{bipy})]_n$ (**23**) consists of a chain built up from only $\{\text{MoO}_4\text{N}_2\}$ corner-sharing octahedral (**O**) motifs: $-\text{O}-\text{O}-$. The remaining polymers are constructed from alternating sequences of one, two or three $\{\text{MoO}_4\text{N}_2\}$ corner-sharing octahedra (**O**) with one $\{\text{MoO}_4\}$ tetrahedron (**T**): $[\text{Mo}_2\text{O}_6(\text{bipy})]_n$ (**24**) showing a $-\text{O}-\text{T}-\text{O}-\text{T}-\text{O}-$ distribution; $[\text{Mo}_3\text{O}_9(\text{bipy})_2]_n$ (**25**) with $-\text{T}-\text{O}-\text{O}-\text{T}-\text{O}-\text{O}-\text{T}-$, and $[\text{Mo}_4\text{O}_{14}(\text{bipy})_3]_n$ (**27**) having $-\text{T}-\text{O}-\text{O}-\text{O}-\text{T}-$ distribution. Another example of a rare polymer containing bipy is $[\text{Mo}_3\text{O}_8(\text{bipy})_2]_n$ (**26**). This compound has a quite distinct 1D backbone because it is composed of binuclear units of edge-sharing $\{\text{MoO}_4\text{N}_2\}$ octahedra linked by $\{\text{MoO}_4\}$ tetrahedra through corner-sharing, *i.e.*, $-\text{T}-(\text{O}-\text{O})-\text{T}-(\text{O}-\text{O})-\text{T}-$. According to the authors this difference can be attributed to the mixed-valence character of the polymer.^[99] Mixed-valence hybrid molybdenum oxides remain highly unexplored in the literature.

Upon inspection of the reaction conditions (hydrothermal) used for the preparation of the polymeric structures it seems that there is no general trend between the final product and the reaction conditions (temperature, duration, or choice of reactants). It is thus clear that the product obtained from the hydrothermal reactions is critically dependent on specific reaction conditions employed for each reaction.

Only two oxide-based molybdenum 1D polymers coordinated to phen were found, namely those published by the groups of Zhou, $[\text{Mo}_3\text{O}_9(\text{phen})_2]_n$,^[101] (**28**) and Cheng, $[\text{Mo}_3\text{O}_9(\text{phen})_2]_n$,^[102] (same structure but with different authors and

refcodes in the Cambridge Structural Database). Zhou was nevertheless the first to describe $[\text{Mo}_3\text{O}_9(\text{phen})_2]_n$. It was described as a 1D chain constructed of repeating pairs of distorted $\{\text{MoO}_4\text{N}_2\}$ octahedra sharing a corner with one $\{\text{MoO}_4\}$ tetrahedron.^[101] The phen rings coordinated to Mo^{VI} are almost parallel to each other owing to π - π interactions.^[101] Zhou further explored the chemical system by using electrospray ionization mass spectra to the solution from which the polymer was collected, immediately after the conclusion of the hydrothermal reaction. The results showed the presence of HMoO_4^- as dominating species in solution, together with other minor amounts of unassigned species. The authors suggested that the nitrogen atoms of the ligand phen attack, under hydrothermal conditions, the structure of the $[\text{Mo}_6\text{O}_{19}]^{2-}$ cage giving mainly monomeric anions, which then coordinate to the nitrogen atoms resulting in the 1D framework.^[101] Four years later Cheng described the same crystallographic structure but using a more complex procedure.

An interesting set of examples, also relying on $\{\text{MoO}_4\text{N}_2\}$ repeating octahedral units, used to build one-dimensional molybdenum oxide polymers were reported by the group of Domasevitch. This group reported the $[\text{Mo}_4\text{O}_{12}(\text{tr}_2\text{eth})_2]$, $[\text{Mo}_2\text{O}_6(\text{tr}_2\text{pr})]$, $[\text{Mo}_2\text{O}_6(\text{tr}_2\text{cy})_2]$, $[\text{Mo}_2\text{O}_6(\text{tr}_2\text{ad})] \cdot 6\text{H}_2\text{O}$, $[\text{Mo}_2\text{O}_6(4,9\text{-tr}_2\text{dia})] \cdot 0.5\text{H}_2\text{O}$, and $[\text{MoO}_3(\text{trtz})]$ hybrid materials (for representations of the ligand structures and abbreviations, see Figure 21), for which the 3D are structures entirely supported by covalent links between the Mo^{VI} oxide subtopologies and the neutral organic components.^[108] The 1D backbone in these materials is generated in a similar fashion to that described previously, *i.e.*, by combinations of oxido organic bridges between the Mo^{VI} ions bearing two *cis*-oriented $\text{Mo}=\text{O}$ bonds: the N^1, N^2 -bidentate triazole ligands form a bridge between adjacent Mo^{VI} ions along the oxo-linked chain $(-\text{MoO}_2-\text{O}-)_n$ through two principal binding modes defined by the author as: Type A when the coordination organic motifs were observed in a 4_1 helix, and Type B when a double triazole bridge was established. Within the first type complexes were $[\text{Mo}_4\text{O}_{12}(\text{tr}_2\text{eth})_2]$, $[\text{Mo}_2\text{O}_6(\text{tr}_2\text{cy})_2]$ and $[\text{MoO}_3(\text{trtz})]$. The Type B were $[\text{Mo}_2\text{O}_6(\text{tr}_2\text{pr})]$, $[\text{Mo}_2\text{O}_6(\text{tr}_2\text{ad})] \cdot 6\text{H}_2\text{O}$ and $[\text{Mo}_2\text{O}_6(4,9\text{-tr}_2\text{dia})] \cdot 0.5\text{H}_2\text{O}$, (see Figure 22).

The results by Domasevitch raise new prospects of how to increase the dimensionality of the structures listed in Table 3.

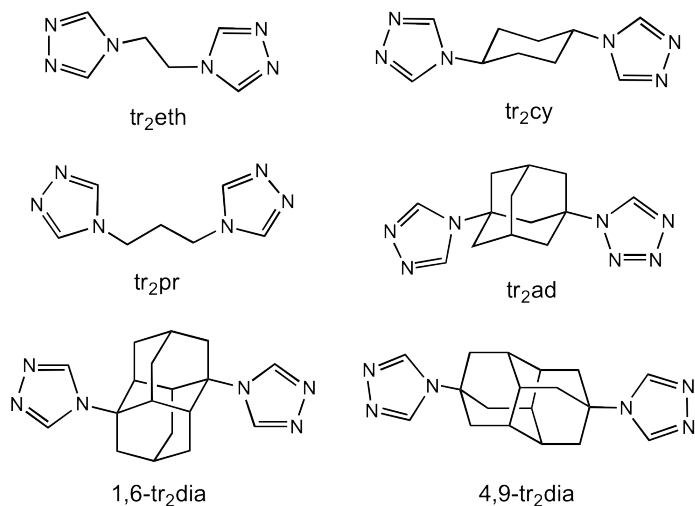


Figure 21. Ligand structure and abbreviations for the organic components used to coordinate to Mo^{VI} complexes prepared by Domasevitch. Image reproduced from reference.^[108]

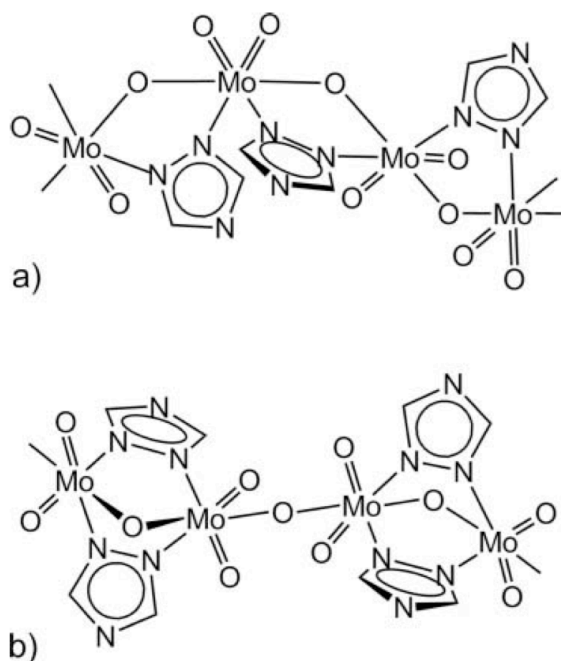


Figure 22. Coordination motifs a) Type A and b) Type B observed in Mo/triazole polymers prepared by Domasevitch and bearing a $\{\text{MoO}_4\text{N}_2\}$ repeating octahedral unit. Images reproduced from reference.^[108]

III.6. USE of OXOMOLYBDENUM(VI) HYBRID MATERIALS as CATALYSTS

The chemistry of Mo^{VI} is prominent in both the industrial and biological areas. In industry, Mo^{VI} is used as a catalyst for a number of important processes such as oxidation, ammoxidation, metathesis, and

hydrocarbon dehydrogenation.^[109] Because the chemistry of Mo^{VI} is largely dominated by complexes having the *cis*- MoO_2^{2+} core, very significant research efforts both by industry and academia have been made to find efficient new catalysts within this structural family.

For monomeric $[\text{MoO}_2\text{X}_m\text{L}_n]$ -type complexes (X = mono/dianionic ligand, L = neutral ligand), and the related cationic derivatives $[\text{MoO}_2\text{X}_m\text{L}_n]^+[\text{Y}]^-$, it has been shown that they are active catalysts or catalyst precursors for homogenous epoxidation of nonfunctionalized olefins usually employing *tert*-butylhydroperoxide (TBHP) as the mono-oxygen. The same behaviour is usually observed for binuclear species of the type $[(\text{MoO}_2\text{X}_m\text{L}_n)_2\text{O}]$ which can be considered a special case of the monomeric species $[\text{MoO}_2\text{X}_m\text{L}_n]$ with $\text{X} = [\text{MoO}_3\text{X}_m\text{L}_n]^-$.^{[110][111][112][113][114]} The motivation to study these discrete homogeneous catalysts stems from the fact that they are well-defined, single site catalysts, which usually favour high activities and selectivities. Furthermore, these homogeneous molecular catalysts are amenable to chemical modification and to detailed mechanistic studies.

III.6.1. OLEFIN EPOXIDATION

An olefin is any unsaturated hydrocarbon containing one or more pairs of adjacent carbon atoms linked by a double bond. Olefins are usually classified as cyclic or acyclic (aliphatic) organic compounds depending on if the double bond location is within a cyclic (closed-ring) or open-chain of the organic group. Depending on the number of double bonds per molecule, they may be defined as *mono*-, *di*-, *tri*-olefins, etc.

The great importance of olefin epoxidation stems from the reactivity of the epoxide ring product which changes the initial olefin into a key substrate for a multitude of other intermediate and/or final products. As shown in Figure 23, this highly reactive, versatile chemical is, or was, a product/precursor of, at least, one material with which we interact on a daily bases. The products of which olefin epoxides are precursors include vicinal diols, also called glycols. A striking example is ethylene glycol that is the common ingredient of antifreeze products. Propane-1,2-diol is used in food and medicine industry. Epoxide compounds also have a wide range of direct applications like components for inks and paints, resins and adhesives.

In general, epoxides can be prepared by the reaction of olefins with hydrogen peroxide or alkylhydroperoxides, catalyzed by transition metal complexes.^{[115][116]} Examples are the dioxomolybdenum(VI) complexes presented in the previous section III.5 and which are generally formulated as $[\text{MoO}_2\text{X}_2]$, $[\text{MoO}_2\text{X}_m\text{L}_n]$ -type or $[\text{MoO}_2\text{X}_m\text{L}_n]^+[\text{Y}]^-$. The interest in these complexes arose in the late 1960's when ARCO and Halcon were granted patents on olefin epoxidation catalyzed by Mo^{VI} compounds in the homogeneous phase.^{[117][118]}

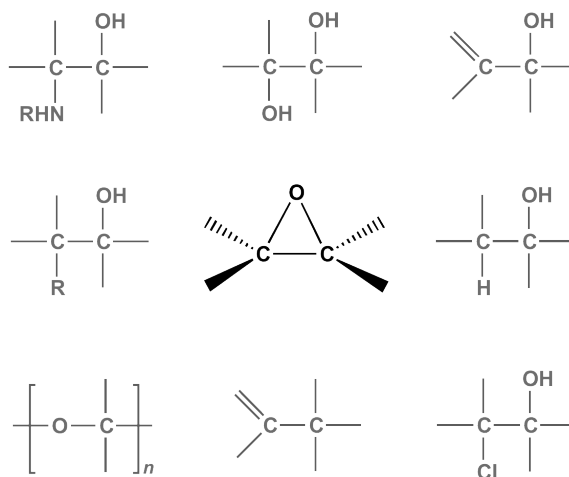


Figure 23. Examples of chemical fragments which can be obtained from a highly reactive epoxide organic core.

III.6.1.1. SUBSTRATES and PRODUCTS

Three examples of olefin substrates that are frequently used to test pre-catalysts or catalysts for olefin epoxidation are: DL-limonene (Lim), cyclooctene (Cy8) and methyl oleate (Ole) (Figure 24).

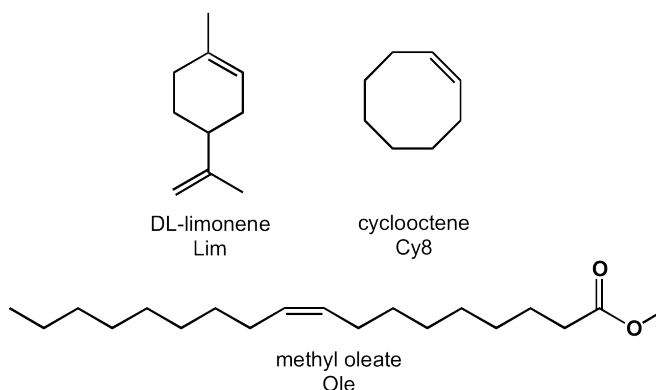


Figure 24. Epoxidation substrate models often used for olefin epoxidation catalyst tests.

DL-LIMONENE

DL-Limonene (present in citrus oil) is a colourless hydrocarbon liquid classified as a cyclic terpene, and is one of the most common naturally occurring monoterpenes. Because it is a chiral molecule, racemic mixtures of both D-limonene ((+)-limonene) and L-limonene ((-)-limonene) isomers exist and are known as dipentene. As represented in Figure 25, the epoxidation of DL-limonene (Lim) gives 1,2-epoxy-*p*-menth-8-ene (LimOx) which is an epoxide monomer with applications that include metal coatings, varnishes, printing inks, and synthesis of biodegradable polycarbonates by copolymerization with CO₂.^[119]

Possible by-products obtained from the epoxidation reaction of DL-limonene are 1,2:8,9-diepoxy-*p*-menthane (LimDiOx) and 1-methyl-4-(1-methylethenyl)-1,2-cyclohexanediol (LimDiol).

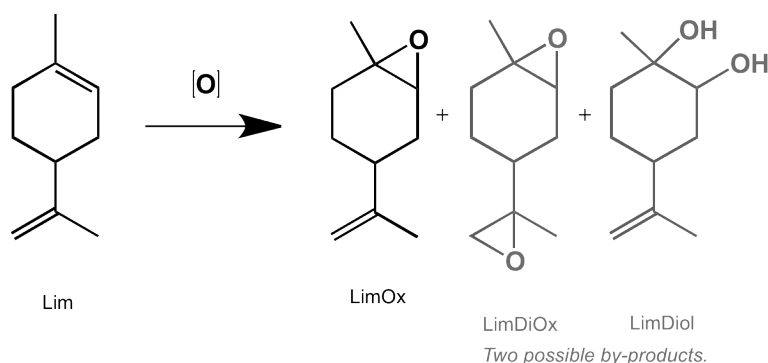


Figure 25. DL-limonene epoxidation products and possible by-products.

CYCLOOCTENE

Cyclooctene is a cycloalkene with an eight membered ring. It is the smallest cycloalkene and it can exist as either the *cis*- or *trans*-isomer. The *cis*-isomer (Cy8) is the more common.

As represented in Figure 26 the *cis*-isomer of cyclooctene is a substrate model notoriously known for high selectivity towards the epoxide and, possibly, low amounts of radical by-products. The reason for this behaviour is that allylic functionalization in *cis*-cyclooctene is more difficult than for other cycloalkenes because of the almost orthogonal allylic C-H bonds. Therefore, if radicals are present they preferentially form the epoxide (via an addition-elimination mechanism) than allylic by-products.^[120]

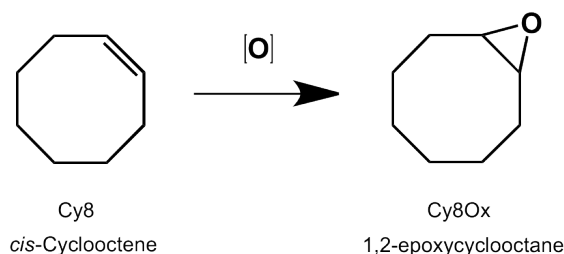


Figure 26. Cyclooctene epoxidation product.

METHYL OLEATE

Methyl oleate (Ole) is a mono-unsaturated fatty acid methyl ester present in methyl oleate soybean oil, which is an abundant natural material. The interest in the reactions of this material stems from the cost-effectiveness of

its derivatives.^[121] The most important reaction of Ole is the epoxidation reaction in which Ole produces methyl 9,10-epoxystearate (OleOx), Figure 27. The OleOx product on the other hand is a key precursor used to prepare several compounds of industrial interest. For example, OleOx is used as i) plasticizer and stabilizer for polyvinyl (PVC) production and ii) as intermediate in the production of biodegradable lubricants.^{[119][122][123][124]}

At the industrial scale epoxidation of unsaturated plant oils is carried out by the Prileshajev reaction using either preformed or in situ generated short chain peroxyacids (e.g., peracetic acid), which react with the unsaturated fatty acid C=C double bond to give the corresponding epoxide.^[119] Some drawbacks of this process include the wide range of byproducts formed (which result in more demanding separation/purification steps and enhanced formation of waste products), equipment corrosion hazards (presence of strong acid in an oxidative environment), and the need for neutralization processes downstream. A potentially interesting alternative that may render the epoxidation of vegetable oils more selective is the use of catalysts based on high-valent transition metals such as molybdenum(VI)^{[124][125][126]}

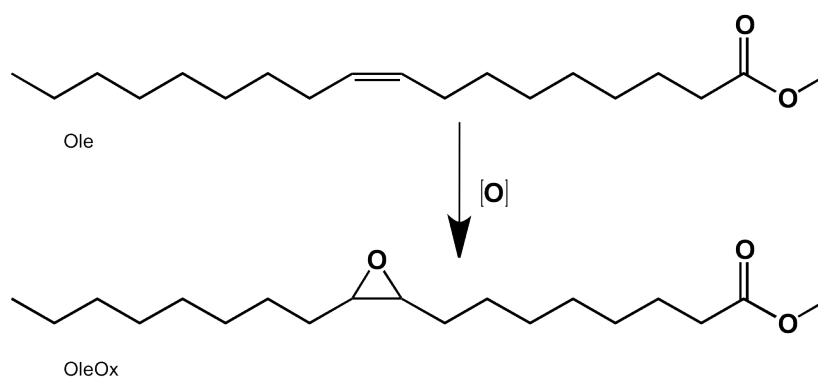


Figure 27. Methyl oleate epoxidation product.

III.6.1.2. LITERATURE RESULTS

A search in the literature revealed that in recent years a good number of oxomolybdenum(VI) complexes bearing the *cis*-MoO₂²⁺ core have been studied as homogeneous catalysts for the reaction of olefins with TBHP. Selected data using Lim and Cy8 are summarized in Tables 4 and 5.

Table 4. Literature data for the reaction of Lim with TBHP in the presence of discrete dioxomolybdenum(VI) complexes.^a

Complex type and substituent	LimOx yield %	Time h	# Fig	Ref.
[MoO ₂ X ₂ L ₂] with X = Cl				
Dimethylformamide	39	—	—	[127]
{OP(CH ₂ CH ₃)(Ph) ₂ }	74	—	—	[128]
L = {PhCHNCH ₂ CH ₂ NCHPh};	15 – 20	—	1b	[79]
L = 2-(1-butyl-3-pyrazolyl)pyridine	95–100	—	2b	[80]
L = bidentate salen ligand	65 ^b	—	—	[129]
[MoO ₂ X ₂ L ₂] with X = CH ₃				
L = N,N'-p-tolyl-2,3-dimethyl-1,4-diazabutadiene	47	4	—	[130]
[MoO ₂ L]				
L = tetradentate salen ligand	50 ^b	—	—	[129]
L = tetradentate oxazoline ligand	59 ^b	—	—	[131]
[CpMo(CO)nL]				
n = 2 and L = η ³ -C ₃ H ₅	70	—	—	[132]
n = 3 and L = Cl	21	6	—	[133]
[Mo ₂ O ₄ (μ ₂ -O)X ₂ (L) ₄] with X= Cl				
L = pyrazole	59 ^b	6	—	[113]

^a Reaction conditions (unless otherwise specified) are 55 °C, 24 h reaction and no co-solvent.

^b Solvent used: dichloroethane

According to Table 4, the best catalytic performance of a complex bearing a *cis*-MoO₂²⁺ core was observed for a [MoO₂X₂L₂]-type complex with L = 2-(1-butyl-3-pyrazolyl)pyridine. The catalytic reaction gave a LimOx yield of approximately 100 % at 24 h reaction time.

Table 5. Literature data for the reaction of Cy8 with TBHP in the presence of discrete dioxodichloromolybdenum(VI) complexes.^a

Complex type and substituent	Cy8Ox yield %	Time h	# Fig.	Ref.
[MoO ₂ Cl ₂ L ₂]				
L = 2-(1-butyl-3-pyrazolyl)pyridine	93	4		[80]
L = ethyl[3-(2-pyridyl)-1-pyrazolyl]acetate)	92	4		[80]
L = di- <i>t</i> -Bu-bipy	55	4	6e	[86]
L = 1,10-phenanthroline-5,6-dione	50	4	8	[87]
L = 4,5-diazafluorene-9-one	~98	4	10	[87]
L = 2,2'-biquinoline-4,4'-dicarboxylic acid diethyl ester	80	4	11	[87]
L = 3,6'-bis-2-pyridyl-pyridazine	~98	4	12	[87]
L = 4,4'-di-ethoxycarbonyl-2,2'-bipyridine	100	4	6h	[87]
L = bidentate salen ligand	98	24		[129]
L = <i>p</i> -tolyl(CH ₃ DAB) ^b	100	4		[130]
L = bidentate salen ligand	98	-		[129]

^a Reaction conditions (unless otherwise specified) are 55 °C, at 24 h with no co-solvent

^b *p*-tolyl(CH₃DAB) = *N,N'*-*p*-tolyl-2,3-dimethyl-1,4-diazabutadiene

^c Co-solvent used: dry dichloroethane

The motivation to prepare this large diversity of [MoO₂X₂L]₂-type complexes with different X = Cl and/or L = *N,N'*-chelating ligand is based on the fact that solubility of the complex and the Lewis acidity of the metal centre can be tuned via chemical modification. Through all approaches performed up to date, researchers have concluded that:

- the catalytic activity of the [MoO₂Cl₂L₂]₂ complexes in olefin epoxidation with TBHP as oxidizing agent is strongly influenced by the nature of the ligand L and its steric demand. As an example, Kühn and co-workers compared a series of [MoO₂Cl₂(bipy)₂]₂ complexes with bipyridine containing different substituent R groups (such as -CH₃, -Br and -COOEt) in the same positions. In accordance with the donor/acceptor capabilities of each ligand L coordinated to the molybdenum centre, the results were that -Br containing complexes are more active than those of -COOEt or -CH₃. This means that the weaker the donor ability of the Lewis base, the more catalytically active is the catalyst.^[87] The donor ability of each ligand L, fine-tuned by the various substituent groups, is more pronounced when the substituents are *trans*-positioned to the oxo ligands;^[87]

- the catalytic activity also depends on the nature of the ligand X. This is well illustrated by an example from Kühn and Romão and co-workers involving complexes of the $[\text{MoO}_2\text{X}_2\text{bipy}]$ (with X = Cl, Br or CH_3) type. Results revealed that when the complexes were tested as catalysts in cyclooctene epoxidation reactions with TBHP, higher activities were reached for X = Cl while the lowest was observed for X = CH_3 .^[83] The authors suggested that steric factors of X may partially account for the activity differences observed.^[83] Literature data reveal that the catalytic activity is also dependent on the **iii**) solvent choice and **iv**) reaction temperature.^[134] Unfortunately, no systematic example of several solvent tests and/or test of temperatures were found for dioxomolybdenum(VI) complexes containing L = bipyridine derivatives and X = Cl ligands.

The epoxidation of pure methyl oleate using molybdenum-based catalysts has not yet been reported. Wang and co-workers, however, reported that the epoxidation of a mixture of methyl oleate (Figure 27) and methyl lineolate (Figure 28) with $\text{H}_2\text{O}_2/\text{NaHCO}_3$ in the presence of the complex $[\text{MoO}(\text{O}_2)_2(8\text{-quinilino})_2]$ gave 92 % total selectivity to epoxides at 72 % conversion, using CH_3CN as a cosolvent at 2 h / 30 °C.^[126] Sobczak and Ziółkowski investigated the epoxidation of oleic acid (*cis*-9-octadecenoic acid, Figure 29) with organic hydroperoxides in the presence of the complexes $[\text{Mo}(\text{CO})_6]$, $\text{H}_2[\text{Mo}_2\text{O}_4(\text{oxalate})_2(\text{H}_2\text{O})_2]\cdot 4\text{H}_2\text{O}\cdot(\text{CH}_3)_2\text{CO}$, $[\text{MoO}_2(\text{acac})_2]$, and $[\text{MoO}_2(\text{SAP})(\text{EtOH})]$ (SAP = dianionic tridentate salicylideneiminophenolate chelating ligand). The latter complex exhibited the best catalytic performance, giving *ca.* 87 % epoxide selectivity to 9,10-epoxystearic acid at 67% conversion of TBHP_{aq}, at 260 min / 80 °C.^[135]

More recently, it was reported that the use of $[\text{MoO}_2(\text{acac})_2]$ as a catalyst in the epoxidation of soybean oil (Figure 30) with TBHP led to 77 % epoxide selectivity at 70 % conversion (2 h / 110 °C).^[125]

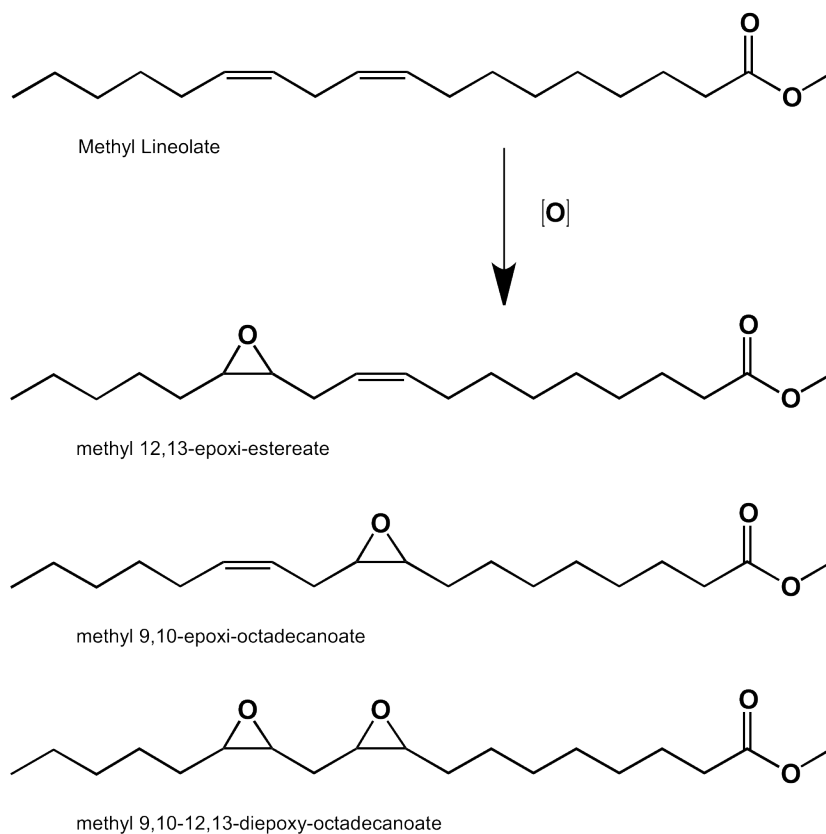


Figure 28. Methyl lineoleate epoxidation products.

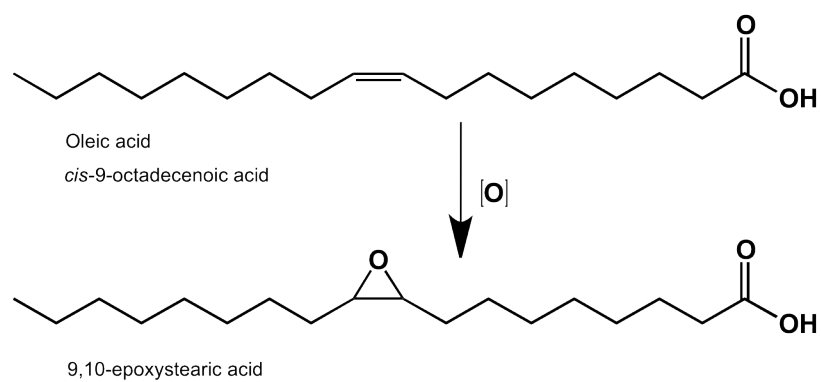


Figure 29. Structures and epoxidation products of oleic acid.

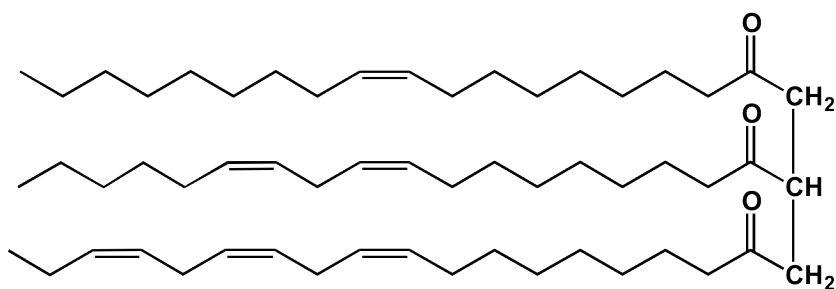


Figure 30. Example of a triglyceride molecule present in Soybean oil. This vegetable oil is a mixture of saturated and poly-unsaturated fatty acids. The major unsaturated fatty acids (80 % of its content) are triglycerides with unsaturated long-chains in approximately 26 % of oleic acid, 52 % of linoleic acid, and 8 % linolenic acid.^[136]

IV. AIM OF THIS WORK

Dioxomolybdenum(VI) complexes of the type $[\text{MoO}_2\text{X}_2]$ and $[\text{MoO}_2\text{X}_2\text{L}]$ are known to be important catalysts or catalyst precursors for the liquid phase epoxidation of nonfunctionalized olefins in the presence of organic peroxides. The motivation to study these discrete, homogeneous catalysts with $\text{L} = \text{N}, \text{N}'$ -chelating ligands in the form of monomeric or dimeric species, stems from the fact that they are well-defined, single site catalysts, usually favouring high activity and selectivities, but also because: i) Mo-catalyzed reactions are economically attractive due to the relatively inexpensive costs of Mo; ii) the complexes have already proven to give good results in important homogeneous catalytic processes such as oxidation; and iii) presence of these Lewis base organic ligands coordinated to Mo has helped to stabilize compounds/catalysts.

Considering the accumulated knowledge (synthesis and catalytic behaviour) of monomeric species, one major step would be the creation of a truly heterogeneous catalyst with, hopefully, the same catalytic properties and kinetics obtainable from the homogeneous counterparts. No approach exists where no second step reaction is needed, *i.e.*, all methods use the immobilization (covalently anchor a functionalized derivative of the molecular catalyst) on to an insoluble solid support of large surface area that can be either an organic polymer or inorganic material. To reduce the catalyst's preparation time and costs we aim to convert these monomeric complexes directly into insoluble materials, designing a new heterogeneous catalyst that would not need to be immobilized. This kind of approach, *i.e.*, the combination of metal oxide monomers to isolate polymeric structures where each metallic unit will be linked by short-distance oxo-bridges, has been practically unexplored. As shown in this introduction, only a handful of examples of polymeric hybrid materials containing N, N' -chelate ligands and the cis-MoO_2^{2+} core are known, with the scarce examples arising from the group of Zubieta. The catalytic potential of

these systems as well as a deeper structural characterization has also yet to be explored.

Alongside with this main objective is also the development of alternative approaches that would create more cost competitive catalytic processes, as *e.g.* testing different Mo^{VI} oxide precursors. We also aim for a pure reproducible product that would be very active, highly selective, stable and re-usable catalyst to be used under mild conditions. These results would have a significant impact on the overall financial cost of the catalytic process, especially because heterogeneous catalysts are easily separated from the reaction mixture and recycled.

The organization of this thesis was made according to the ligand used within each case study. Each chapter describes the synthesis, structure and catalytic performance of the resultant material. In the conclusion all experimental and catalytic results are joined and critically compared.

SYNTHESIS and STRUCTURE of a POLYMERIC COMPOUND CONTAINING 2,2'-BIPYRIDINE

1.1. SUMMARY

Recently our research group^[98] was able to isolate the polymer $[\text{MoO}_3(\text{bipy})]_n$ (see Introduction, Table 3, compound **23**) discovered by Zubieta,^[59] when using an oxidative decarbonylation of *cis*- $[\text{Mo}(\text{CO})_4(\text{bipy})]$ with TBHP under relatively mild conditions (4 h at ambient temperature).

These studies led us to investigate alternative soft chemistry routes (performed in water) toward new polymeric hybrid materials: the hydrolysis and condensation of monomeric *cis*-dioxomolybdenum(VI) complexes such as $[\text{MoO}_2\text{Cl}_2(\text{bipy})]$. The chemistry of $[\text{MoO}_2\text{X}_n\text{L}_m]$ in water is usually not considered as a viable pathway to obtain Mo^{6+} oxide-based organic-inorganic hybrids. This is most likely due to the general assumption that water is incompatible with this type of chemistry and would only promote an anarchic disruption of all metal-ligand bonds. There are, nevertheless, a handful of reports showing that the coordinated organic ligands in $[\text{MoO}_2\text{X}_n\text{L}_m]$ -type complexes may be partially resistant to protic environments.^[137] This opens new possibilities concerning the synthetic pathways employed toward the synthesis of these functional compounds, in particular the use of those based on more environmentally-friendly solvents such as water.

1.2. $\{[\text{MoO}_3(\text{bipy})][\text{MoO}_3(\text{H}_2\text{O})]\}_n$ (1.2)

In this section it is described the use of the monomeric $[\text{MoO}_2\text{Cl}_2(\text{bipy})]$ (1.1) complex to prepare the Mo^{6+} oxide polymeric hybrid material $\{[\text{MoO}_3(\text{bipy})][\text{MoO}_3(\text{H}_2\text{O})]\}_n$ (1.2) (Figure 1.1). A detailed structural characterization of the polymeric material is presented, which includes FT-IR vibrational spectroscopy, thermogravimetric analysis, electron microscopy and a complete structural description from powder X-ray diffraction studies using high-resolution synchrotron data. The catalytic performance of both 1.1 and 1.2 was studied in the conversion of *cis*-cyclooctene (Cy8) into 1,2-epoxycyclooctane (Cy8Ox), and analysed in a comparative fashion. Additional studies were performed to understand the effect of adding (or otherwise) a co-solvent such as 1,2-dichloroethane (DCE) or *n*-hexane (1 mL), or using 70% aqueous TBHP or 30% aqueous H_2O_2 instead of TBHP *dec.*

Methods used to prepare the polymeric 1D hybrid material containing 2,2'-bipyridine

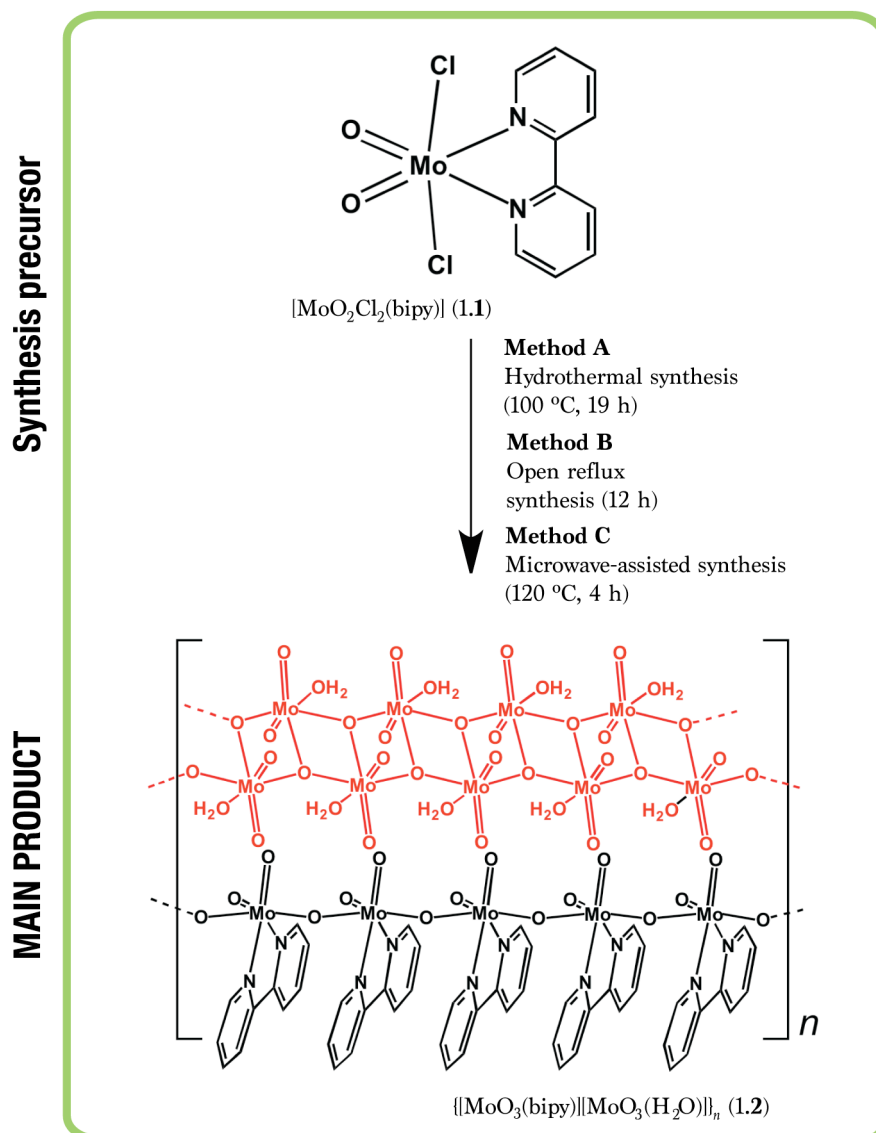


Figure 1.1. Methods used to prepare the polymeric 1D hybrid material $\{[\text{MoO}_3(\text{bipy})][\text{MoO}_3(\text{H}_2\text{O})]\}_n$ (1.2).

1.2.1. SYNTHESIS

The reaction of $[\text{MoO}_2\text{Cl}_2(\text{bipy})]$ (**1.1**) with water was carried out either in i) a Teflon-lined stainless steel autoclave (autogenous pressure, 100 °C, 19 h), ii) in an open reflux system in open air (12 h, oil bath heating), or iii) in a sealed glass vessel with microwave-assisted heating (120 °C, 4 h). In each case, a white solid suspended in a pink acidic solution (pH = 2-3) was obtained. The solid was recovered by centrifugation, washed with water and organic solvents, and dried at 100 °C in air. Identical elemental analysis, FT-IR and powder X-ray diffraction data were obtained for all three solid products indicating that the heating method had no significant influence on the outcome of the reaction. EDS analyses confirmed the absence of chlorine in the products. On the basis of the characterization data and the crystal structure solution described below, the product was formulated as $\{[\text{MoO}_3(\text{bipy})][\text{MoO}_3(\text{H}_2\text{O})]\}_n$ (**1.2**). This compound is a 1 : 1 adduct of two one-dimensional (1D) polymers. Yields were 72% for the hydrothermal method and 91-92% for the microwave-assisted and reflux methods.

1.2.2. FT-IR

For comparison the FT-IR spectra of the free ligand, the precursor **1.1**, the product **1.2**, and of the polymer $[\text{MoO}_3(\text{bipy})]_n$ are depicted in Figure 1.2.

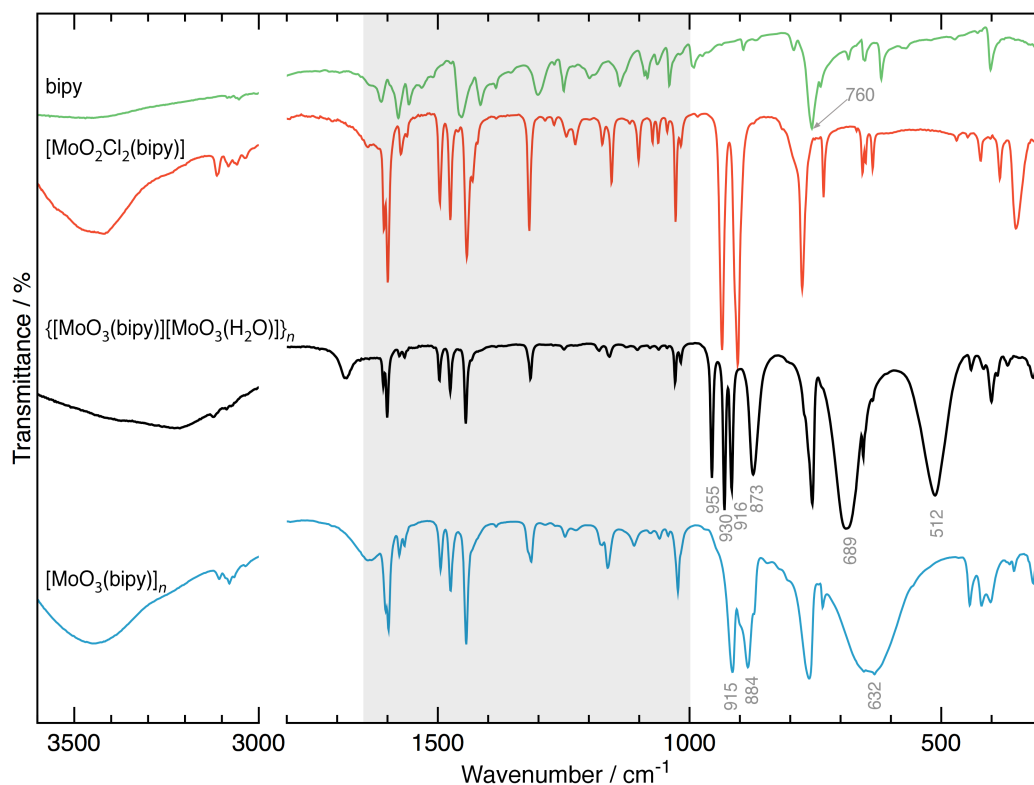


Figure 1.2. Comparison of the FT-IR spectra of 2,2'-bipyridine (bipy), the precursor $[\text{MoO}_2\text{Cl}_2(\text{bipy})]$ (**1.1**), and the polymers $\{[\text{MoO}_3(\text{bipy})][\text{MoO}_3(\text{H}_2\text{O})]\}_n$ (**1.2**) and $[\text{MoO}_3(\text{bipy})]_n$. Spectra were collected using KBr pellets.

The FT-IR spectrum of **1.2** presents the characteristic bands of the coordinated 2,2'-bipyridine ligand appearing at around 3100 cm^{-1} , in the range of *ca.* $1610\text{--}1000\text{ cm}^{-1}$ and at around 760 cm^{-1} . These bands are coincident with those registered for the monomer $[\text{MoO}_2\text{Cl}_2(\text{bipy})]$ (**1.1**)^[138] and with those of the known organic-inorganic hybrid compound $[\text{MoO}_3(\text{bipy})]_n$ (Table 3, compound **23**).^[98]

Strong bands centred at *ca.* 955 , 930 , 916 , 873 , 689 , and 512 cm^{-1} may be assigned to various types of Mo–O vibrational modes. For comparison, the polymer $[\text{MoO}_3(\text{bipy})]_n$ presents Mo–O vibrations at *ca.* 915 , 884 , and 632 cm^{-1} . Taking into account the crystal structure of **1.2** (described in section 1.2.5), the four bands at *ca.* 955 , 930 , 916 , and 873 cm^{-1} may be attributed to $\nu(\text{Mo}=\text{O})$ stretching vibrations from two distinct *cis*- $[\text{MoO}_2]^{2+}$ units. As expected, the bands in this region differ from the pair of $\nu(\text{Mo}=\text{O})$ stretching vibrations exhibited by the precursor complex $[\text{MoO}_2\text{Cl}_2(\text{bipy})]$ (**1.1**) (found at *ca.* 936 and 904 cm^{-1}).^[83] The intense, broad bands at *ca.* 689 and 512 cm^{-1} can be assigned to stretching vibrations of bridging Mo–O–Mo and OMo_3 units, respectively.^[139] A very broad band at around 3200 cm^{-1} and another at *ca.* 1679 cm^{-1} are indicative of the presence of water molecules in the structure corresponding, respectively, to the typical stretching and deformation vibration modes of these moieties.

1.2.3. THERMOGRAVIMETRIC ANALYSES

Thermogravimetric studies on a representative portion of the polymeric compound $\{[\text{MoO}_3(\text{bipy})][\text{MoO}_3(\text{H}_2\text{O})]\}_n$ (**1.2**) were performed between ambient temperature and *ca.* $800\text{ }^\circ\text{C}$. No weight losses were observed up to *ca.* $200\text{ }^\circ\text{C}$ (Figure 1.3). The first weight loss of about 4.1% occurs at around $205\text{ }^\circ\text{C}$ and agrees well with the release of one water molecule per formula unit as indicated by the empirical formula (calculated value of *ca.* 3.9%). The high temperature for the release of this water molecule is coherent with the proposed crystal structure: the structure does not call for water molecules of crystallization, instead only coordinated molecules appear in the crystal structure, hence the high temperature at which they are released. Above *ca.* $205\text{ }^\circ\text{C}$, and up to *ca.* $455\text{ }^\circ\text{C}$, there is a four-step decomposition of the organic component with a total weight loss of *ca.* 33.7% (which coincides with the calculated value). Above *ca.* $455\text{ }^\circ\text{C}$, and below *ca.* $720\text{ }^\circ\text{C}$, the obtained residue (*ca.* 62.3%) corresponds to the stoichiometric formation of MoO_3 (which once again matches perfectly the calculated value). At temperatures higher than *ca.* $720\text{ }^\circ\text{C}$ a further weight loss is attributed to the sublimation of MoO_3 .^{[140][141]}

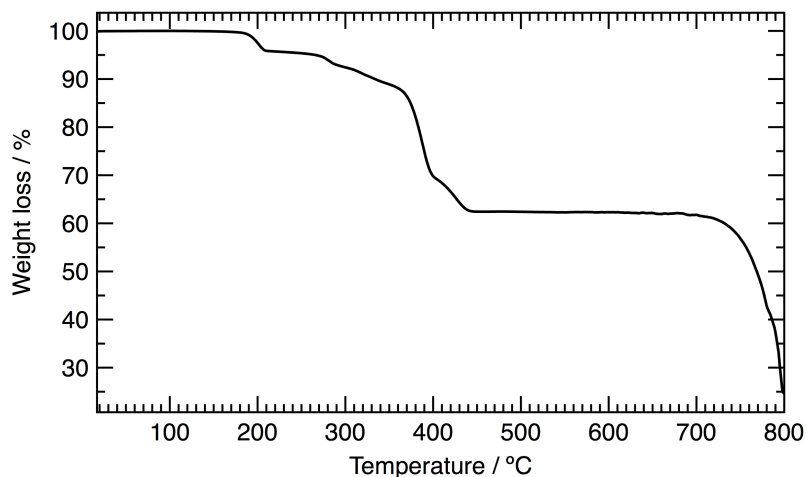


Figure 1.3. Thermogram of $\{[\text{MoO}_3(\text{bipy})][\text{MoO}_3(\text{H}_2\text{O})]\}_n$ (1.2).

1.2.4. SCANNING ELECTRON MICROSCOPY

Scanning Electron Microscopy studies on representative portions of $\{[\text{MoO}_3(\text{bipy})][\text{MoO}_3(\text{H}_2\text{O})]\}_n$ (1.2) reveal that the material is composed of a uniform distribution of needle-like shaped crystallites as shown in the inset in Figure 1.4.

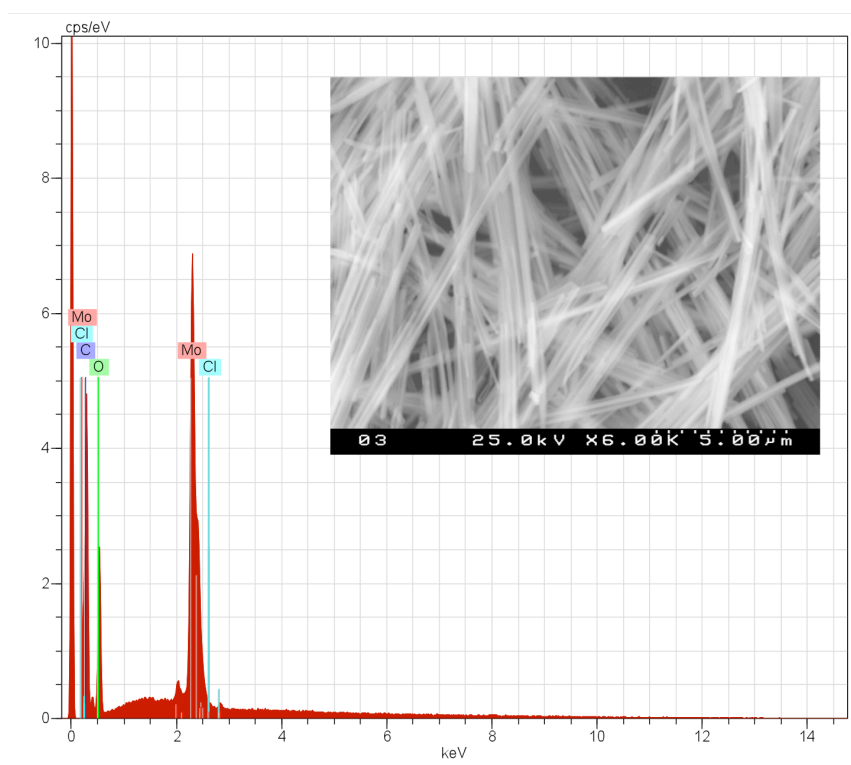


Figure 1.4. Dispersive X-ray spectroscopy (EDS) spectrum of $\{[\text{MoO}_3(\text{bipy})][\text{MoO}_3(\text{H}_2\text{O})]\}_n$ (1.2) the inset corresponds to a SEM image collected at an operating energy work of 25 kV, with a magnification of 6000x.

Even though the needles are relatively long (*i.e.*, length greater than *ca.* 10 μm), they were systematically very thin (in the nano-size range – see inset

in Figure 1.4). This morphological feature prevented the use of single-crystal X-ray diffraction for a complete structural elucidation of 1.2. As described in section 1.2.5, only by employing *ab initio* methods based on high-resolution synchrotron powder X-ray diffraction data could the structural details be unveiled.

Energy-dispersive X-ray spectroscopy on various portions of the as-prepared compound 1.2 (from different batches) confirmed the absence of chlorine in the material (Figure 1.4). This further signifies that the precursor 1.1 was not dispersed in 1.2 as a physical mixture (as confirmed from powder X-ray diffraction).

1.2.5. X-RAY DIFFRACTION: CRYSTAL STRUCTURE DESCRIPTION

Through the use of high-resolution synchrotron powder X-ray diffraction data (Figure 1.5), in combination with data derived from other characterization methods, the crystal structure was fully determined and formulated as $\{[\text{MoO}_3(\text{bipy})][\text{MoO}_3(\text{H}_2\text{O})]\}_n$ (1.2).^[142]

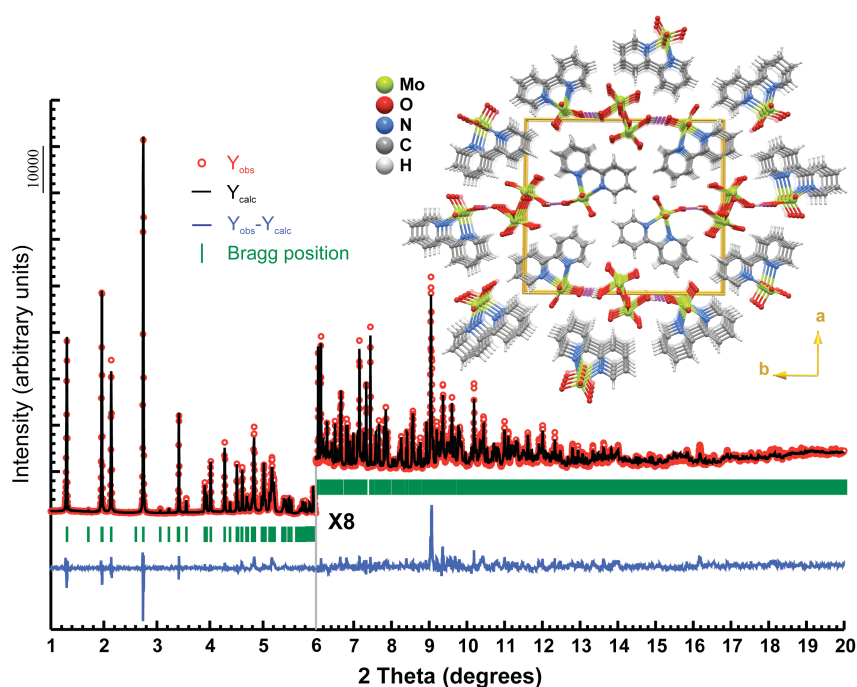


Figure 1.5. Final Rietveld plot (synchrotron powder X-ray diffraction data) of $\{[\text{MoO}_3(\text{bipy})][\text{MoO}_3(\text{H}_2\text{O})]\}_n$ (1.2). Observed data points are indicated as red circles; the best fit profile (upper trace) and the difference pattern (lower trace) are drawn as solid black and blue lines, respectively. Green vertical bars indicate the angular positions of the allowed Bragg reflections. The inset shows a ball-and-stick crystal packing representation of 1.2 viewed along the [001] crystallographic direction.

As depicted in Figure 1.6, the hybrid material 1.2 is composed of two distinct neutral one-dimensional polymers: one organic-inorganic polymer,

$[\text{MoO}_3(\text{bipy})]_n$, and a purely inorganic chain, $[\text{MoO}_3(\text{H}_2\text{O})]_n$, both based on Mo^{6+} metal centres (as unequivocally confirmed by bond valence calculations based on the crystal structure).

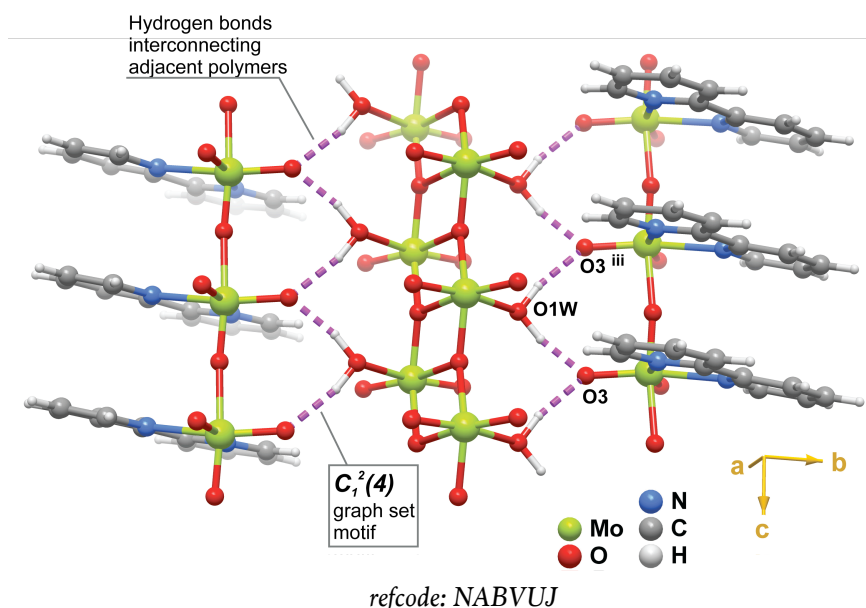


Figure 1.6. O–H \cdots O hydrogen bonding interactions (dashed pink lines) interconnecting adjacent inorganic, $[\text{MoO}_3(\text{H}_2\text{O})]_n$, and hybrid, $[\text{MoO}_3(\text{bipy})]_n$, polymers in 1.2. The supramolecular contacts describe a $C_1^2(4)$ graph set motif running parallel to the [001] direction of the unit cell. Symmetry transformation used to generate equivalent atoms: (iii) $x, y, 1+z$. Geometrical parameters for the hydrogen bonds present in 1.2: $d(\text{D}\cdots\text{A}) = \text{O1W}-\text{H1B}\cdots\text{O3}$ 2.6166(19) Å, $\angle(\text{D}\cdots\text{A}) = 167^\circ$; $\text{O1W}-\text{H1C}\cdots\text{O3}^{\text{iii}}$ 2.7959(19) Å, $\angle(\text{D}\cdots\text{A}) = 168^\circ$.

Hybrid polymer

In the 1D hybrid polymer $[\text{MoO}_3(\text{bipy})]_n$ (Figure 1.7) the crystallographically independent Mo1 centre is coordinated to two terminal oxido groups, one *N,N*-chelated bipy organic molecule and two symmetry-related μ_2 -bridging oxido groups. The overall $\{\text{MoN}_2\text{O}_4\}$ coordination geometry resembles a distorted octahedron as shown in Figure 1.8. The Mo–(N,O) distances range from 1.7829(14) to 2.3569(17) Å, and the internal (N,O)–Mo1–(N,O) *cis* and *trans* octahedral angles fall in the ranges of 76.83(6)–102.85(6) $^\circ$ and 160.27(6)–166.09(8) $^\circ$, respectively.

The distortion of the Mo1 coordination environment seems to arise from the combination of a significant *trans* effect of the Mo=O groups (which are *trans*-coordinated to the N-donor atoms of the organic moiety; Figure 1.8), and to the distinct apical Mo–O distances of the μ_2 -bridges [1.6932(13) and 2.0933(13) Å]. Nevertheless, this hybrid polymer is characterized by only one intermetallic Mo \cdots Mo distance of 3.759(1) Å.

In the related $[\text{MoO}_3(\text{bipy})]_n$ polymer reported by Zubietta and co-workers (see Introduction, Table 3, polymer **23**),^[59] all of the *N,N'*-chelated organic ligands are aligned so as to minimize mutual steric repulsion leading to a

pseudo-star distribution along the direction of the polymer. In contrast, in **1.2** the same hybrid polymer $[\text{MoO}_3(\text{bipy})]_n$ has instead all of the organic molecules perfectly aligned (*i.e.*, eclipsed) in the growth direction of the polymer. The aforementioned distortion of the Mo^{6+} coordination environment is, nevertheless, also found in polymer **23**. For example, the octahedral apical Mo–O distances of the μ_2 -bridges are also unsymmetrical [1.822(4) and 2.031(3) Å], thus giving rise to an infinite $\{\cdots\text{O}=\text{Mo}\cdots\text{O}=\text{Mo}\}$ chain with alternating short-long Mo–O distances, respectively. In the material reported by Zubietta there is also a single intermetallic $\text{Mo}\cdots\text{Mo}$ distance of *ca.* 3.70 Å, which agrees with that observed in **1.2**.

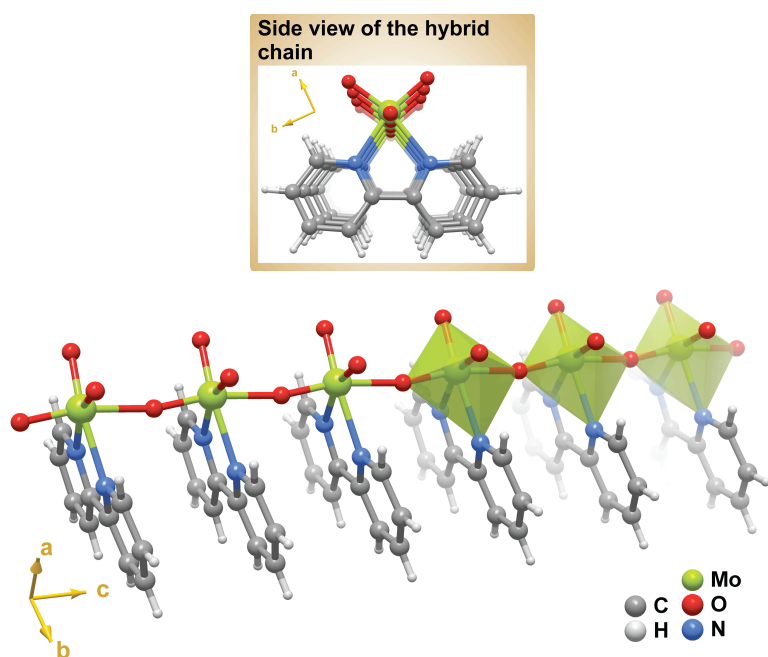


Figure 1.7. Mixed ball-and-stick and polyhedral representations of the neutral $[\text{MoO}_3(\text{bipy})]_n$ hybrid polymer present in **1.2**, which runs parallel to the [001] direction of the unit cell.

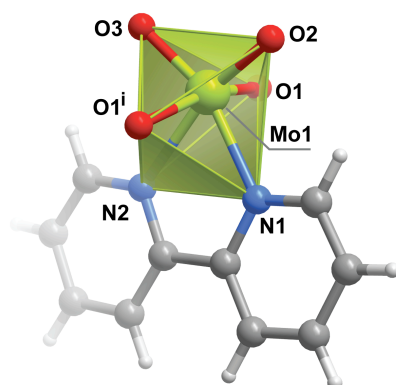


Figure 1.8. Schematic representation of the highly distorted $\{\text{MoN}_2\text{O}_4\}$ octahedral coordination environment of Mo1. Symmetry transformation used to generate equivalent atoms: (i) $x, y, -1+z$.

Inorganic polymer

The inorganic 1D polymer $[\text{MoO}_3(\text{H}_2\text{O})]_n$ (Figure 1.9) is based on the other crystallographically independent Mo^{6+} metallic centre, Mo2, which is coordinated to three μ_3 -bridging oxido groups, two terminal oxido groups, and one water molecule. The octahedral $\{\text{MoO}_6\}$ coordination environment (Figure 1.10) is more distorted than that for Mo1: the internal O–Mo2–O octahedral *trans* angles lie in the wide range of $139.67(7)$ – $168.57(6)^\circ$ and the *cis* angles are found in the range of $68.57(5)$ – $107.43(6)^\circ$ (Table 1.1).

Table 1.1. Selected bond lengths (Å) and angles (in degrees) for the two Mo^{6+} coordination environments present in compound $\{[\text{MoO}_3(\text{bipy})][\text{MoO}_3(\text{H}_2\text{O})]\}_n$ (1.2).^a

Mo1–O1	1.6932(13)	Mo2–O4	1.9117(12)
Mo1–O1 ⁱ	2.0933(13)	Mo2–O4 ⁱⁱⁱ	2.0921(12)
Mo1–O2	1.7892(15)	Mo2–O4 ^{iv}	2.2381(12)
Mo1–O3	1.7829(14)	Mo2–O5 ⁱⁱ	1.7892(15)
Mo1–N1	2.2261(17)	Mo2–O6	1.7461(14)
Mo1–N2	2.3569(17)	Mo2–O1W	2.2506(15)
O1–Mo1–O1 ⁱ	166.09(8)	O4–Mo2–O4 ⁱⁱⁱ	139.67(7)
O1–Mo1–O2	95.29(6)	O4–Mo2–O4 ^{iv}	68.57(5)
O1–Mo1–O3	97.03(6)	O4–Mo2–O1W	76.56(6)
O1–Mo1–N1	93.15(7)	O4 ⁱⁱⁱ –Mo2–O4 ^{iv}	74.32(5)
O1 ⁱ –Mo1–N1	76.83(6)	O4 ⁱⁱⁱ –Mo2–O1W	80.82(5)
O1 ⁱ –Mo1–N2	78.35(5)	O4 ^{iv} –Mo2–O1W	77.84(5)
O1–Mo1–N2	89.30(7)	O5 ⁱⁱ –Mo2–O4	97.07(6)
O2–Mo1–N1	92.96(6)	O5 ⁱⁱ –Mo2–O4 ⁱⁱⁱ	98.86(6)
O2–Mo1–N2	163.29(6)	O5 ⁱⁱ –Mo2–O4 ^{iv}	91.04(6)
O3–Mo1–N1	160.27(6)	O5 ⁱⁱ –Mo2–O1W	168.57(6)
O2–Mo1–O1 ⁱ	94.94(6)	O6–Mo2–O4	107.43(6)
O3–Mo1–O1 ⁱ	89.96(6)	O6–Mo2–O4 ⁱⁱⁱ	103.03(5)
O3–Mo1–O2	102.85(6)	O6–Mo2–O4 ^{iv}	162.26(6)
O3–Mo1–N2	92.52(6)	O6–Mo2–O5 ⁱⁱ	106.67(7)
N1–Mo1–N2	70.69(6)	O6–Mo2–O1W	84.43(6)

^a Symmetry transformations used to generate equivalent atoms:

(i) $x, y, -1+z$; (ii) $x, 1+y, z$; (iii) $x, y, 1+z$; (iv) $1-x, 2-y, 1-z$.

Nevertheless, the range found for the Mo2–O bond distances [$1.7461(14)$ to $2.2506(15)$ Å] is comparable with that found for the $\{\text{MoN}_2\text{O}_4\}$ coordination environment of Mo1. The bond distance with the coordinated water molecule

[2.2506(15) Å] is typical for dioxomolybdenum(VI) compounds, as revealed by a search in the CSD: for 33 entries, all Mo–O_{water} distances were found in the range of 2.20–2.44 Å with a median of 2.29 Å. Indeed, the possibility of the presence of a terminal hydroxyl group was discarded due to, on the one hand, bond valence calculations and, on the other, the fact that for the only known dioxomolybdenum(VI) compound with a terminal –OH group the bond distance to this moiety (*ca.* 1.97 Å) is significantly shorter than that registered for 1.2.^[143]

The three symmetry-related O4 atoms composing the {MoO₆} coordination sphere, and structurally located in the equatorial plane of the octahedron, act as μ_3 -bridges leading to the formation of an inorganic tape with all Mo⁶⁺ centres distributed in a zigzag fashion along the [001] direction. This arrangement leads to a slightly asymmetric distribution of intermetallic Mo \cdots Mo distances along the chain: 3.434(1) and 3.452(1) Å.

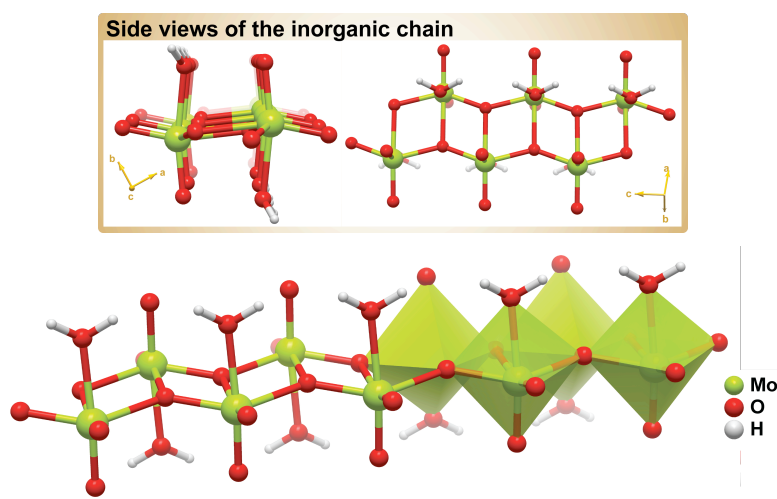


Figure 1.9. Mixed ball-and-stick and polyhedral representations of the neutral [MoO₃(H₂O)]_n inorganic polymer present in 1.2 and running parallel to the [001] direction of the unit cell.

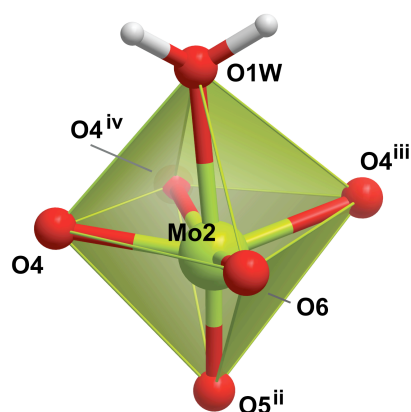


Figure 1.10. Schematic representation of the highly distorted {MoO₆} octahedral coordination environment of Mo2. Symmetry transformations used to generate equivalent atoms: (ii) $x, 1+y, z$; (iii) $x, y, 1+z$; (iv) $1-x, 2-y, 1-z$.



The two polymers in $\{[\text{MoO}_3(\text{bipy})][\text{MoO}_3(\text{H}_2\text{O})]\}_n$ (1.2) are linked by O–H \cdots O hydrogen bonding interactions in which the coordinated water molecule of $[\text{MoO}_3(\text{H}_2\text{O})]_n$ donates the two hydrogen atoms to neighbouring O3 atoms of the terminal Mo=O oxido groups of the adjacent $[\text{MoO}_3(\text{bipy})]_n$ polymer (Figure 1.6). These interactions are strong [$d_{\text{D}\cdots\text{A}}$ ranging between *ca.* 2.62 and 2.80 Å] and highly directional. The recursive and cooperative fashion in which these interactions create supramolecular bridges along the [001] direction between the polymers leads to a $\text{C}_1^2(4)$ graph set motif^[144] running parallel to the *c*-axis. This arrangement produces a new supramolecular entity composed of two hybrid polymers and one inorganic chain (Figure 1.6), which close packs in the *ab* plane of the unit cell in a brickwall-like fashion to yield the crystal structure of 1.2 (inset in Figure 1.5). The closest intermetallic Mo \cdots Mo distance across polymers within this new entity is 5.811(1) Å.

1.2.6. HETEROGENEOUS CATALYSIS

The catalytic performance of 1.2 for olefin epoxidation was investigated at 55 °C for the model substrate Cy8 while using TBHP_{dec} (5.5 M in decane) as the oxygen source. The catalyst : substrate : oxidant molar ratio was set to 1 : 100 : 150, respectively. Biphasic solid-liquid mixtures were always obtained, even in the presence of a co-solvent [1,2-dichloroethane (DCE) or *n*-hexane], and 1,2-epoxycyclooctane (Cy8Ox) was the sole product of Cy8 oxidation. As depicted in Figure 1.11 (with symbol **o**), epoxide yields at 48 h were: 49% for no co-solvent (Figure 1.11a); 62% when using DCE (Figure 1.11c); and 34% when using *n*-hexane (Figure 1.11d). These yields are all higher than those observed in the absence of the molybdenum-containing catalyst (**+**) *i.e.*, 11, 11 and 19% for the same reaction conditions as above, respectively. These results clearly indicate that 1.2 contains active metal species that function as catalytic sites in the investigated reaction.

After each reaction run of 48 h, the solid phase was recovered by centrifugation, washed with *n*-hexane, and dried at ambient temperature overnight. The recovered amount of 1.2 was *ca.* 78% (no co-solvent) and *ca.* 88% (when either DCE or *n*-hexane were used). This indicates that the catalyst is poorly soluble in the tested reaction media solvent. The nature of each catalytic reaction (homogeneous and/or heterogeneous) was investigated by performing a CatFilt experiment (for more details see Experimental chapter). This test consists of comparing the increase in conversion between 1 and 24 h of reaction [denoted as $\Delta\text{X}(\text{CatFilt})$], with the results obtained either for the same reaction in the presence of 1.2 but when no filtration step was taken [$\Delta\text{X}(\text{NoFilt})$] or, in the absence of 1.2 [$\Delta\text{X}(\text{NoCat})$]. The observed values for $\Delta\text{X}(\text{NoFilt})$, $\Delta\text{X}(\text{CatFilt})$, and $\Delta\text{X}(\text{NoCat})$ are summarized in Table 1.2.

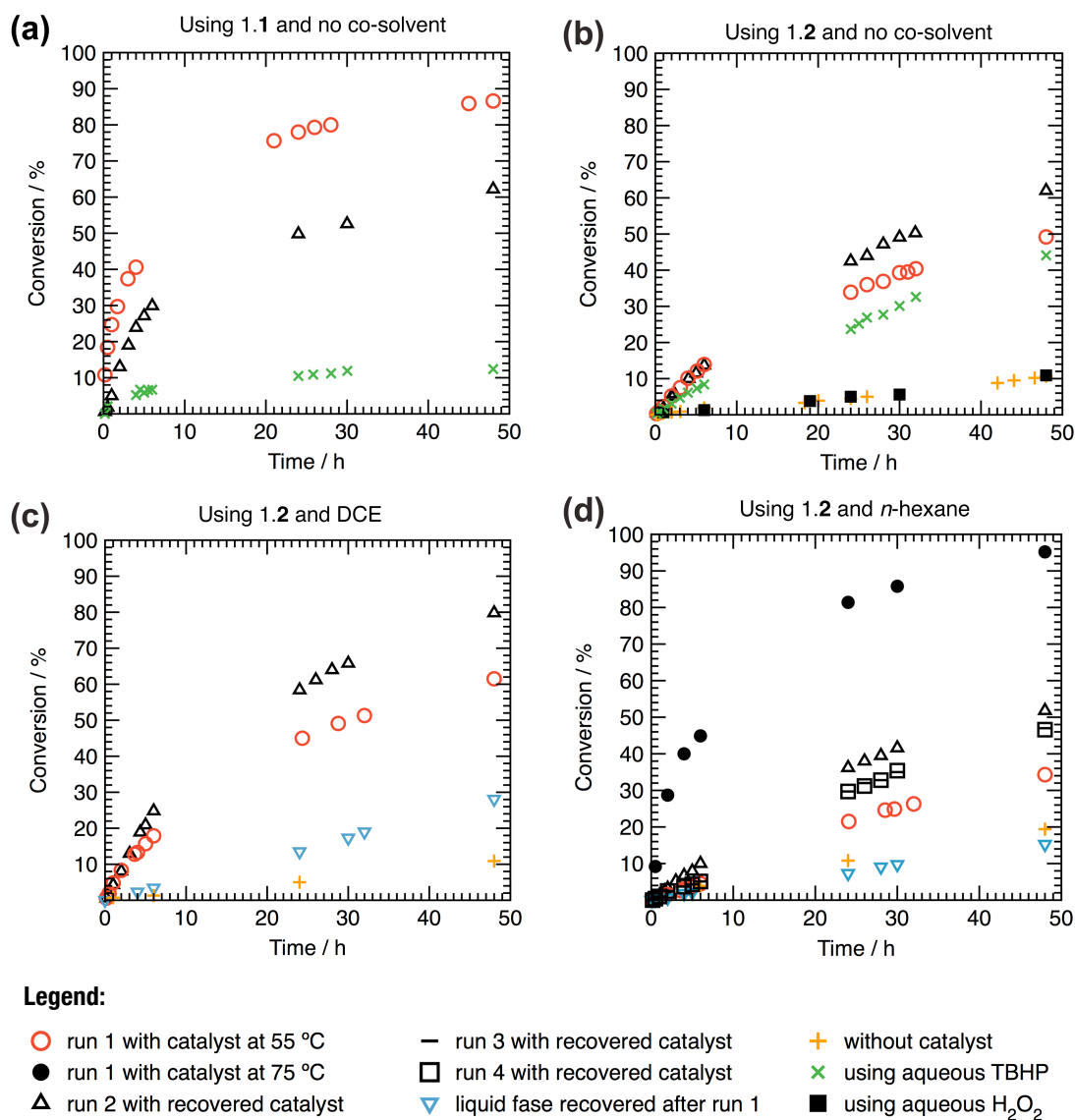


Figure 1.11. Epoxidation of *cis*-cyclooctene at 55 °C (unless otherwise stated) using: (a) [MoO₂Cl₂(bipy)] (1.1) and no additional co-solvent; (b) 1.2 and no additional co-solvent; (c) 1.2 and 1,2-dichloroethane; (d) 1.2 and *n*-hexane. Results of the reactions carried out with TBHP_{dec} as the oxidant, and the catalytic runs using aqueous TBHP or aqueous H₂O₂ are also represented.

The fraction $\Delta X(\text{CatFilt})/\Delta X(\text{NoCat})$ decreases in the following order: no co-solvent > DCE > *n*-hexane. Accordingly, the contribution from the homogeneous phase reaction is more significant in the absence of co-solvent than for the presence of DCE. When *n*-hexane was used this contribution is negligible. Results unequivocally indicate that, in the beginning of the reaction, the degree of dissolution of the molybdenum-containing active species is strongly influenced by the solvent. This dissolution is enhanced for more polar solvents, which may act on the material by disrupting O–H···O hydrogen bonds.

Table 1.2. Results for the CatFilt experiment used to determine the nature of each catalytic reaction depending on the solvent used.

	No filtration	After filtration	Absence of Catalyst	
Co-solvent	$\Delta X(\text{NoFilt})$	$\Delta X(\text{CatFilt})$	$\Delta X(\text{NoCat})$	$\Delta X(\text{CatFilt})/\Delta X(\text{NoCat})^*$
No solvent	32	23	5	5.7
DCE	39	13	6	2.3
<i>n</i> -hexane	21	10	10	1

* The higher the value of $\Delta X(\text{CatFilt})/\Delta X(\text{NoCat})$ the greater the homogeneous contribution to the nature of the reaction.

As discussed ahead, structural data for pristine 1.2 and that of the recovered catalysts are similar. This indicates that the homogeneous contribution may possibly be happening due to the dissolution of a fraction (*i.e.*, “oligomers”) of 1.2 rather than to its full decomposition into soluble, active metal species.

To verify that the catalytic reaction with 1.2 is essentially heterogeneous when *n*-hexane was employed, a Liquid Phase Recovered Study (LPRS) was performed. In this test the reaction solution was recovered after a normal (*i.e.*, unfiltered) catalytic first run of 48 h at 55 °C with 1.2 and *n*-hexane. Similar amounts of fresh olefin and oxidant were then added to the recovered solution, and the amount of epoxide was determined. As shown in Figure 1.11d (see symbol ▽), the conversion of Cy8 into Cy8O_x in the homogeneous phase using *n*-hexane as co-solvent was lower than that observed without a catalyst (possibly due to dilution effects). Atomic Absorption Spectroscopy (AAS) analysis of the recovered solution from the second homogeneous run revealed that no measurable amount of molybdenum was detected, *i.e.*, less than 1 ppm (detection limit). Thus, as expected from the CatFilt tests, 1.2 acts as a true heterogeneous catalyst when using *n*-hexane as co-solvent.

With *n*-hexane the epoxidation reaction in the presence or absence of 1.2 at 55 °C (Figure 1.11d, +) gives comparable epoxide yields up to *ca.* 6 h. Afterwards, the reaction is faster if the catalyst is present. This induction period may be partly due to diffusion limitations that seem to be overruled if the reaction temperature is increased to, at least, 75 °C (Figure 1.11d, see symbol ●).

The same LPRS and CatFilt tests were performed when DCE was used as co-solvent. Results revealed that the solution contains active species, giving 14 and 28% epoxide yield within a 24 and 48 h of reaction, respectively. Without a catalyst (+), the epoxide yields were only 7 and 11%. These results allowed us to conclude that when using DCE the reaction could not be defined as purely heterogeneous. The same result could be derived from the CatFilt test approach.

Stability and reusability

To study the stability and reusability of 1.2 within each reaction run, the solid recovered at 48 h (on each particular system of different co-solvents) was used in a second consecutive run. For the procedure used for the recovery of the solid see Experimental chapter and Catalysis section corresponding to chapter 1.

Results for each co-solvent were reproducible during an initial period of time concerning the epoxide conversion of runs 1 and 2. After this initial period, epoxide yields were higher for run 2, particularly when using *n*-hexane as co-solvent. Two additional runs (run 3 and 4) were carried out and it was observed that the kinetic curves (represented on Figure 1.11d with the symbols - and □) are roughly coincident and lie between those of runs 1 and 2. On every 48 h second run (*i.e.*, run 2) the solids were recovered by filtration, washed and dried. Recovered catalysts were studied using powder X-ray diffraction and ATR FT-IR studies. For the solid recovered after the first run when *n*-hexane was used, powder X-ray data (Figure 1.12) suggest that the material is structurally identical to the as-prepared solid 1.2.

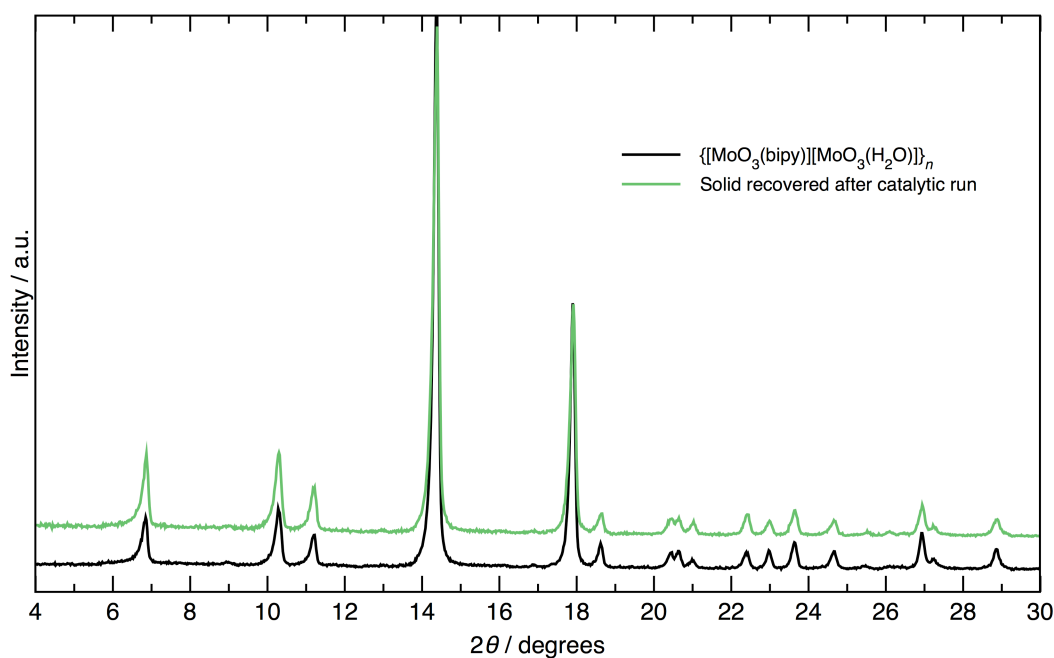


Figure 1.12. Powder X-ray diffraction patterns of the as-prepared $\{[\text{MoO}_3(\text{bipy})][\text{MoO}_3(\text{H}_2\text{O})]\}_n$ (1.2) material and the solid recovered after epoxidation of Cy8 carried out at 55 °C for 48 h, with *n*-hexane as the co-solvent and TBHP_{dec} as the oxidant.

The ATR FT-IR spectrum of the solid recovered after the catalytic run 2 performed without co-solvent and using TBHP_{dec} as oxidant, is similar to that of 1.2 in the 300-1750 cm⁻¹ spectral range (Figure 1.13). This constitutes further evidence that the two solids are identical. In short, these two bulk characterization techniques did not provide any irrefutable evidence suggesting

any degree of structural modification for the solids recovered when *n*-hexane or no co-solvent were used during the catalytic reactions. CHN microanalyses were performed for the recovered catalysts in the latter situation, with the results being also comparable with those obtained for as-prepared 1.2.

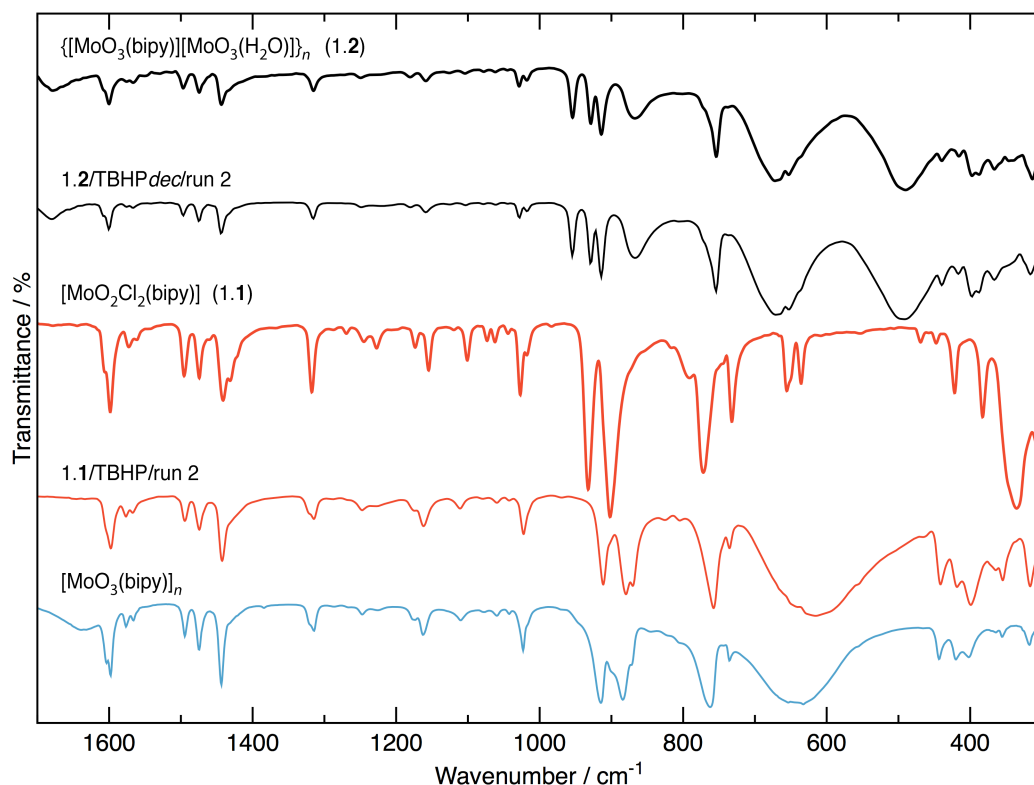


Figure 1.13. Comparison of the ATR FT-IR spectra of $\{[\text{MoO}_3(\text{bipy})][\text{MoO}_3(\text{H}_2\text{O})]\}_n$ (1.2) and $[\text{MoO}_2\text{Cl}_2(\text{bipy})]$ (1.1) with the spectra of the solids recovered after the epoxidation runs 1.2/TBHP*dec*/run 2, 1.1/TBHP*aq*/run 1, respectively. The spectrum of the hybrid polymer $[\text{MoO}_3(\text{bipy})]_n$ is also represented for comparative purposes.

COMPARISON of the CATALYTIC PERFORMANCE of 1.1 and 1.2

- Oxidative agent in organic medium (TBHP*dec*)

The catalytic performance of the precursor $[\text{MoO}_2\text{Cl}_2(\text{bipy})]$ (1.1) was also investigated for comparative purposes (conditions: no co-solvent, TBHP*dec* at 55 °C). Results are graphically summarized in Figure 1.11 (○). In the first run the epoxide was the only product formed in 78 / 87% yields at 24 / 48 h, respectively. This compound outperformed 1.2 for which the observed yields at identical periods were 34 / 49%, respectively (Figure 1.11b, (○)). Noteworthy, the catalytic reaction mixture with 1.1 (no co-solvent) was also biphasic solid-liquid. The amount of solid recovered after the first 48 h was, however, lower corresponding to *ca.* 56% (Figure 1.11a) of the initially loaded 1.1. The recovered solid was further reused in a 48 h second run (Figure 1.11a). After the first

10 minutes the reaction was already slower than in the first run, as clearly shown by the calculated epoxide yields: 78 / 87% and 50 / 62% at 24 / 48 h for runs 1 and 2, respectively.

Figure 1.13 shows the ATR FT-IR spectra of the precursor $[\text{MoO}_2\text{Cl}_2(\text{bipy})]$ (**1.1**), the solid recovered after the 2nd run (Cy8, TBHP_{dec} and no co-solvent) and of the polymeric hybrid material $[\text{MoO}_3(\text{bipy})]_n$. Looking at the 300-1000 cm^{-1} spectral range, it is clear that under the employed catalytic conditions the precursor **1.1** is transformed *in situ* into $[\text{MoO}_3(\text{bipy})]_n$.^[98]

This assumption was further investigated by scaling up in a round-bottomed flask the reaction 10 times (to isolate more catalyst). After 24 hours of reaction, the dispersed solid was isolated by filtration, washed and vacuum-dried. FT-IR and elemental analysis (CHN) were performed and, as expected, data matched those of polymeric $[\text{MoO}_3(\text{bipy})]_n$. The observed transformation probably occurs due to the presence of vestigial amounts of water (the supplied TBHP solution was used as received and may contain up to 4% water), which promotes the hydrolysis of the Mo-Cl bonds.

Using *n*-hexane and TBHP the catalytic activity of **1.2** is considerably improved when the temperature is raised from 55 to 75 °C (Figure 1.11d, ●). The CatFilt experiment performed at 75 °C gave: $\Delta X(\text{CatFilt}) = 9\%$, $\Delta X(\text{NoFilt}) = 36\%$ and $\Delta X(\text{CatFilt}) / \Delta X(\text{NoCat})$ approximately 1. This indicates that the reaction is, essentially, heterogeneous in nature.

- Oxidative agent (TBHP or H₂O₂) in water

The catalytic performances of $[\text{MoO}_2\text{Cl}_2(\text{bipy})]$ (**1.1**) and $\{[\text{MoO}_3(\text{bipy})]-[\text{MoO}_3(\text{H}_2\text{O})]\}_n$ (**1.2**) were studied using aqueous 70% TBHP or 30% H₂O₂. Triphasic solid-organic-aqueous mixtures were always formed. Selectivity to the epoxide was always 100%. Using aqueous TBHP promoted much slower reactions than those observed when TBHP_{dec} was used instead (Figure 1.11). These results may be attributed to mass transfer limitations of the oxidant between the aqueous and organic phases.

The presence of excess of water in the catalytic medium has strong implications in the type of the recovered catalyst. Indeed, using aqueous TBHP (no co-solvent), **1.1** is transformed to the polymeric **1.2** material. This can be easily followed using ATR FT-IR (Figure 1.14): the strong bands centred at *ca.* 340 $[\nu(\text{Mo}-\text{Cl}_{\text{asym}})]$, 904 $[\nu(\text{Mo}=\text{O}_{\text{asym}})]$, and 935 cm^{-1} $[\nu(\text{Mo}=\text{O}_{\text{sym}})]$ present in the spectrum of **1.1** spectrum are replaced by bands centred at *ca.* 317, 355, 871 (sh), 881, and 913 cm^{-1} in the recovered solids.

Studies with aqueous H₂O₂ show that the polymeric compound **1.2** is unable to activate the oxidant: the kinetic curve is nearly coincident with that observed for the reaction of Cy8 with TBHP_{dec} in the absence of catalyst (Figure 1.11).

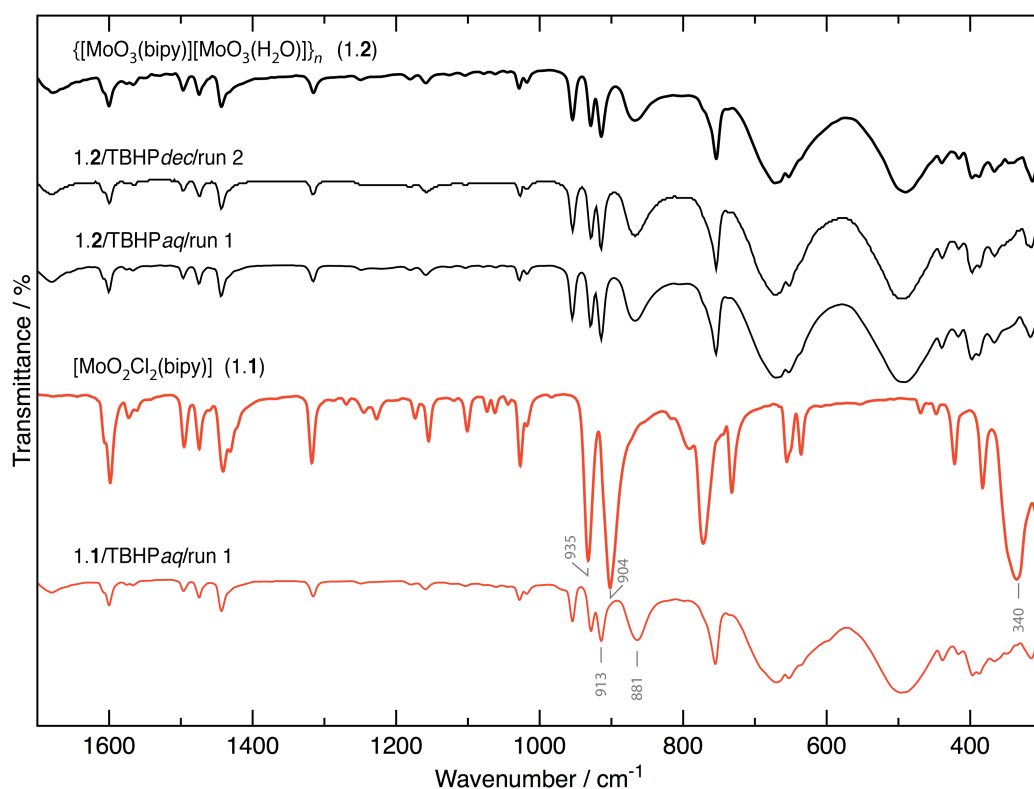


Figure 1.14. Comparison between the ATR FT-IR spectra of $\{[\text{MoO}_3(\text{bipy})][\text{MoO}_3(\text{H}_2\text{O})]\}_n$ (1.2) and the solids recovered after the first and second catalytic epoxidation runs. The spectra of the precursor $[\text{MoO}_2\text{Cl}_2(\text{bipy})]$ (1.1) and the solid recovered from the catalytic epoxidation of 1.1/TBHPaq/run 1 are also provided for comparative purposes.

1.4. CONCLUDING REMARKS

In this chapter it was shown that even though the reaction in water of $[\text{MoO}_2\text{Cl}_2(\text{bipy})]$ (1.1) was expected to produce the hybrid material $[\text{MoO}_3(\text{bipy})]_n$, which is known to be an active, highly selective, and stable catalyst for the epoxidation of Cy8 with TBHP, the result was instead the polymeric compound $\{[\text{MoO}_3(\text{bipy})][\text{MoO}_3(\text{H}_2\text{O})]\}_n$ (1.2). It is demonstrated that regardless of the heating method used, the hydrolysis reaction only produced in high yields 1.2. By using *n*-hexane as co-solvent this material was found to be a moderately effective, highly selective and stable heterogeneous catalyst in the epoxidation of Cy8 at 55 °C with TBHP_{dec}.

Literature searches on polymeric organic-inorganic hybrid structures containing organic *N,N'*-organic ligands bonded to a molybdenum oxide skeleton showed that only a handful of related hybrid structures have been reported to date (see Introduction, Table 3). A close structural comparison reveals that compound 1.2 is truly unprecedented: i) it differs from most of these previously reported structures in the fact that the hybrid polymer is composed solely of one type of monomer, while in most of the aforementioned structures $[\text{MoO}_4]$

tetrahedra (**T**) periodically intercalate the monomers containing the organic ligand (either bipy or 1,10-phenanthroline); ii) in contrast to the structure of $[\text{MoO}_3(\text{bipy})]_n$ reported by Zubietta, **1.2** has all of the organic molecules eclipsed in the growth direction of the polymer; iii) this material is a 1 : 1 adduct of two one-dimensional polymers, in which one is a purely inorganic structure.

Using **1.2** with TBHP_{aq} the epoxidation of Cy8 also occurs although, in this case, reactions were slower than those performed using TBHP_{dec} (i.e., 5.5 M TBHP in decane).

Tests reveal that when the precursor **1.1** is employed as catalyst and the reaction is carried out using TBHP_{dec}, the hybrid material $[\text{MoO}_3(\text{bipy})]_n$ was formed *in situ*, presumably due to the presence of some residual water arising from the oxidant. In the presence of an excess of water, for example when 70% aqueous TBHP was used, compound **1.2** was isolated at the end of the catalytic run from **1.1**.

In summary, the hybrid polymer $\{[\text{MoO}_3(\text{bipy})][\text{MoO}_3(\text{H}_2\text{O})]\}_n$ (**1.2**) and the discrete complex $[\text{MoO}_3(\text{bipy})]$ are potentially interesting water-tolerant catalysts for the epoxidation of non-functionalized olefins because of their good performance, activity, selectivity and stability. The Cy8 conversion at 24 h for **1.2** (45%) is, however, lower than that registered for $[\text{MoO}_3(\text{bipy})]_n$ (81%). From the results in this chapter, and the examples given in the Introduction, it is clear that the next challenge should focus on how to fine-tune the chemical properties of the catalysts by judiciously changing the organic ligand in the starting $[\text{MoO}_2\text{X}_m\text{L}_n]$ complex. This approach can lead to the design of new materials with different structural features and improved heterogeneous catalytic properties, capable of higher conversions and yields.

DISCRETE COMPLEXES with Di-*tert*-Butyl-2,2'-BIPYRIDINE

2.1. SUMMARY

In the previous chapter the controlled hydrolysis and condensation of the mononuclear complex $[\text{MoO}_2\text{Cl}_2(\text{bipy})]$ (1.1) was the distinct route used to prepare the polymeric hybrid material $[\text{MoO}_3(\text{bipy})][\text{MoO}_3(\text{H}_2\text{O})]_n$ (1.2). The latter material proved to be an active, selective, and stable catalyst for the epoxidation of Cy8. This compound was, nevertheless, only a moderately effective heterogeneous catalyst. This chapter describes the attempts to prepare more active heterogeneous catalysts capable of addressing more demanding epoxidations and/or other types of oxidation reactions. The strategy employed was similar to that of chapter 1: a $[\text{MoO}_2\text{Cl}_2(\text{L})]$ -type complex was used as the precursor in water to isolate new hybrid materials.

di-*tert*-Butyl-2,2'-bipyridine (di-*t*-Bu-bipy) was selected as the N,N' -chelating ligand because: i) it is more soluble than 2,2'-bipyridine in inorganic solvents; ii) it is an effective N,N' -chelating ligand for the preparation of both mononuclear and dinuclear oxomolybdenum(VI) hybrid catalyst materials, namely $[\text{MoO}_2(\text{NCS})_2(\text{di-}t\text{-Bu-bipy})]$,^{[114][145][146][147]} $[\text{Mo}_2\text{O}_5(\text{NCS})_2(\text{di-}t\text{-Bu-bipy})_2]$,^[114] $[\text{Mo}_2\text{O}_5\text{Cl}_2(\text{di-}t\text{-Bu-bipy})_2] \cdot 0.2\text{H}_2\text{O}$ ^[96] $[\text{Mo}_2\text{O}_5\text{Cl}_2(\text{di-}t\text{-Bu-bipy})_2]$ ^[97] and $[\text{V}_2\text{O}_2(\mu\text{-MeO})_2(\mu\text{-MO}_4)_2(\text{di-}t\text{-Bu-bipy})_2]$ ^[148] (where M = Mo, W). These complexes reported in the literature are effective oxygen atom transfer agents and/or pre-catalysts for alcohol oxidation and olefin epoxidation.

This chapter describes the reaction of $[\text{MoO}_2\text{Cl}_2(\text{di-}t\text{-Bu-bipy})]$ (2.1) in water at 100–120 °C, using three different heating methods: hydrothermal, reflux and microwave-assisted synthesis. All approaches produced the discrete octanuclear complex $[\text{Mo}_8\text{O}_{22}(\text{OH})_4(\text{di-}t\text{-Bu-bipy})_4]$ (2.2). This complex is formed by a purely inorganic cationic core, $[\text{Mo}_4\text{O}_8(\mu_3\text{-OH})_2(\mu_2\text{-O})_2]^{2+}$, attached to two peripheral oxo-bridged binuclear anionic units, $[\text{Mo}_2\text{O}_4(\mu_2\text{-O})_2(\text{OH})(\text{di-}t\text{-Bu-bipy})_2]$. Single-crystals suitable for X-ray diffraction could only be isolated from conventional hydrothermal synthesis using MoO_3 (metallic source) and di-*t*-Bu-bipy (ligand). The dinuclear complex $[\text{Mo}_2\text{O}_6(\text{di-}t\text{-Bu-bipy})_2]$ (2.3) was isolated from the filtered aqueous mother liquor by slow evaporation. The catalytic performance of both 2.2 and 2.3 in the epoxidation of non-functionalized olefins is described.

2.2. $[\text{Mo}_8\text{O}_{22}(\text{OH})_4(\text{di-}t\text{-Bu-bipy})_4]$ (2.2)

This section describes the use of the complex $[\text{MoO}_2\text{Cl}_2(\text{di-}t\text{-Bu-bipy})]$ (2.1) to prepare the Mo^{6+} oxide discrete hybrid material $[\text{Mo}_8\text{O}_{22}(\text{OH})_4(\text{di-}t\text{-Bu-bipy})]$ (2.2). A detailed structural characterization of the discrete material is presented, which includes FT-IR spectroscopy, solid-state NMR, thermogravimetric analysis, electron microscopy and a detailed structural description based on single-crystal X-ray diffraction studies. The catalytic performance of 2.2 was investigated in the conversion of DL-limonene (Lim) and methyl oleate (Ole) into 1,2-epoxy-*p*-menth-8-ene (LimOx) and 9,10-epoxystearate (OleOx), respectively. These catalytic substrates were chosen due to their relevance in the usage of plant biomass as a renewable feedstock for the chemical industry.^{[119][122][125][126][135]}

2.2.1. SYNTHESIS

Hybrid precursor: $[\text{MoO}_2\text{Cl}_2(\text{di-}t\text{-Bu-bipy})]$ (2.1)

The reaction of $[\text{MoO}_2\text{Cl}_2(\text{di-}t\text{-Bu-bipy})]$ (2.1) (di-*t*-Bu-bipy = 4,4'-di-*tert*-butyl-2,2'-bipyridine) with water was carried out using different synthetic approaches: i) sealed glass vessel using microwave heating (120 °C, 4.5 h, irradiation power 150 W; method A); ii) open reflux system in the air (18 h, OB heating, method B); iii) sealed Teflon-lined stainless steel autoclave (autogenous pressure, 100 °C, 19 h, method C), Figure 2.1.

For all methods a white solid suspended in a pink acidic solution (pH \cong 2) was isolated. The solid was recovered by centrifugation, washed with water and organic solvents, and finally vacuum-dried. Identical characterization results were obtained for all three solid products indicating that the heating method had no significant influence on the outcome of the reaction. To the pink solution (of method A) acetone was added and after slow diffusion of diethyl ether to the solution, the result was the formation of yellow crystals that were characterized as being the oxodiperoxo complex $[\text{Mo}(\text{O}_2)_2(\text{di-}t\text{-Bu-bipy})]$.^[149]

Inorganic precursor: MoO_3

The hydrothermal reaction of MoO_3 , di-*t*-Bu-bipy and H_2O in the molar ratio of 1 : 1 : 580, respectively, at 160 °C for 3 days in a Teflon-lined autoclave rotating at 25 rpm (dynamic hydrothermal synthesis - method D; see Experimental chapter) afforded a crystalline material, Figure 2.1. The bulk sample was composed of small crystals. For this method (and precursor) the size of the crystals are at the low limit of what can be studied using single-crystal X-ray diffraction. The performed crystallographic studies revealed, nevertheless, that the material was formed by discrete octanuclear complexes formulated as

$[\text{Mo}_8\text{O}_{22}(\text{OH})_4(\text{di-}t\text{-Bu-bipy})_4]$ (**2.2**). Characterization studies (e.g., elemental analysis, FT-IR and powder X-ray diffraction) were in good agreement with the data previously gathered for the same compound when **2.1** was used as the precursor. Figure 2.1 depicts all four methods employed to obtain the octanuclear complex $[\text{Mo}_8\text{O}_{22}(\text{OH})_4(\text{di-}t\text{-Bu-bipy})_4]$ (**2.2**), and the possible secondary products which could be isolated from each one.

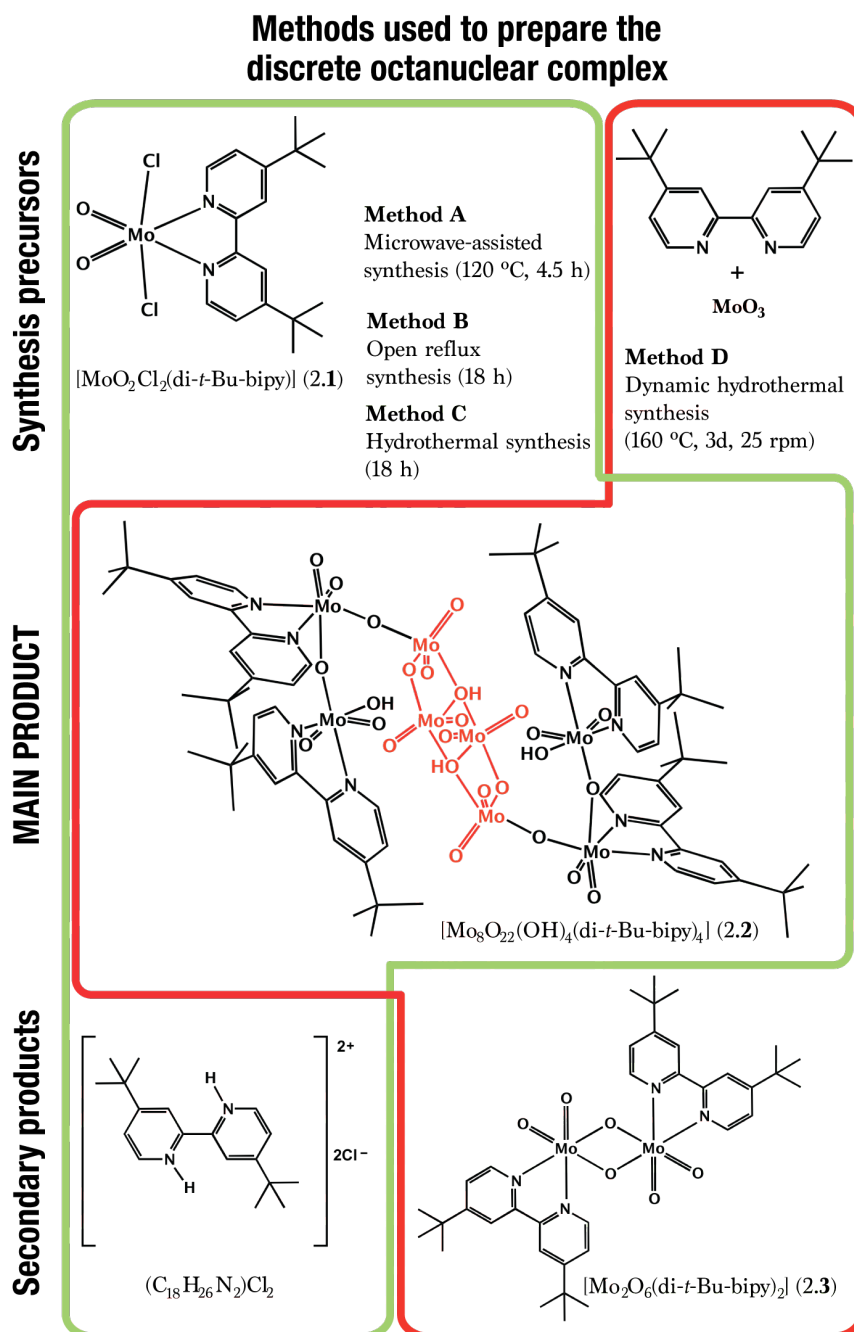


Figure 2.1. Methods used to prepare the octanuclear complex $[\text{Mo}_8\text{O}_{22}(\text{OH})_4(\text{di-}t\text{-Bu-bipy})_4]$ (**2.2**). Depending on whether the metallic source was the discrete complex $[\text{MoO}_2\text{Cl}_2(\text{di-}t\text{-Bu-bipy})]$ (**2.1**) or inorganic MoO_3 (plus the free organic ligand *di-t-Bu-bipy*), the secondary products which could be obtained are: $(\text{C}_{18}\text{H}_{26}\text{N}_2)\text{Cl}_2$ (left) and $[\text{Mo}_2\text{O}_6(\text{di-}t\text{-Bu-bipy})_2]$ (**2.3**) (right). All syntheses were carried out in water. For characterization details on the organic salt $(\text{C}_{18}\text{H}_{26}\text{N}_2)\text{Cl}_2$ see Experimental chapter.

The same crystalline product could be prepared from distinct synthetic methods (A to D). Almost all characterization data for **2.2** presented in this chapter were, nevertheless, acquired using the solid obtained with method C. An exception is the SEM data where solid **2.2** was prepared instead using method D. Noteworthy, using method D the synthesis of phase-pure $[\text{Mo}_8\text{O}_{22}(\text{OH})_4(\text{di-}t\text{-Bu-bipy})_4]$ (**2.2**) could not be achieved without employing rotation of the reaction vessels: the main product **2.2** would be otherwise contaminated with unreacted MoO_3 . Performing the same reaction using MoO_3 but under similar conditions to those employed in methods A and B, *i.e.*, microwave-assisted synthesis or open reflux (Figure 2.1), the result was either a mixture of unreacted MoO_3 plus **2.2** (method A), or a mixture of product **2.2** plus the dinuclear complex $[\text{Mo}_2\text{O}_6(\text{di-}t\text{-Bu-bipy})]_2$ (**2.3**) (method B).

2.2.2. FT-IR

Figure 2.2 shows the FT-IR spectrum of $[\text{Mo}_8(\text{OH})_4\text{O}_{22}(\text{di-}t\text{-Bu-bipy})_4]$ (**2.2**) compared to those of the ligand and of the mononuclear precursor $[\text{MoO}_2\text{Cl}_2(\text{di-}t\text{-Bu-bipy})]$ (**2.1**).

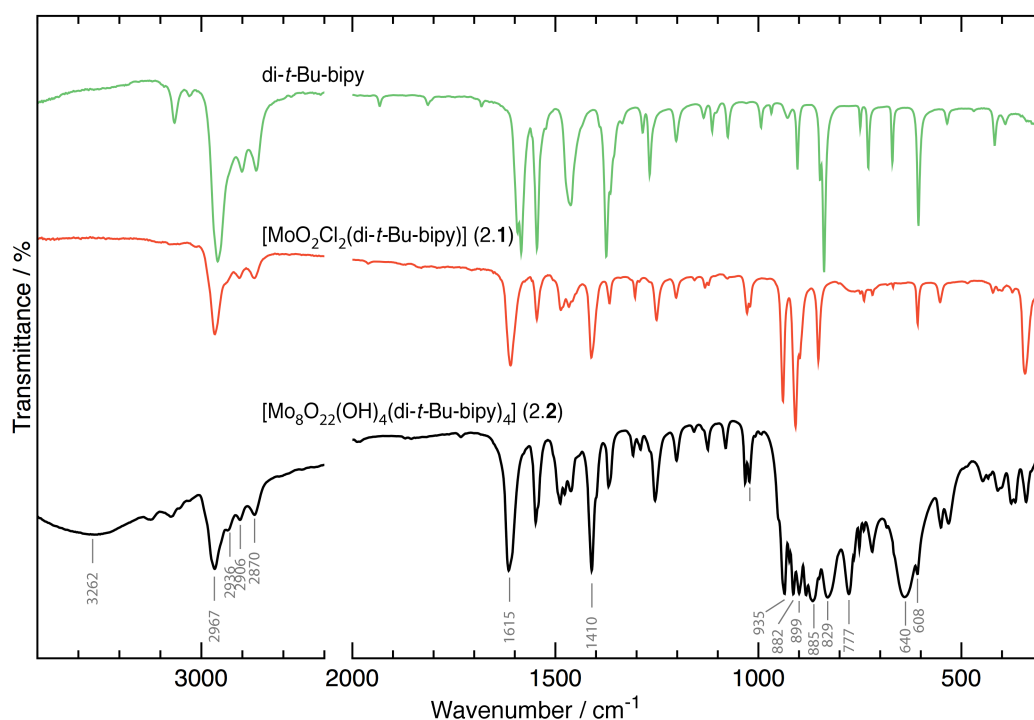


Figure 2.2. Comparison between the FT-IR spectrum of $[\text{Mo}_8(\text{OH})_4\text{O}_{22}(\text{di-}t\text{-Bu-bipy})_4]$ (**2.2**), obtained from the microwave-assisted synthesis (method C), with the spectra of the *di-}t\text{-Bu-bipy}* ligand and of the monomer $[\text{MoO}_2\text{Cl}_2(\text{di-}t\text{-Bu-bipy})]$ (**2.1**).

di-*t*-Bu-bipy

The FT-IR spectrum of di-*t*-Bu-bipy exhibits prominent bands above 3000 cm⁻¹ that are attributed to the alkene and aromatic C-H stretching vibrations, *i.e.*, $\nu(\text{C-H})$. The strong bands immediately below 3000 cm⁻¹, centred at *ca.* 2960, 2901 and 2866 cm⁻¹, are assigned to the C-H stretching vibrations of the alkane *tert*-butyl groups, $\nu(\text{C-H})_{t\text{-Bu}}$. Several other bands in the range of *ca.* 2000-1600 cm⁻¹ may be attributed to overtones of the aromatic rings. The strong bands at *ca.* 1584 cm⁻¹ and 1374 cm⁻¹ are attributed to the C=C and C=N stretching of the aromatic rings, *i.e.*, $[\nu(\text{C=C}) + \nu(\text{C=N})]_{\text{py}}$. At *ca.* 837 cm⁻¹ a strong band is attributed to the out-of-plane bending $\gamma(\text{CH-CH})$ of the pyridine aromatic rings. The two bands centred at *ca.* 605 cm⁻¹ and 418 cm⁻¹ are attributed to the in-plane bending of the C-H from the pyridyl rings, usually indicated as $\delta(\text{C-H})_{\text{py}}$.^[150]

[MoO₂Cl₂(di-*t*-Bu-bipy)] (2.1)

Upon coordination of di-*t*-Bu-bipy to the MoO₂Cl₂ fragment the spectrum of the obtained product [MoO₂Cl₂(di-*t*-Bu-bipy)] (2.1) exhibits bands typical of both precursors. For instance, above *ca.* 3000 cm⁻¹ the alkene and aromatic C-H stretching vibrations from the organic ligand are still present. At *ca.* 1610 cm⁻¹ and *ca.* 1411 cm⁻¹ two strong bands appear attributed to the C=C and C=N stretching that are red-shifted with respect to those of the uncoordinated ligand (located at *ca.* 1584 cm⁻¹ and 1374 cm⁻¹).

At *ca.* 343 cm⁻¹ a medium-to-strong band is attributed to the presence of chloride anions bound to the metal centre, *i.e.*, $\nu(\text{Mo-Cl})$. As expected for a complex having a *cis*-MoO₂²⁺ core there are two strong bands between *ca.* 950 and 850 cm⁻¹ attributed to the $\nu(\text{Mo=O})$ stretching vibrational modes arising from this functional group.

[Mo₈O₂₂(OH)₄(di-*t*-Bu-bipy)₄] (2.2)

In common with the mononuclear precursor 2.1 the FT-IR spectrum of [Mo₈O₂₂(OH)₄(di-*t*-Bu-bipy)₄] (2.2) exhibits two strong pyridyl ring stretching vibrational modes centred at *ca.* 1615 cm⁻¹ and 1410 cm⁻¹, which can be ultimately attributed to the bidentate coordination mode of the di-*t*-Bu-bipy ligands with the Mo⁶⁺ centers. In addition, a complex pattern of bands appearing in the *ca.* 600–950 cm⁻¹ range is attributable to various Mo–O vibrational modes in accordance with the crystal structure.

2.2.3. SOLID-STATE NMR

$^{13}\text{C}\{^1\text{H}\}$ CP MAS NMR studies provided additional information on the structure of the compound, in particular the composition of the asymmetric unit. Data clearly shows three main spectral regions, two attributed to the aromatic portion (from *ca.* 170 to 110 ppm) and another to the aliphatic one of the ligand (from *ca.* 38 to 30 ppm), *i.e.*, the *tert*-butyl groups (Figure 2.3).

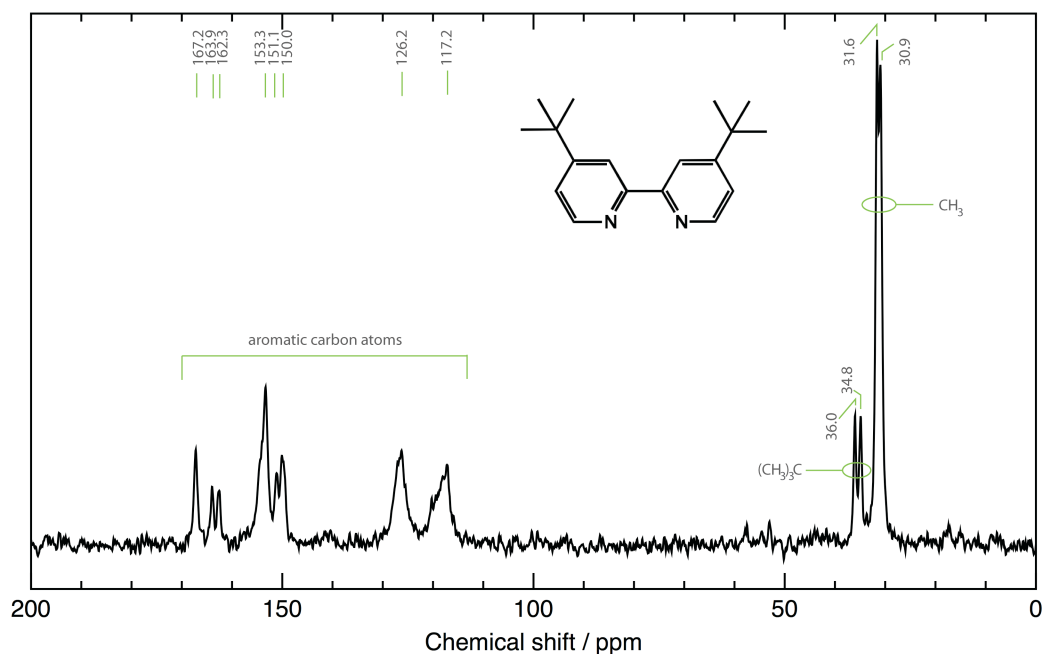


Figure 2.3. Solid state $^{13}\text{C}\{^1\text{H}\}$ CP MAS NMR spectrum of $[\text{Mo}_8\text{O}_{22}(\text{OH})_4(\text{di-}t\text{-Bu-bipy})_4]$ (2.2). Spinning rate of 11 kHz using a Bruker Avance 400 spectrometer (9.4 T) at 100.62 MHz. Chemical shifts are quoted in parts per million (ppm) with respect to TMS.

Two resonances at 30.9 and 31.6 ppm are attributed to the methyl carbons of the *tert*-butyl groups: $(\text{CH}_3)_3\text{-C}$ and $(\text{CH}_3)_3\text{-C}'$. The presence of two distinct resonances is further evidence to the existence of, at least, two methyl carbons that are crystallographically independent. The resonances centred at 34.8 and 36.0 ppm are attributed to the two quaternary carbon atoms attached to the *tert*-butyl groups: $(\text{CH}_3)_3\text{-C}$ and $(\text{CH}_3)_3\text{-C}'$. The section of the spectrum assigned to the aromatic carbon atoms can be divided into two main regions: between *ca.* 110 to 140 ppm and 140 to 170 ppm. In the former region, two broad resonances centred at 117.2 and 126.2 ppm are attributed to the carbon atoms immediately bonded to the quaternary ones. The broadening may be caused by the overlap of more resonances related to the crystallographically independent carbons of the same type. The second region of the spectrum, with a total of six resonances, may be attributed to the remaining aromatic carbon atoms, including at the higher frequency region the less shielded aromatic quaternary carbon. For the ^{13}C solid-state NMR studies it would be expected a total of seven resonances if only one di-*t*-Bu-bipy organic ligand would be present in the asymmetric unit.

The presence of more resonances comes in line with the performed crystallographic studies showing that the asymmetric unit is, indeed, composed of more than one of such chemical moieties.

2.2.4. THERMOGRAVIMETRIC ANALYSES

Thermogravimetric studies between ambient temperature and *ca.* 800 °C revealed that bulk $[\text{Mo}_8\text{O}_{22}(\text{OH})_4(\text{di-}t\text{-Bu-bipy})_4]$ (**2.2**) has no weight losses up to *ca.* 185 °C (Figure 2.4). Above this temperature and up to *ca.* 550 °C there is a multi-step thermal decomposition that is mainly attributed to the thermal decomposition of the organic component and to the liberation of the various hydroxyl groups, most likely in the form of water molecules. At *ca.* 550 °C the observed residue is of *ca.* 51.0% which agrees well with the stoichiometric formation of MoO_3 (calculated value of 50.9%). Above *ca.* 700 °C, as registered in the previous chapter, the MoO_3 starts to sublime, hence the continuous weight loss above this temperature.^{[140][141]}

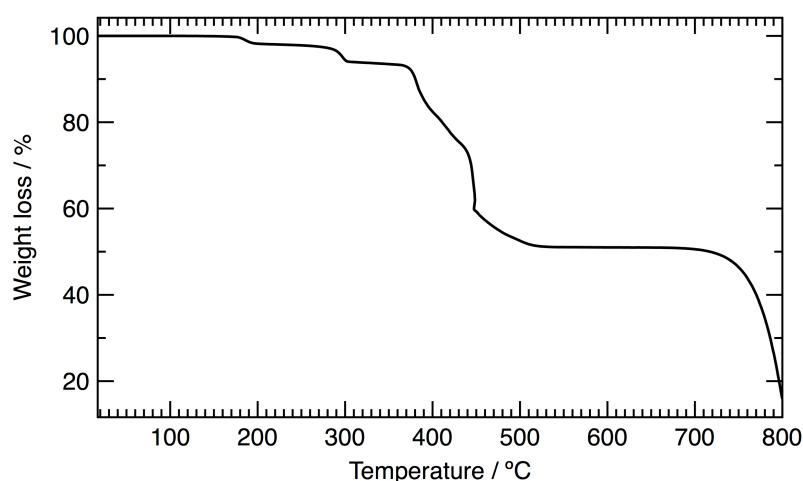


Figure 2.4. Thermogram of $[\text{Mo}_8\text{O}_{22}(\text{OH})_4(\text{di-}t\text{-Bu-bipy})_4]$ (**2.2**).

2.2.5. SCANNING ELECTRON MICROSCOPY

Scanning Electron Microscopy studies on the octanuclear complex $[\text{Mo}_8\text{O}_{22}(\text{OH})_4(\text{di-}t\text{-Bu-bipy})_4]$ (**2.2**) were performed for all products obtained from the various synthetic methods mentioned in previous sections (Figure 2.1). This was performed so as to further confirm the structural similarities between the various products. For simplicity, the results presented in this sub-section correspond solely to the material prepared using method D.

SEM studies were performed on a representative portion of **2.2**, with the results revealing that the material is homogeneously composed of block-like crystallites with a wide range of sizes (Figure 2.5). Even though small size

crystals were predominant in the bulk material, larger crystals with sizes which could achieve *ca.* 10 μm \times 10 μm \times 10 μm were present (Figure 2.5, *right*). Indeed, the presence of these larger crystals of the material was the crucial step that allowed the detailed structural characterization using single-crystal X-ray diffraction described in section 2.2.6.

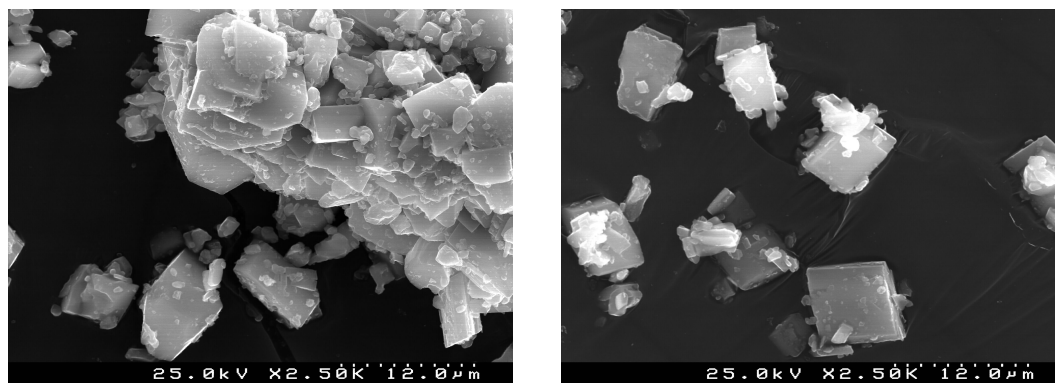


Figure 2.5. Scanning electron microscopy studies on representative portions of $[\text{Mo}_8\text{O}_{22}(\text{OH})_4(\text{di-}t\text{-Bu-bipy})_4]$ (2.2). Images collected on a Hitachi S4100 equipment at an operating energy work of 25 kV. Magnification of 25000x.

2.2.6. X-RAY DIFFRACTION: CRYSTAL STRUCTURE DESCRIPTION

As mentioned in the previous sub-section, single crystals of 2.2 suitable for X-ray diffraction were obtained by the reaction of MoO_3 and di-*t*-Bu-bipy in water at 160 $^\circ\text{C}$ for 3 days (method D). Due to the very small dimensions of the isolated crystals, X-ray diffraction at high angles was poor.^[151] Analysis of the available data set produced, nevertheless, a structural model fully consistent with the remaining characterization data that includes powder X-ray diffraction of the microcrystalline powders obtained from methods A to D (Figure 2.10, page 76).

Compound 2.2 crystallizes as discrete centrosymmetric octanuclear units, being formulated as $[\text{Mo}_8\text{O}_{22}(\text{OH})_4(\text{di-}t\text{-Bu-bipy})_4]$ on the basis of the crystallographic studies in conjunction with elemental analysis. The octanuclear complex can be divided into two distinct sections (Figure 2.6a): the inner core, composed of four Mo^{6+} centers, $\text{Mo}_4\text{O}_8(\mu_3\text{-OH})_2(\mu_2\text{-O})_2$, is purely inorganic and is attached to two peripheral symmetry-related oxo-bridged dinuclear units, each containing *N,N'*-chelated di-*t*-Bu-bipy moieties in the coordination spheres of the metal centers.

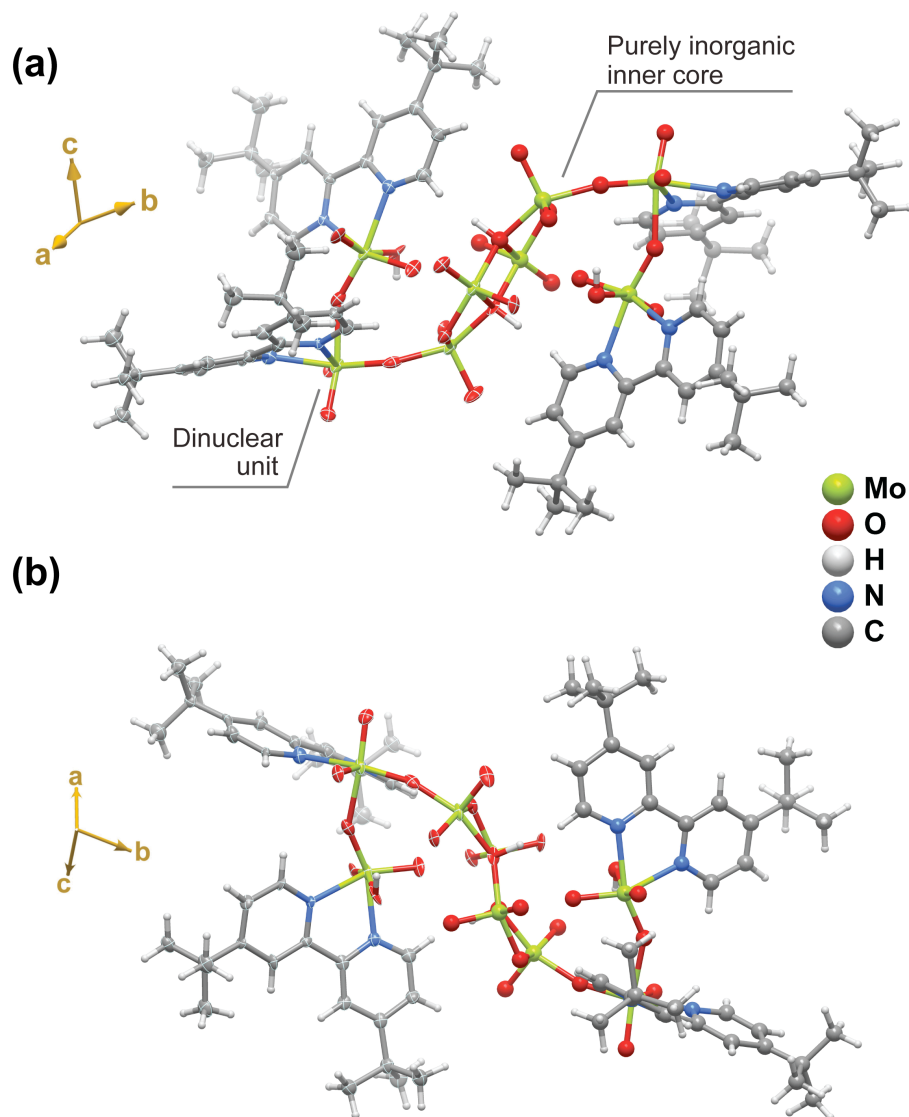


Figure 2.6. Schematic representation of the centrosymmetric $[\text{Mo}_8\text{O}_{22}(\text{OH})_4(\text{di-}t\text{-Bu-bipy})_4]$ molecular unit viewed in perspective along two distinct crystallographic directions. Atoms belonging to the asymmetric unit are represented as thermal ellipsoids drawn at the 30% probability level. Hydrogen atoms are represented as small spheres with arbitrary radii.

Due to the steric repulsion associated with these bulky organic ligands, the octanuclear complex adopts a highly distorted form strongly resembling an “S”-shaped molecular unit. The complex is composed of four crystallographically independent Mo^{6+} centres: Mo1 and Mo2 compose the aforementioned $\text{Mo}_4\text{O}_8(\mu_3\text{-OH})_2(\mu_2\text{-O})_2$ inorganic core, while Mo3 and Mo4 are peripheral to this core, each being coordinated to one N,N' -chelated di-*t*-Bu-bipy ligand (Figure 2.7). Mo1 and Mo2 centers exhibit significantly distorted square pyramidal coordination environments with the overall Mo–O bond lengths ranging from 1.688(14) to 2.283(14) Å (Figure 2.7a), and the *cis* O–Mo–O_{basal} and O–Mo–O_{apical} polyhedral angles lying in the 70.9(6)–102.6(7)° and 99.8(7)–107.5(8)° ranges, respectively.^[151]

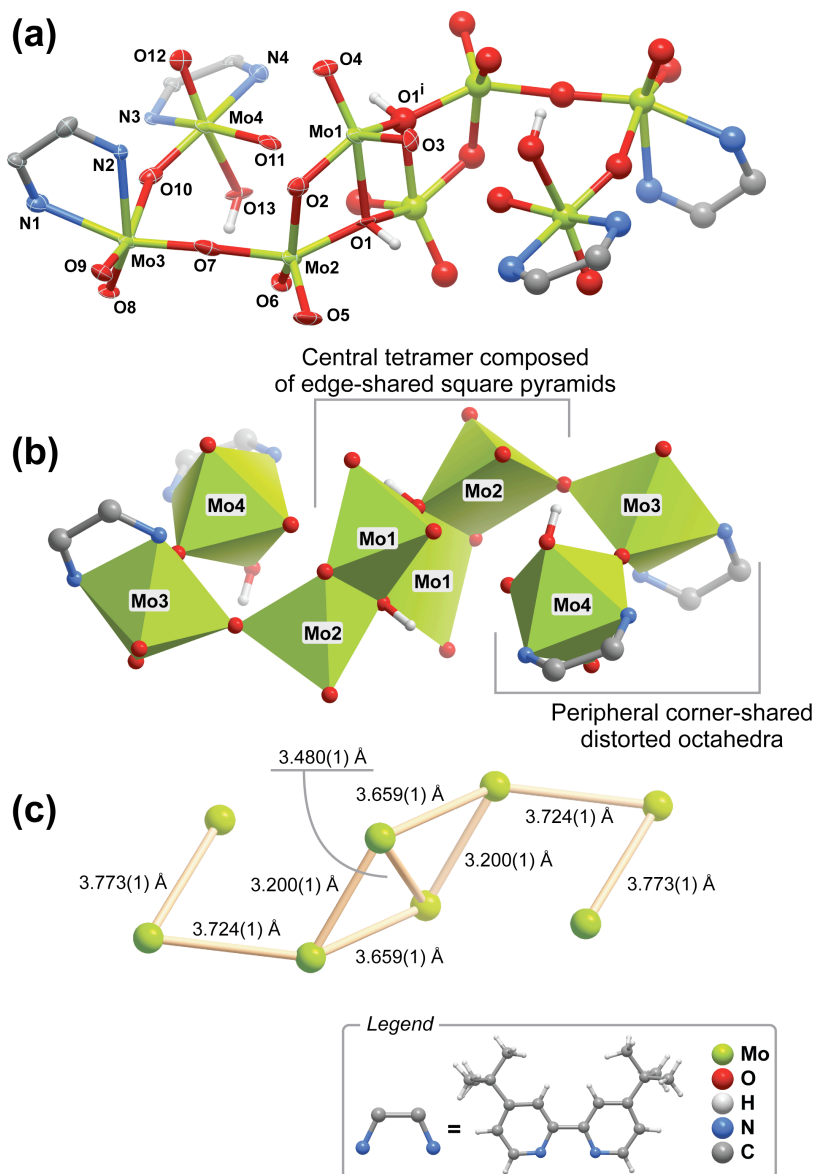


Figure 2.7. (a) Detailed view of the octanuclear core of the centrosymmetric $[\text{Mo}_8\text{O}_{22}(\text{OH})_4(\text{di-}t\text{-Bu-bipy})_4]$ molecular unit. Atoms belonging to the asymmetric unit are represented as thermal ellipsoids drawn at the 30% probability level. Hydrogen atoms are represented as small spheres with arbitrary radii. The labelling scheme is provided for all atoms composing the first coordination spheres of the four crystallographically independent Mo^{6+} centres. (b) Polyhedral representation of the same octanuclear core. (c) Intermetallic distances and angles in the represented coordination polyhedra. Symmetry transformation used to generate equivalent atoms: (i) $1-x, 2-y, -z$.

The $\{\text{MoO}_5\}$ coordination environment of Mo1 is significantly more distorted than that of Mo2 due to its close proximity to a symmetry-related (by inversion) Mo1 [$\text{Mo1}\cdots\text{Mo1}$ distance of $3.480(1)$ Å, Figure 2.7c]. This creates a significant electrostatic repulsion between the two spatially close Mo^{6+} cores, concomitantly leading to a highly distorted coordination environment.

The $\text{Mo}_4\text{O}_8(\mu_3\text{-OH})_2(\mu_2\text{-O})_2$ inorganic core is composed of a truly unique assembly of four $\{\text{MoO}_5\}$ distorted square pyramids connected to each other *via* edge-sharing, with the $\text{Mo}\cdots\text{Mo}$ distances ranging from 3.200(1) to 3.659(1) Å (Figures 2.7b and c). A search in the Cambridge Structural Database (CSD)^{[36][37]} version 5.34 (November 2013 with 3 updates) revealed the existence of only a handful of structures containing edge-shared $\{\text{MoO}_5\}$ polyhedra, in particular, various assemblies of three $\{\text{MoO}_5\}$ fused to an octahedron,^{[152][153][154]} or two $\{\text{MoO}_5\}$ fused to two octahedra.^{[60][155]} Compound 2.2 was the first compound described in the literature with an inorganic core based on four edge-fused $\{\text{MoO}_5\}$ units.^[151]

Another interesting feature concerns the fact that the $\text{Mo}=\text{O}$ apical bonds of the Mo1 and Mo2 polyhedra are *cis* to each other with respect to the mean plane of the two bases of the pyramids (Figure 2.7b). Even though the Mo1 coordination environment is more distorted than that of Mo2, the two Mo^{6+} centers are raised from the average coordination basal planes by approximately the same distance (0.42 Å for Mo1 and 0.49 Å for Mo2).

The two remaining Mo^{6+} centers, Mo3 and Mo4, exhibit highly distorted octahedral $\{\text{MoN}_2\text{O}_4\}$ coordination environments, with each being coordinated to one *N,N'*-chelated di-*t*-Bu-bipy ligand and four oxygen-containing groups. In Mo3 two of these oxygens belong to μ_2 -bridging oxido groups [establishing connections to the inorganic core (O7) and to the neighboring Mo4 metal center (O10), Figure 2.7a]. For Mo4 one of these oxygen-based groups is a terminal charge-balancing hydroxyl moiety (O13, Figure 2.7a). The octahedral coordination environments of Mo3 and Mo4 are highly distorted due to the presence of two $\text{Mo}=\text{O}$ groups in their coordination spheres, which exert a marked *trans* effect on the coordination polyhedra by displacing the metal cations from their geometrical centers: for the two coordination polyhedra, while the $\text{Mo}-(\text{N},\text{O})$ bond lengths range from 1.683(15) to 2.300(17) Å, the *cis* and *trans* $(\text{N},\text{O})-\text{Mo}-(\text{N},\text{O})$ internal octahedral angles are found in the 69.0(6)–108.2(7)° and 151.8(7)–161.6(6)° ranges, respectively. Because the connections between adjacent $\{\text{MoN}_2\text{O}_4\}$ octahedra, and between the $\text{Mo}_4\text{O}_8(\mu_3\text{-OH})_2(\mu_2\text{-O})_2$ inorganic core and Mo3, are based on corner sharing (Figure 2.7b), the $\text{Mo}\cdots\text{Mo}$ separations are concomitantly longer: 3.724(1) and 3.773(1) Å for $\text{Mo}2\cdots\text{Mo}3$ and $\text{Mo}3\cdots\text{Mo}4$, respectively (Figure 2.7c).^[151]

Despite the highly asymmetric shape of the octanuclear complex 2.2, the close packing of individual units is relatively efficient, being moderated by a number of supramolecular contacts. As shown in Figure 2.8a, individual complexes close pack in a parallel fashion along the [010] direction of the unit cell in such a way that the inorganic cores are clearly separated from the external hybrid portion of the complexes. In addition, the terminal O13 hydroxyl groups bound to Mo4 are engaged in relatively strong $\text{O}-\text{H}\cdots\text{O}$ hydrogen bonding interactions with the O8 oxido groups of an adjacent inorganic core (Figure 2.8b).

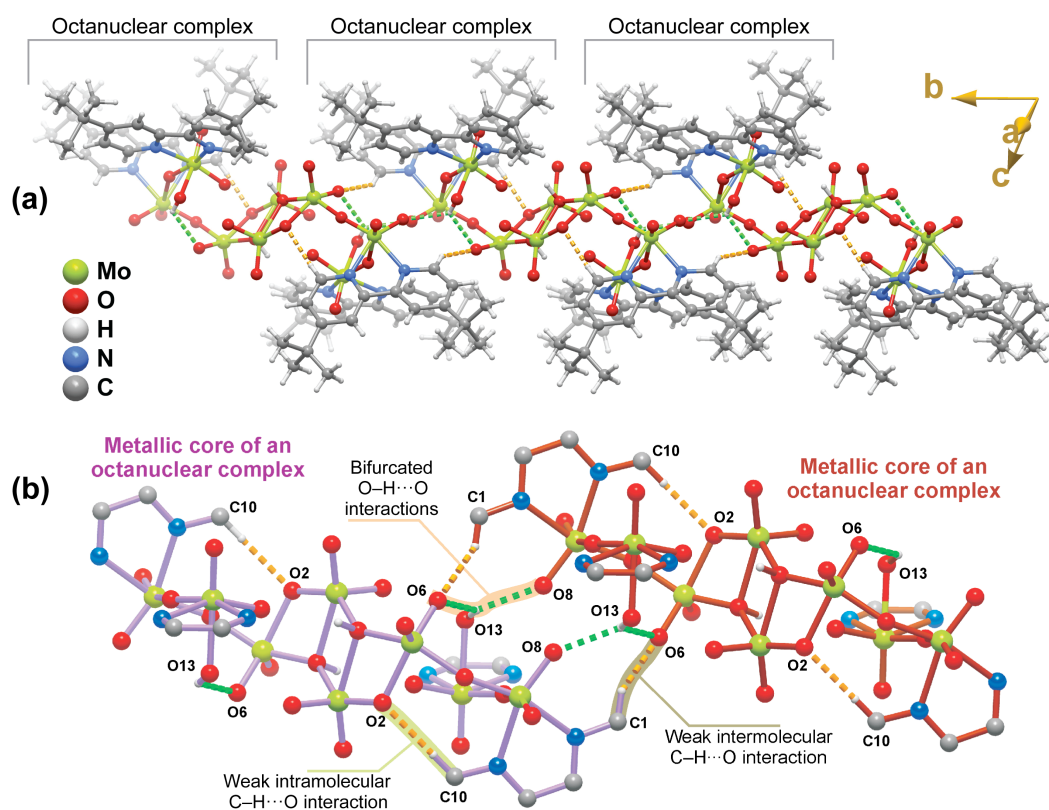


Figure 2.8. (a) Schematic representation of the way adjacent octanuclear $[\text{Mo}_8\text{O}_{22}(\text{OH})_4(\text{di-}t\text{-Bu-bipy})_4]$ complexes close pack along the $[010]$ direction of the unit cell of compound 2.2, with the process being mediated by various intra- and intermolecular weak $\text{C-H}\cdots\text{O}$ interactions and bifurcated $\text{O-H}\cdots\text{O}$ hydrogen bonds. (b) Detailed view of the supramolecular contacts present between the octanuclear core of adjacent centrosymmetric $[\text{Mo}_8\text{O}_{22}(\text{OH})_4(\text{di-}t\text{-Bu-bipy})_4]$ molecular units. For geometrical details on the represented contacts see reference [151]. Symmetry codes associated with symmetry-equivalent atoms have been omitted for clarity.

The strengths of these inter-core connections are further cooperatively increased by the existence of a number of intermolecular $\text{C-H}\cdots\text{O}$ interactions: for example, the C1 atom of a coordinated *di-t-Bu-bipy* ligand interacts with the O6 oxido group *via* a strong [$d_{\text{C}\cdots\text{O}} = 3.17(2) \text{ \AA}$] and relatively directional [$\angle(\text{CHO}) = 146^\circ$] contact. A number of weak intramolecular $\text{C-H}\cdots\text{O}$ contacts exist in the crystal structure (see Table 2.1 for geometrical details on the hydrogen bonds). The combination of all of these supramolecular contacts leads to the formation of robust one-dimensional supramolecular chains running parallel to the *b*-axis of the unit cell. Individual chains close pack in the *ac* plane of the unit cell mediated by purely geometrical reasons. This occurs because the contacts between spatially-close *di-t-Bu-bipy* organic molecules are, essentially, of the van der Waals type (Figure 2.9).

Table 2.1. Hydrogen bonding and close contact (both inter- and intramolecular) geometrical details for $[\text{Mo}_8\text{O}_{22}(\text{OH})_4(\text{di-}t\text{-Bu-bipy})_4]$ (2.2).^a

D–H \cdots A	d(D \cdots A) / Å	$\angle(\text{DHA}) / ^\circ$
O13–H13 \cdots O2 ⁱ	2.73(2)	121
O13–H13 \cdots O6	2.93(2)	124
C10–H10 \cdots O2 (<i>intramolecular</i>)	3.28(2)	169
C1–H1 \cdots O6 ⁱ (<i>intermolecular</i>)	3.17(2)	146
C7–H7 \cdots O9 ⁱⁱ (<i>intermolecular</i>)	3.05(2)	127
C16–H16C \cdots O9 ⁱⁱ (<i>intermolecular</i>)	3.43(2)	165
C32–H32B \cdots O4 ⁱⁱⁱ (<i>intermolecular</i>)	3.49(2)	153

^a Symmetry transformations used to generate equivalent atoms: (i) $1-x, 1-y, -z$; (ii) $2-x, 1-y, -z$; (iii) $1-x, 1-y, 1-z$.

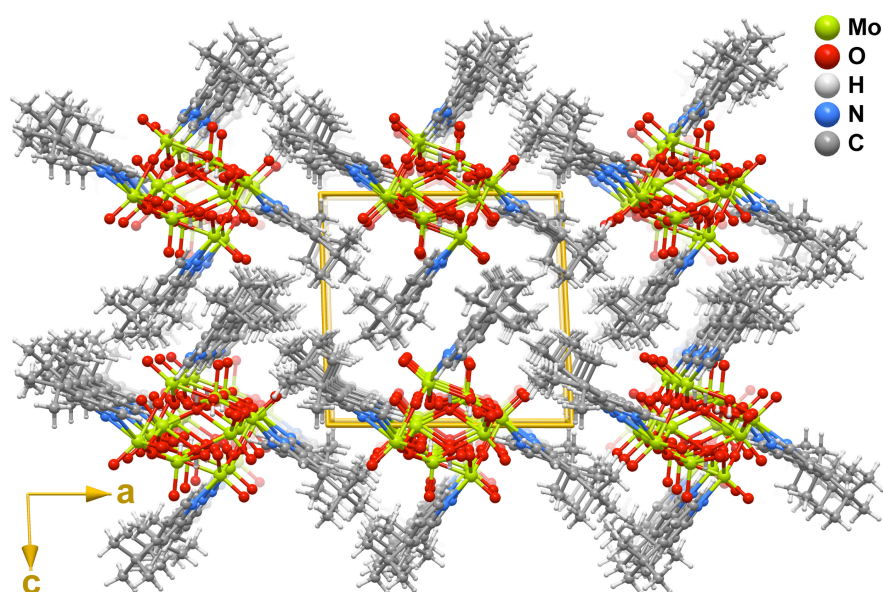


Figure 2.9. Crystal packing of $[\text{Mo}_8\text{O}_{22}(\text{OH})_4(\text{di-}t\text{-Bu-bipy})_4]$ (2.2) viewed in perspective along the $[010]$ direction of the unit cell. Weak C–H \cdots O interactions and O–H \cdots O hydrogen bonds, which mediate the crystal packing along the b -axis, have been omitted for clarity.

2.2.7. POWDER X-RAY DIFFRACTION STUDIES

The powder X-ray diffraction patterns depicted on Figure 2.10 indicate that the white powder isolated on each employed synthetic method is microcrystalline and a monophasic material. Moreover, these patterns agree well

with a simulation based on the single-crystal X-ray diffraction structure of (2.2) (solved from small crystals obtained using method D). It is, thus, possible to infer that the $[\text{Mo}_8(\text{OH})_4\text{O}_{22}(\text{di-}t\text{-Bu-bipy})_4]$ molybdenum complex determined by single-crystal X-ray diffraction is representative of the bulk 2.2 materials isolated in methods A to D. This assumption was further confirmed using the remaining characterization data: elemental analysis, FT-IR, solid-state NMR and thermogravimetric analysis.

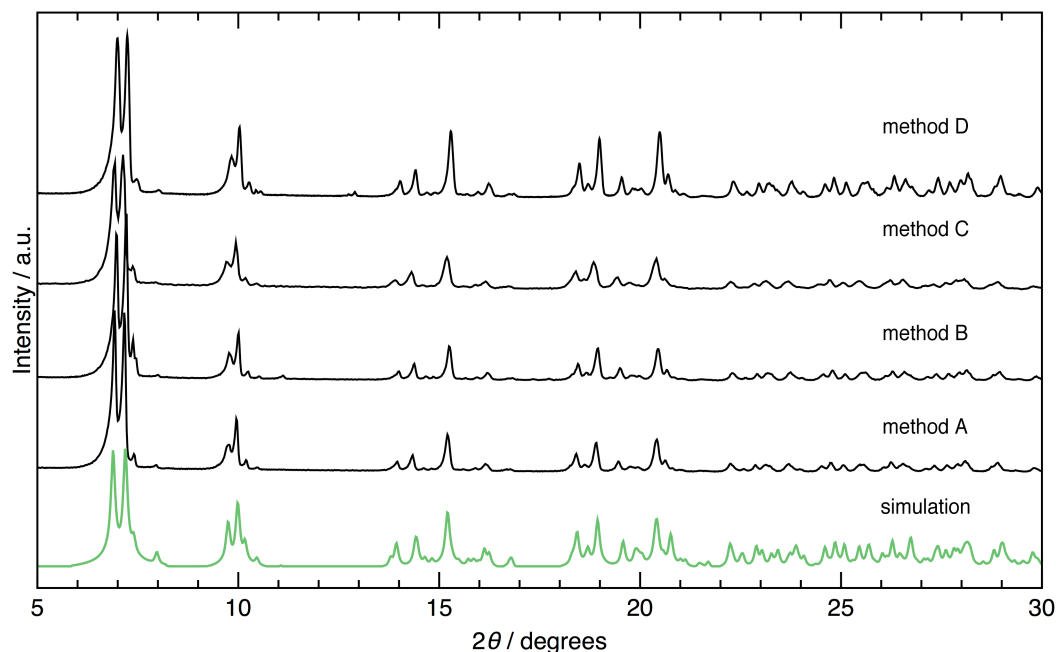


Figure 2.10. Comparison between the experimental powder X-ray diffraction patterns of the white solid products obtained from methods A to D, with a simulation based on the single-crystal X-ray structure of $[\text{Mo}_8(\text{OH})_4\text{O}_{22}(\text{di-}t\text{-Bu-bipy})_4]$ (2.2).

2.2.8. CATALYSIS

This section summarizes the results obtained when using $[\text{Mo}_8(\text{OH})_4\text{O}_{22}(\text{di-}t\text{-Bu-bipy})_4]$ (2.2) as a catalyst in epoxidation reactions of DL-limonene (Lim) and methyl oleate (Ole) into 1,2-epoxy-*p*-menth-8-ene (LimOx) and 9,10-epoxystearate (OleOx), respectively.

2.2.8.1. DL-LIMONENE (Lim)

The catalytic performance of $[\text{Mo}_8(\text{OH})_4\text{O}_{22}(\text{di-}t\text{-Bu-bipy})_4]$ (2.2) in the olefin epoxidation was investigated at 55 °C for the substrate Lim while using TBHP_{dec} (5.5 M in decane) or TBHP (either in decane or water) as the oxygen source. Depending on the oxidant media and the co-solvent choice, five different systems (or series) were investigated:

- i) TBHP_{dec}/no co-solvent;
- ii) TBHP_{dec}/DCE;

- iii) TBHP/DCE;
- iv) TBHP_{dec}/BTF;
- v) TBHP/EtOH.

Details on the experimental procedures used to prepare systems iii) and v) are described in last chapter of this thesis.

For the first three series LimOx was always the main product, formed in similar amounts after 24 h of reaction. The selectivity range stood between 84 and 89%, with conversions of 94 to 96%, respectively (Figure 2.11). In the absence of 2.2 LimOx was formed in less than 4% yield after 24 h of reaction.

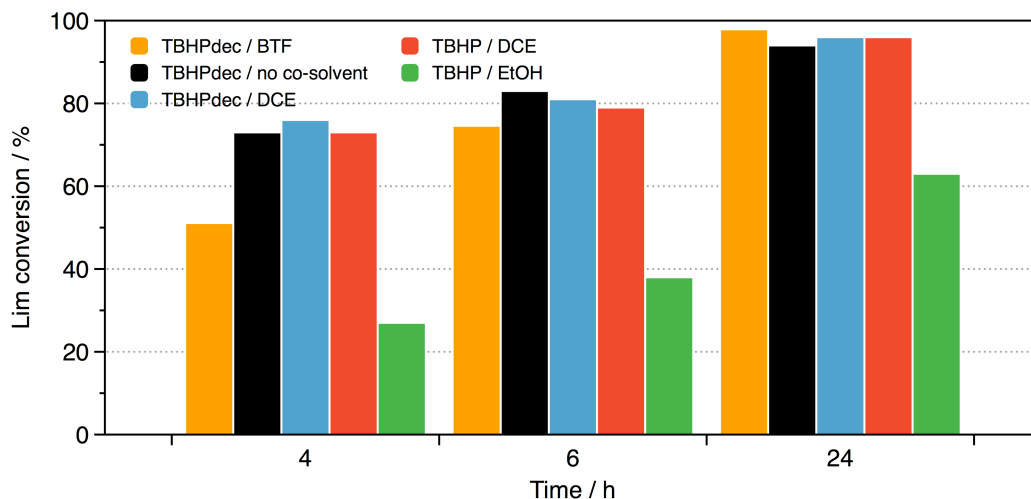


Figure 2.11. Kinetic profiles for the epoxidation reaction of Lim at 55 °C in the presence of $[\text{Mo}_8(\text{OH})_4\text{O}_{22}(\text{di-}t\text{-Bu-bipy})_4]$ (2.2).

- TBHP_{dec} series

Comparing the TBHP_{dec} conditions with no co-solvent or with DCE, it was found that no significant dilution effects were present in these cases. For the TBHP_{dec}/BTF system, the initial reaction rate of Lim was lower than that observed for TBHP_{dec}/DCE, although similarly high conversions were reached after 6 h reaction; the product LimOx and the by-product LimDiOx were formed in 76% and 22% yields at 98% conversion and 24 h reaction, respectively. At this point the by-product LimDiol was not detected. This decrease in LimOx selectivity and concomitant increase of LimDiOx suggests that LimOx is an intermediate product in the formation of LimDiOx. In fact, the selectivity to LimOx tends to decrease for conversions of Lim greater than *ca.* 80% (Figure 2.12): for all tested reaction systems (excluding TBHP_{dec}/BTF) this trend is accompanied by the formation of a new by-product, denoted as LimDiol, reaching a maximum yield at 24 h of 11% for the TBHP_{dec}/no co-solvent system.

Noteworthy, with the TBHP_{dec}/BTF system the initial reaction rate of Lim was lower than that observed for TBHP_{dec}/DCE. The reason for this may be intrinsic to the differences in the solvent polarities, *i.e.*, BTF has a dipole moment of *ca.* 2.86 D while that for DCE is *ca.* 1.83 D.

- TBHP series

In the TBHP/DCE system, for which the oxidant solution was prepared by mixing 70% aqueous TBHP and DCE, followed by the removal of excess water using MgSO_4 , besides the desired product LimOx, both by-products LimDiOx and LimDiol were formed at 24 h, albeit in only 8% yield at 24 h for LimDiOx (Figure 2.12). These results indicate very high regioselectivity toward the epoxidation of the endocyclic double bond relative to the exocyclic one. As in the previous TBHP_{dec}/BTF system there is a decrease in LimOx selectivity with the concomitant increase in selectivities to the secondary by-products LimDiol and LimDiOx. These results suggest that LimOx is not just an intermediate product in the formation of LimDiOx (e.g., TBHP_{dec}/BTF) but also an intermediate product to LimDiol. This LimDiol formation may take place *via* the hydrolysis of LimOx with residual water present in the reaction media. Accordingly, the presence of water influences product distribution by favouring the LimOx to LimDiol conversion, which may take place in parallel with the LimOx to LimDiOx conversion.

The comparable LimOx yields at 24 h for the TBHP_{dec}/BTF, TBHP_{dec}/DCE and TBHP/DCE series suggest that it may be feasible to use TBHP_{aq} (coupled with a drying procedure) instead of TBHP_{dec}, and to substitute decane (b.p. *ca.* 174 °C) for solvents with lower boiling points, thereby avoiding energy-intensive separation/purification processes.

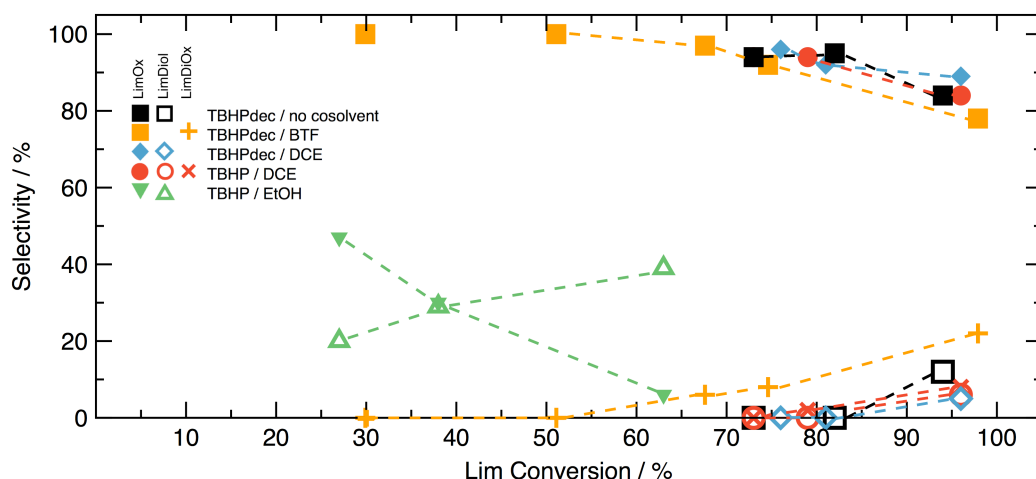


Figure 2.12. Dependence of the selectivity to LimOx, LimDiol and LimDiOx on Lim conversion for the five different series employed using $[\text{Mo}_8(\text{OH})_4\text{O}_{22}(\text{di-}t\text{-Bu-bipy})_4]$ (2.2) as the catalyst. Solid-filled symbols, white-filled symbols and math symbols represent the LimOx, LimDiol and LimDiOx results, respectively.

- TBHP series with bioderived solvents

Aiming at the use of more environmentally attractive solvents, DCE and BTF were replaced with a bioderived alternative. The epoxidation of Lim was, in this way, carried out at 55 °C using the TBHP/EtOH series and

[Mo₈(OH)₄O₂₂(di-*t*-Bu-bipy)₄] (2.2) as the catalyst. Results showed that the reaction of Lim was considerably slower than when using TBHP/DCE (Figure 2.11), and selectivity to LimOx decreased considerably from 47% (at 27% conversion) to just 6% (at 63% conversion reached at 24 h reaction). It was further observed the concomitant formation of several by-products that include LimDiol (39% selectivity at 63% conversion, Figure 2.12). In the absence of the catalyst, but under similar reaction conditions, conversion of Lim was less than 3% Lim (reached at 24 h). A possible explanation for the slower reaction of Lim when using EtOH as the co-solvent instead of (non-coordinating) DCE concerns the fact that the EtOH molecules may compete with the reagents in the coordination to the metal centre.^{[83][156][157]}

The enhanced formation of the secondary product LimDiol for the TBHP/EtOH series may be partly due to the less efficient removal of water from this mixture prior to the catalytic reaction (see Experimental chapter - Catalysis section). Besides LimDiol, ethoxy alcohol products were also formed possibly *via* the ethanolysis of the epoxide products. The formation of such products was reported for the reaction of LimOx with ethanol in the presence of BF₃·O(C₂H₅)₂ or EtONa.^[158]

Independent of the employed conditions, all tested reaction systems were always biphasic solid-liquid mixtures. After each reaction the solid phase was recovered and characterized by ATR FT-IR. As shown in Experimental chapter correspondent section, all spectra from the recovered solids are similar to that of the fresh catalyst. The solid recovered from the catalytic reaction using TBHPdec/DCE was reused in a second 24 h batch run, under similar reaction conditions. The results for LimOx selectivity (89 / 88% at 74 / 95% conversion, respectively) were comparable to those registered for first run at 6 / 24 h: 92 / 89% at 79 / 96% conversion, respectively. The “productive consumption” of TBHP was ascertained by iodometric titrations, which indicated that no measurable decomposition of TBHP (to give *tert*-butanol and molecular oxygen) took place in the presence of 2.2 (without olefin) at 55 °C.

- Investigation into the nature of the catalytic reaction

The homogeneous or heterogeneous nature of the catalytic reaction performed using TBHP/DCE was checked by filtering the reaction mixture through a 0.2 µm PTFE membrane after 1 h and then leaving the filtrate to react at 55 °C for a further 5 h. The increment in conversion between 1 and 6 h was 32%, which is comparable to that observed in the presence of the solid catalyst (36%). Hence, it is inferred that the catalytic reaction takes place in the homogeneous phase. Additional tests revealed, however, that [Mo₈(OH)₄O₂₂(di-*t*-Bu-bipy)₄] (2.2) did not dissolve completely, even when the amount charged to the reactor was decreased from 1 mol % (Mo/Lim) to 0.2 mol %. The kinetic behavior of the catalytic reaction in the homogeneous phase using 0.2 mol% was similar (94 / 91% LimOx selectivity at 74 / 91% conversion for 6 / 24 h, respectively) to that measured for 1 mol % (94 / 84% LimOx selectivity at 79 / 96% conversion, respectively).

- Catalytic behaviour of the precursors

The catalytic performance of the octanuclear complex present in **2.2** was compared with that of MoO₃ and a commercial ammonium heptamolybdate [(NH₄)₆Mo₇O₂₄]·4H₂O, 99% p.a., Merck], under similar reaction conditions to those of the TBHP_{dec}/DCE series. *Please note:* the MoO₃ inorganic compound was freshly prepared from MoO₂Cl₂ under the same experimental conditions of method D, but while omitting the organic ligand.

After 6 h of reaction, conversion of Lim was negligible for both MoO₃ and the heptamolybdate source. When compared with other previously investigated oxomolybdenum complexes, or their carbonyl precursors tested as catalysts in the same reaction, using TBHP as an oxidant at 55 °C (Introduction, Table 4), the catalytic performance of **2.2** is outstanding concerning the yield of LimOx.

2.2.4.2. METHYL OLEATE (Ole)

The catalytic performance of [Mo₈(OH)₄O₂₂(di-*t*-Bu-bipy)₄] (**2.2**) was further investigated at 55 °C for the production of bio-based epoxidized vegetable oils. Methyl oleate (Ole, see Introduction for details) was the model substrate, TBHP_{dec} the oxygen donor and DCE, BTF, ethyl acetate (EtOAc), or acetonitrile (CH₃CN) the co-solvents used. The main reaction product was independent of the solvent choice and methyl 9,10-epoxystearate (OleOx) was always the sole product formed in at least 91% selectivity and at high conversions (up to 94%, Figure 2.13, *bottom*). Without a catalyst and under similar reaction conditions the reaction did not occur.

As shown in Figure 2.13 (*top*), the highest initial catalytic activity was found for DCE and BTF. The highest OleOx yield (*i.e.*, 92%) at the highest conversion (*i.e.*, 99%) was registered for the latter co-solvent. When using EtOAc or CH₃CN as co-solvents, OleOx selectivity was 95–97% at *ca.* 60% conversion (24 h reaction).

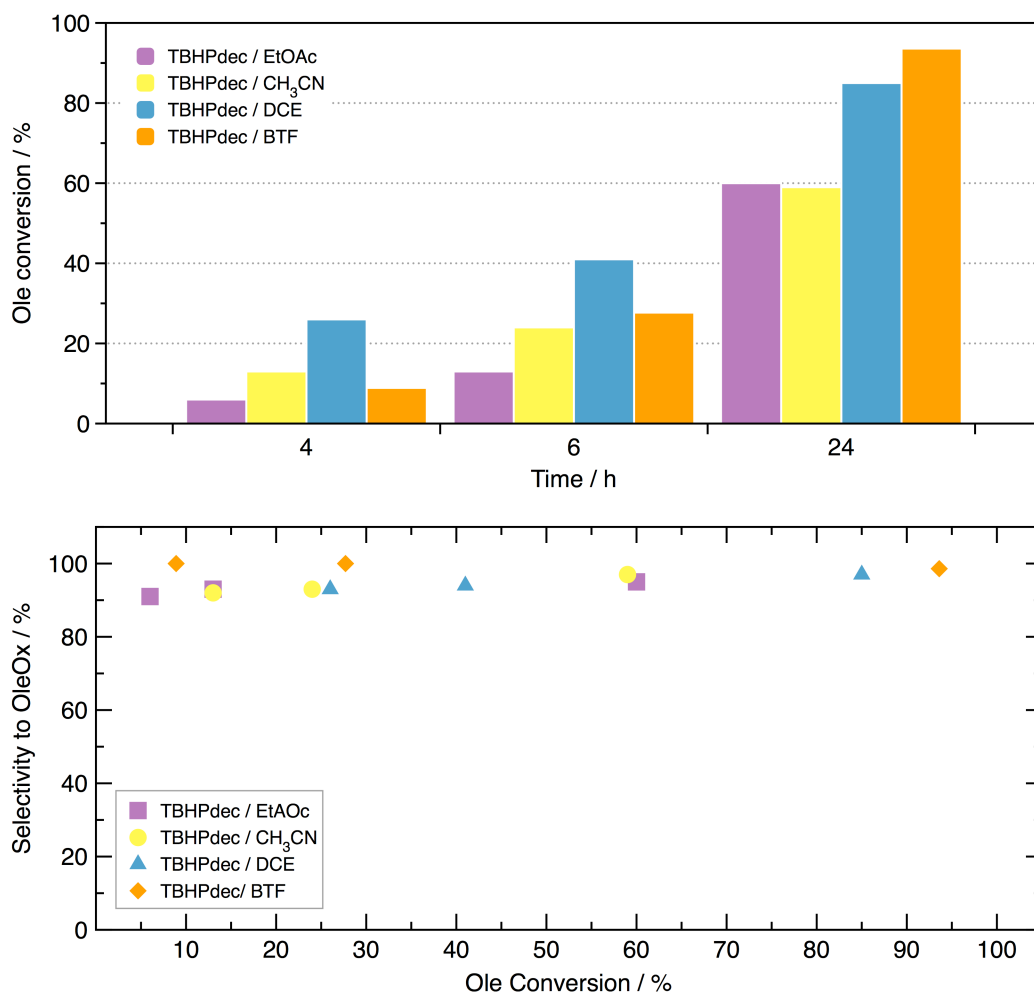


Figure 2.13. (Top) Kinetic profiles for the catalytic reaction of Ole using $[\text{Mo}_8(\text{OH})_4\text{O}_{22}(\text{di-}t\text{-Bu-bipy})_4]$ (2.2) as the catalyst. (Bottom) Dependence of the selectivity toward OleOx in the catalysed Ole conversion.

All catalytic systems were biphasic. The solid phase was once again recovered after a 24 h batch and its ATR FT-IR spectrum was collected. These studies unequivocally confirmed that all recovered solids were structurally similar to 2.2 (Experimental chapter - Catalysis section). The fact that the catalytic reaction is slower when using EtOAc and CH₃CN as the co-solvent may be due to their ability to compete with the reagents in the coordination to the metal centre. This was already observed for the catalytic reaction of Lim when employing EtOH as the co-solvent (see previous sub-sections).

A search in the literature shows that the aforementioned study is the most complete reported to date for the epoxidation of pure Ole using a molybdenum-based catalytic system.^[151] A handful of research groups have, however, investigated the epoxidation of a mixture of Ole and methyl lineolate (Introduction, section III.6.1)

As described in the crystallographic studies, compound 2.2 consists of a molybdenum oxide/organic assembly strongly resembling a metallic cluster. In this way, steric effects may partly explain the higher reactivity of Lim in comparison to the bulkier substrate Ole while using similar reaction conditions

(e.g., TBHP_{dec}/DCE). On the other hand, the unique structural features of **2.2** may hinder the various catalyst auto-degradation pathways, ultimately explaining the fairly high catalyst stability.

2.2.9. BY-PRODUCTS of the SYNTHESIS of [Mo₈O₂₂(OH)₄(di-*t*-Bu-bipy)₄] (**2.2**)

In methods A to C, for which the metal precursor was the complex [MoO₂Cl₂(di-*t*-Bu-bipy)] (**2.2**) (Figure 2.1), it was possible to isolate a white solid suspended in an acidic pink solution (pH = 2). To investigate the contents of the aqueous mother liquor from these reactions, the solvent was allowed to slowly evaporate. Irregular, poorly-formed crystals of the 4,4'-di-*tert*-butyl-2,2'-dipyridinium dichloride salt, (H₂-di-*t*-Bu-bipy)Cl₂, were isolated as a minor secondary product. This result allowed a better understanding of the whole reactive system: for example, it allowed a quick assessment if this secondary product was, or otherwise, a contaminant when the main product **2.2** was isolated (using powder X-ray diffraction screening tests); if this was the case, it permitted to derive the better experimental procedure to eliminate this secondary product from the main one. The characterization performed for (H₂-di-*t*-Bu-bipy)Cl₂ is presented in the Experimental chapter.

The reaction between MoO₃ and di-*t*-Bu-bipy (Figure 2.1, method D) led to the formation of the same octanuclear [Mo₈O₂₂(OH)₄(di-*t*-Bu-bipy)₄] (**2.2**) product, which was isolated as a white solid suspended in a colourless aqueous mother liquor with pH = 6. Slow evaporation of this solution led to the isolation of single crystals formulated as the dinuclear complex [Mo₂O₆(di-*t*-Bu-bipy)₂] (**2.3**). The distinct structural features and its potential use in oxygen atom transfer processes motivated the isolation of this dimer in larger quantities, with the main objective to perform a more detailed structural characterization and tests as catalyst in olefin epoxidation. The results from these studies are presented in the following sub-section.

2.3. [Mo₂O₆(di-*t*-Bu-bipy)₂]·2H₂O (**2.3**)

The dinuclear complex [Mo₂O₆(di-*t*-Bu-bipy)₂] present in compound **2.3** (which contains two additional water molecules besides the molecular complex) was repeatedly obtained as a by-product (≅ 5 % yield) from the hydrothermal reaction of MoO₃ and di-*t*-Bu-bipy (method D, Figure 2.1). The complex was structurally characterized by single-crystal X-ray diffraction analysis and tested as a catalyst in the epoxidation reaction of several non-functionalized olefins using TBHP_{dec} as the oxidant.^[159] This section presents the details of the structure and catalytic performance of [Mo₂O₆(di-*t*-Bu-bipy)₂]·2H₂O (**2.3**).

2.3.1. SYNTHESIS

Single crystals of $[\text{Mo}_2\text{O}_6(\text{di-}t\text{-Bu-bipy})_2]\cdot 2\text{H}_2\text{O}$ (**2.3**) were abundantly isolated from the slow evaporation (at ambient temperature) of the filtered colourless aqueous mother liquor (pH = 6) isolated from method D employed to prepare $[\text{Mo}_8(\text{OH})_4\text{O}_{22}(\text{di-}t\text{-Bu-bipy})_4]$ (**2.2**).

Forcing the removal of the solvent by using a vacuum line, the same product was also isolated. Using this faster approach a microcrystalline powder of **2.3** was instead obtained (Figure 2.1, page 65). This solid was washed with diethyl ether and characterized by elemental analysis, the spectroscopic methods FT-IR and ^1H NMR, and by powder X-ray diffraction.

2.3.2. FT-IR

The FT-IR spectra of the previously discussed octanuclear complex $[\text{Mo}_8\text{O}_{22}(\text{OH})_4(\text{di-}t\text{-Bu-bipy})_4]$ (**2.2**) and of the dinuclear $[\text{Mo}_2\text{O}_6(\text{di-}t\text{-Bu-bipy})_2]\cdot 2\text{H}_2\text{O}$ (**2.3**) are represented in Figure 2.14.

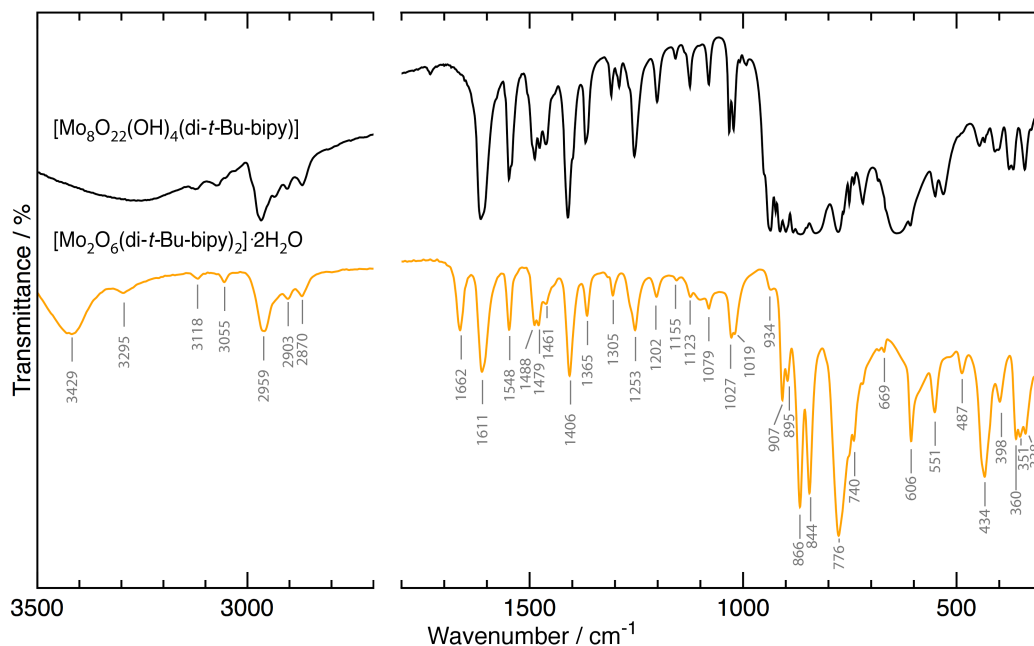


Figure 2.14. FT-IR spectra of the two products isolated using method D: the main product is the octanuclear complex present in $[\text{Mo}_8\text{O}_{22}(\text{OH})_4(\text{di-}t\text{-Bu-bipy})_4]$ (**2.2**) (top spectrum), and the secondary product is the dinuclear complex composing the crystal structure of $[\text{Mo}_2\text{O}_6(\text{di-}t\text{-Bu-bipy})_2]\cdot 2\text{H}_2\text{O}$ (**2.3**) (bottom spectrum). The spectral 2700-1700 cm^{-1} region was omitted for clarity.

The spectrum of **2.3** exhibits weak-to-medium intensity bands in the *ca.* 2800-3200 cm^{-1} spectral range, which are attributed to the aromatic and aliphatic stretching vibrations of the C-H bonds present in the di-*t*-Bu-bipy ligand.^[150] Additional vibrational modes arising from the ligand are found in the

ca. 1000-1700 cm^{-1} range: for example, the presence of the typical pyridyl ring stretching vibrational band centred at *ca.* 1611 cm^{-1} is indicative of the bidentate coordination mode of the di-*t*-Bu-bipy ligands to the Mo^{6+} centers.^{[146][114][149]} A very strong ligand band at *ca.* 844 cm^{-1} might be assigned to the out-of-plane bending $\gamma(\text{CH}-\text{CH})$ of the C-H groups composing the pyridyl aromatic rings.

The bands found in the *ca.* 840-950 cm^{-1} range, with intensity varying from the medium to the very strong, could be assigned to the typical $\nu(\text{Mo}=\text{O})$ stretching vibrational modes. A very strong band arising at *ca.* 777 cm^{-1} is typical of the $\text{Mo}_2(\mu_2\text{-O})_2$ intermetallic moiety *via* the bridging oxido groups.^{[114][113][111][160][110]}

2.3.3. POWDER X-RAY DIFFRACTION STUDIES

Figure 2.15 compares the experimental powder pattern of the microcrystalline material directly isolated from the filtrate of the reaction with a theoretical simulation based on the collected single-crystal data. The main goal was to unequivocally prove that microcrystalline solid 2.3 shared the same crystalline structure with the material isolated as single crystals. Besides some small differences related to the low level of crystallinity, there is a strong similarity between the two patterns. This is indicative that the bulk powdered material shares the same crystal structure with compound 2.3.

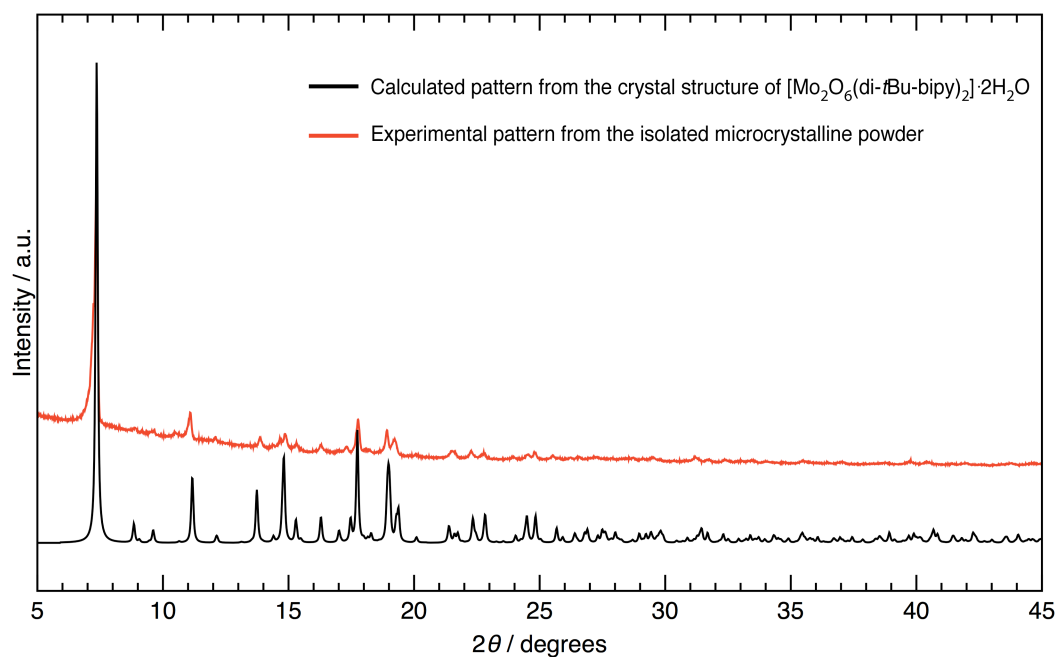
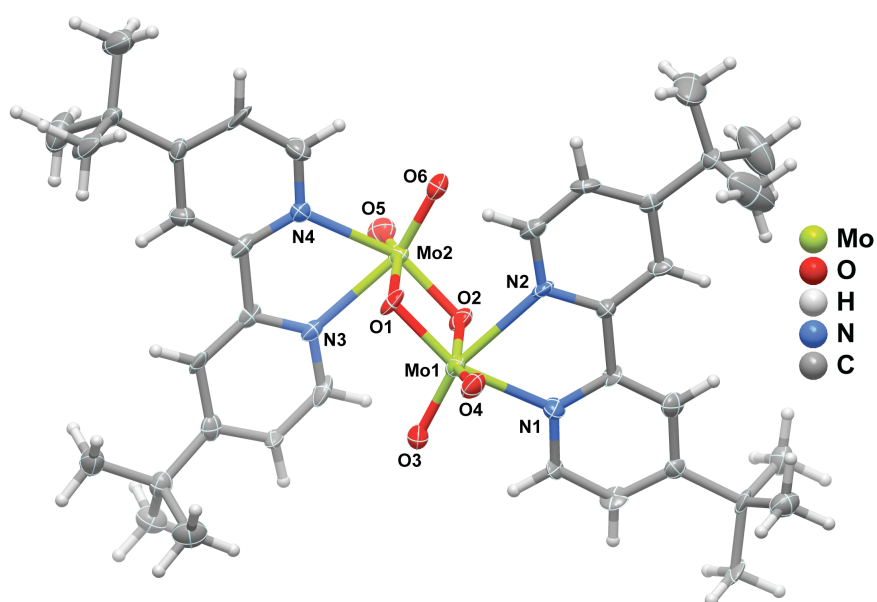


Figure 2.15. Comparison between the experimental and simulated (based on single-crystal data) powder X-ray diffraction of $[\text{Mo}_2\text{O}_6(\text{di-}t\text{-Bu-bipy})_2]\cdot 2\text{H}_2\text{O}$ (2.3). The simulation was performed using CCDC Mercury software while using a FWHM of 0.10 2θ .

2.3.4. CRYSTAL STRUCTURE DESCRIPTION

Single-crystal X-ray diffraction studies (reference ^[159] for procedure details) revealed that compound $[\text{Mo}_2\text{O}_6(\text{di-}t\text{-Bu-bipy})_2]\cdot 2\text{H}_2\text{O}$ (**2.3**) crystallizes in the monoclinic space group $P2_1/n$ with the asymmetric unit comprising a whole molecular unit of $[\text{Mo}_2\text{O}_6(\text{di-}t\text{-Bu-bipy})_2]$ (Figure 2.16) and two water molecules of crystallization strongly hydrogen bonded to the hybrid complexes. The crystallographically independent dinuclear neutral complex is approximately centrosymmetric, but the overall crystal symmetry does not reflect this local feature. This occurs because of the combined effect of i) conformational rotations associated with the large and peripheral *tert*-butyl groups attached to the N,N' -chelated di-*t*-Bu-bipy ligands, and ii) twisting around the central C–C bond of the organic molecule. Table 2.2 summarizes the selected bond lengths and angles for the coordination sphere of each Mo^{6+} centre.



refcode: TEJCES

Figure 2.16. $[\text{Mo}_2\text{O}_6(\text{di-}t\text{-Bu-bipy})_2]$ molecular unit composing the crystal structure of **2.3**. Non-hydrogen atoms are represented as thermal ellipsoids drawn at the 70% probability level, and hydrogen atoms as small spheres with arbitrary radii. Table 2.2 summarizes the most relevant bond lengths and angles.

Table 2.2. Selected bond lengths and angles for the two Mo⁶⁺ metallic centers present in the crystal structure of 2.3.

Bond lengths (Å)		Bond angles (°)	
Mo1-O1	1.805(4)	O1-Mo1-O2	77.05(18)
Mo1-O2	2.217(5)	O3-Mo1-O1	107.4(2)
Mo1-O3	1.707(4)	O3-Mo1-O2	92.6(2)
Mo1-O4	1.714(5)	O3-Mo1-O4	104.1(2)
Mo1-N1	2.277(5)	O4-Mo1-O1	105.0(2)
Mo1-N2	2.339(5)	O4-Mo1-O2	161.5(2)
		N1-Mo1-N2	68.96(18)
Mo2-O1	2.198(4)	O2-Mo2-O1	77.70(18)
Mo2-O2	1.798(4)	O5-Mo2-O1	162.7(2)
Mo2-O5	1.720(5)	O5-Mo2-O2	105.8(2)
Mo2-O6	1.716(5)	O6-Mo2-O1	90.7(2)
Mo2-N3	2.311(5)	O6-Mo2-O2	106.9(2)
Mo2-N4	2.270(5)	O6-Mo2-O5	104.0(2)
		N4-Mo2-N3	69.16(19)

A search in the literature and in the CSD^[36] showed that [Mo₂O₆(di-*t*-Bu-bipy)₂] is the first dinuclear complex for which the Mo⁶⁺ coordination environments are defined by the MoO₂(μ₂-O)₂(NN) core (where NN represents a *N,N*-chelate ligand). Removing this structural restriction, the search yields only three related complexes with cores of the MoO₂(μ₂-O)₂(NO)^{[154][161]} and MoO₂(μ₂-O)₂(OO)^[162] types (NO and OO correspond to the donor atoms from chelate ligands). All these reported complexes crystallize in either the space groups *P*₂₁/*n* or *P*₂₁/*c* (two alternate settings of the same space group). Remarkably, only [Mo₂O₆(di-*t*-Bu-bipy)₂] is not truly centrosymmetric, illustrating well the significant structural influence of the various conformations that the di-*t*-Bu-bipy organic ligands can adopt while coordinated to the metal centres.

In this way, [Mo₂O₆(di-*t*-Bu-bipy)₂] is composed of two crystallographically distinct Mo⁶⁺ centres whose coordination polyhedra are edge-shared, a feature only encountered in a handful of related molybdenum complexes.^[162] The Mo⋯Mo separation in [Mo₂O₆(di-*t*-Bu-bipy)₂] is 3.1394(8) Å, which is within the range found in the aforementioned related compounds (*ca.* 3.12–3.18 Å).

Mo1 and Mo2 exhibit almost similar highly distorted octahedral coordination environments, [MoN₂O₄]: besides the two terminal oxido groups, each metal centre is further coordinated to two μ₂-bridging oxido moieties and one *N,N'*-chelated di-*t*-Bu-bipy ligand (Figure 2.16). Because the terminal oxido groups markedly exert the well-known *trans* influence in the coordination environments (*i.e.*, each Mo⁶⁺ is displaced from the geometrical centre of the

coordination polyhedron, leading to long *trans* connections to the oxido groups), the overall geometry is highly distorted for both Mo⁶⁺: on the one hand, the Mo–(N,O) bond lengths are found in the 1.707(4) to 2.339(5) Å range, and, on the other, the *cis*- and *trans*–(N,O)–Mo–(N,O) octahedral angles fall within the relatively wide 68.96(18)–107.4(2)° and 152.3(2)–162.7(2)° ranges, respectively (Figure 2.16). The extreme values between which all registered lengths and angles vary were mainly observed for Mo1. This distortion seems to compensate the high planarity of the two coordinated aromatic rings: indeed, while the two pyridine rings coordinated to Mo1 are mutually rotated by only *ca.* 3.5°, the analogous value for Mo2 is nearly four times larger (*ca.* 11.9°); as a consequence, the steric pressure imposed on Mo1 seems to be higher, leading to a more distorted coordination environment.

The two water molecules of crystallization are engaged in strong ($d_{D\cdots A}$ usually below 3 Å) and highly directional [$\angle(DHA)$ usually above *ca.* 150°] O–H \cdots O hydrogen bonding interactions with the dinuclear [Mo₂O₆(di-*t*-Bu-bipy)₂] complexes, ultimately describing two R₄⁴(16) graph set motifs which alternate along the [100] direction of the unit cell (Figure 2.17).

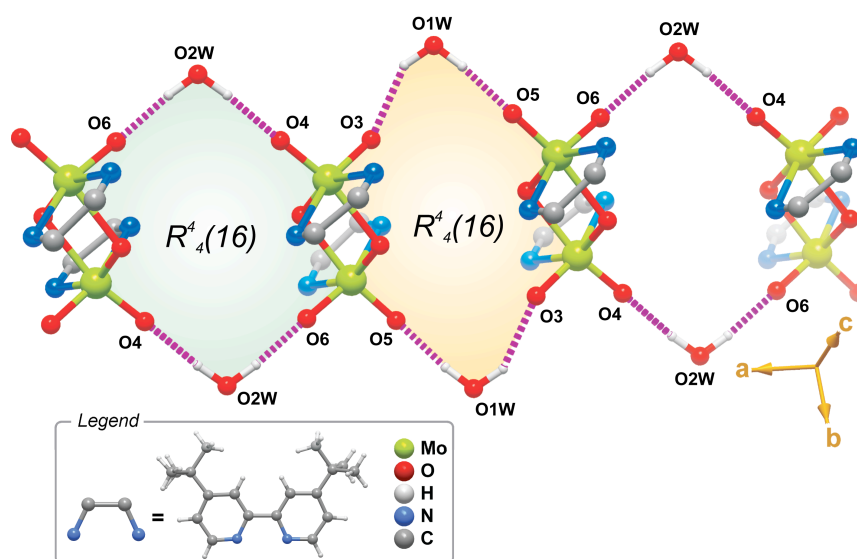


Figure 2.17. Schematic representation of the strong and highly directional O–H \cdots O hydrogen bonds (dashed pink lines) mediated by the two water molecules of crystallization, which establish supramolecular bridges between adjacent molecular units along the *a*-axis of the unit cell (Table 2.3). Each assembly of four adjacent moieties (two water molecules and two neutral complexes) describe R₄⁴(16) graph set motifs.^[37] Symmetry codes associated with symmetry-equivalent atoms have been omitted for clarity.

Table 2.3. Geometrical details of the hydrogen bonds and intermolecular close contacts present in compound **2.3**.^a

D-H...A	$d(\text{D}\cdots\text{A})/\text{\AA}$	$\angle(\text{DHA})/^\circ$
O1W-H1X...O5 ⁱ	2.789(7)	174(6)
O1W-H1Y...O5 ⁱⁱ	3.021(7)	148(5)
O2W-H2X...O6 ⁱⁱⁱ	2.778(6)	173(6)
O2W-H2Y...O4 ⁱⁱ	2.843(7)	169(6)
C4-H4...O1W ^{iv}	3.491(8)	168
C22-H22...O2W ^v	3.415(8)	171
C25-H25...O2W ^v	3.314(8)	167
C1-H1...O5 ^{vi}	3.306(9)	136
C9-H9...O4 ^{vii}	3.306(9)	136
C19-H19...O2 ^{vii}	3.090(8)	125

^aSymmetry transformations used to generate equivalent atoms:

- (i) $1+x, 1+y, z$; (ii) $1-x, 1-y, 2-z$; (iii) $x, 1+y, z$;
(iv) $-1/2-x, 1/2-y, 1/2+z$; (v) $1/2-x, -1/2+y, 1.5-z$;
(vi) $-x, -y, 2-z$; (vii) $1-x, -y, 2-z$.

This arrangement leads to the formation of a one-dimensional supramolecular tape which close packs in a typical herringbone fashion in the *bc* plane of the unit cell to yield the crystal structure of **2.3** (Figure 2.18). Water molecules of a given tape are further interacting with the coordinated di-*t*-Bu-bipy ligands from an adjacent tape by way of several weak C-H...O interactions (not shown, see Table 2.3 for geometrical details). Indeed, even though the internuclear C...O distances are relatively long (varying between *ca.* 3.31 and 3.49 Å), the $\angle(\text{DHA})$ interaction angles for these connections are very close to linearity (all above *ca.* 167°), which clearly confirms their structural relevance in the crystal packing of **2.3**. Other intermolecular C-H...O contacts exist in the structure (last three entries in Table 2.3). Despite their low directionality, these contacts help to strengthen the connections between neighbouring complexes.

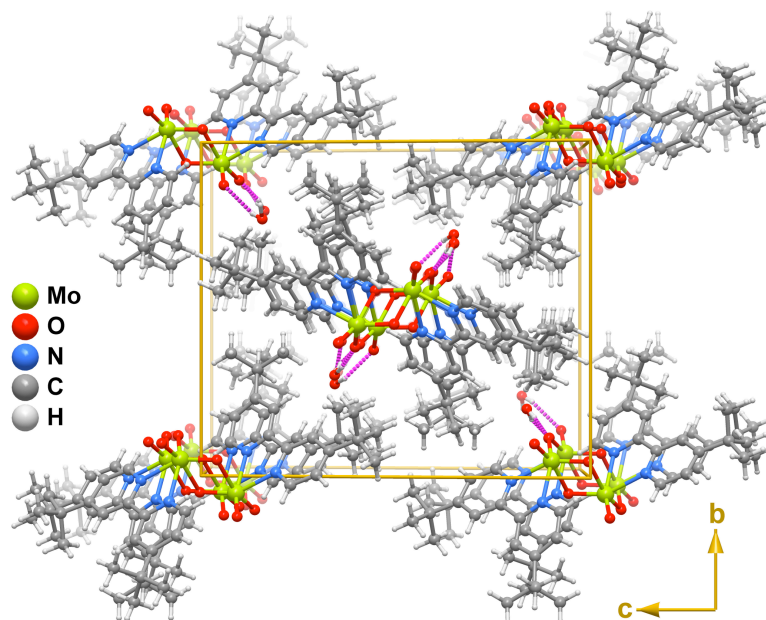


Figure 2.18. Crystal packing of $[\text{Mo}_2\text{O}_6(\text{di-}t\text{-Bu-bipy})_2]\cdot 2\text{H}_2\text{O}$ (2.3) viewed in perspective along the $[100]$ direction of the unit cell. $\text{O-H}\cdots\text{O}$ hydrogen bonding interactions connecting adjacent molecular units along the a -axis of the unit cell are represented as dashed pink lines.

2.3.5. CATALYSIS TESTS

The catalytic performance of $[\text{Mo}_2\text{O}_6(\text{di-}t\text{-Bu-bipy})_2]\cdot 2\text{H}_2\text{O}$ (2.3) was investigated at 55 °C using TBHP_{dec} as the oxygen source for the epoxidation of *cis*-cyclooctene (Cy8), DL-limonene (Lim), cyclododecene (Cy12), 1-octene and *trans*-2-octene. Figure 2.19 shows all substrate structures used in these studies.

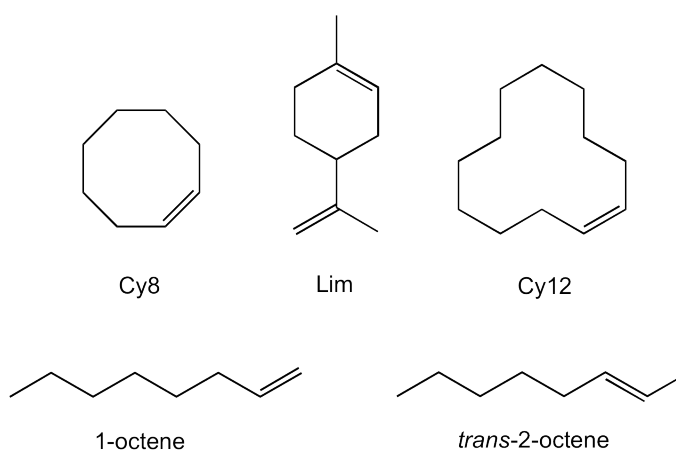


Figure 2.19. Substrates used to investigate the catalytic performance of 2.3: *cis*-cyclooctene (Cy8), DL-limonene (Lim), cyclododecene (Cy12), 1-octene and *trans*-2-octene.

2.3.5.1. *Cis*-CYCLOOCTENE (Cy8)

For the epoxidation of Cy8 the catalytic reaction using **2.3** was investigated in a batch-wise homogeneous phase. As shown in Figure 2.20, the conversion of Cy8 into Cy8Ox had a 93 / 100% yield at 6 / 24 h reaction, respectively. The absence of the catalyst led to a negligible formation of Cy8Ox.

Table 2.4 summarizes the results from a literature search on oxomolybdenum(VI) complexes possessing the same organic ligand (*di-t*-Bu-bipy) that were employed as catalysts in the same reaction under similar conditions (unless otherwise specified). This search clearly shows that the catalytic performance of compound **2.3** is fairly similar to that of related materials.

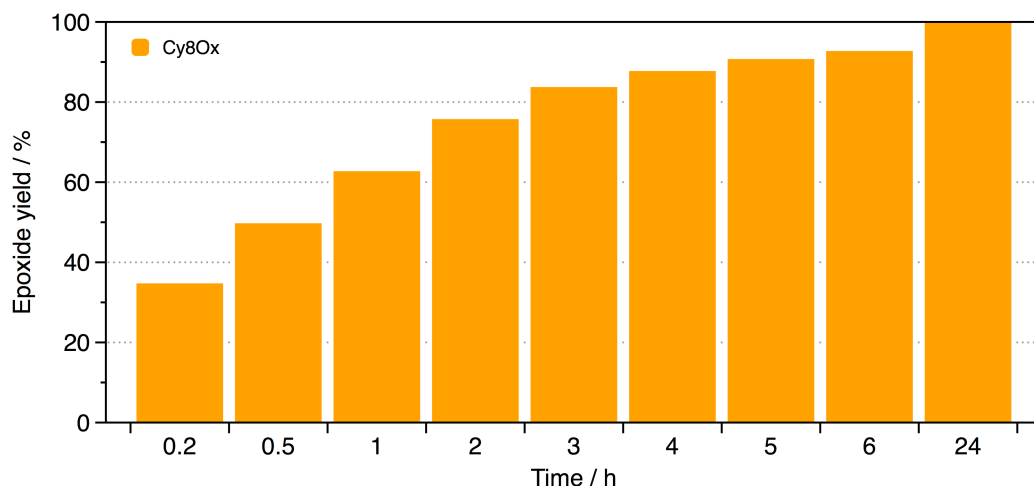


Figure 2.20. Performance profile, while using TBHP_{dec} as the oxygen source, for the epoxidation of *cis*-cyclooctane (Cy8) into 1,2-epoxycyclooctane (Cy8Ox) at 55 °C in the presence of [Mo₂O₆(*di-t*-Bu-bipy)₂]**·**2H₂O (**2.3**).

Table 2.4. Catalytic performance of oxomolybdenum(VI) complexes possessing *di-t*-Bu-bipy (L) as the organic ligand and used as catalysts for the epoxidation of Cy8 into Cy8Ox.

Complex	Cy8Ox yield (in %)	Time (in hours)	Ref.
2.3	93 / 100	6 / 24	--
[MoO ₂ Cl ₂ L]	79 / 90	6 / 24	[114]
	53 / 70	4 / 24	[86]
[Mo ₈ O ₂₄ L ₄]	65	6 ^a	[98]
	97	6 ^b	[98]
[MoO ₂ (NCS) ₂ L]	45 / 40 (at 45 / 50% conversion)	6 / 24	[114]
[Mo ₂ O ₅ (NCS) ₂ L ₂]	49 / 60 (at 52 / 64% conversion)	6 / 24	[114]

^a 1,2-Dichloroethane used as co-solvent

^b Use of microwave heating

Comparing at the same reaction time the catalytic performance of **2.3** with the mononuclear complex $[\text{MoO}_2\text{Cl}_2(\text{di-}t\text{-Bu-bipy})]$, the observed differences were surprising. The considerably distinct yields can be partially attributed to differences in the initial heating rate of the reaction mixtures and/or stirring rates. Noteworthy, the results derived for compound **2.3** are favourably compared to those given by the previously described octanuclear complex $[\text{Mo}_8\text{O}_{24}(\text{di-}t\text{-Bu-bipy})_4]$.^[98]

Omitted from Table 2.4 is a dinuclear complex of the type $[\text{Mo}_2\text{O}_4\text{L}]$, where $\text{L} = 1,4\text{-}(2,6\text{-di-methyl})\text{-phenyl-}2,3\text{-dimethyldiazabutadiene}$, reported by the groups of Calhorda and Valente.^[163] This complex was theoretically proposed as the active species formed when the dicarbonyl complex $[\text{Mo}(\eta^3\text{-C}_3\text{H}_5)\text{Cl}(\text{CO})_2\text{L}]$ was tested as a catalyst precursor in the same reaction under similar conditions. This complex gave an experimental conversion of 75% Cy8Ox yield at 24 h reaction.^[163]

2.3.5.2. DL-LIMONENE (Lim), CYCLODODECENE (Cy12), 1-OCTENE and *trans*-2-OCTENE

The catalytic performance of **2.3** was investigated for the remaining model substrates using the same conditions employed before (55 °C using TBHP_{dec}): DL-limonene (Lim), cyclododecene (Cy12), 1-octene and *trans*-2-octene. Results are summarized in Table 2.5.

The reaction of Cy12 gave the respective epoxide as the main product and a minor amount of the diol. A comparison of the results for Cy12 and Cy8 (Table 2.5) shows that the former is a less reactive olefin, which may be partly due to the larger steric hindrance of the substrate molecule. For the linear olefins 1-octene and *trans*-2-octene the respective epoxides were always the sole reaction products, and *trans*-2-octene was more reactive than 1-octene. It is possible to conclude that the epoxidation of internal C=C bonds is favoured in relation to that of terminal ones, most likely due to electronic effects. Mechanistic studies reported in the literature for the epoxidation of olefins with hydroperoxides as oxidants, in the presence of oxomolybdenum complexes, refer that the oxygen atom transfer to the olefin may involve an intermediate electrophilic alkylperoxo complex.^{[83][156][157]} Accordingly, the epoxidation of the internal C=C bonds is expected to be more favourable than that of the terminal ones because the former possess higher electron density. This feature makes the complex in **2.3** particularly attractive as a catalyst for the epoxidation of olefins possessing both internal and terminal C=C bonds because it may lead to relatively high regioselectivity.

Table 2.5. Epoxidation of olefins with TBHP_{dec} at 55 °C in the presence of 2.3.

Olefin	Conversion ^a (in %)	Product(s)	Selectivity ^a (in %)
Cy8	93 / 100	Cy8Ox	100 / 100
Lim	94 / 99	LimOx	76 / 72
		LimDiol	2 / 3
Cy12	78 / 92	1,2-epoxycyclododecane	95 / 95
		cyclododecane-1,2-diol	5 / 5
1-octene	7 / 27	1,2-epoxyoctane	100 / 100
<i>trans</i> -2-octene	28 / 54	2,3-epoxyoctane	100 / 100

^a Olefin conversion and product selectivity at 6 / 24 h reaction.

Epoxidation of Lim is of great industrial interest because the epoxide products are bio-renewable and have commercial use as, for example, reactive diluents in cationic and UV cure applications^[164] The epoxidation of Lim, which possesses endocyclic and terminal C-C bonds, with TBHP in the presence of 2.3 gave mainly LimOx in 71% yield within 24 h of reaction. The regioselectivity to the endocyclic C-C bond was 75% and calculated as follows:

$$\frac{(\text{moles of LimOx})}{(\text{moles of LimOx}) + (\text{moles of LimDiOx})} \times 100 \quad \text{Equation 2.1}$$

The work presented in this chapter constitutes the first systematic report on the use of a molybdenum complex possessing the di-*t*-Bu-bipy ligand as a pre-catalyst for the epoxidation of Lim.

Comparing to previously investigated oxomolybdenum complexes tested as catalysts in the reaction of Lim with TBHP at 55 °C, the catalytic results for compound 2.3 seem fairly good in terms of LimOx yield at 80–100% conversion and regioselectivity to LimOx. Several parameters were not taken into consideration in these comparisons, such as the amount of water in the reaction mixture, which favours the formation of LimDiol.

To summarize, compound 2.3 represents a new member of the increasingly large family of oxomolybdenum complexes containing the *N,N*-chelating ligand 4,4'-di-*tert*-butyl-2,2'-bipyridine. Within this family this compound stands out as being a particularly active and regioselective catalyst for the epoxidation of non-functionalized olefins.

2.4. CONCLUDING REMARKS

The results presented in this chapter reinforce the idea that the hydrolysis and condensation of complexes of the type [MoO₂Cl₂L] is a potentially interesting route to obtain new oxomolybdenum(VI) hybrid materials. Reactions

in water at 100–120 °C using $[\text{MoO}_2\text{Cl}_2\text{L}]$ as the metal precursor produced the polymeric material $\{[\text{MoO}_3(\text{bipy})][\text{MoO}_3(\text{H}_2\text{O})]\}_n$ (**1.2**) ($\text{L} = 2,2'$ -bipyridine, chapter 1) in large yields. Octanuclear species $[\text{Mo}_8\text{O}_{22}(\text{OH})_4(\text{di-}t\text{-Bu-bipy})_4]$ (**2.2**) were formed instead if 4,4'-di-*tert*-butyl-2,2'-bipyridine was the initial choice for the *N,N*-chelated ligand.

The large complex $[\text{Mo}_8\text{O}_{22}(\text{OH})_4(\text{di-}t\text{-Bu-bipy})_4]$ (**2.2**) is composed of a purely inorganic cationic core, $[\text{Mo}_4\text{O}_8(\mu_3\text{-OH})_2(\mu_2\text{-O})_2]^{2+}$, attached to two peripheral oxo-bridged binuclear anionic units, $[\text{Mo}_2\text{O}_4(\mu_2\text{-O})_2(\text{OH})(\text{di-}t\text{-Bu-bipy})_2]^-$. When investigated as a heterogeneous catalyst using the substrate models Lim and Ole under various conditions, **2.2** exhibited some steric effects that may partly explain the higher reactivity of Lim in comparison to the bulkier substrate Ole. In addition, the structural features of **2.2** may hinder the catalyst autodegradation pathways, which may partly explain the fairly high catalyst stability observed.

While using an alternative method to isolate **2.2**, *i.e.*, the hydrothermal reaction of MoO_3 with 4,4'-di-*tert*-butyl-2,2'-bipyridine, the dinuclear complex $[\text{Mo}_2\text{O}_6(\text{di-}t\text{-Bu-bipy})_2] \cdot 2\text{H}_2\text{O}$ (**2.3**) was isolated as a trace compound. Even though the $\{\text{MoO}_2(\mu\text{-O})\text{MoO}_2\}^{2+}$ core structure is quite common in oxomolybdenum(VI) chemistry, only a handful of dinuclear complexes displaying the dioxo-bridged neutral unit $\{\text{MoO}_2(\mu\text{-O})_2\text{MoO}_2\}$ have been reported to date. In this context, the structural features and the catalytic performance of **2.3** in the epoxidation of non-functionalized olefins were investigated in detail. Compound **2.3** stood out as being a particularly active and regioselective catalyst for the epoxidation of non-functionalized olefins, particularly in the conversion of bio-derived olefins into added value epoxides.

SYNTHESIS and STRUCTURE of a POLYMERIC COMPOUND CONTAINING 2,2'-BIPYRIDINE-5,5'-DICARBOXYLIC ACID

3.1. SUMMARY

2,2'-Bipyridine-5,5'-dicarboxylic acid (H_2bpdc) is a potential multidentate ligand which has been employed in the synthesis of organic-inorganic hybrid materials.^[165] The main advantage of H_2bpdc compared to other molecules concerns its versatile coordination fashion: while strongly bound to a metal ion by way of a typical *N,N*-chelate (primary coordination mode), it may also participate in additional bonding interactions through the peripheral carboxylic acid groups (secondary coordination mode). Noteworthy, these substituent groups embody this molecule with additional structural versatility: i) on the one hand, they may permit the formation of several supramolecular interactions based on strong hydrogen bonds (some even charged if the groups are deprotonated); ii) on the other, deprotonation of these groups may also lead to the formation of new coordinative bonds to metal ions; iii) additionally, the carboxylic acid groups are amenable to chemical functionalization.^{[166][167]}

A remarkable example of the use of H_2bpdc comes from the research group of Zubietta whom, through the use of standard hydrothermal synthesis, prepared new two-dimensional (2D) coordination networks with 1st row transition metals (particularly Cu^{2+}), which feature both the aforementioned *N,N*-chelate and metal bridges via the peripheral carboxylate groups.^{[168][169]}

The research work presented in this chapter was essentially motivated by the great potential of H_2bpdc to lead to novel Mo^{6+} oxide hybrid materials with intriguing structures, which could also embody the obtained compounds with promising catalytic properties. Moreover, this organic ligand belongs to the large family of 2,2'-bipyridine molecules typically employed in the preparation of Mo^{6+} hybrid catalysts, some of which have been used in previous chapters of this thesis. The transposition of synthetic procedures used for other molecules was, therefore, relatively straightforward when H_2bpdc was used instead.

The hydrothermal reaction of H_2bpdc with MoO_3 in water and dimethylformamide (DMF, used because of solubility issues of the ligand) produced a new polymeric hybrid material formulated as

(DMA)[MoO₃(Hbpdc)]·*n*H₂O (3.1) (where DMA = dimethylammonium). Catalytic studies using the bioderived olefins DL-limonene and methyl oleate revealed that the catalytic epoxidation in the presence of 3.1 was homogeneous in nature. Recyclable catalytic systems involving 3.1 were achieved by using ionic liquids (IL) as solvents.^[170] This approach is a simple and more efficient way to either use other co-solvents (as employed in other chapters of this thesis), or even to immobilize the catalyst in solid supports. Indeed, this latter approach is much more complex as it requires additional modification of the catalyst in a solid support (Introduction), with frequently partial loss of activity. This process is, thus, unattractive for potential industrial applications.

3.2. (DMA)[MoO₃(Hbpdc)]·*n*H₂O (3.1)

This section describes the synthesis and characterization of (DMA)[MoO₃(Hbpdc)]·*n*H₂O (3.1). This polymeric material was precipitated from the solution obtained by the dynamic solvothermal (H₂O : DMF) treatment of MoO₃ with 2,2'-bipyridine-5,5'-dicarboxylic acid (H₂bpdc). A detailed structural characterization of 3.1 including FT-IR, solid-state NMR, thermogravimetric analyses, scanning electron microscopy and a complete structural description based on powder X-ray diffraction studies is presented. The catalytic performance of this polymeric material was investigated in the epoxidation reactions (at 55 or 75 °C) of the bioderived olefins Ole and Lim, using TBHP_{dec}/DCE or TBHP_{dec}/BTF (oxidant/co-solvent) systems. For the same reaction temperatures, substrates and oxidant the catalytic performance of 3.1 was further studied using the ionic liquids:

- i) 1-butyl-3-methylimidazolium tetrafluoroborate ([bmim]BF₄),
- ii) 1-butyl-3-methylimidazolium bis(trifluoromethylsulfonyl)imide ([bmim]NTf₂)
- iii) 1-butyl-3-methylpyridinium tetrafluoroborate ([bmpy]BF₄)

as co-solvents instead of DCE or BTF.

3.2.1. SYNTHESIS

Several synthetic approaches similar to those described in chapters 1 and 2 were used to tentatively prepare hybrid materials with 2,2'-bipyridine-5,5'-dicarboxylic acid (H₂bpdc). The treatment of neutral [MoO₂Cl₂(H₂bpdc)] or charged [MoO₂Cl₂(bpdc)]²⁻ (as a salt) as precursors under typical hydrothermal synthetic conditions led to the systematic isolation of reagent/product mixtures that proved to be very difficult to analyse and even identify.

In a similar fashion to that employed in the preparation of [Mo₈O₂₂(OH)₄(di-*t*-Bu-bipy)₄] (2.2), H₂bpdc was made to react with MoO₃ using dynamic hydrothermal synthesis (Figure 3.1). Nevertheless, powder X-ray

diffraction studies revealed once again that the obtained product was a mixture of phases.

A search in the literature concerning the use of 2,2'-bipyridine-5,5'-dicarboxylic acid as an organic ligand revealed that this molecule could present some solubility issues when the solvent employed is only water. Indeed, the research group of Ziessel showed that the formation of the $[(\eta^5\text{-Me}_5\text{C}_5)\text{Ir}(2,2'\text{-bipy-4,4'-(COOH)}_2)]^{[171]}$ complex could only be achieved when the ligand was dissolved in DMF.

These results led to a shift in employed synthetic strategy: instead of using only water as the solvent medium (*i.e.*, hydrothermal conditions), DMF was also added to the initial reaction mixture (*i.e.*, solvothermal conditions) in order to improve the solubility of the organic ligand. The solvent ratio employed was always *ca.* 19 : 6 v/v for H₂O : DMF. In this way, the reaction between MoO₃ and H₂bpdcc occurred inside a Teflon-lined stainless steel autoclave (autogenous pressure, 150 °C, 3 d), which was kept rotating during the entire period (at *ca.* 10 rpm) of the reaction leading to the isolation of a clear orange solution. A white microcrystalline solid started to precipitate, with a gradual change in colour of the solution from orange to pink. To isolate quantitative amounts of the product (yield 56%), the solution/precipitate mixture was allowed to stand at ambient temperature for a period of 4 days. The precipitate was then recovered by filtration, washed, dried and fully characterized in the solid state. The compound was formulated as a novel oxomolybdenum(VI)-bipyridinedicarboxylate hybrid material: (DMA)[MoO₃(Hbpdcc)]·*n*H₂O (3.1). Despite the crystallization of 3.1 being slow (*i.e.*, thermodynamically driven), attempts to control this step and isolate crystals suitable for single-crystal X-ray diffraction were unsuccessful. The structural details were then unveiled from *ab initio* methods based on high-resolution synchrotron powder X-ray diffraction data. The systematic isolation of 3.1 as a microcrystalline powder clearly suggests that nucleation is fast, occurring randomly, while crystal growth is in turn slow and strongly dependent on the self-assembly of the individual building units from solution. Because DMA⁺ cations are important in the crystal structure of 3.1 (more details in the section dedicated to the structural description), it is reasonable to assume that the formation of this cation from the solvent DMF limits in some way the rate of formation of the resultant polymeric material.

Solvothermal methods used use to prepared polynuclear material

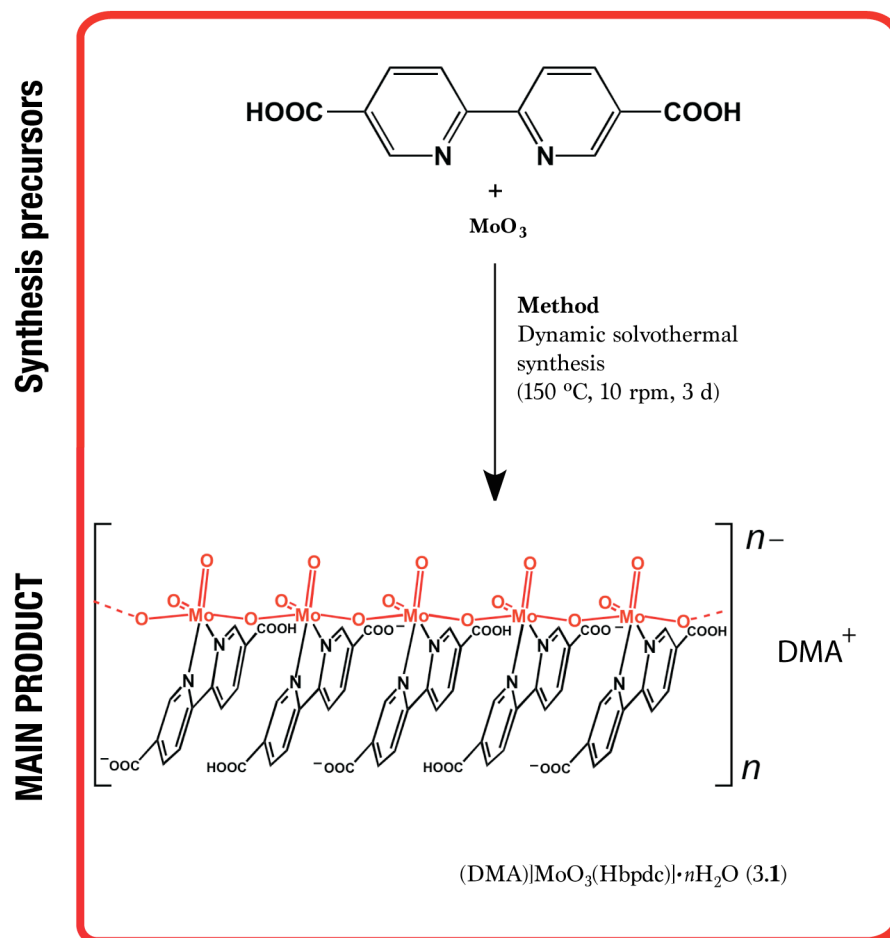


Figure 3.1. Method used to prepare the polymeric complex $(\text{DMA})[\text{MoO}_3(\text{Hbpdcc})] \cdot n\text{H}_2\text{O}$ (3.1).

3.2.2. FT-IR

Figure 3.2 compares the FT-IR spectrum of the free ligand H_2bpdcc with that of the polymeric $(\text{DMA})[\text{MoO}_3(\text{Hbpdcc})] \cdot n\text{H}_2\text{O}$ (3.1) material. The FT-IR spectrum of 3.1 exhibits strong, sharp bands centred at *ca.* 901 and 922 cm^{-1} that can be assigned to $\nu(\text{Mo}=\text{O})$ stretching modes arising from the *cis*- $[\text{MoO}_2]^{2+}$ units, and a broad, intense band at *ca.* 576 cm^{-1} attributed to $\nu(\text{Mo}-\text{O}-\text{Mo})$.^[172] Noteworthy, both $[\text{MoO}_3(\text{bipy})]_n$ (first reported by Zubietta and discussed in chapter 1) and the hybrid material 1.2 exhibit a similar set of bands.^{[59][98]}

A strong (and sharp) band at *ca.* 1602 cm^{-1} in the spectrum of 3.1 (cf. 1598 cm^{-1} in the Raman spectrum) is assigned to the pyridyl ring stretching vibration, and it is shifted by about 10 cm^{-1} to higher frequency when compared with the corresponding band for the free ligand. This shift to higher wavenumbers constitutes solid evidence for coordination of the ligand to the metal center.

The bands at *ca.* 1648 cm^{-1} and 3442 cm^{-1} are associated with water molecules of crystallization involved in hydrogen-bonding interactions. The very

broad band centred at *ca.* 3442 cm^{-1} with medium-to-strong intensity is attributed to the asymmetric H-O-H stretching vibrational modes of lattice water molecules. The high frequency of this band clearly indicates that this moiety is weakly interacting *via* hydrogen bonds with the remaining framework.^[150] In fact, the thermogravimetric analysis shows a continuous weight loss at low temperatures, which can be attributed to weakly bound water molecules trapped in the crystal structure.

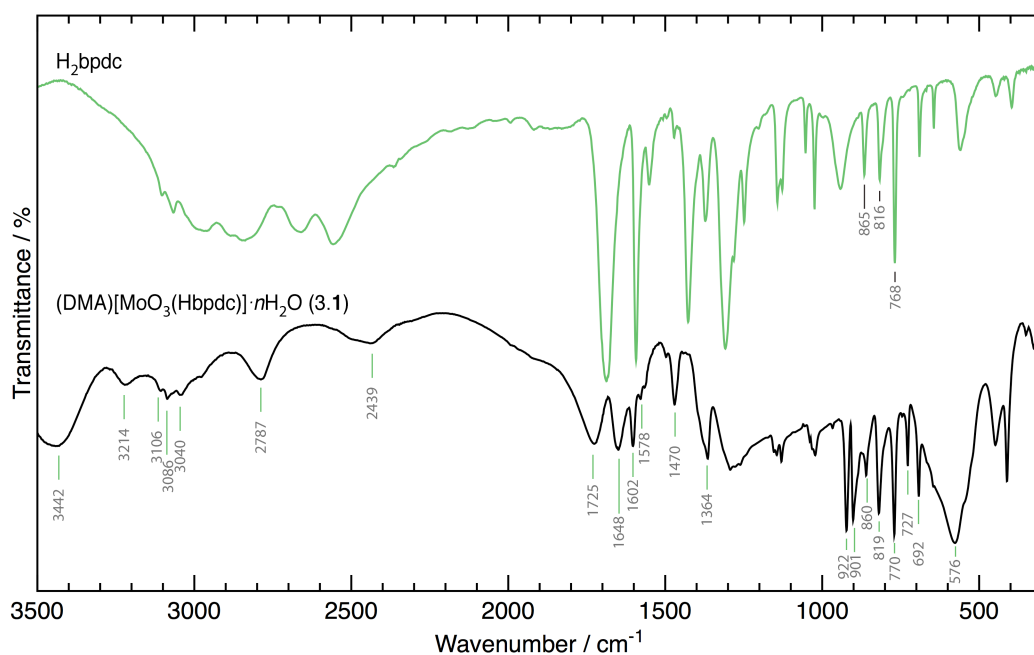


Figure 3.2. Comparison between the FT-IR spectra of the polymeric hybrid material (DMA)[MoO₃(Hbpdc)]·*n*H₂O (3.1) and that of the free ligand H₂bpdc.

The medium-intensity band at *ca.* 1648 cm^{-1} likely overlaps with a number of functional groups: i) the asymmetric stretching vibrational mode of deprotonated carboxylic acid groups [$\nu_{\text{as}}(\text{COO}^-)$]; ii) the bending deformation of water.^[150] The increase in intensity of the band centred at *ca.* 1364 cm^{-1} when compared to that of the free organic ligand seems however to strongly indicate that the pair *ca.* 1648 / 1364 cm^{-1} might be attributed to the asymmetric/symmetric stretching vibrational modes of carboxylates.

A broad, medium-intensity band centred at *ca.* 1725 cm^{-1} proves the existence of both carboxylate and carbonyl groups (C=O).^[150] The existence of carboxylate groups in the crystal structure implies the presence of a cation, most likely DMA⁺, a common product of decomposition of DMF *via in situ* hydrolysis.^[173] Indeed several bands in the spectral range 2400–3250 cm^{-1} support this assumption. In particular, the medium-intensity (and broad) bands peaking at *ca.* 3214 cm^{-1} and 2787 cm^{-1} can be attributed to the $\nu(\text{NH}_2^+)$ and $\nu(\text{CH}_3)$ stretching modes, respectively.^{[174][175][176]} Several overlapping bands in the range

2979-3110 cm^{-1} arise from $\nu(\text{NH}_2^+)$, $\nu(\text{CH}_3)$ and aromatic $\nu(\text{C-H})$ stretching vibrations. In addition, a shoulder at *ca.* 2838 cm^{-1} can be assigned to the C-H stretching of the corresponding N-C-H groups.

It is important to emphasize that the decomposition of DMF under hydrothermal conditions is quite a common occurrence and there are a number of examples in the literature where the resultant $(\text{CH}_3)_2\text{NH}_2^+$ cation (DMA^+) is incorporated as a counter-cation in an anionic coordination network.^{[177][178][179]} In this system the hydrolysis of DMF could be metal-catalyzed and/or promoted by acidic conditions during the initial stages of reaction.

3.2.3. SOLID-STATE NMR

^1H and ^{13}C solid-state NMR studies are particularly informative providing additional structural information on the crystal structure of the compound, in particular regarding the composition of the asymmetric unit.

The $^{13}\text{C}\{^1\text{H}\}$ MAS NMR spectrum shows three distinct spectral regions. The first portion is composed of two resonances centred at 169.0 and 168.0 ppm that are attributed to two crystallographically independent carbonyl (C=O) groups from the carboxylic acid groups in the organic molecule. The absence of additional resonances in this spectral region constitutes strong evidence for the absence of DMF molecules in the crystal structure. Indeed, the carbonyl group of this solvent molecule appears typically at *ca.* 162 ppm and, as shown in Figure 3.3, this region is completely clear.

The aromatic portion of the spectrum can be subdivided into two regions: between *ca.* 150 and 139 ppm five resonances arise (150.0, 148.5, 146.4, 142.4 and 139.4 ppm), being attributed to the *ortho* and *para* carbon atoms from the heterocyclic rings; between *ca.* 130 and 123 ppm a total of three resonances (peaking at 130.2, 124.3 and 123.3 ppm) are instead attributed to the *meta* carbon atoms of the same rings. Indeed, the carboxylic acid groups decrease the electron density of the benzene rings, with this effect being more pronounced in the *ortho* and *para* positions causing the deprotection of the hydrogen atoms.^[180] Worth of note is the fact that the splitting of the resonances into, respectively, 5 and 3 for the bipyridyl carbon atoms is a clear indication that the two pyridyl rings are indeed non equivalent. In addition, as noted above, this result is in agreement with the presence of two non-equivalent carbonyl groups. As described in the section dedicated to the X-ray diffraction structural studies, these results from solid-state NMR are in perfect agreement with the presence of a crystallographically independent organic molecule coordinated to the Mo^{6+} metallic centre.

The third spectral region appears in the lower frequency part of the spectrum where a notable broad resonance centred at 36.1 ppm, and overlapped with the spinning sidebands, is assigned to the $-\text{CH}_3$ groups of the DMA^+ charge-balancing cation.

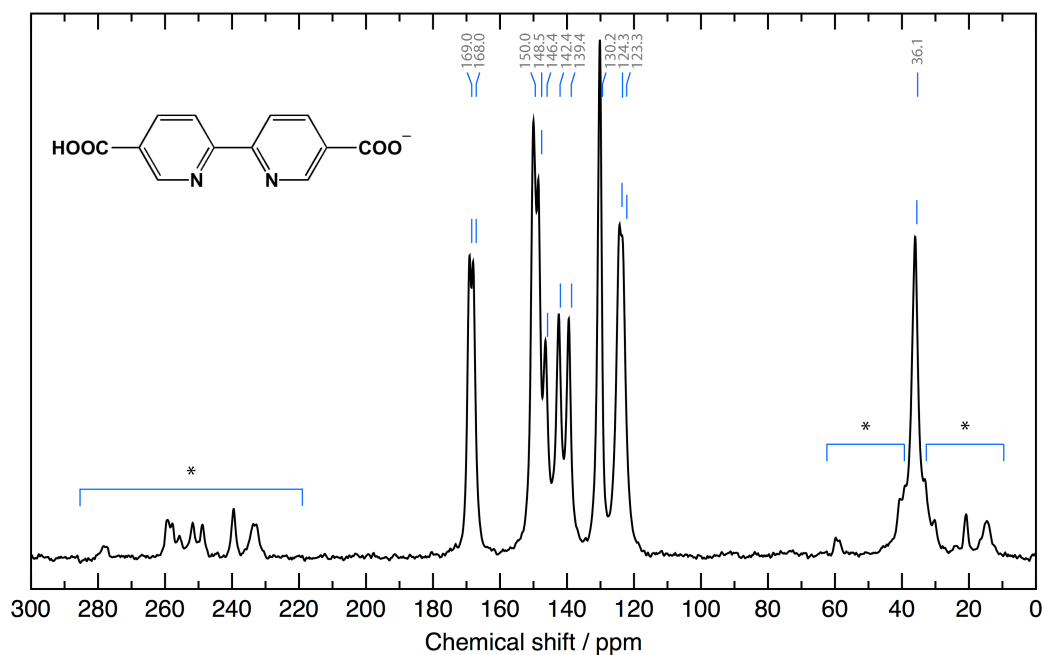


Figure 3.3. Solid-state $^{13}\text{C}\{^1\text{H}\}$ CP MAS NMR spectrum of $(\text{DMA})[\text{MoO}_3(\text{HbpdC})]\cdot n\text{H}_2\text{O}$ (3.1) collected at a spinning rate of 10 kHz. Chemical shifts are quoted in parts per million (ppm) with respect to TMS and the spinning sidebands are indicated with an asterisk.

The ^1H MAS NMR spectrum shows five well-resolved resonances in the 20-0 ppm spectral region (Figure 3.4). The most striking resonance appears centred at 18.4 ppm, being a very broad resonance characteristic of a highly unprotected proton. This resonance (which appears *ca.* 4 ppm upfield with respect to the free ligand: 14.2 ppm) can be attributed to the proton establishing the hydrogen bonding connection between neighbouring carboxylic acid groups. This large variation of chemical shift is attributed to the strong deshielding effects of the supramolecular assembly involving neighbouring carboxylate groups (Figure 3.10).^[181]

The broad resonance centred at *ca.* 8.2 ppm may be attributed to the various aromatic protons that have very close resonances. A spectrum of the same compound acquired at a higher spinning rate (15 kHz) showed a small splitting of this band into two broad signals. This unequivocally indicated that this resonance is composed of more than one type of protons.

The remaining resonances centred at 5.0, 3.7 and 1.3 ppm are attributed to the extra-polymer species, namely the water molecule of crystallization and the DMA^+ cation. Noteworthy, these resonances are much sharper than the remaining ones, which is a clear indication that they correspond to more mobile moieties in the crystal structure. Indeed, both the DMA^+ cations and the water molecules are only bound to the remaining network *via* hydrogen bonds, which are much weaker than the strong coordinative ones of the polymer, hence the increased mobility of these species.

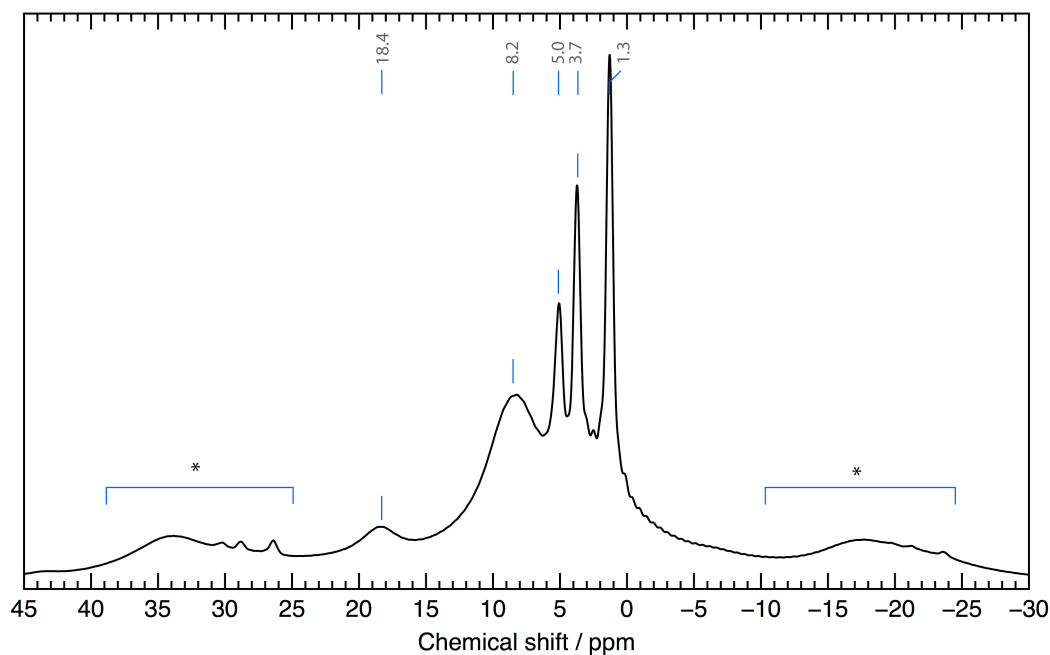


Figure 3.4. Solid-state ^1H MAS NMR spectrum of **3.1** collected at spinning rate of 10 kHz. Chemical shifts are quoted in parts per million (ppm) with respect to TMS and the spinning sidebands are indicated with an asterisk.

3.2.4. THERMOGRAVIMETRIC ANALYSES and VARIABLE TEMPERATURE POWDER X-RAY DIFFRACTION STUDIES

The thermogravimetric analyses of a representative portion of compound **3.1** were performed under air in the temperature range from 25 to 800 °C. In addition, a variable-temperature powder X-ray diffraction (VTPXRD) was also performed in air in the temperature range from ambient temperature to 500 °C.

As depicted in Figure 3.5, the thermogram has a continuous weight loss of *ca.* 6.6% up to *ca.* 210 °C. This corresponds to the release of a total of *ca.* 1.7 water molecules per formula unit (calcd. weight loss value of *ca.* 6.8%). This result is in very good agreement with the chemical composition determined from CHN elemental analyses (see experimental chapter), but contradicts somehow the crystallographic studies that were only able to unequivocally show the presence of one water molecule per formula unit. This may ultimately indicate that some of the water molecules in the bulk material are not of structural nature and are either physisorbed on the crystallites or occupying small voids within crystal defects. In this context, the remaining discussion in this section will assume that the composition of the material is in fact $(\text{DMA})[\text{MoO}_3(\text{Hbpd})]1.7\text{H}_2\text{O}$.

In the 25-210 °C temperature range there is a clear two-step weight loss (see magnification in Figure 3.5). The first of about 3.8% occurs at around 100 °C and is mainly attributed to the desorption of one water molecule per formula unit (could be a combination of physisorbed with crystallographic ones). This low temperature of water desorption is also coherent with the

fragmentation of the crystals under the electron beam during the SEM studies (see, for example, Figure 3.7). The second loss of *ca.* 2.8% peaks at approximately 210 °C and may be attributed to the release of the remaining water molecules (according to the crystal structure description there is one water molecule of crystallization per formula unit, which corresponds to 4.0% by weight).

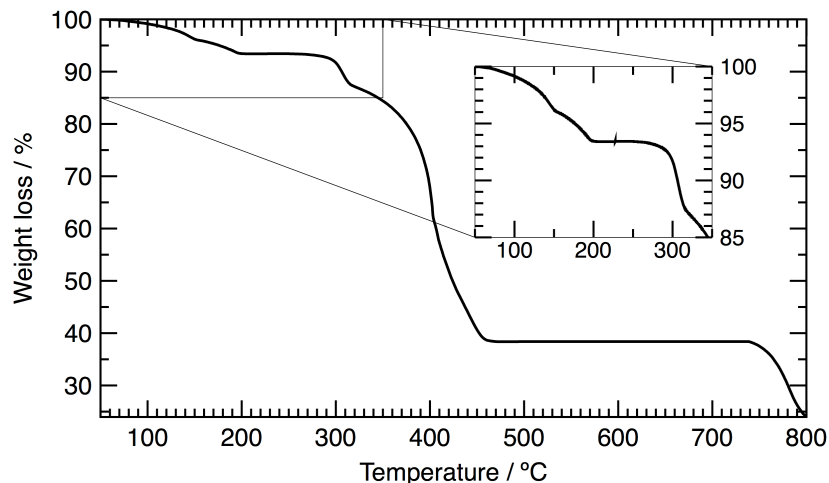


Figure 3.5. Thermogram for the polymeric compound $(\text{DMA})[\text{MoO}_3(\text{HbpdC})]1.7\text{H}_2\text{O}$ between ambient temperature and *ca.* 800 °C.

As shown from the VTPXRD studies within this temperature range the crystalline structure of $(\text{DMA})[\text{MoO}_3(\text{HbpdC})]1.7\text{H}_2\text{O}$ immediately starts to change at *ca.* 100 °C and then (after *ca.* 120 °C) remains unaltered until *ca.* 220 °C, at which temperature the sample starts to lose its crystallinity.

In the thermogram and above *ca.* 210 °C and up to *ca.* 470 °C, there is a three-step decomposition of the organic component with a total weight loss of *ca.* 55.0%, which agrees with the calculated value of 68.9% if it is considered that the decomposition of the organic component is not complete and a small amount of amorphous carbon remains in the sample holder (see the following paragraph).

Above *ca.* 470 °C a solid residue is obtained at which is attributed to the formation of MoO_3 from the various decomposition steps. A separate experiment using a combination of calcination and powder X-ray diffraction studies clearly showed that the residue obtained in the thermogravimetric studies is crystalline MoO_3 (Figure 3.6). The residue obtained in the thermogravimetric analysis is, nevertheless, darker than that obtained for the powder X-ray diffraction studies, which is a clear indication for the presence of carbon in the former residue. This is further supported by the registered mass of residue at *ca.* 470 °C (*ca.* 38.3%), which is significantly higher than that expected for the stoichiometric amount of MoO_3 (calculated as *ca.* 30.9%).

For temperatures higher than *ca.* 720 °C a further weight loss is observed which is attributed to the simultaneous release of the remaining carbon in the sample and also to the sublimation of MoO_3 .^{[140][141]}

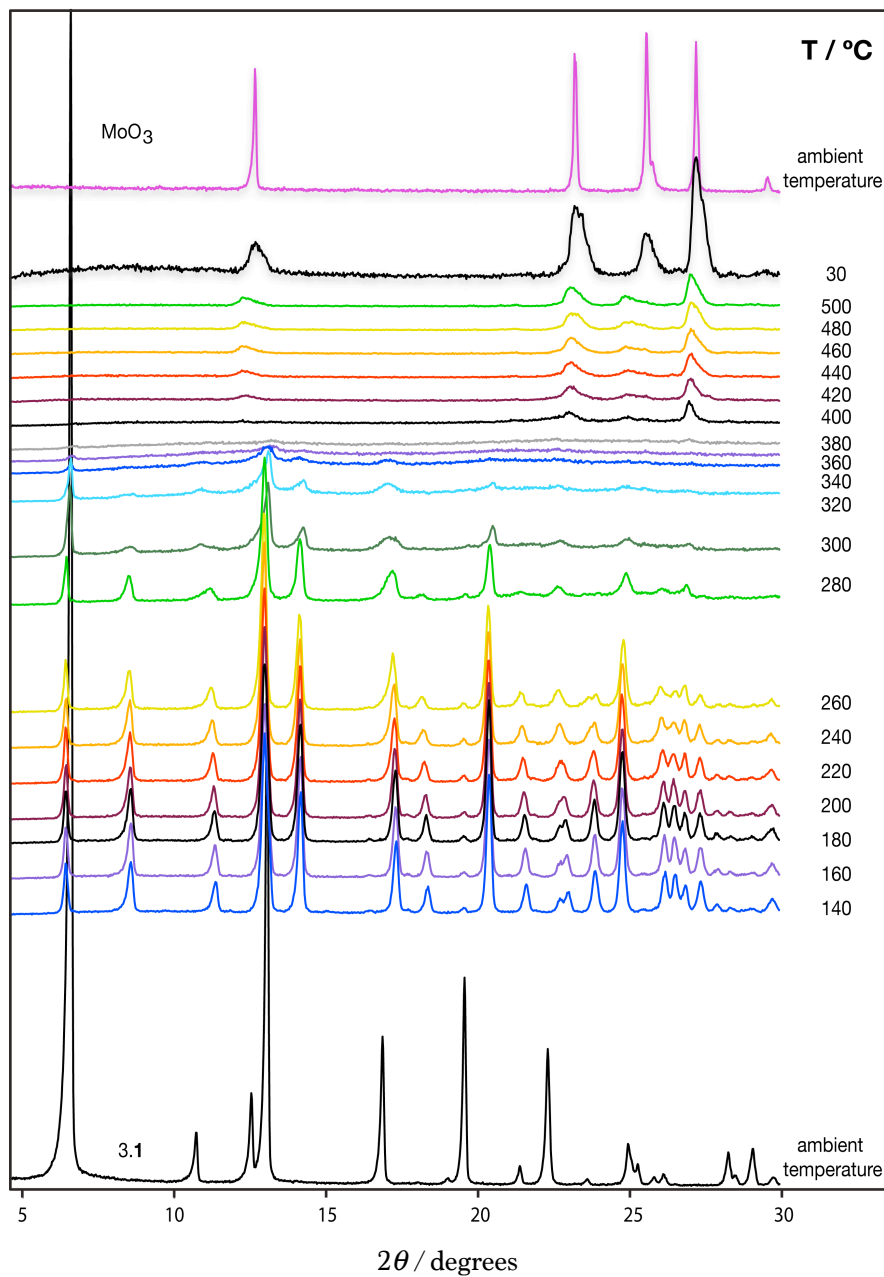


Figure 3.6. Variable-temperature powder X-ray diffraction study (in air atmosphere) on a representative portion of $(\text{DMA})[\text{MoO}_3(\text{HbpdC})] \cdot n\text{H}_2\text{O}$ (**3.1**). The diffraction pattern of MoO_3 is also represented for comparison.

3.2.5. SCANNING ELECTRON MICROSCOPY

Scanning electron microscopy studies were performed on a representative portion of $(\text{DMA})[\text{MoO}_3(\text{Hbpdc})] \cdot n\text{H}_2\text{O}$ (3.1). Studies indicated that the material 3.1 is composed of very thin slab-like crystallites with an average size up to $12 \mu\text{m}$ in length. This rectangular shape of the flat plates may indicate a preferential growth direction, most likely related to the presence of 1D hybrid chains parallel to the crystallographic c -axis (see Figure 3.9).

The crystal cracking shown in Figure 3.7 was directly observed under the electron beam and is attributed to the release of the water molecules upon exposure to the electron beam. Indeed, as described below in the crystallographic section, the water molecules are disposed in a small channel parallel to the c -axis of the unit cell (Figure 3.8), which may facilitate their release and ultimately promote crystal cracking.

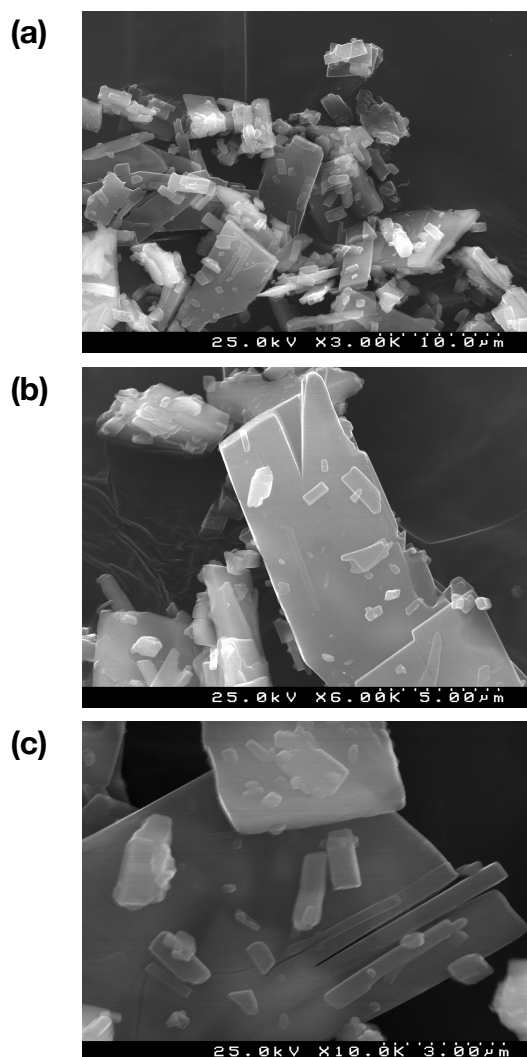


Figure 3.7. Representative SEM images of compound $(\text{DMA})[\text{MoO}_3(\text{Hbpdc})] \cdot n\text{H}_2\text{O}$ (3.1).

3.2.6. X-RAY DIFFRACTION: CRYSTAL STRUCTURE DESCRIPTION

A detailed crystallographic description of $(\text{DMA})[\text{MoO}_3(\text{Hbpd})] \cdot n\text{H}_2\text{O}$ (**3.1**) was obtained by using *ab initio* methods based on high-resolution synchrotron powder X-ray diffraction data collected at 100 K on the powder diffractometer at the ID31 beam line of the ESRF, Grenoble, France (Figure 3.8; see the experimental chapter for details on X-ray data collection, crystal data and structure refinement).^[182]

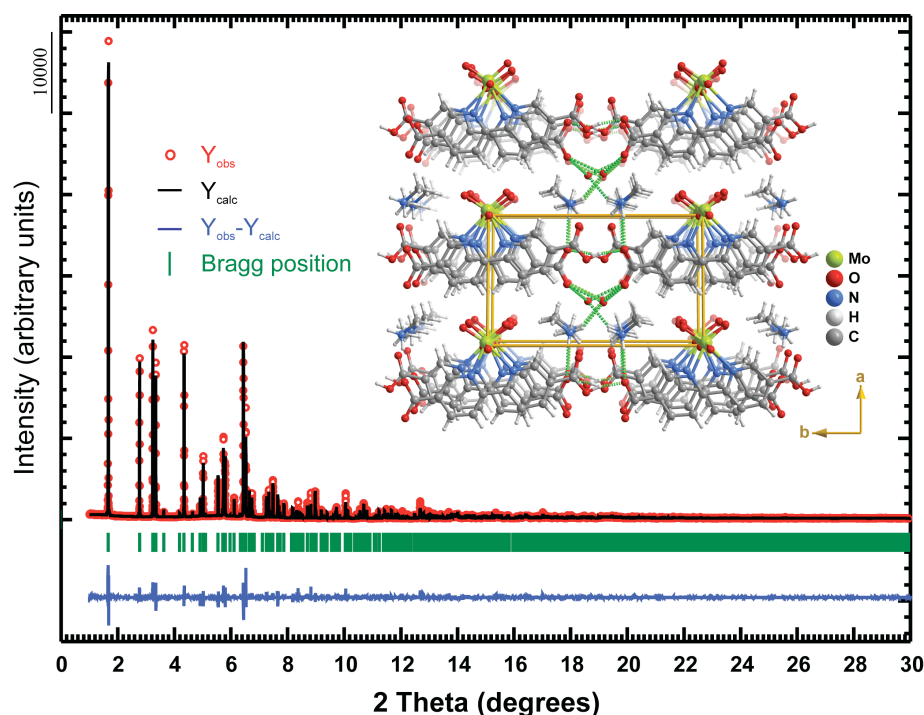


Figure 3.8. Final Rietveld plot (synchrotron PXRD data) of $\{(\text{DMA})[\text{MoO}_3(\text{Hbpd})] \cdot n\text{H}_2\text{O}\}$ (**3.1**) Observed data points are indicated as red circles; the best fit profile (upper trace) and the difference pattern (lower trace) are drawn as solid black and blue lines, respectively. Green vertical bars indicate the angular positions of the allowed Bragg reflections. A ball-and-stick crystal packing representation of **3.1** viewed along the $[001]$ crystallographic direction is provided as an inset.

As shown in Figure 3.9 the material is composed of an anionic 1D organic-inorganic hybrid polymer, $[\text{MoO}_3(\text{Hbpd})]_n^{n-}$, which cocrystallizes with charge-balancing DMA^+ cations and one water molecule per metal center.

A search in the literature (see Introduction for additional details) confirms that this hybrid material is truly unique. 1D polymers based on dioxomolybdenum(VI) units N,N' -chelated by organic ligands, in some cases intercalated by tetrahedral $[\text{MoO}_4]^{2-}$ units, have been only reported by Zapf *et al.*^[59] with 2,2'-bipyridine ($[\text{MoO}_3(\text{bipy})]_n$ see Introduction, Table 3, polymer **23** and $[\text{Mo}_2\text{O}_6(\text{bipy})]_n$, polymer **24**), Kim *et al.* ($[\text{Mo}_4\text{O}_{12}(\text{bipy})_3]_n$, polymer **27**),^[100] and Zhou *et al.* with 1,10-phenanthroline ($[\text{Mo}_3\text{O}_9(\text{phen})_2]_n$, polymer **28**).^[101]

In all these materials the hybrid polymers are, nevertheless, neutral. The anionic $[\text{MoO}_3(\text{Hbpd})]_n^{n-}$ polymer reported in this chapter constitutes the first of such polymeric compounds which is negatively charged, even though it is formed, just like the $[\text{MoO}_3(\text{bipy})]_n$ polymer reported by the group of Zubietta, by a standard -O-O-O-O- alternation of octahedral building units (see Introduction for additional details).

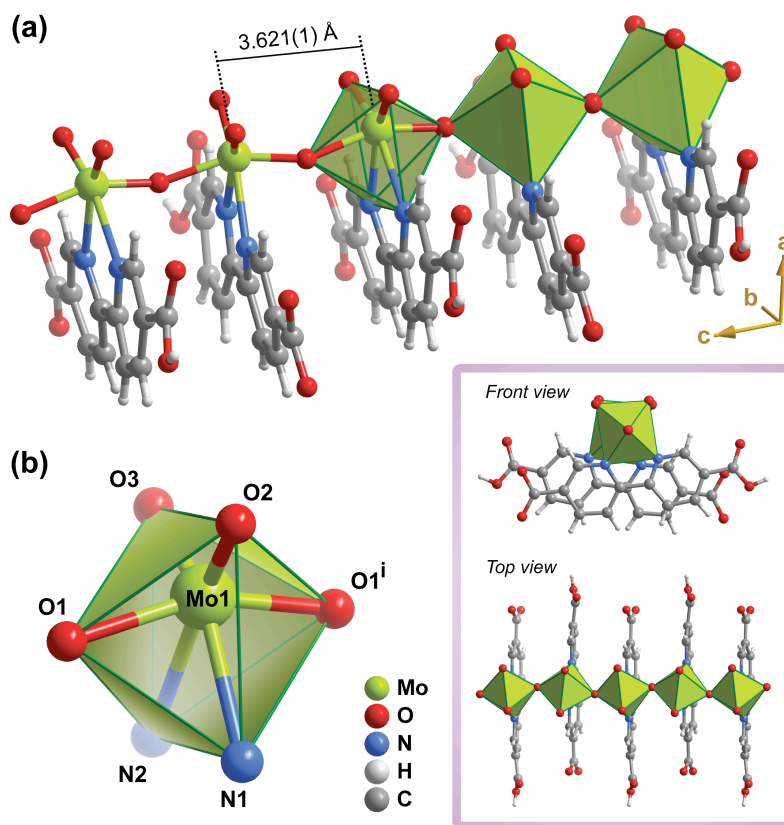


Figure 3.9 (a) Mixed ball-and-stick and polyhedral representation of the anionic one-dimensional $[\text{MoO}_3(\text{Hbpd})]_n^{n-}$ hybrid polymer present in compound 3.1 running parallel to the [001] direction of the unit cell. (b) Schematic representation of the highly distorted $[\text{MoN}_2\text{O}_4]$ octahedral coordination geometry of Mo1. Symmetry transformation used to generate equivalent atoms: (i) $x, -y, -\frac{1}{2}+z$.

Branched cationic polymers having similar environments for the Mo^{6+} centres are known, and were crystallographically reported for the first time just a handful of years ago by Li *et al.*^[183] and, much more recently, by Dai *et al.*^[184] However, such crystalline architectures could only be achieved by the systematic use of large polyoxometalate anions serving as templates. Furthermore, in these described materials, the 1D chains are not markedly linear, being branched at some point that may also serve as a coordination site for other metals such as found in the material reported by Li *et al.*^[183]

The anionic 1D organic-inorganic hybrid polymer, $[\text{MoO}_3(\text{Hbpcd})]_n^{n-}$ (Figure 3.9a), present in the crystal structure of **3.1** is formed by a single crystallographically independent Mo^{6+} metal centre coordinated to two symmetry-related μ_2 -bridging oxido groups (in apical positions), two terminal $\text{Mo}=\text{O}$ groups, and one N,N' -chelated Hbpcd^- anionic ligand, ultimately describing a highly distorted $\{\text{MoN}_2\text{O}_4\}$ octahedral (O) coordination environment for which the equatorial plane is composed of the two latter coordinating groups (Figure 3.9b): while the internal (N,O)–Mo–(N,O) octahedral *trans* angles were found in the 156.9(12)–165.5(13) $^\circ$ range, the *cis* angles are instead in the 68.3(11)–99.8(13) $^\circ$ range; the Mo–(N,O) bond distances range from 1.67(3) to 2.43(3) Å.

Most of the octahedral distortion arises from within the equatorial plane of the $\{\text{MoN}_2\text{O}_4\}$ octahedron due to the strong *trans* influence of the two terminal oxido groups with respect to the N,N' -chelated Hbpcd^- anionic ligand. Even though the observed amplitudes for these physical parameters are large, a search in the CSD^{[37][36]} version 5.34 (November 2012 with 3 updates), for the geometrical parameters of $\{\text{MoN}_2\text{O}_4\}$ octahedra showed that the typical Mo–(N,O) bond distances and (N,O)–Mo–(N,O) angles are found in the *ca.* 1.70–2.37 Å and 72.1–166.1 $^\circ$ ranges (median values for each limit; from 188 hits in the database), clearly supporting the chemical feasibility of the structural model derived for compound **3.1**.

As depicted in Figure 3.9b, the two symmetry-related μ_2 -bridging O1 oxido groups are at the genesis of the 1D $[\text{MoO}_3(\text{Hbpcd})]_n^{n-}$ polymer establishing physical connections between adjacent units. This feature imposes an intermetallic $\text{Mo1}^i \cdots \text{Mo1}^i$ separation of 3.621(1) Å (*i.e.*, half of the *c*-axis) and a "kink" $\text{Mo1}-\text{O1}-\text{Mo1}^i$ angle of 154.4(12) $^\circ$. A search in the literature for similar values in Mo^{6+} -containing polymeric materials reveals that the intermetallic distances are typically found in the 3.66–3.96 Å range (median 3.72 Å), while the "kink" angles of μ_2 -bridging oxido groups are instead described in the wide 135.8–175.4 $^\circ$ range (median 157.2 $^\circ$). This data clearly shows that while the observed bridging "kink" angle for **3.1** is rather typical, the intermetallic separation is markedly shorter than in related materials. This structural feature can be rationalized by taking into consideration the various supramolecular contacts mediating the crystal packing of the material and contributing to the overall structural robustness.

Within the anionic $[\text{MoO}_3(\text{Hbpcd})]_n^{n-}$ polymer, which runs parallel to the *c*-axis of the unit cell, symmetry-related N,N' -chelated Hbpcd^- ligands alternate (concerning the location of the protonated carboxylic acid group) and are slightly tilted with respect to the $\text{Mo} \rightarrow \text{O} \rightarrow \text{Mo}$ vector along the polymer (this is particularly notable from a front view of the polymer as depicted in Figure 3.9): the dihedral angle between the two ligands is *ca.* 19.8 $^\circ$. An analogous dihedral angle of *ca.* 49.6 $^\circ$ was previously reported by Zapf *et al.* for the neutral polymer $[\text{MoO}_3(\text{bipy})]_n$ (see Introduction, Table 3, polymer **23**).^[59] The striking difference between these two dihedral angles is attributed mainly to the type of

supramolecular interactions mediating the packing of adjacent polymers: while in the anionic polymer reported in this chapter the 5,5'-disubstituted carboxylic acid groups are mutually engaged in strong and highly directional O–H⋯O hydrogen bonds (Figure 3.10), which drive the molecules to be almost aligned along the direction of the polymer, in the close packing of $[\text{MoO}_3(\text{bipy})]_n$ only weak contacts are present, thus allowing the mutual rotation of adjacent bipy molecules so as to minimize steric repulsion. This is also the structural reason why the exact opposite was observed in the material $\{[\text{MoO}_3(\text{bipy})][\text{MoO}_3(\text{H}_2\text{O})]\}_n$ previously described in chapter 1: in that situation the bipy ligands of the neutral $[\text{MoO}_3(\text{bipy})]_n$ polymer were perfectly aligned so as to minimize steric repulsion with the adjacent $[\text{MoO}_3(\text{H}_2\text{O})]_n$ polymers.

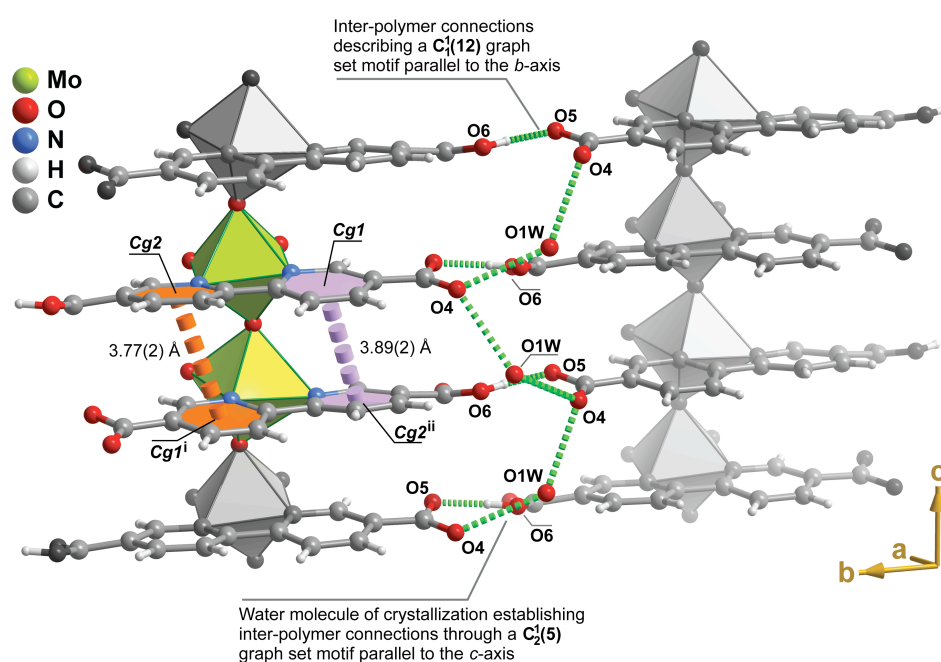


Figure 3.10. Mixed ball-and-stick and polyhedral representation of the supramolecular contacts (O–H⋯O hydrogen bonds and π - π contacts) involving adjacent anionic 1D $[\text{MoO}_3(\text{Hbpd})]_n^{n-}$ hybrid polymers in the crystal structure of 3.1. Symmetry transformations used to generate equivalent centroids: (i) $x, -y, -1/2+z$; (ii) $x, -y, 1/2-z$ (please note: transformation operations involving the inter-polymer $C_1(12)$ and $C_2(5)$ graph set motifs^[144] have been omitted for clarity).

The close packing of individual anionic $[\text{MoO}_3(\text{Hbpd})]_n^{n-}$ polymers, DMA^+ cations and water molecules of crystallization to yield the crystal structure of 3.1 is mediated by a series of supramolecular contacts. The most striking interactions concern the strong [$d_{\text{D}\cdots\text{A}} = 2.49(2) \text{ \AA}$] and highly directional [$\angle(\text{DHA}) = 169^\circ$] O6–H6⋯O5 hydrogen bonds involving the carboxylic acid groups of adjacent anionic $[\text{MoO}_3(\text{Hbpd})]_n^{n-}$ polymers, establishing an effective physical connection between polymers along the [010] direction of the unit cell

and describing an interpolymer $C_1^1(12)$ graph set motif (Figure 3.10).^[144] Additionally, adjacent coordinated Hbpd c^- ligands interact via offset π - π contacts, with the inter-centroid distances ranging from *ca.* 3.77(2) to 3.89(2) Å. The cooperative effect of both these O-H \cdots O hydrogen bonds and π - π contacts seems to be the reason why in 3.1 the intermetallic Mo1 \cdots Mo1 separation is among the shortest reported to date. Inter-polymer connections are also ensured by the water molecule of crystallization that is involved in a $C_2^1(5)$ graph set motif parallel to the [001] direction, donating the two hydrogen atoms to neighbouring carboxylic acid groups (Figure 3.10 and 3.11).

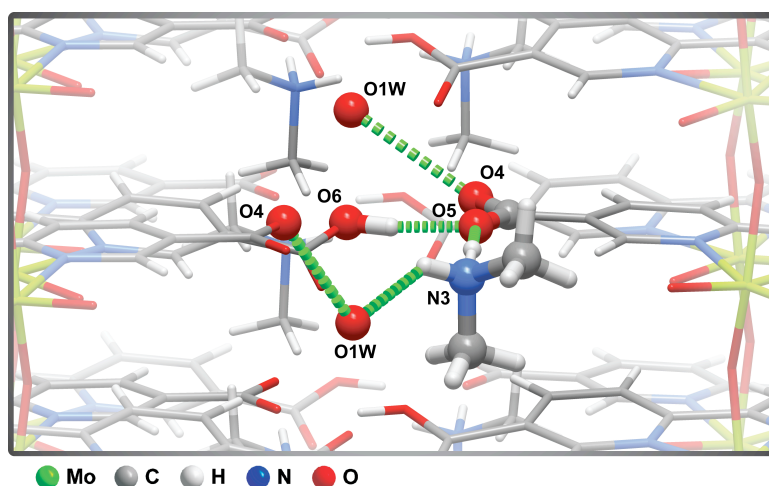


Figure 3.11. Detailed view of the strong and highly directional (N,O)-H \cdots O hydrogen bond interactions (dashed green lines) interconnecting anionic $[\text{MoO}_3(\text{Hbpd}c)]_n^{n-}$ hybrid polymers, DMA $^+$ cations and water molecules of crystallization. Symmetry transformations used to generate equivalent atoms have been omitted for clarity.

The DMA $^+$ cation is engaged in both strong (N $^+$ -H \cdots O $^-$) and weak (C-H \cdots O) hydrogen bonds with oxido and carboxylic acid groups belonging to adjacent anionic $[\text{MoO}_3(\text{Hbpd}c)]_n^{n-}$ polymers and water molecules of crystallization (Figure 3.11). The most notable interaction concerns the charged N $^+$ -H \cdots O $^-$ hydrogen bond that this cation establishes with the neighbouring carboxylate group. Despite being relatively long [$d_{\text{D}\cdots\text{A}} = 2.97(4)$ Å], this interaction remains somewhat directional [$\angle(\text{DHA}) = 158^\circ$]. The other hydrogen from the protonated -NH $_2^+$ moiety is in turn donated to the neighbouring water molecule. Weak C-H \cdots O hydrogen bonds are also present in the crystal structure, connecting not only the DMA $^+$ cation to adjacent moieties (such as the anionic polymer and water molecules), but also promoting inter-polymer connections (the most striking example concerns the C7-H7 \cdots O3 interaction - not shown). Despite these supramolecular interactions being of rather weak nature they are, nevertheless, numerous in the crystal structure of 3.1 and, in general, they are relatively directional [all $\angle(\text{DHA})$ angles are greater than 127°].

The cooperative effects of the various supramolecular contacts described in the previous paragraphs contribute significantly towards the structural robustness of the material, and further help to explain why the self-assembly of the material from solution produces such highly crystalline material.

3.2.7. CATALYTIC STUDIES

The catalytic performance of $(\text{DMA})[\text{MoO}_3(\text{Hbpd})] \cdot n\text{H}_2\text{O}$ (**3.1**) was investigated in epoxidation reactions (at 55 or 75 °C) of the bioderived olefins Ole and Lim, using TBHP_{dec} as the oxygen donor and DCE or BTF as the organic co-solvents.

TBHP_{dec} was the only oxidant chosen for these studies because as shown in chapter 1 and in published reports^[98] the catalytic performance of oligo-/polymeric oxomolybdenum(VI) hybrid compounds for olefin epoxidation tends to be superior when using organic hydroperoxides as oxidants rather than, for example, H_2O_2 . Moreover, TBHP possesses relatively small molecular dimensions, which is important to avoid steric constraints, since the reaction mechanism typically involves coordination of the organic hydroperoxide to the metal centre to give the active oxidizing species responsible for the oxygen transfer reaction to the olefin.

3.2.7.1. Ole EPOXIDATION

At 55 °C, the reaction of Ole with TBHP_{dec} in the presence of **3.1** gave OleOx (see Figure 3.12) as the main product (yields of ca. 77-83% at 24 h). Note that without the catalyst the Ole conversion was negligible.

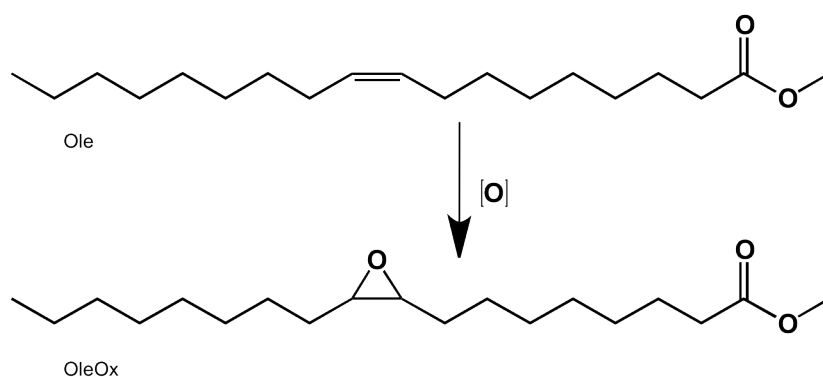


Figure 3.12. Methyl oleate epoxidation product.

As shown in Figure 3.13, the rate of formation of OleOx was comparable, within the temperature choice, for both co-solvents. On the other hand, in Figure 3.14 it is observed that while for BTF the OleOx selectivity was 100% at

high conversions, for DCE there was a slight decrease in product selectivity at comparably high conversions. This fact was concomitant with the formation of OleDiol as a by-product (ca. 4% of OleDiol yield at 87% conversion). The outstanding epoxide selectivity while using BTF is possibly related to the high hydrophobicity of this solvent, thereby avoiding water in the reaction system.

Increasing the reaction temperature from 55 to 75 °C the reaction rate enhanced, for instance, at 6 h reaction, from ca. 42% to 89-93% conversion using either DCE or BTF co-solvents (Figure 3.13). The increase in temperature did not significantly affect the dependence of OleOx yields on Ole conversion. At 75 °C the reaction of Ole was complete within 24 h, giving an excellent OleOx yield of 98% with BTF as co-solvent (see Figure 3.13 at 24 h time).

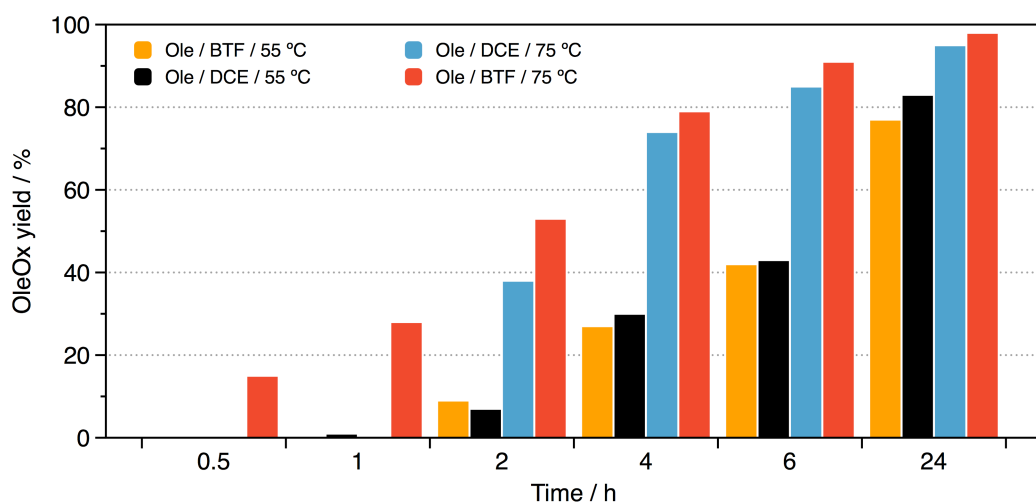


Figure 3.13. Dependence of OleOx yield on the reaction time for the reaction of Ole with TBHP_{dec} in the presence of (DMA)[MoO₃(Hbpdc)]·*n*H₂O (3.1).

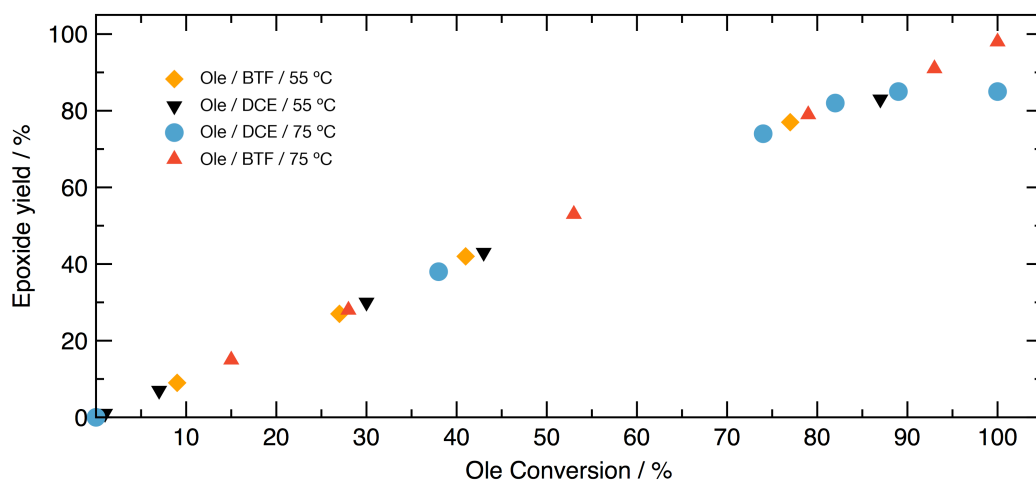


Figure 3.14. Dependence of OleOx yield on the Ole conversion for the reaction of Ole with TBHP_{dec} in the presence of (DMA)[MoO₃(Hbpdc)]·*n*H₂O (3.1).

3.2.7.2. Lim EPOXIDATION

As showed in Figure 3.16 the epoxidation of Lim (Figure 3.15) at 55 °C leads to LimOx as the main reaction product in similar yields (*ca.* 85% at 24 h time) for either DCE or BTF co-solvents. In the temperature range of 55-75 °C, regioselectivity was very high toward the epoxidation of the endocyclic C=C bond. At Lim conversions greater than *ca.* 90% (*i.e.*, 6 h reaction time), the LimOx yield decreased slightly with the concomitant increase in LimDiOx yield (range from 3-7% yield; Figure 3.17), suggesting that LimOx is an intermediate in the formation of LimDiOx.

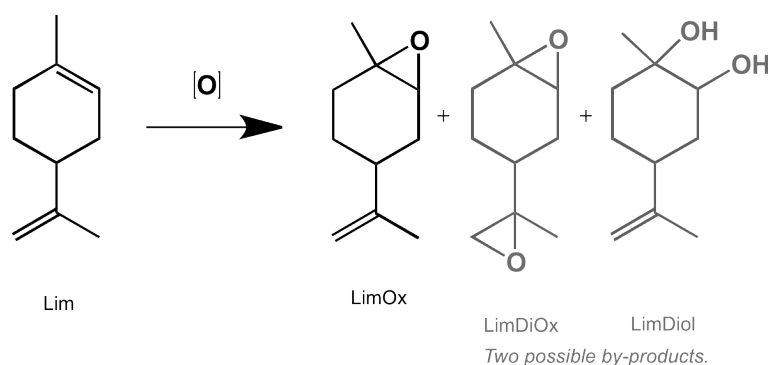


Figure 3.15. DL-limonene epoxidation products and possible by-products.

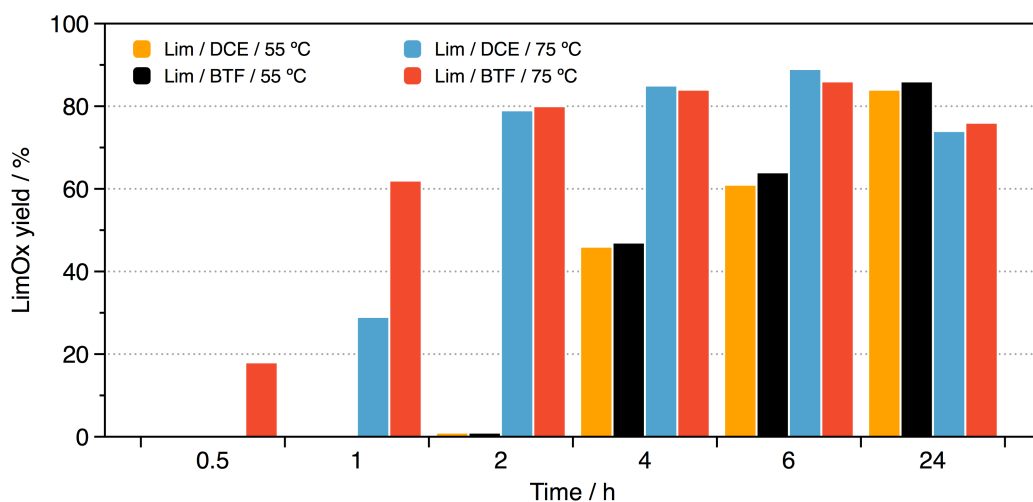


Figure 3.16 Dependence of LimOx yield on the reaction time for the reaction of Lim with TBHP_{dec} in the presence of (DMA)[MoO₃(HbpdC)]·*n*H₂O (3.1).

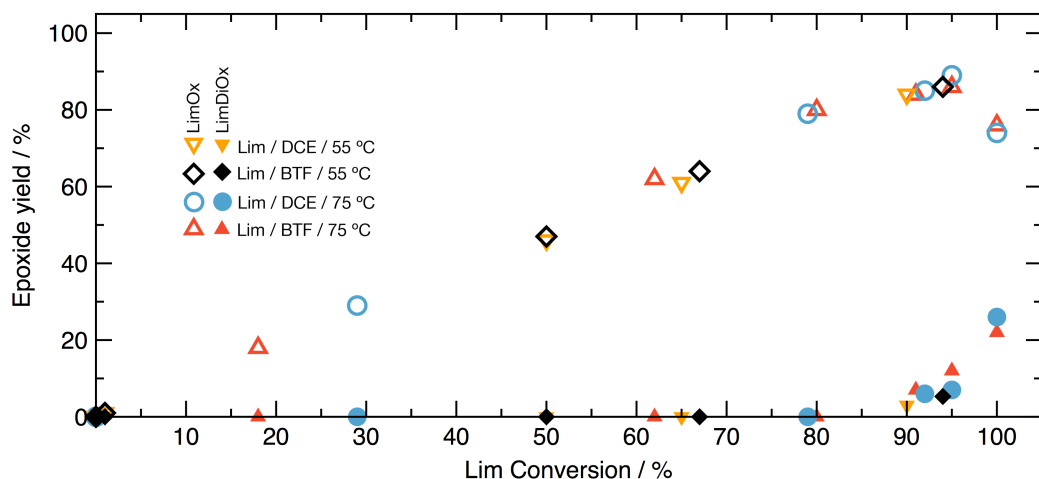


Figure 3.17 Dependence of LimOx (*open symbols*) and LimDiOx (*filled symbols*) yields on Lim conversion for the reaction of Lim with TBHP_{dec} in the presence of (DMA)[MoO₃(HbpdC)]·*n*H₂O (3.1) and the co-solvents DCE and BTF at 55 or 75 °C.

For both substrates and both co-solvents, an initial induction period was observed at 55 °C (*i.e.*, *ca.* 1 h for Ole and 2 h for Lim). After increasing the temperature from 55 to 75 °C the initial reaction rates increased, and the induction period was only observed for DCE. These results may be explained by the fact that the co-solvent BTF may better solubilize the metal species (notice that the reaction mixtures with the organic co-solvents were always biphasic solid-liquid). Such hypothesis assumes that the catalytic reaction takes place in the homogeneous phase, which was confirmed by the CatFilt test (details given in the Experimental chapter) for the system 3.1 / Ole / TBHP_{dec} / BTF / 75 °C. A $\Delta\text{Filt} / \Delta\text{cat}$ ratio equal to 1 was obtained for this system, suggesting that the catalytic reaction is homogeneous in nature. A 4-fold decrease in the initial mass of 3.1 using BTF at 75 °C, led to a slower reaction of Ole, with OleOx obtained as the only product in 65 / 92% yield at 6 / 24 h (under these conditions, the reaction mixture was also biphasic solid-liquid).

The dependence of the reaction rate on the initial amount of catalyst was surprising because the catalytic reaction takes place in the homogeneous phase and 3.1 was never fully dissolved in the reaction medium (*i.e.*, the reaction mixture was apparently saturated with metal compound). The initial rate of dissolution of the metal species in the liquid medium is most likely the limiting factor to the overall reaction process. Similar effects have been reported for molybdenum-based epoxidation catalysts in the model reaction of Cy8.^[185]

3.2.7.3. IONIC LIQUIDS

Homogeneous metal-based catalysis has the industrial drawback of being expensive and with highly difficult steps to recover and reuse the catalyst. Thus, in addition to the homogeneous catalytic studies performed up until now (e.g., in chapter 2) in this chapter a new approach was made in an attempt to facilitate the catalyst recycling process. The work consisted of using the ionic liquids (ILs): [bmim]BF₄, [bmim]NTf₂ or [bmpy]BF₄ instead of the co-solvents DCE or BTF. These particular ILs were chosen due to their commercial availability, relatively low price and stability under the reaction conditions used. [bmim]BF₄ and [bmim]NTf₂ have already been successfully used as co-solvents for the epoxidation of olefins in the presence of Mo-based homogeneous catalysts.^{[126][170][186][187][188][189][190][191][192]}

Table 3.1 summarizes the results for the 3.1 / TBHP_{dec} / IL / 75 °C systems studied for Ole and Lim epoxidation reactions. The “non-productive” decomposition of TBHP (into *tert*-butanol and molecular oxygen) in the systems (without the olefin) was determined by iodometric titration and found to be less than 6% after 6 h. For the same systems with Ole but without catalyst no reaction took place.

The dependence of OleOx yield on Ole conversion was similar for the organic and IL solvent systems examined in this work. A comparison of the results for the three ILs shows that the formation of OleOx was faster for [bmim]NTf₂ (60 / 76% yield at 60 / 79% conversion reached at 6 / 24 h of reaction, respectively; Figure 3.18). The ILs containing BF₄⁻ led to 50–52% OleOx yield (with 100% selectivity) at 24 h (Table 3.1, Figure 3.18).

Table 3.1. Conversion and epoxide yield of the Ole and Lim epoxidation reactions with TBHP_{dec} at 75 °C using the ILs [bmim]NTf₂ and [bmpy]BF₄ as co-solvents.

Substrate	Ionic Liquid	Olefin Conversion (%) ^a (6 / 24 h)	Epoxide yield (%) ^a (6 / 24 h)
Ole	[bmim]NTf ₂	60 / 79 (- / 74) ^b	60 / 76 (- / 73) ^b
	[bmpy]BF ₄	17 / 52	17 / 52
	[bmpy]BF ₄	23 / 50	23 / 50
Lim	[bmim]NTf ₂	74 / 76 (76 / 79) ^b	67 / 61 (66 / 64) ^b
	[bmpy]BF ₄	52 / 72	47 / 65

^a Reaction using initial molar ratios Mo : olefin : TBHP = 1 : 103 : 160.

^b Values inside the parentheses correspond to a second catalytic batch run.

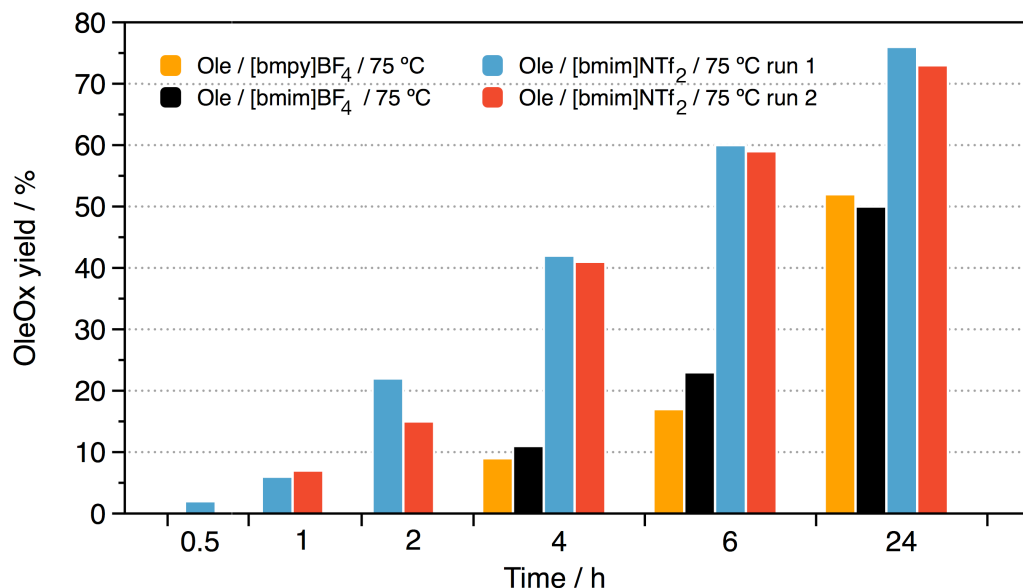


Figure 3.18 Dependence of OleOx yield on the reaction time for the reaction of Ole with TBHPdec in the presence of (DMA)[MoO₃(HbpdC)]·nH₂O (3.1).

In contrast to that observed for the BF₄⁻ containing ILs, the reagents were completely dissolved in [bmim]NTf₂. Considering the good solubilization properties and relatively low viscosity of [bmim]NTf₂, mass transfer limitations may be less important. The recyclability of the catalyst/[bmim]NTf₂ system was investigated by carrying out a second 24 h batch run of the reaction of Ole at 75 °C, using the recovered catalyst/[bmim]NTf₂ mixture (please see the Experimental chapter for additional details). The catalytic results were similar for the two consecutive runs, suggesting that the 3.1/[bmim]NTf₂ system can be effectively recycled (Table 3.1). In parallel to that observed for Ole, the formation of LimOx from Lim was faster for [bmim]NTf₂ than for [bmim]BF₄, and similar catalytic results were obtained in the two consecutive 24 h batch runs using [bmim]NTf₂ as co-solvent (Figure 3.18).

3.3. CONCLUDING REMARKS

This chapter described the solvothermal synthesis of the new 1D organic-inorganic polymeric material: (DMA)[MoO₃(HbpdC)]·nH₂O (3.1). While in previous chapters the solvothermal synthesis always occurred with water as the reactive medium (*i.e.*, hydrothermal conditions), in this study a solvent mixture of H₂O : DMF had to be employed in order to increase the solubility of the organic ligand. This solvothermal approach afforded an orange solution from which microcrystalline powdered 3.1 continuously precipitated over a period of 4 days.

As for materials described in other chapters, the crystal structure details of 3.1 were found from a combination of several solid-state characterization

techniques, including solid-state NMR, thermogravimetry, vibrational spectroscopy and high-resolution powder X-ray diffraction investigations.

The crystal structure of **3.1** is formed by an anionic 1D $[\text{MoO}_3(\text{Hbpd})]_n^{n-}$ organic-inorganic hybrid polymer that cocrystallizes with charge-balancing DMA^+ cations and one water molecule per metal center. This novel hybrid material is truly unique: on the one hand, it is the first negatively-charged polymeric compound of its kind; moreover, it is the first 1D polymer based on dioxomolybdenum(VI) units coordinated to a N,N' -chelate ligand which also has other possible coordinative sites (*i.e.*, the *exo*-located carboxylic acid groups).

Several synthetic investigations were made in order to try to increase the crystallite size of **3.1** and they were all unsuccessful. Indeed, the structural resolution based on powder X-ray diffraction data showed that the material had to have DMA^+ cations in its composition. These chemical species had to be, however, formed *in situ* from the solvent DMF. This transformation process seems to limit somehow the crystal growth rate, improving instead the rate of crystal nucleation, hence systematically leading to the isolation of a microcrystalline powder.

Comparing the crystal structure of **3.1** with related structures described in the literature, particularly that by Zubietta and co-workers, $[\text{MoO}_3(\text{bipy})]_n$ (Introduction, Table 3, polymer **23**), and $\{[\text{MoO}_3(\text{bipy})][\text{MoO}_3(\text{H}_2\text{O})]\}_n$ (**1.2**, chapter 1), it is clear that the use of H_2bpd leads to significantly stronger interactions between adjacent polymers.

In **1.2**, the two neutral 1D polymers, *i.e.*, $[\text{MoO}_3(\text{bipy})]_n$ and $[\text{MoO}_3(\text{H}_2\text{O})]_n$, are linked by $\text{O}-\text{H}\cdots\text{O}$ hydrogen bonding interactions [$d_{\text{D}\cdots\text{A}} = 2.6166(19)$ and $2.7959(19)$ Å] established between the coordinated water molecule and neighbouring atoms of the terminal $\text{Mo}=\text{O}$ oxido groups of an adjacent polymer. Even though these connections are still very strong and approximately similar to those present in **3.1**, in this latter compound there is a negative charge involved in the interaction, ultimately boosting robustness. Indeed, the distance between the donor and the acceptor atoms is only of $d_{\text{D}\cdots\text{A}} = 2.49(2)$ Å for **3.1**.

This structurally relevant, and very strong hydrogen bond also leads to a displacement of the N,N' -chelated moiety in **3.1** from the growth direction of the polymer. Indeed, both in $\{[\text{MoO}_3(\text{bipy})][\text{MoO}_3(\text{H}_2\text{O})]\}_n$ (**1.2**) and $[\text{MoO}_3(\text{bipy})]_n$ reported by Zubietta the N,N' -chelated 2,2'-bipyridine molecules are perfectly eclipsed along the direction of the polymer. This can be attributed to the absence of strong supramolecular interactions involving the organic moiety (only $\text{C}-\text{H}\cdots\text{O}$ contacts exist). Conversely, in **3.1** the presence of the two carboxylic acid groups permits the existence of much stronger interactions, making the ligand adopt a crystallographic position that is not eclipsed (instead it shifts so as to maximize the supramolecular contacts).

When **3.1** was employed as catalyst in the olefin epoxidation of Ole and Lim using TBHP_{dec} as oxidant and DCE or BTF as the organic co-solvents, the catalytic reactions were homogeneous in nature. In addition, the obtained

results for Ole are comparable to those reported for other mono-/polymeric molybdenum compounds possessing mono-/bidentate (bi)pyridine-type ligands. For Lim epoxidation, **3.1** also compares favourably with other related materials.

When IL solvent systems were employed instead of the organic co-solvents the homogeneity issue was successfully addressed. As a result, the TBHP_{dec} / IL / 75 °C systems were effectively recycled as in a typical heterogeneous catalysis process.

SYNTHESES of DISCRETE and POLYMERIC HYBRID COMPOUNDS with 2-[3(5)-PYRAZOLYL]PYRIDINE

4.1. SUMMARY

In this chapter the hydrolysis and condensation of the mononuclear complex $[\text{MoO}_2\text{Cl}_2(\text{L})]$ ($\text{L} = \text{pzpy}$; 2-[3(5)-pyrazolyl]pyridine) was used to extend the studies performed aimed at expanding the structural diversity of molybdenum oxide-based organic inorganic hybrid materials. The selection of pzpy as a N,N' -chelate ligand is based on a handful of reports available in the literature that show that this molecule is a suitable organic ligand toward the design of active molybdenum(VI) catalysts for olefin epoxidation.^{[49][81]}

The treatment of the dichlorodioxomolybdenum(VI) complex with water under hydrothermal, open reflux or microwave-assisted heating conditions led to the isolation of the inorganic-organic hybrid $[\text{Mo}_3\text{O}_9(\text{pzpy})]_n$ (4.2), whose crystal structure has been determined from synchrotron powder X-ray diffraction data in conjunction with other characterization studies. Material 4.2 has also been isolated from the hydrothermal treatment of an aqueous solution containing MoO_3 and pzpy. The molybdenum-catalyzed epoxidation of *cis*-cyclooctene was chosen as a model reaction to assess the catalytic properties of 4.2.

4.2. $[\text{Mo}_3\text{O}_9(\text{pzpy})]_n$ (4.2)

This section summarizes the efforts toward the use of the complex $[\text{MoO}_2\text{Cl}_2(\text{pzpy})]$ (4.1) to prepare the Mo^{6+} oxide hybrid polymeric compound $[\text{Mo}_3\text{O}_9(\text{pzpy})]_n$ (4.2). The compound was obtained from the treatment of 4.1 with water under three distinct reaction conditions: i) hydrothermal synthesis (with induction heating); ii) open reflux system; and iii) microwave-assisted synthesis. Compound 4.2 was obtained from the hydrothermal reaction of MoO_3 and the ligand pzpy in H_2O . Two secondary products were isolated from the aqueous mother liquors resulting from the aforementioned reactions: the salt $(\text{pzpyH})_2(\text{MoCl}_4)$ (pzpyH = 2-(1*H*-pyrazol-3-yl)pyridin-1-ium; for more details see the Experimental chapter) and the known tetranuclear compound $[\text{Mo}_4\text{O}_{12}(\text{pzpy})_4]$ (4.3) (Figure 4.1) whose structure was described by the research group of Zhang,^[48] (see Introduction). A detailed structural characterization of 4.2 is presented which includes FT-IR, FT-Raman and $^{13}\text{C}\{^1\text{H}\}$ CP MAS NMR spectroscopies.

The catalytic performance of 4.2 in the epoxidation of Cy8 with TBHP_{dec} was assessed and is described in detail.

4.2.1. SYNTHESIS

Hybrid precursor: $[\text{MoO}_2\text{Cl}_2(\text{pzpy})]$ (4.1)

The complex $[\text{MoO}_2\text{Cl}_2(\text{pzpy})]$ (4.1) was prepared following literature procedures: 2-[3(5)-pyrazolyl]pyridine (pzpy) was added to a solution of $[\text{MoO}_2\text{Cl}_2(\text{THF})_2]$ in THF.^[81]

The reaction of 4.1 with water was carried out either in an open reflux system under nitrogen (16 h, oil bath heating, method A), in a sealed glass vessel with microwave-assisted heating (120 °C, 2 h, method B), or in a sealed Teflon-lined stainless steel autoclave (autogenous pressure, 100 °C, 19 h, method C). The Experimental chapter contains more details on each procedure employed. In each case a pale blue solid suspended in an acidic solution (pH of about 1-3) was obtained, which was recovered by filtration, washed with water and organic solvents, and vacuum-dried. Practically identical elemental analysis, FT-IR and powder X-ray diffraction data were obtained for all three solid products, indicating that the heating method had no significant influence on the outcome of the reaction (see, as an example, X-ray diffraction Figure presented in the Experimental chapter). EDS analyses confirmed the absence of chlorine in the final product 4.2. Based on the characterization data and the crystal structure solution described below, the product was formulated as the polymeric material $[\text{Mo}_3\text{O}_9(\text{pzpy})]_n$ (4.2) (Figure 4.1).

The yield of 4.2 was in the range of 72-79% for all three methods. In the case of method C, concentration of the filtrate led to the appearance of small crystals, which were identified by single-crystal X-ray diffraction as the salt

(pzpyH)₂(MoCl₄) (see Experimental chapter for full details of the structural elucidation).

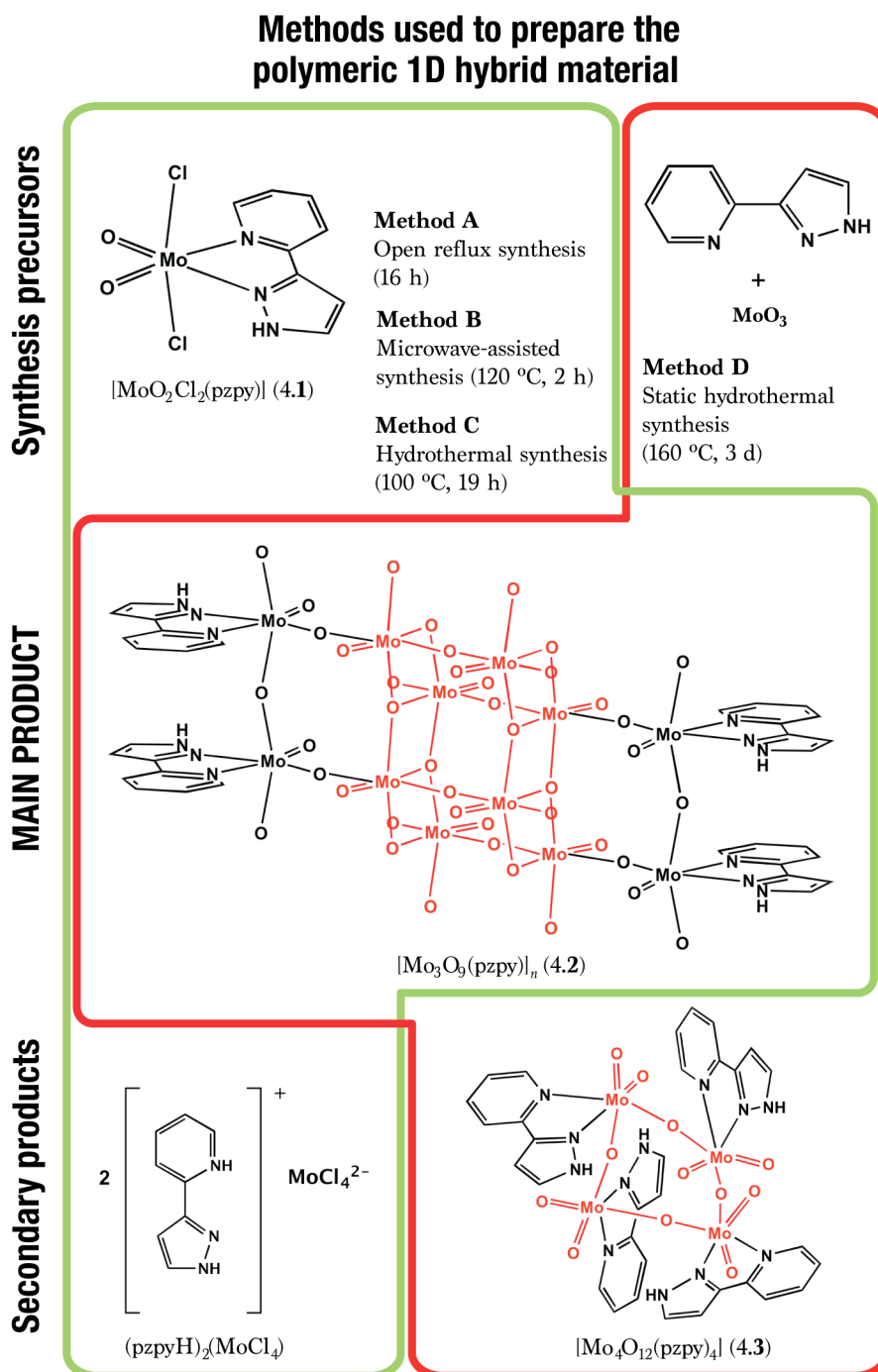


Figure 4.1. Methods used to prepare the 1D hybrid material [Mo₃O₉(pzpy)]_n (4.2). When the metallic source was the inorganic MoO₃ (plus the free organic ligand pzpy), the secondary product isolated from the solution was the tetranuclear [Mo₄O₁₂(pzpy)₄] (4.3) discrete complex. From method C and after concentrating the filtrate under reduced pressure, small crystals of the salt (pzpyH)₂(MoCl₄) were obtained.

Metallic precursor: MoO₃

Polymeric compound 4.2 could also be isolated in poor yields (*ca.* 29%) by the reaction of MoO₃, pzpy and H₂O in the mole ratio of *ca.* 1 : 1 : 560 at 160 °C for 3 d in a teflon-lined autoclave (method D, Figure 4.1). The pale yellow filtrate from this reaction was evaporated to dryness and the resultant solid identified as the known tetranuclear compound [Mo₄O₁₂(pzpy)₄] (4.3) (Figure 4.1) by a comparison of the experimental powder X-ray diffraction pattern with a simulation based on the crystal structure data reported by Zhang and co-workers.^[48] Even though, these authors obtained crystals of 4.3 by using the same hydrothermal method, they did not report the formation of an insoluble product which could be identical to polymeric 4.2.

4.2.2. SCANNING ELECTRON MICROSCOPY

Even though several attempts were performed to isolate large single crystals of 4.2, this material was systematically isolated as a microcrystalline powder regardless of the synthetic method A to D employed.

Scanning electron microscopy studies were performed on a representative portion of the [Mo₃O₉(pzpy)]_{*n*} (4.2) material obtained from method C (Figure 4.2). Studies indicated that 4.2 is composed of very thin and long (hair-like) crystallites with an average size up to 2 μm in length. This long shape morphology may indicate a preferential growth direction. Energy dispersive X-ray analyses (EDS) confirmed the absence of Cl in 4.2.

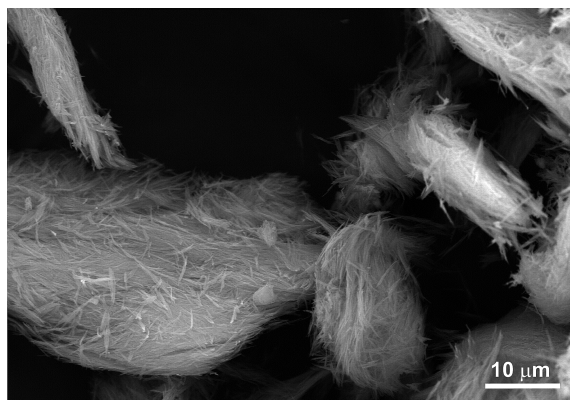


Figure 4.2. Scanning Electron Microscopy (SEM) image of material 4.2 obtained using the synthetic method C.

4.2.3. X-RAY DIFFRACTION: CRYSTAL STRUCTURE DESCRIPTION

A full structural elucidation could only be achieved by using *ab initio* powder X-ray diffraction methods based on high-resolution synchrotron X-ray data (Figure 4.3) in combination with other relevant characterization techniques.

It is noted that this tandem approach was used to unveil the structural features of other novel molybdenum oxide-organic hybrid materials such as $\{[\text{MoO}_3(\text{bipy})][\text{MoO}_3(\text{H}_2\text{O})]\}_n$ (1.2) (where bipy = 2,2'-bipyridine)^[142] and $(\text{DMA})[\text{MoO}_3(\text{Hbpydc})]_n \cdot \text{H}_2\text{O}$ (3.1) (where DMA^+ = dimethylammonium; H_2bpydc = 2,2'-bipyridine-5,5'-dicarboxylic acid)^[182] and which have been described in chapters 1 and 3, respectively.

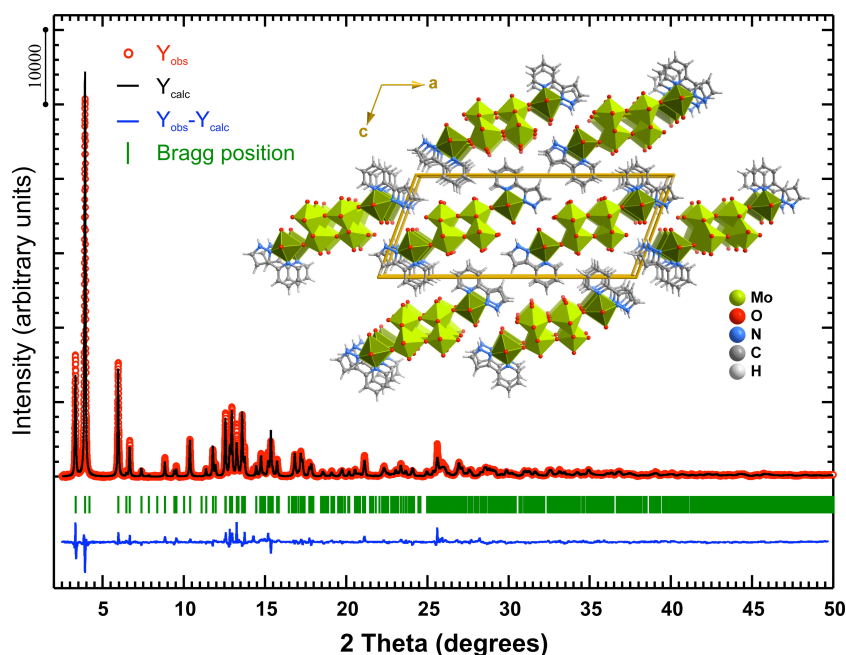


Figure 4.3. Final Rietveld plot (synchrotron powder X-ray diffraction data) of $[\text{Mo}_3\text{O}_9(\text{pzpy})]_n$ (4.2). Observed data points are indicated as red circles, and the best fit profile (upper trace) and the difference pattern (lower trace) are drawn as solid black and blue lines, respectively. Green vertical bars indicate the angular positions of the allowed Bragg reflections. Refinement details are given in Experimental chapter. A mixed ball-and-stick and polyhedral crystal packing representation of 4.2 viewed down the [010] crystallographic direction is provided as an inset.

The crystal structure of $[\text{Mo}_3\text{O}_9(\text{pzpy})]_n$ (4.2) is based on three crystallographically independent Mo^{6+} metal centers and one pzpy organic ligand. These four moieties are structurally located on special positions belonging to the mirror plane of the $C2/m$ monoclinic unit cell, alongside with 7 (out of the 9) crystallographically independent oxygen atoms. The three single Mo^{6+} centers (Mo1, Mo2 and Mo3) have considerably distinct coordination environments as well as distinct structural functions in the crystal structure of 4.2 (Figures 4.4a and 4.4c-e). Only Mo1 has the organic ligand in its coordination environment in a typical N,N' -chelate fashion, with the overall $\{\text{MoN}_2\text{O}_4\}$ coordination geometry resembling a distorted octahedron

(Figure 4.4c): the Mo1–(N,O) distances range from 1.909(3) to 2.35(2) Å, and the *cis* and *trans* octahedral angles were found in the 66.8(10)-117.9(8)° and 146.5(9)-162.4(9)° ranges, respectively (Tables 3 and 4). The coordination spheres of Mo2 and Mo3 are uniquely composed of oxygen atoms, {MoO₆} (Figures 4.4d and 4.4e), and exhibit very similar geometrical features: the Mo–O distances for the two metal environments were found in the 1.691(16)-2.325(18) Å range, and the *cis* and *trans* octahedral angles were in the 149.8(8)-179.5(8)° and 73.6(8)-104.3(7)° intervals, respectively (Tables 4.1 and 4.2). From these data, it is difficult to properly evaluate and compare the degree of distortion for each Mo⁶⁺ octahedron: while the presence of pzpy in the coordination sphere of Mo1 seems to visually indicate a more distorted octahedron (Figure 4.4c), the values for the angles and distances are, on average, more spread out for Mo2 and Mo3. To further help in the evaluation of the variation of the degree of distortion of the Mo⁶⁺ octahedra, it was decided to employ an adaptation of a simple method proposed by Baur^[193] to calculate a distortion index (DI) for bonds and angles:

Equation 4.1

$$DI_{Bond} = \frac{\sum_{i=1}^n \left| d(Mo-(N,O))_i - d(Mo-(N,O))_{average} \right|}{\sum_{i=1}^n \left| d(Mo-(N,O))_i \right|}$$

Equation 4.2

$$DI_{Angle} = \frac{\sum_{i=1}^n \left| \angle((N,O)-Mo-(N,O))_i - \angle((N,O)-Mo-(N,O))_{ideal} \right|}{\sum_{i=1}^n \left| \angle((N,O)-Mo-(N,O))_i \right|}$$

where the subscripts *i* and *average/ideal* correspond to individual and average/ideal bond lengths and angles. For the sake of comparison, the value of DI_{Angle} should be, for an octahedron, calculated independently for the *cis* and *trans* angles. Even though the initial model by Baur^[193] suggested that DI_{Angle} should also be calculated with respect to the average values observed for the polyhedra, we believe that only when comparing with the ideal values of an octahedron (*i.e.*, 90 and 180° for the *cis* and *trans* angles, respectively) can one derive correct comparative conclusions on the degrees of distortion for each individual Mo⁶⁺ coordination environment. Having this in mind, the DI_{Bond} values for the three crystallographically independent Mo⁶⁺ metallic centers are 0.086, 0.068 and 0.085 for Mo1, Mo2, and Mo3, respectively. The corresponding DI_{Angle} values for the *cis/trans* angles are 0.120/0.164, 0.101/0.117 and 0.104/0.096

for Mo1, Mo2, and Mo3, respectively. These results are significantly more clear indicating that when one compares the polyhedra to the ideal Archimedean solid, Mo1 is significantly more distorted concerning the angle spread, while Mo2 and Mo3 are, as expected, more structurally similar. In addition, it is possible to further conclude that the variation of the distances is approximately identical for all three Mo⁶⁺ metal centers, with the environment of Mo2 being slightly more regular than the other two.

Table 4.1. Selected bond lengths (in Å) for the three crystallographically independent molybdenum coordination environments present in [Mo₃O₉(pzpy)]_n (4.2).^a

Mo1-O3	2.00(2)	Mo1-O7 ⁱ	1.909(3)
Mo1-O5	1.671(15)	Mo1-N1	2.35(2)
Mo1-O7	1.909(3)	Mo1-N2	2.17(3)
Mo2-O1	2.32(2)	Mo2-O3	2.02(2)
Mo2-O2	1.930(5)	Mo2-O4	2.02(2)
Mo2-O2 ⁱ	1.930(5)	Mo2-O8	1.691(16)
Mo3-O1 ⁱⁱ	1.927(5)	Mo3-O4	2.03(2)
Mo3-O1 ⁱⁱⁱ	1.927(5)	Mo3-O6	1.678(17)
Mo3-O2 ⁱⁱ	2.325(18)	Mo3-O9	1.702(18)

^aSymmetry transformations used to generate equivalent atoms: (i) $x, -1+y, z$; (ii) $\frac{1}{2}-x, -\frac{1}{2}+y, 1-z$; (iii) $\frac{1}{2}-x, \frac{1}{2}+y, 1-z$.

The three Mo⁶⁺ polyhedra coalesce along the [010] direction of the unit cell to produce the hybrid organic-inorganic 1D polymer ∞^1 [Mo₃O₉(pzpy)] depicted in Figure 4.4a. This polymer is truly unique and it can be divided into two very distinct components. Interconnection between solely the Mo2 and Mo3 polyhedra leads to the formation of a double ladder-type inorganic core reminiscent of the crystal structure of MoO₃ (Figure 4.5). Indeed, the Mo \cdots Mo intermetallic distances within the inorganic core of ∞^1 [Mo₃O₉(pzpy)] range from 3.368(1) to 4.040(1) Å (Figure 4.4b), which are very similar to those found in the crystal structure of the inorganic precursor (from *ca.* 3.43 to 3.96 Å). The small differences are mainly attributed to crystal packing effects in 4.2 that induce small distortions in the polyhedra so as to promote a more effective packing of the polymers in the solid state. A portion of this inorganic core has already been found in the polymeric compound $\{[(\text{MoO}_3)(\text{bipy})][\text{MoO}_3(\text{H}_2\text{O})]\}_n$ (1.1)^[142] described in chapter 1. As described previously, the hybrid and the inorganic polymers are segregated in the crystal structure of the latter material, mutually interacting through supramolecular interactions. The inorganic ladder present in ∞^1 [MoO₃(H₂O)] is solely composed of one zigzag chain of Mo⁶⁺ centers

interconnected through μ_3 -bridging oxido groups (in contrast to two such ladders in $\infty^1[\text{Mo}_3\text{O}_9(\text{pzpy})]$ – see Figures 4.4 and 4.5), for which the $\text{Mo}\cdots\text{Mo}$ intermetallic distances along the chain have an average value of *ca.* 3.44 Å.

Table 4.2. Selected bond angles (in degrees) for the three crystallographically independent molybdenum coordination environments present in $[\text{Mo}_3\text{O}_9(\text{pzpy})]_n$ (4.2).^a

O3–Mo1–O5	117.9(8)	O5–Mo1–N2	95.6(9)
O3–Mo1–O7	90.2(6)	O7–Mo1–N1	77.8(4)
O3–Mo1–O7 ⁱ	90.2(6)	O7 ⁱ –Mo1–N1	77.8(4)
O3–Mo1–N1	79.7(9)	O7–Mo1–N2	83.0(6)
O3–Mo1–N2	146.5(9)	O7 ⁱ –Mo1–N2	83.0(6)
O5–Mo1–O7	100.9(5)	O7–Mo1–O7 ⁱ	155.1(6)
O5–Mo1–O7 ⁱ	100.9(5)	N1–Mo1–N2	66.8(10)
O5–Mo1–N1	162.4(9)		
O1–Mo2–O2	75.5(5)	O2–Mo2–O4	96.7(5)
O1–Mo2–O2 ⁱ	75.5(5)	O2 ⁱ –Mo2–O4	96.7(5)
O1–Mo2–O3	89.8(7)	O2–Mo2–O8	102.6(5)
O1–Mo2–O4	100.0(7)	O2 ⁱ –Mo2–O8	102.6(5)
O1–Mo2–O8	163.4(8)	O3–Mo2–O4	170.1(8)
O2–Mo2–O2 ⁱ	149.8(8)	O3–Mo2–O8	73.6(8)
O2–Mo2–O3	85.7(5)	O4–Mo2–O8	96.5(9)
O2 ⁱ –Mo2–O3	85.7(5)		
O1 ⁱⁱ –Mo3–O1 ⁱⁱⁱ	150.6(8)	O1 ⁱⁱⁱ –Mo3–O9	103.4(6)
O1 ⁱⁱ –Mo3–O2 ⁱⁱ	75.4(6)	O2 ⁱⁱ –Mo3–O4	76.2(7)
O1 ⁱⁱⁱ –Mo3–O2 ⁱⁱ	75.4(6)	O2 ⁱⁱ –Mo3–O6	104.3(7)
O1 ⁱⁱ –Mo3–O4	84.9(6)	O2 ⁱⁱ –Mo3–O9	162.6(8)
O1 ⁱⁱⁱ –Mo3–O4	84.9(6)	O4–Mo3–O6	179.5(8)
O1 ⁱⁱ –Mo3–O6	95.3(6)	O4–Mo3–O9	86.4(9)
O1 ⁱⁱⁱ –Mo3–O6	95.3(6)	O6–Mo3–O9	93.1(9)
O1 ⁱⁱ –Mo3–O9	103.4(6)		

^a Symmetry transformations used to generate equivalent atoms: (i) $x, -1+y, z$; (ii) $\frac{1}{2}-x, -\frac{1}{2}+y, 1-z$; (iii) $\frac{1}{2}-x, \frac{1}{2}+y, 1-z$.

Looking only at the structural behaviour of the Mo1 polyhedra, the interconnection along the [010] direction via μ_2 -bridging oxido groups leads to the formation of a 1D polymer topologically similar to that reported by Zubieta in $[\text{MoO}_3(\text{bipy})]_n$ ^[59] and in $\{[\text{MoO}_3(\text{bipy})][\text{MoO}_3(\text{H}_2\text{O})]\}_n$ (1.2)^[142] and (DMA)[$\text{MoO}_3(\text{Hbpydc})$]_n·H₂O (3.1)^[182] described in chapters 1 and 3, respectively. All these hybrid polymers exhibit a typical –O–O–O–O–O– distribution of the

oligomeric building units. Indeed, the Mo \cdots Mo intermetallic distance along this polymer in the compound reported in this chapter [3.727(1) Å – Figure 4.4b] compares well with those of the aforementioned structures described in previous chapters, which range from *ca.* 3.61 to 3.76 Å. As found for [MoO₃(bipy)]_n and {[MoO₃(bipy)][MoO₃(H₂O)]_n (1.2), the *N,N*-chelated moieties in 4.2 are eclipsed along the grow direction of the polymer (Figure 4.4).

Connections between the hybrid 1D polymers and the inorganic core in [Mo₃O₉(pzpy)]_n are ensured by a common oxido group which acts as a μ_2 -bridging moiety imposing a Mo \cdots Mo separation of 3.918(1) Å (Figures 4.4 and 4.5). In this way, the individual structure-composing compound 4.2 comprises an inorganic core, based on MoO₃, decorated at the periphery by two hybrid polymers. Remarkably, compound 4.2 finds a structural parallel in the material {[MoO₃(bipy)][MoO₃(H₂O)]_n (1.2), in which each individual ∞^1 [MoO₃(H₂O)] polymer interacts with two peripheral ∞^1 [MoO₃(bipy)]_n moieties *via* strong hydrogen bonds (see section 1.2.5 in chapter 1).^[142]

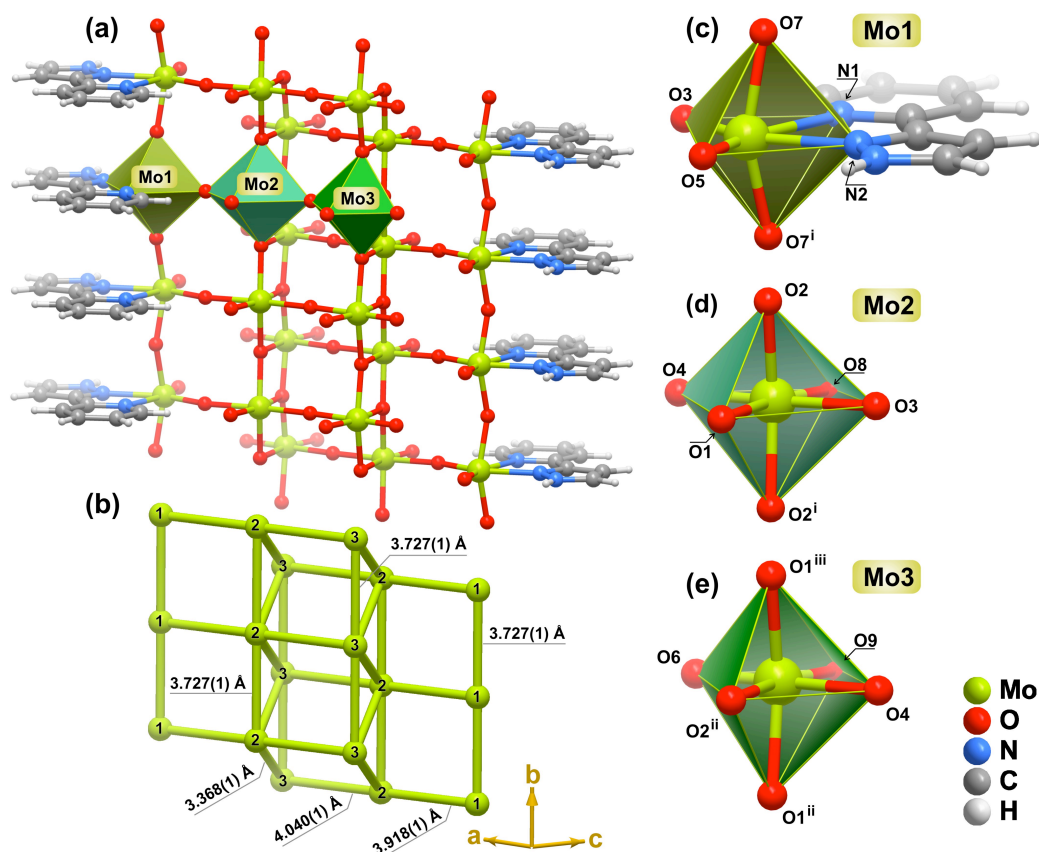


Figure 4.4. One-dimensional neutral ∞^1 [Mo₃O₉(pzpy)] hybrid polymer present in the crystal structure of 4.2 running parallel to the *b*-axis, emphasizing the (a) three crystallographically independent Mo⁶⁺ metal centers and the respective (b) intermetallic distances within the polymer. Schematic representation of the distorted octahedral coordination environments of: (c) Mo1, (d) Mo2 and (e) Mo3. Selected bond lengths and angles are listed in Tables 4.1 and 4.2. Symmetry transformations used to generate equivalent atoms: (i) *x*, -1+*y*, *z*; (ii) $\frac{1}{2}$ -*x*, - $\frac{1}{2}$ +*y*, 1-*z*; (iii) $\frac{1}{2}$ -*x*, $\frac{1}{2}$ +*y*, 1-*z*.

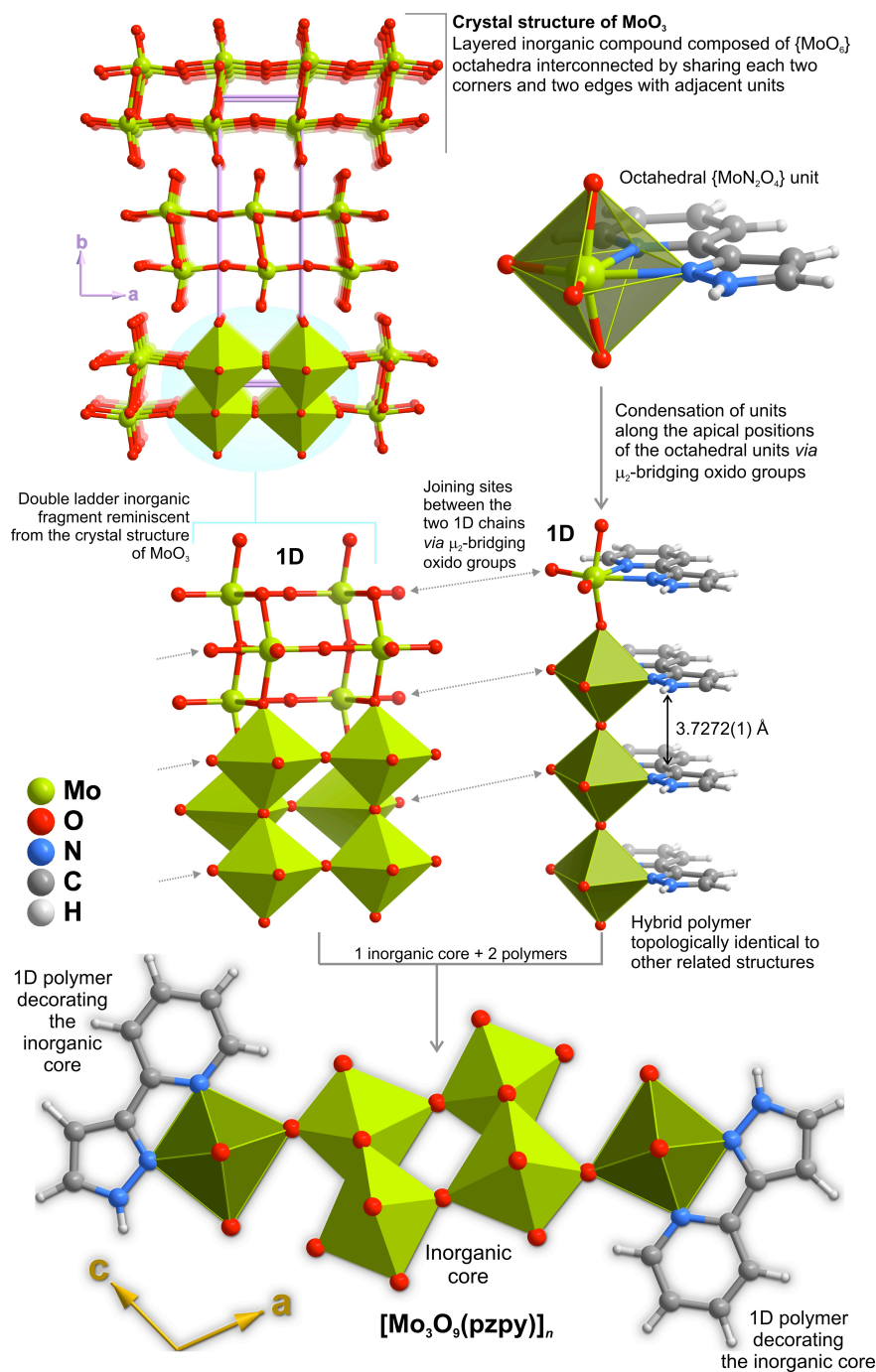


Figure 4.5. Relationship between the 1D neutral $\infty^1[\text{Mo}_3\text{O}_9(\text{pzpy})]$ hybrid polymer present in compound 4.2 and the topological features reported for related hybrid polymers in the literature and the parent MoO₃ inorganic compound.

The crystal structure of 4.2 is largely dominated by the close packing of individual 1D $\infty^1[\text{Mo}_3\text{O}_9(\text{pzpy})]$ polymers as shown in the inset in Figure 4.3. The most striking supramolecular contacts present in the structure concern the strong and highly directional N3–H1···O5 hydrogen bonds which, by way of a $\mathbf{R}^2_2(10)$ graph set motif,^[194] interconnect adjacent 1D polymers forming supramolecular layers in the *ab* plane of the unit cell (see Table 4.2 for geometrical details). Figure 4.6 emphasizes the distribution of these graph sets, which due to their strong cooperative effect along the [010] direction increase the structural robustness of 4.2. There are also a handful of weaker supramolecular

interactions, particularly onset π - π stacking interactions involving the pyridine and pyrazole rings of the organic ligand (Figure 4.6), and some weak intra-polymer C-H \cdots O hydrogen bonds (see Table 4.3 for geometrical details).

Table 4.3. Supramolecular contacts present in $[\text{Mo}_3\text{O}_9(\text{pzpy})]_n$ (4.2).^a

D-H \cdots A	d(D \cdots A) / Å	$\angle(\text{DHA}) / ^\circ$
N3-H1 \cdots O5 ⁱ	2.88(3)	174
(intra) C1-H2 \cdots O3	2.84(3)	121
(intra) C1-H2 \cdots O8	3.15(3)	179

^a Symmetry transformation used to generate equivalent atoms: (i) 1-x, y, 1-z.

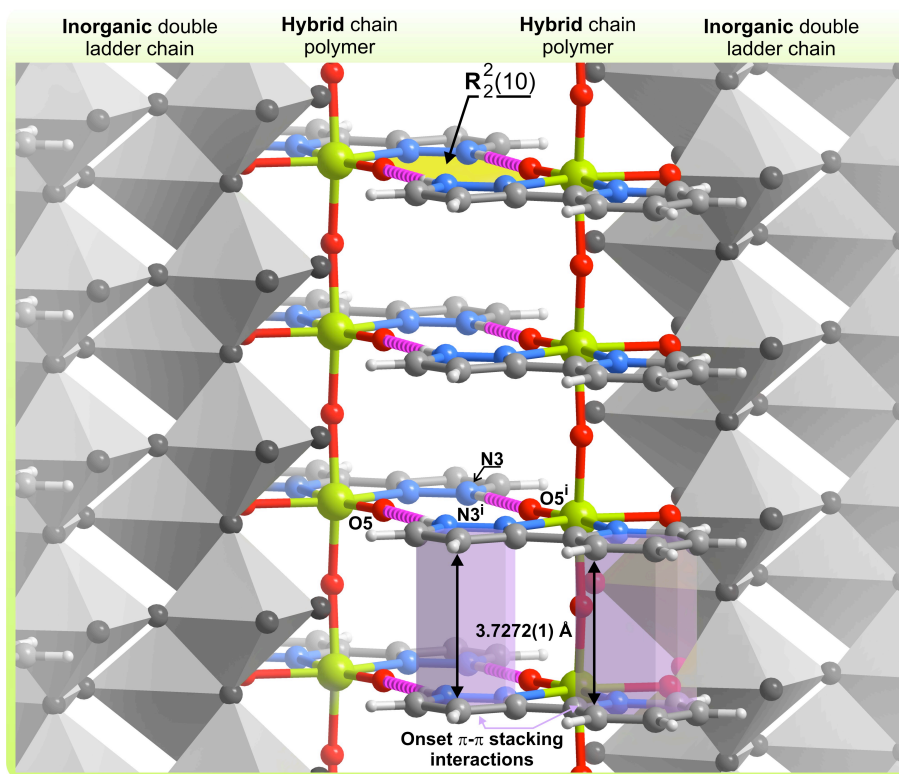


Figure 4.6. Detailed view of the strong and highly directional N-H \cdots O hydrogen bonding interactions (dashed purple lines) interconnecting adjacent neutral 1D $\infty^1[\text{Mo}_3\text{O}_9(\text{pzpy})]$ hybrid polymers, describing $\mathbf{R}_2^2(10)$ graph set motifs along the direction of the polymers. Onset π - π stacking interactions involving the pyridine and pyrazole rings of the organic ligand are represented in violet (inter-centroid distances of 3.7272(1) Å). Table 4.3 gives geometrical details on the represented interactions. Symmetry transformation used to generate equivalent atoms: (i) 1-x, y, 1-z.

A search in the literature concerning related polymeric structures (*i.e.*, Mo⁶⁺ inorganic cores coordinated to *N,N*-chelated ligands) showed unequivocally that 4.2 was the one with the highest metal content (concerning the metal:ligand ratio) found to date: (DMA)[(MoO₃)(Hbpdc)]·*n*H₂O with 1:1 (described in chapter 3),^[182] {[MoO₃(bipy)||MoO₃(H₂O)]}_{*n*} with 2:1 (described in chapter 1),^[142] [MoO₃(bipy)]_{*n*} with 1:1,^[59] [Mo₂O₆(bipy)]_{*n*} with 2:1,^[59] [Mo₃O₉(bipy)₂]_{*n*} with 3:2,^[59] [Mo₃O₈(bipy)₂]_{*n*} with 3:2,^[99] [Mo₄O₁₂(bipy)₃]_{*n*} with 4:3,^[100] and [Mo₃O₉(phen)₂]_{*n*} with 3:2 (where phen = 1,10-phenanthroline).^{[102][103][101]} These prior results clearly show that the Mo⁶⁺ content is never above 2 (in relation to the organic ligand), with this circumstance only occurring in exceptional cases for materials containing a large fraction of inorganic components (please note: compounds having isolated polyoxometalates^{[184][183]} as templates were excluded from this search): while in {[MoO₃(bipy)||MoO₃(H₂O)]}_{*n*} (1.1) the material is composed of a hybrid 1D structure co-crystallizing with a purely inorganic polymer,^[142] in [Mo₂O₆(bipy)]_{*n*} reported by Zubieta^[59] the polymer is instead formed by alternating octahedral complexes (**O**, having the *N,N*-chelated ligand composing the equatorial plane) and tetrahedral (**T**) MoO₄²⁻ inorganic units in a typical **-O-T-O-T-O-** fashion.

4.2.4. SOLID-STATE NMR

The material 4.2 was further characterized by ¹³C{¹H} CP MAS NMR as shown in Figure 4.7. The spectrum displays several sharp signals between *ca.* 160 and 100 ppm that can be readily assigned to the 8 carbon atoms of the pyrazolylpyridine ligand (Figure 4.7). The resonances at 146.9, 145.9 and 143.4 ppm are attributed to the carbons (C3, C7, C11) immediately bonded to the nitrogen atoms present in the two heterocyclic rings of the pzpy ligand.

The resonance centred at 133.1 ppm has a FWHM larger than all other aromatic signals suggesting there must be a superimposition of two carbon atoms. This was attributed to the carbons C5 and C9. The remaining three resonances at 125.6, 120.6 and 99.8 ppm are attributed to the two pyridine carbons C10, C8 and to one pyrazole carbon C4, accordingly.

Noteworthy, ¹³C{¹H} CP MAS NMR studies were of crucial importance because they unequivocally showed that the asymmetric unit of [Mo₃O₉(pzpy)]_{*n*} (4.2) was composed of a single organic ligand, with this information being essential in the use of *ab initio* powder X-ray diffraction methods.

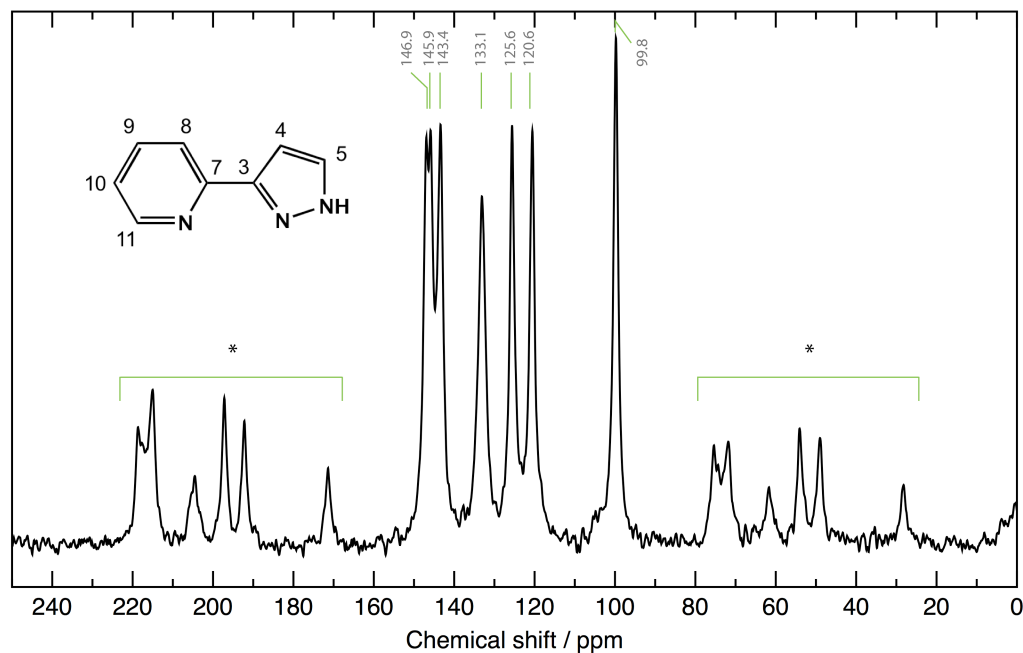


Figure 4.7. Solid-state $^{13}\text{C}\{^1\text{H}\}$ CP MAS NMR spectrum of $[\text{Mo}_3\text{O}_9(\text{pzpy})]_n$ (4.2). Data collected using a spinning rate of 9 kHz in a Bruker Avance 500 spectrometer at 125.76 MHz. Chemical shifts are quoted in parts per million (ppm) with respect to TMS. Spinning sidebands are denoted by an asterisk.

4.3. BY-PRODUCT $[\text{MoO}(\text{O}_2)_2(\text{pzpy})]$ (4.4) of CATALYSIS TESTS using 4.2

In an attempt to obtain a better understanding of the Mo-containing species formed during the catalytic olefin epoxidation with compound $[\text{Mo}_3\text{O}_9(\text{pzpy})]_n$ (4.2) as the pre-catalyst for the reaction of 4.2 in DCE with a large excess (*ca.* 150 equiv.) of the oxidant TBHP_{dec} was performed separately. After heating at 55 °C for 24 h, the reaction mixture was centrifuged and pentane/diethyl ether were added to the liquid phase, resulting in the precipitation of a pale yellow solid, which was identified as the oxodiperoxido complex $[\text{MoO}(\text{O}_2)_2(\text{pzpy})]$ (4.4) (Figure 4.8) by elemental analysis, powder X-ray diffraction, FT-IR and NMR spectroscopies. In addition, large single crystals of 4.4 suitable for X-ray diffraction were obtained by slow diffusion of diethyl ether into a concentrated solution of 4.4 in DMF.

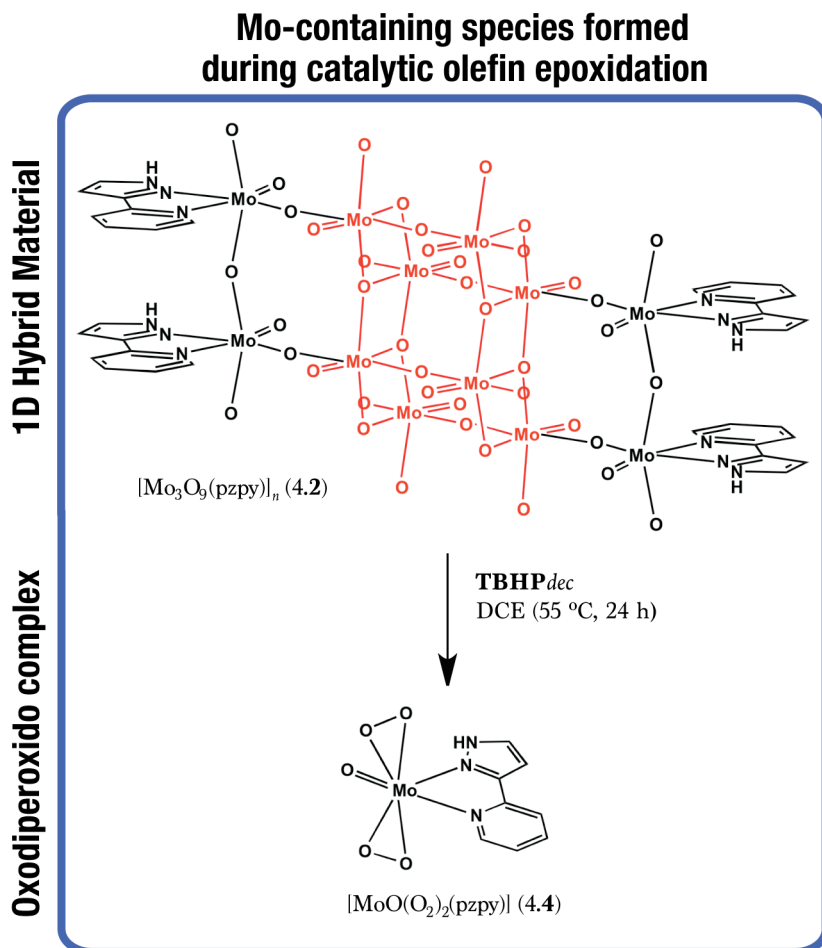


Figure 4.8. Schematic representation of the reaction of $[\text{Mo}_3\text{O}_9(\text{pzpy})]_n$ (4.2) in DCE with the oxidant TBHP_{dec} and the consequent precipitation of the solid identified as the oxodiperoxido complex $[\text{MoO}(\text{O}_2)_2(\text{pzpy})]$ (4.4).

4.3.1. X-RAY DIFFRACTION: CRYSTAL STRUCTURE DESCRIPTION

Compound $[\text{MoO}(\text{O}_2)_2(\text{pzpy})]$ (4.4) crystallizes in the centrosymmetric orthorhombic space group $Pbca$ with the asymmetric unit being composed of a whole molecular unit as depicted in Figure 4.9. The single Mo^{6+} metal center is coordinated to one N,N' -chelated pzpy organic moiety, two peroxido groups and one terminal oxido group. A search in the literature and in the CSD (Version 5.34, November 2012 with three updates)^{[36][37]} reveals the existence of a handful related structures (*i.e.*, sharing the same coordination environment) with various types of N,N' -chelating organic ligands bound to the metal center.^{[111][149][195][196][197][198][199][200][201]} The coordination environment of Mo^{6+} in all these structures is identical to that found in compound 4.4: i) overall coordination number of 7 (see Table 4.4 for selected bond lengths and angles concerning the coordination polyhedron); ii) two peroxido groups are *cis*-positioned with respect to the oxido one.

Table 4.4. Bond distances (in Å) and angles (in degrees) for the crystallographically independent Mo⁶⁺ metal center present in [MoO(O₂)₂(pzpy)] (4.4).

Mo1-O1	1.902(3)	Mo1-O5	1.689(2)
Mo1-O2	1.945(3)	Mo1-N1	2.157(3)
Mo1-O3	1.916(3)	Mo1-N3	2.358(3)
Mo1-O4	1.974(3)		
Mo1-Cg _{O1,O2}	1.779(3)	Mo1-Cg _{O3,O4}	1.805(3)
O1-Mo1-O2	44.67(11)	O3-Mo1-N3	85.81(10)
O1-Mo1-O3	88.40(11)	O4-Mo1-N1	89.40(11)
O1-Mo1-O4	130.25(11)	O4-Mo1-N3	78.52(10)
O1-Mo1-N1	129.65(11)	O5-Mo1-O1	106.31(11)
O1-Mo1-N3	86.99(10)	O5-Mo1-O2	102.07(11)
O2-Mo1-O4	157.32(10)	O5-Mo1-O3	105.65(11)
O2-Mo1-N1	86.26(11)	O5-Mo1-O4	100.34(11)
O2-Mo1-N3	79.07(9)	O5-Mo1-N1	92.34(10)
O3-Mo1-O2	130.81(11)	O5-Mo1-N3	162.39(11)
O3-Mo1-O4	43.68(10)	N1-Mo1-N3	70.13(10)
O3-Mo1-N1	131.46(11)		

The oxido group in 4.4 exerts its typical *trans* effect pulling the Mo⁶⁺ from the average equatorial plane by *ca.* 0.37 Å. This displacement value falls well within the range observed in the aforementioned related structures: from *ca.* 0.30 to 0.40 Å with a median value of 0.36 Å.^{[111][149][195][196][197][198][199][200][201]} This *trans* effect is concomitantly accompanied by the presence of a much longer Mo-N bond length [Mo1-N3 = 2.358(3) Å - see Table 4.4]; this value in [MoO(O₂)₂(pzpy)] is, nevertheless, well within the expected range (from *ca.* 2.29 to 2.43 Å with median of *ca.* 2.35 Å). As shown in Figure 4.9, the equatorial plane of the coordination polyhedron is composed of the two peroxido groups plus the nitrogen atom from the pyrazole ring. In a simplified approach taking the centers of gravity of the latter moieties as the coordination sites (*i.e.*, Cg_{O1,O2} and Cg_{O3,O4}), the overall coordination environment can be envisaged as a highly distorted trigonal bipyramid: the *cis* equatorial and apical polyhedral angles are found in the *ca.* 107.8-130.2° and 70.1-105.3° ranges, respectively, and the Mo1-(N,O,Cg) distances are spread in the wide 1.689(2)-2.358(3) Å range (Table 4.4 and Figure 4.9).

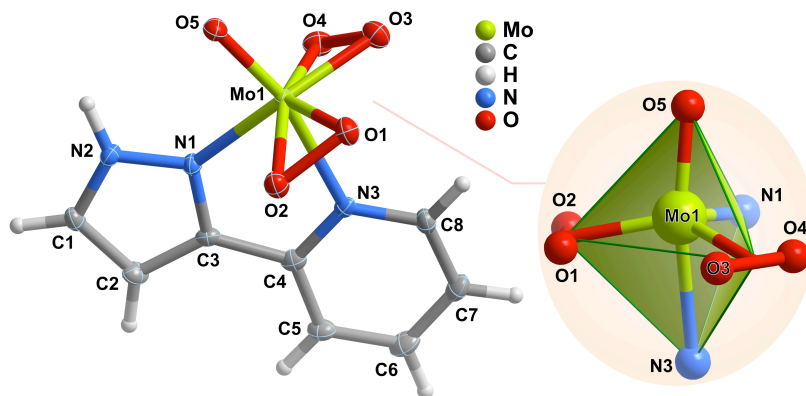


Figure 4.9. Schematic representation of the crystallographically independent molecular unit composing the asymmetric unit of $[\text{MoO}(\text{O}_2)_2(\text{pzpy})]$ (**4.4**). Non-hydrogen atoms are represented as thermal ellipsoids drawn at the 50% probability level. Hydrogen atoms are represented as small spheres with arbitrary radii. The inset emphasizes the distorted trigonal bipyramidal coordination environment of Mo1 when each peroxide ligand is considered as a single coordination site. Table 4.4 lists selected bond lengths and angles.

Even though the complex $[\text{MoO}(\text{O}_2)_2(\text{pzpy})]$ is rich in atoms capable of acting as acceptors in strong hydrogen bonds (due to the presence of various terminal oxygen atoms), there are not many donor groups in the crystal structure that can facilitate these supramolecular interactions. It is thus not surprising that the crystal packing of **4.4** is mostly mediated by the maximization of the sole $\text{N2-H1}\cdots\text{O4}$ hydrogen bond present in the crystal structure (Figure 4.10). This interaction, very strong and highly directional (see Table 4.5 for geometrical parameters), occurs between neighbouring individual complexes leading to the formation of a $\text{C}^1_1(5)$ graph set motif parallel to the *b*-axis of the unit cell.^[194] Each complex is involved in two such motifs in the *ab* plane, which creates a two-dimensional supramolecular layer (Figure 4.11). Besides this strong interaction, a handful of C-H groups from the organic ligand are engaged in weak C-H \cdots O interactions (not shown; see Table 4.5 for geometrical details).

Table 4.5. Supramolecular contacts present in $[\text{MoO}(\text{O}_2)_2(\text{pzpy})]$ (**4.4**).^a

D-H \cdots A	$d(\text{D}\cdots\text{A}) / \text{\AA}$	$\angle(\text{DHA}) / ^\circ$
$\text{N2-H1}\cdots\text{O4}^{\text{i}}$	2.772(4)	169
$\text{C1-H1}\cdots\text{O3}^{\text{ii}}$	3.307(4)	135
$\text{C5-H5}\cdots\text{O4}^{\text{iii}}$	2.921(4)	107
$\text{C6-H6}\cdots\text{O2}^{\text{iv}}$	3.282(4)	151

^a Symmetry transformations used to generate equivalent atoms:

(i) $-x, \frac{1}{2}+y, \frac{1}{2}-z$; (ii) $x, 1+y, z$; (iii) $-x, -y, 1-z$; (iv) $\frac{1}{2}-x, -y, \frac{1}{2}+z$.

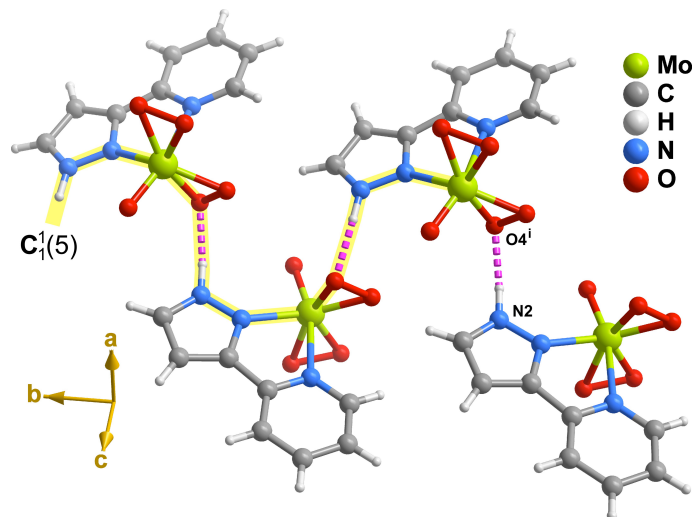


Figure 4.10. Schematic representation of the strong and highly directional N-H...O hydrogen bonds (dashed purple lines) interconnecting adjacent [MoO(O₂)₂(pzpy)] complexes in the crystal structure of 4.4, ultimately leading to the formation of a C₁¹(5) graph set motif.^[194] For geometrical details associated with the represented hydrogen bonds see Table 4.5. Symmetry transformation used to generate equivalent atoms: (i) $-x, \frac{1}{2}+y, \frac{1}{2}-z$.

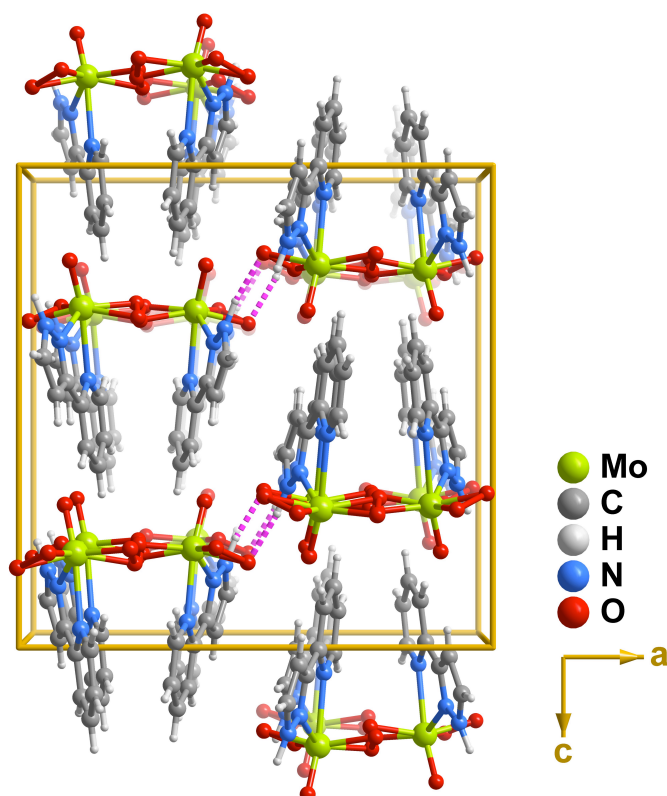


Figure 4.11. Crystal packing of compound [MoO(O₂)₂(pzpy)] (4.4) viewed in perspective along the [010] direction of the unit cell. Hydrogen bonding interactions connecting adjacent molecular units are represented as dashed purple lines. For geometrical details on the represented hydrogen bonds see Table 4.5.

4.4. FT-IR COMPARISON STUDIES: 4.1, 4.2, 4.3 and 4.4

This section focuses on a detailed FT-IR comparison study, involving both experimental and calculated bands, for all four hybrid materials studied in this chapter (Figure 4.1 and 4.8): $[\text{MoO}_2\text{Cl}_2(\text{pzpy})]$ (4.1), $[\text{Mo}_3\text{O}_9(\text{pzpy})]_n$ (4.2), $[\text{Mo}_4\text{O}_{12}(\text{pzpy})]$ (4.3) and $[\text{MoO}(\text{O}_2)_2(\text{pzpy})]$ (4.4).

Table 4.6. Selected FT-IR bands (cm^{-1}) for 4.1, 4.2, 4.3 and 4.4, and calculated (B3LYP) values.

Compound	calcd ^a	IR	assignment ^b	
4.1	932	940s	$\nu(\text{Mo}=\text{O})_{\text{sym}}$	
		918	906vs	$\nu(\text{Mo}=\text{O})_{\text{asym}}$
		337	395w	$\gamma(\text{MoO}_2)$
		308	345m	$\nu(\text{Mo}-\text{Cl})_{\text{asym}}$
		276	--	$\nu(\text{Mo}-\text{Cl})_{\text{sym}}$
		151	--	$\nu(\text{Mo}-\text{N})_{\text{sym}}$
		137	--	$\nu(\text{Mo}-\text{N})_{\text{asym}}$
4.2	--	967	$\nu(\text{Mo}=\text{O})_{\text{asym or sym}}$	
	--	941	$\nu(\text{Mo}=\text{O})_{\text{asym or sym}}$	
	--	935	$\nu(\text{Mo}=\text{O})_{\text{asym or sym}}$	
	--	930	$\nu(\text{Mo}=\text{O})_{\text{asym or sym}}$	
4.3	857	--	$\nu(\text{Mo}=\text{O})_{\text{sym}}$	
	850	--	$\nu(\text{Mo}=\text{O})_{\text{asym}}$	
	802	818/849s	$\nu(\text{Mo}-\text{O}-\text{Mo})_{\text{asym}}$	
	348	436m	$\delta(\text{Mo}-\text{O}-\text{Mo})$	
	331	402s	$\nu(\text{Mo}-\text{O}-\text{Mo})_{\text{sym}}$	
	322	343m	$\gamma(\text{MoO}_2)$	
4.4	929	950vs ^c	$\nu(\text{Mo}=\text{O})$	
	876	875sh	$\nu(\text{O}-\text{O})_{\text{sym}}$	
	875	864s	$\nu(\text{O}-\text{O})_{\text{asym}}$	
	583	584s	$\nu(\text{Mo}-\text{O})_{\text{peroxido}}$	
	543	539m	$\nu(\text{Mo}-\text{O})_{\text{peroxido}}$	
	494	512s	$\nu(\text{Mo}-\text{O})_{\text{peroxido}}$	
	463	492m	$\nu(\text{Mo}-\text{O})_{\text{peroxido}}$	
	298	393m	$\gamma(\text{O}=\text{Mo}(\text{O}_2)_2)$	
	160	--	$\nu(\text{Mo}-\text{N})_{\text{sym}}$	
	103	--	$\nu(\text{Mo}-\text{N})_{\text{asym}}$	

^a Scaled values (scale factor = 0.961).

^b For schematic representations of the vibrational modes see Experimental chapter.

^c Overlap with strong $\gamma(\text{CH})$ bands of the pzpy ligand.

For simplicity Table 4.6 lists the most characteristic and representative metal-ligand vibrations calculated and experimentally observed for compounds 4.1, 4.3 and 4.4. Overall, there is a good qualitative agreement between the experimental and calculated values despite the simplification of the calculated model, namely, only the isolated molecules were considered. Due to the large size of the system, no computational investigation was performed for 4.2 and tentative band assignments are based on the information provided by the comparison with the other molybdenum systems described in this chapter as well as on the literature data found for related molybdenum^[98] and tungsten^[202] compounds. The latter experimental values are also presented in Table 4.6.

4.4.1. Discussion

The bands arising from Mo=O vibrations are intense and characteristic in both 4.1 and 4.3 FT-IR spectra of the *cis*-dioxo complexes, being expected two Mo=O stretching modes $\nu(\text{Mo}=\text{O})$ and a deformation mode $\gamma(\text{MoO}_2)$.^[203] For compounds 4.1 and 4.2, the pairs of intense FT-IR bands at *ca.* 940/906 cm^{-1} and (930/935/941)/967 cm^{-1} are assigned to the asymmetric and symmetric stretching vibrations of the *cis*-[MoO₂]²⁺ core (Figure 4.12). The presence of molybdenum systems with higher complexity in material 4.2 and 4.3 is indicated by the FT-IR bands related with the bridging Mo–O–Mo unit, which are not present in the spectrum of 4.1 (Figure 4.12). On the basis of the DFT calculations performed for 4.3, the band at *ca.* 402 cm^{-1} is assigned as the symmetric stretching mode, $\nu(\text{Mo}-\text{O}-\text{Mo})_{\text{sym}}$, while the band at *ca.* 436 cm^{-1} is assigned to the out-of-plane deformation $\delta(\text{Mo}-\text{O}-\text{Mo})$. The pair of strong bands assigned to the Mo–O asymmetric stretching vibration of the Mo–O–Mo bridge appears at *ca.* 818 and 849 cm^{-1} , in agreement with previous studies.^{[89][111][114]} For compound 4.2, while the $\nu(\text{Mo}-\text{O}-\text{Mo})_{\text{asym}}$ mode appears as a broad FT-IR band at *ca.* 847 cm^{-1} (similar to 4.3), the broad FT-IR bands at *ca.* 672 and 535 cm^{-1} can be related with $\delta(\text{Mo}-\text{O}-\text{Mo})$ and $\nu(\text{Mo}-\text{O}-\text{Mo})_{\text{sym}}$ modes, respectively, somewhat higher than those observed for complex 4.3. These shifts to higher wavenumbers can be explained by the large decrease in the degree of linearity of the oxido bridges between the two Mo⁶⁺ centers on going from compound 4.3 (Mo–O–Mo = 175.4°) to compound 4.2 (Mo–O–Mo = 155.1°). Additionally, the C–H out-of-plane bending mode of the pzpy ligand observed at *ca.* 785 cm^{-1} for 4.1 and at *ca.* 778 cm^{-1} for 4.3 and 4.4, shifts to lower wavenumber, at *ca.* 748 cm^{-1} , for 4.2, probably because this material is richer in terms of supramolecular contacts, with several hydrogen bonding interactions involving the C–H oscillator. All these observations are in full agreement with the crystallographic studies performed for compound 4.2.

The vibrational Mo=O and O–O stretching modes for complex 4.4 are clearly distinguished in the spectrum as sharp and very strong bands. The FT-IR spectrum (Figure 4.12) shows the $\nu(\text{Mo}=\text{O})$ band at *ca.* 950 cm^{-1} , while two bands

at *ca.* 875 and 864 cm^{-1} are found for the asymmetric and symmetric peroxido stretching $\nu(\text{O-O})$ modes, respectively. Additionally, four bands assigned to the metal–peroxido stretching modes, $\nu(\text{Mo-O})_{\text{peroxido}}$, appear (*ca.* 584, 539, 512, 492 cm^{-1} , Figure 4.12). The observed $\nu(\text{Mo=O})$ and $\nu(\text{O-O})$ wavenumbers are similar to the values reported for related compounds.^{[111][149]} The bands identified in Figure 4.12 as L are assigned to pzpy ligand vibrations.

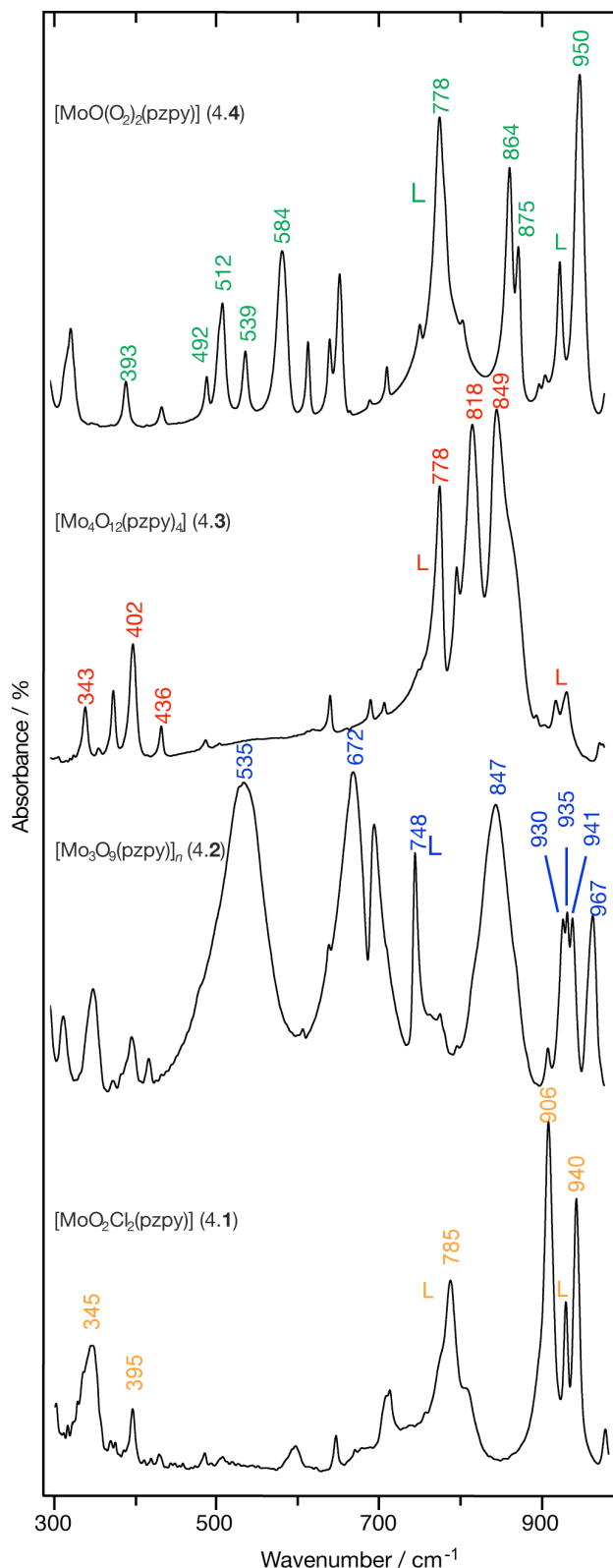


Figure 4.12. FT-IR spectra of compounds 4.1 to 4.4 in the *ca.* 300-1000 cm^{-1} spectral region.

The detailed analysis of the vibrational spectra of compounds 4.1 to 4.4 in the *ca.* 1550-1650 cm^{-1} region, demonstrates structural changes in the pzpy ligand upon complexation. In this region, the bands arising from the ligand N-C-C-N fragment, from the C-C pyridine vibrations and from the C-N ring stretching vibrations, reflect a general trend, observed for the remaining complexes, to be shifted to higher wavenumbers upon coordination to the Mo^{6+} center, in agreement with previous work.^{[81][80]} The bands of pzpy at *ca.* 1565 cm^{-1} (pzpy C-C inter-ring stretching mode), *ca.* 1590 cm^{-1} (py C-N stretching mode) and *ca.* 1597 cm^{-1} (py C-C stretching mode) are shifted to *ca.* 1570/1613, 1570/1607, 1567/1607 and 1570/1610 cm^{-1} for compounds 4.1, 4.2, 4.3 and 4.4, in that order.

4.5. CATALYSIS: Cy8 substrate

This section discusses the catalytic performance of $[\text{Mo}_3\text{O}_9(\text{pzpy})]$ (4.2) for the conversion of Cy8 into Cy8Ox using TBHP_{dec} as oxidant, at 55 or 75 °C, with no co-solvent or using one of the following organic co-solvents: 1,2-dichloroethane (DCE) or (trifluoromethyl)benzene (BTF).

For all reaction conditions (see Figure 4.13) where $[\text{Mo}_3\text{O}_9(\text{pzpy})]$ (4.2) was used as catalyst, Cy8Ox was the only reaction product (100% selectivity). In contrast, when no catalyst was added, 1,2-cyclooctanediol was formed in 2-10% yield at 75 °C / 24 h. The molybdenum species play, thus, an important role in the selective epoxidation of the olefin.

The reaction of Cy8 in the presence of 4.2 at 55 °C gave 29 /51% Cy8Ox yield at 6 /24 h. These results are inferior to those previously reported for the mononuclear $[\text{MoO}_2\text{Cl}_2(\text{pzpy})]$ ^[81] or tetranuclear molybdenum $[\text{Mo}_4\text{O}_{12}(\text{pzpy})]$ ^[49] complexes tested as pre-catalysts for the same reaction under similar conditions (Table 4.8). These different catalytic performances may be partly due to the polymeric nature of 4.2 having a lower amount of effective active species in comparison to the mono- and tetranuclear complexes, and/or differences in catalyst stability. A comparison of the catalytic results for 4.2 with those reported in the literature for polymeric molybdenum-containing compounds bearing organic ligands different from pzpy, tested as pre-catalysts in the same reaction under similar conditions, shows that the catalytic activity of 4.2 (based on Cy8Ox yield at 24 h, 55 °C, no co-solvent) stands on a similar footing to that of $[\text{Mo}_2\text{O}_6(\text{HpypzA})]$ (57%),^[172] inferior to that of $[\text{MoO}_3(\text{bipy})]_n$ (78%)^[98] and $[\text{Mo}_8\text{O}_{24}(\text{pypzEA})_4]$ (92%; pypzEA = ethyl[3-(pyridin-2-yl)-1H-pyrazol-1-yl]acetate),^[49] and superior to that of $\{[\text{MoO}_3(\text{bipy})][\text{MoO}_3(\text{H}_2\text{O})]\}_n$ (1.1) (34%),^[142] the hybrid material presented in chapter 1 of this thesis.

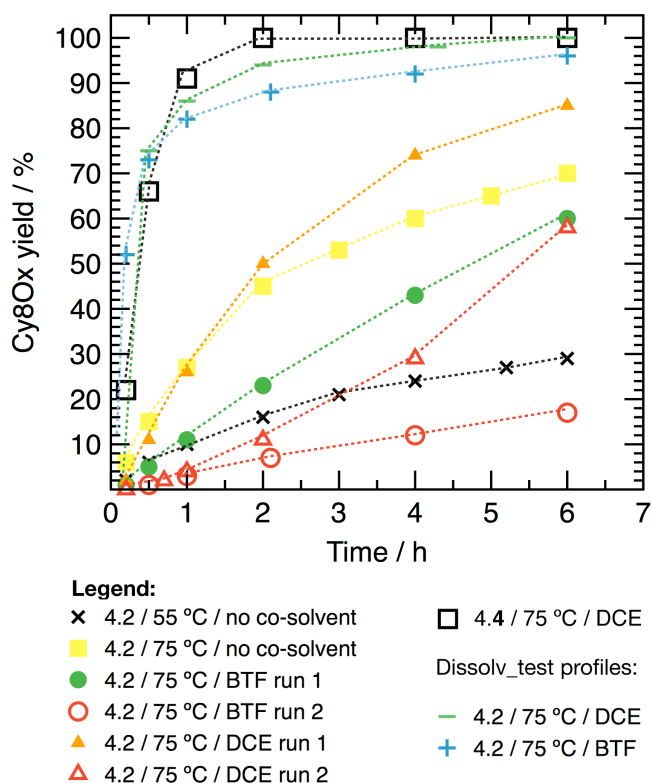


Figure 4.13. Dependence of *cis*-cyclooctene oxide (Cy8Ox) yield with the reaction time in the epoxidation of *cis*-cyclooctene (Cy8). TBHP_{dec} was used as the oxidant in the initial molar ratio of Mo : Cy8 : TBHP_{dec} = 1 : 100 : 152 for 4.2 and 0.3 : 100 : 152 for 4.4. Catalysts/co-solvent systems and the Dissolv_Test profiles are detailed in the legend. Dashed guidelines connect adjacent points for clarity.

Increasing the reaction temperature from 55 to 75 °C led to faster reaction of Cy8: 70% CyO yield at 6 h and quantitative Cy8Ox yield at 24 h. It has been reported for hybrid organic-inorganic molybdenum-containing polymers that the use of halogenated and non-coordinating co-solvents such as DCE and BTF may have a beneficial effect on the catalytic reaction rate of Cy8 with TBHP_{dec}.^{[172][142]} For 4.2 at least 98% conversion was reached at 24 h using these co-solvents (or no co-solvent) at 75 °C, and Cy8Ox was always the only product (Table 4.7). Differences in reaction rates were observed in the initial stages: conversion at 6 h followed the order DCE > no co-solvent > BTF (Figure 4.13). The catalytic performance of 4.2 using DCE / 75 °C is comparable to that reported for [Mo₈O₂₄(di-*t*-Bu-bipy)₄], which led to 100% Cy8Ox yield at 24 h.^[98]

Table 4.7. Epoxidation of *cis*-cyclooctene with TBHP_{dec} in the presence of [Mo₃O₉(pzpy)] (4.2), and the catalytic results for the Dissolv_Test.^a

Co-solvent	Reaction temperature (°C)	Epoxide yield (%) at 6 / 24 h reaction	ΔCatFilt/ΔNoCat ^b
no co-solvent	55	29 / 51	-
no co-solvent	75	70 / 98	2
BTF	75	60 / 100 (17 / 47) ^c	2
DCE	75	85 / 100 (58 / 98) ^c	6
BTF (Dissolv_Test) ^b	75	96 / 99	-
DCE (Dissolv_Test) ^b	75	100 / 100	-

^a Reaction conditions: initial molar ratios of Mo : Cy8 : TBHP_{dec} \cong 1 : 100 : 152, initial concentration of Cy8 = 1 M.

^b Details for ΔFiltCat/ΔNoCat and Dissolv_Test are given in the Experimental chapter.

^c Values in parentheses are for a second batch run using the recovered solid.

Table 4.8. Epoxidation of *cis*-cyclooctene with TBHP_{dec} in the presence of molybdenum compounds possessing the ligand L = pzpy, at 55 °C.^a

Compound	Epoxide yield (%) at 6 / 24 h reaction ^b	Metal species ^c	Ref.
4.2	29 / 51	LP = [MoO(O ₂) ₂ L] (4.4) SP = unknown polymer or molybdenum oxide cluster	--
[MoO ₂ Cl ₂ L]	66 / 90		[81]
[MoO ₂ (OSiPh ₃) ₂ L]	66 / 90	SP = [Mo ₄ O ₁₂ L ₄]	[81]
[Mo(CO) ₄ L]	51 / 78 (61 / 91) ^d	SP = [Mo ₄ O ₁₂ L ₄]	[49]
[Mo ₄ O ₁₂ L ₄]	55 / 92 (57 / 89) ^d	SP = [Mo ₄ O ₁₂ L ₄]	[49]

^a Reaction conditions: molar ratios of Mo : Cy8 : TBHP \cong 1 : 100 : 152, without co-solvent, 55 °C.

^b Epoxide was always the only reaction product.

^c Metal species identified or characterized after a 24 h catalytic batch run.

^d Values in parentheses refer to epoxide yield at 6 / 24 h of reaction for the second batch run.

SP - Denotes the recovered solid;

LP - Denotes the solid isolated from solution by precipitation with an organic solvent.

Reaction nature

In order to better understand the influence of the solvent, it was important to check whether the catalytic reaction was homogeneous or heterogeneous in nature, and assess the stability of the catalyst. The CatFilt experiment (details

given in the Experimental chapter) was carried out for the no co-solvent, BTF and DCE co-solvent systems at 75 °C. Without adding a catalyst the conversions at 6 / 24 h were 6 / 13%, 3 / 5% and 2 / 4%, respectively. The ratio $\Delta\text{CatFilt}/\Delta\text{NoCat}$ was always greater than unity, suggesting that a homogeneous catalytic contribution is present (Table 4.7). For each solvent system the value of $\Delta\text{FiltCat}$ was however much smaller than the increment in conversion observed in the presence of 4.2 (without filtration) for the same interval of time. These results suggest that the dissolved species in the corresponding filtrates were not the only ones responsible for the catalytic reaction. Thus, catalysis should also have a heterogeneous contribution.

Catalysts stability

The powder X-ray diffraction patterns and ATR FT-IR spectra of the solids recovered after 24 h batch runs (denoted 4.2 / 75 °C / no co-solvent, 4.2 / 75 °C / DCE and 4.2 / 75 °C / BTF and 4.2 / 55 °C / no co-solvent), were very similar to that for pristine $[\text{Mo}_3\text{O}_9(\text{pzpy})]_n$ (4.2), indicating that the crystalline structure remained essentially unchanged during the catalytic reactions (Figures 4.14 and 4.15). Some morphological changes were, however, apparent in the SEM images. As depicted in Figure 4.16, the SEM images generally revealed a decrease in the particle size of 4.2 after a batch run.

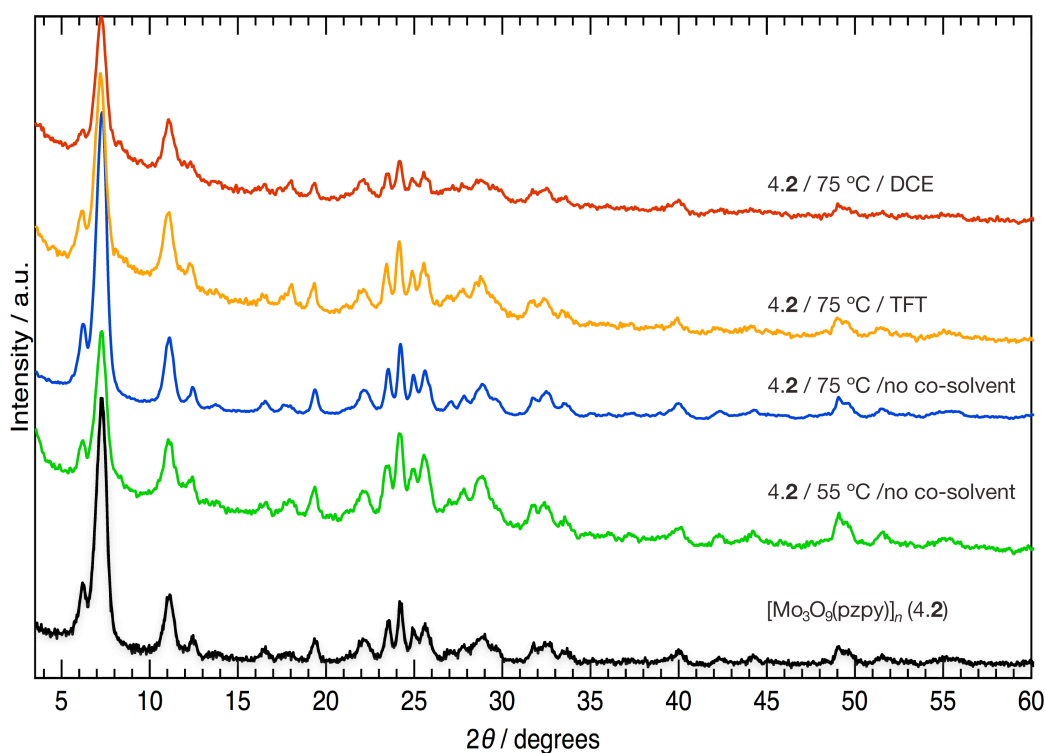


Figure 4.14. Comparison between the powder X-ray diffraction patterns of the pre-catalyst $[\text{Mo}_3\text{O}_9(\text{pzpy})]_n$ (4.2) and of the solids recovered from the different catalytic systems.

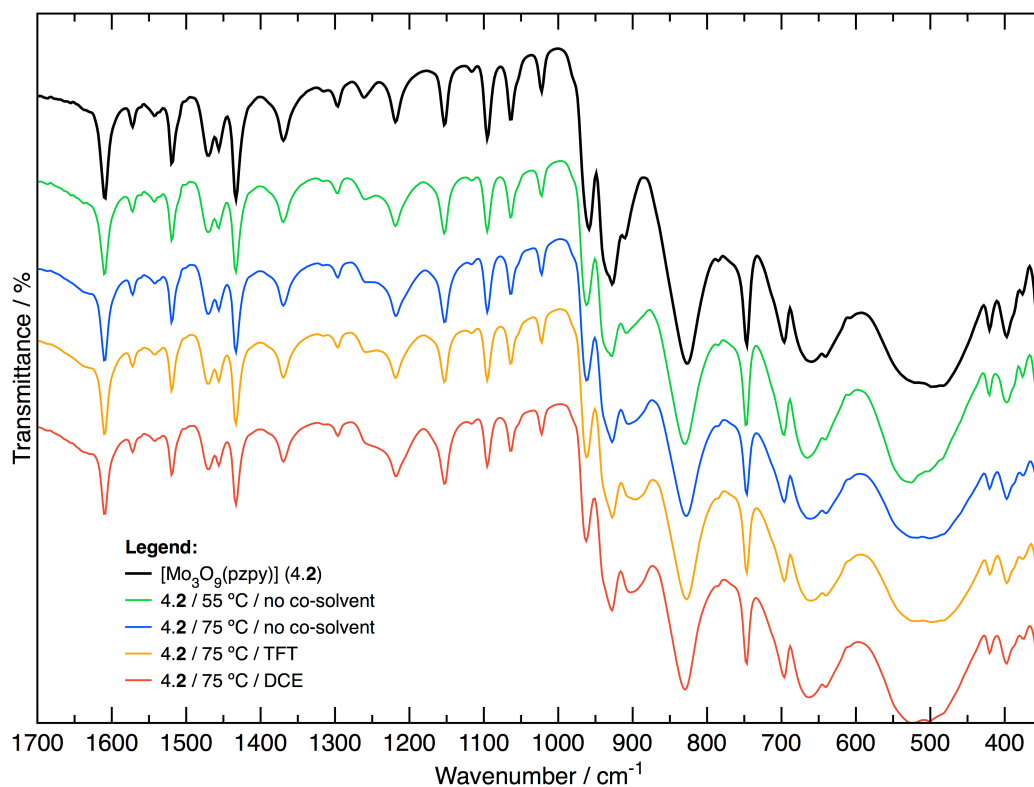


Figure 4.15. Comparison between the ATR FT-IR spectrum (in the region of *ca.* 350-1700 cm^{-1}) of the as-prepared compound 4.2 and those of the solids recovered from the catalytic epoxidation tests.

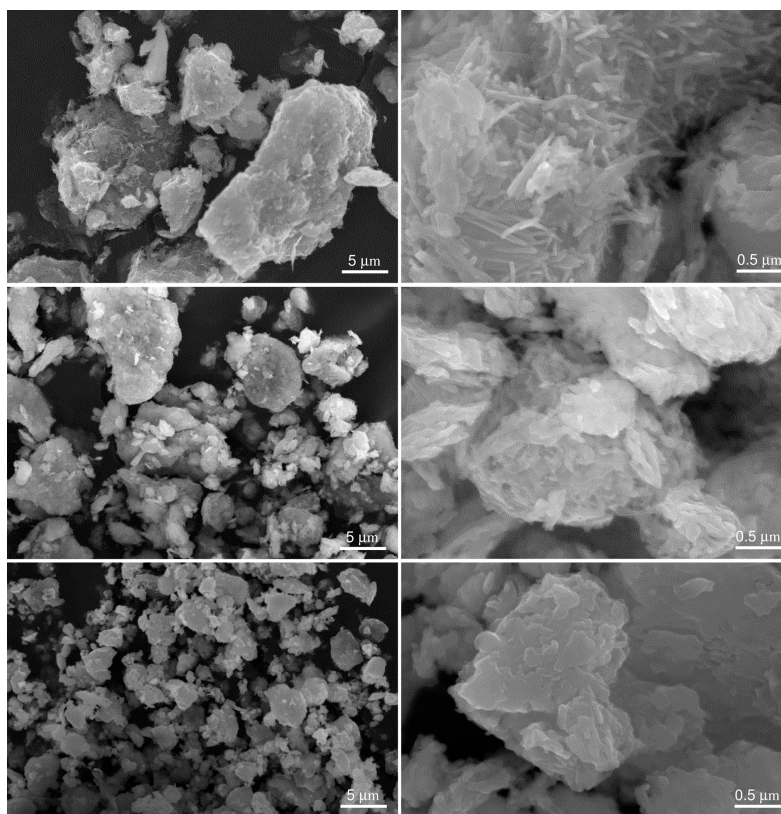


Figure 4.16. SEM images of the as-prepared compound 4.2 (*top*) and of the solids recovered after the first and second catalytic runs (*middle* and *bottom*, respectively) of the system 4.2 / 75 °C / BTF.

Second batch run using DCE and BTF

A second batch run was carried out for the DCE and BTF solvent systems using similar conditions to those used in the first run. A significant decrease in the reaction rate was observed (see Figure 4.13). These results are somewhat surprising since the characterization of the recovered solids did not reveal drastic structural changes, and the CatFilt_Test suggested that the catalytic reaction was to a certain extent heterogeneous in nature. A possible explanation for these results is that compound **4.2** acts as a source of active soluble species which are present in different amounts in runs 1 and 2. Accordingly, the erroneous results for the CatFilt_Test may be due to slow dissolution of metal species, and saturation concentration was not reached at the instant of the filtration. In order to check this hypothesis the Dissolv_Test (details given in the Experimental chapter) experiment was carried out for the solvent systems DCE and BTF, at 75 °C (filtration was carried out at 24 h, whereas for the CatFilt_Test it was carried out at 2 h reaction). The catalytic results were roughly similar for the two solvents, and the reaction rates were much higher than those for the corresponding typical catalytic tests (Figure 4.13). These results support the hypothesis that **4.2** acts as a source of active soluble species, and the type of active soluble species is possibly similar for the two co-solvents. The greater value of $\Delta\text{FiltCat}/\Delta\text{NoCat}$ for DCE in comparison to BTF is possibly due to the higher solubility of the active species in the former solvent.

The difference in concentration of the active species between runs 1 and 2, for each co-solvent, is not clearly understood at this moment. As noted above, the SEM images revealed smaller particle sizes after run 1, and this effect seemed to be more pronounced for the solid recovered after run 2 (Figure 4.16). The gradual reduction in particle size could favour the dissolution of active metal species and enhance the reaction rate in consecutive batch runs, which was not observed. In an attempt to isolate and identify the soluble active species, a large scale (30 fold increase) experiment was carried out for **4.2** / TBHP_{dec} / DCE (without olefin; please see the Experimental chapter for details). Addition of pentane/diethyl ether to the liquid phase resulted in the precipitation of a pale yellow solid, which was identified as the oxodiperoxo complex $[\text{MoO}(\text{O}_2)_2(\text{pzpy})]$ (**4.4**) by elemental analysis, single-crystal and powder X-ray diffraction, FT-IR and NMR spectroscopies. Thiel *et al.* reported the catalytic performance of **4.4** for the reaction of Cy8 with TBHP_{dec} (at 30, 50 or 65 °C; chloroform or toluene as co-solvent; TBHP_{dec} in chloroform).^[204] A catalytic test was carried out for **4.4** (TBHP_{dec} / DCE / 75 °C) using an equivalent molar amount of complex as that used for **4.2** under typical reaction conditions; this amount of **4.4** used corresponds to that calculated assuming that the moieties of **4.2** which possess a pzpy ligand are completely transformed into species of the type **4.4**, in a 1:1 stoichiometric ratio. The reaction was complete within 2 h, indicating that **4.4** is a very active catalyst (Figure 4.13). These

results are somewhat consistent with the relatively fast reaction of Cy8 for the Dissolv_Test experiments. Hence, it seems that 4.2 is poorly soluble in the reaction media, and it is gradually converted into 4.4, which is at least partly responsible for the catalytic reaction of Cy8. The amount of solid recovered after a batch run using 4.2 was much lower than that corresponding to the initial amount of 4.4 used: *ca.* 5 wt% (relative to the initial mass of 4.2) of solid was recovered from the catalytic reaction using 4.2, whereas 4.4 was used in an amount equivalent to 17 wt% of 4.2. However, the initial reaction rate for 4.4 was lower than that observed for the Dissolv_Test experiments. Hence, we cannot rule out the possibility of different active species being involved. The decrease in reaction rate from runs 1 to 2 may be due to gradual structural modifications of 4.2 that lead to different amounts of active species in solution.

4.6. CONCLUDING REMARKS

The hydrolysis and condensation of complexes of the type $[\text{MoO}_2\text{Cl}_2\text{L}]$ was proved once again to be an important route to molybdenum oxide/organic assemblies. In this chapter the polymeric compound $[\text{Mo}_3\text{O}_9(\text{pzpy})]_n$ (4.2) (pzpy = 3-(2-pyridyl)pyrazol) has been prepared and structurally characterized. Of all the molybdenum oxide-organic hybrid materials described in this thesis, $\{[\text{MoO}_3(\text{bipy})][\text{MoO}_3(\text{H}_2\text{O})]\}_n$ (1.1),^[142] $[\text{Mo}_8\text{O}_{22}(\text{OH})_4(\text{di-}t\text{-Bu-bipy})_4]$ (2.2),^[151] and $(\text{DMA})[\text{MoO}_3(\text{Hbpdc})] \cdot n\text{H}_2\text{O}$ (3.1),^[182] this $[\text{Mo}_3\text{O}_9(\text{pzpy})]_n$ (4.2) polymeric compound is the one with the highest metal : ligand ratio. It finds a structural parallel in the material $\{[\text{MoO}_3(\text{bipy})][\text{MoO}_3(\text{H}_2\text{O})]\}_n$ (1.1), in which each individual $\infty^1[\text{MoO}_3(\text{H}_2\text{O})]$ polymer interacts with two peripheral $\infty^1[\text{MoO}_3(\text{bipy})]_n$ moieties *via* strong hydrogen bonds. However, in 4.2, the MoO_3 -based inorganic core is linked covalently at the periphery to two hybrid polymers consisting of corner-sharing distorted $\{\text{MoO}_4\text{N}_2\}$ octahedra.

A comparison of the catalytic results for 4.2 with those reported in the literature for polymeric molybdenum-containing compounds bearing organic ligands different from pzpy shows that the catalytic activity of 4.2 (based on Cy8Ox yield at 24 h, 55 °C, no co-solvent) is similar to that of $[\text{Mo}_2\text{O}_6(\text{HpypzA})]$ (57%),^[172] inferior to that of polymeric $[\text{MoO}_3(\text{bipy})]_n$ (78%)^[98] and $[\text{Mo}_8\text{O}_{24}(\text{pypzEA})_4]$ (92%; pypzEA = ethyl[3-(pyridin-2-yl)-1H-pyrazol-1-yl]acetate),^[49] and superior to that of $\{[\text{MoO}_3(\text{bipy})][\text{MoO}_3(\text{H}_2\text{O})]\}_n$ (1.1) (34%) (see chapter 1 for additional details).^[142] When the DCE and BTF solvent systems were used the CatFilt_Test results suggested that the catalytic reaction was partially heterogeneous in nature.

OXOMOLYBDENUM(VI) COMPLEXES with a NOVEL *N,N'*-CHELATE LIGAND with a LONG ALKYL CHAIN

5.1. SUMMARY

Previous chapters reported new catalytic materials, covering from discrete complexes to polymeric compounds, based on either commercially-available *N,N'*-chelating ligands or those whose synthetic route has been extensively reported: 2,2'-bipyridine, 2,2'-bipyridine-5,5'-dicarboxylic acid, 2-[3(5)-pyrazolyl]pyridine or 4,4'-di-*tert*-butyl-2,2'-bipyridine. In this way, the reaction of the mononuclear $[\text{MoO}_2\text{Cl}_2\text{L}]$ complex type (where L corresponds to the aforementioned *N,N'*-chelating ligands) in excess of water produced: $\{[\text{MoO}_3(\text{bipy})][\text{MoO}_3(\text{H}_2\text{O})]\}_n$ (1.2),^[142] $(\text{DMA})[\text{MoO}_3(\text{Hbpd})] \cdot n\text{H}_2\text{O}$ (3.1),^[182] $[\text{Mo}_3\text{O}_9(\text{pypzH})]_n$, and $[\text{Mo}_8\text{O}_{22}(\text{OH})_4(\text{di-}t\text{-Bu-bipy})_4]$ (2.2),^[151] an octanuclear compound. It is further noted that this same strategy was employed by Gonçalves and co-workers using other ligands, namely [3-(pyridinium-2-yl)-1H-pyrazol-1-yl]acetate (HpypzA), which led to the isolation of another polymeric material formulated as $[\text{Mo}_2\text{O}_6(\text{HpypzA})]_n$.^[172]

This chapter aims to further explore the chemistry and catalytic potential of Mo^{VI} -pyrazolylpyridine compounds by using the novel ligand 2-(1-pentyl-3-pyrazolyl)pyridine (5.1, abbreviated as pent-pp). This molecule is capable of acting as a *N,N*-chelating ligand in the coordination sphere of the $[\text{MoO}_2\text{Cl}_2\text{L}]$ complex. As shown by the detailed literature search (see Introduction), bipyridines and pyrazolylpyridines appear to be the optimal choice to prepare oxomolybdenum(VI) complexes because they are usually resistant to oxidative degradation and/or to exchange reactions under the investigated catalytic conditions.^{[73][80][81][83][85][88][157][205]}

The dioxomolybdenum(VI) complex $[\text{MoO}_2\text{Cl}_2(\text{pent-pp})]$ (5.2) was prepared by simple ligand exchange with the solvent adduct $[\text{MoO}_2\text{Cl}_2(\text{THF})_2]$ (Introduction, Figure 19). The treatment of $[\text{MoO}_2\text{Cl}_2(\text{pent-pp})]$ (5.2) with water led to the isolation of a new organic-inorganic hybrid material with chemical composition $[\text{Mo}_2\text{O}_6(\text{pent-pp})]$ (5.3). The molybdenum-catalysed epoxidation of Cy8 was chosen as a model reaction to assess the catalytic properties of 5.2 and 5.3. The material 5.3 was further examined in the epoxidation of the bio-derived olefins DL-limonene and methyl oleate.

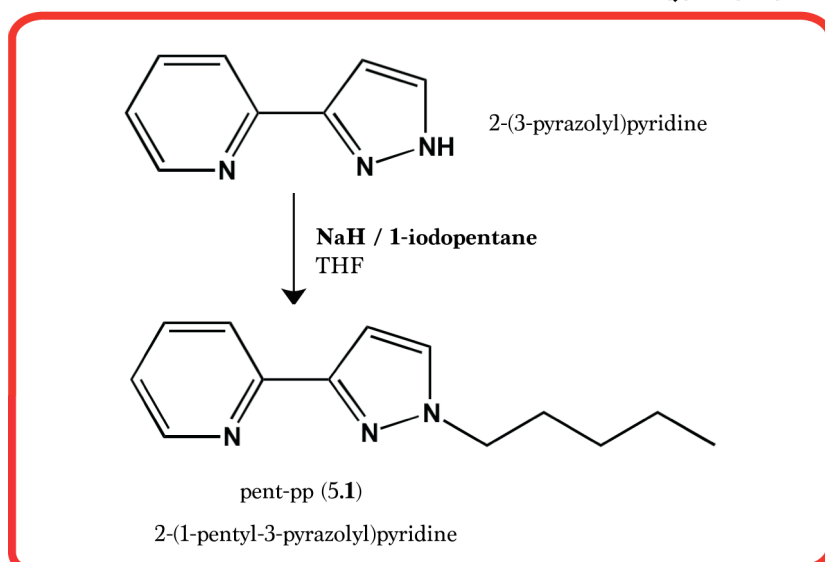
5.2. SYNTHESIS and CHARACTERIZATION

This section describes the synthesis of the new organic ligand 2-(1-pentyl-3-pyrazolyl)pyridine (5.1, pent-pp), the dichlorodioxomolybdenum(VI) complex $[\text{MoO}_2\text{Cl}_2(\text{pent-pp})]$ (5.2), and its hydrothermal treatment which led to the preparation of an organic-inorganic hybrid material with composition $[\text{Mo}_2\text{O}_6(\text{pent-pp})]$ (5.3). The structural characterization of these compounds, which includes elemental analysis, FT-IR and NMR spectroscopies, and single-crystal X-ray studies, is discussed.

5.2.1. 2-(1-pentyl-3-pyrazolyl)pyridine (pent-pp (5.1))

The preparation of the novel organic ligand 2-(1-pentyl-3-pyrazolyl)pyridine (pent-pp) was performed by modifying published procedures while using standard Schlenk techniques under inert atmosphere.^[204] A dry solution of THF was added to NaH dispersed in oil. The resulting solution was removed by filtration under inert atmosphere, and another portion of THF was added to the resulting grey NaH powder. PypzH in dry THF was then added dropwise to the stirring NaH THF solution. Special care needs to be taken because this reaction releases H_2 . Using a syringe, 1-iodopentane was then added and the resulting mixture stirred at 70 °C for 48 h (Equation 5.1). After reacting, THF was evaporated in the vacuum line and a yellow solid was obtained. The solid was extracted with *n*-hexane and pentane. The combined extracts were evaporated to dryness, giving the ligand 5.1 as an oil. This free organic ligand was prepared in good yields: 1.68 g, 76%. Characterization data (elemental analysis, FT-IR, ^1H and ^{13}C solution NMR) were in line with those reported by Thiel *et al.* for other 2-(1-alkyl-3-pyrazolyl)pyridine derivatives.^[204] For more details on the collected characterization data see the experimental chapter.

EQUATION 5.1



5.2.1.1. X-RAY DIFFRACTION: CRYSTAL STRUCTURE DESCRIPTION

As described above, the ligand pent-pp was isolated as oil. Several attempts were performed to promote its crystallization but no single crystals could ever be isolated. Crystals of the hydrochloride salt (**5.1**·HCl) suitable for X-ray diffraction were, however, isolated from the aqueous mother liquor obtained after the reaction of complex **5.2** with water to prepare material **5.3**. This aqueous mother liquor was slowly concentrated by allowing it to stand in open air and at ambient temperature for several days. This crystallographic result was an additional proof of the successful deprotonation of 2-(3-pyrazolyl)pyridine followed by addition of 1-iodopentane resulting in the formation of ligand **5.1**.

5.1·HCl crystallises in the centrosymmetric monoclinic space group $P2_1/c$ with the asymmetric unit being composed of a whole protonated molecular unit plus a charge-balancing chloride anion (Figure 5.1). The pentyl substituent is affected by positional disorder, most likely due to the high conformational flexibility allied to the inexistence of structurally relevant supramolecular contacts associated with this portion of the molecule. Nevertheless, one conformation is predominant in the crystal structure, with a refined rate of occupancy of 70.4(7)%. As found in related structures, the crystal structure of the uncoordinated molecule has the two central rings rotated along the central C5–C6 bond so as to minimize steric repulsion between the lone pairs of the nitrogen atoms. The pyridine and the 2-(3-pyrazole) rings in **5.1**·HCl are almost coplanar, with the average planes subtending a dihedral angle of only 4.40(9)° (Figure 5.1).

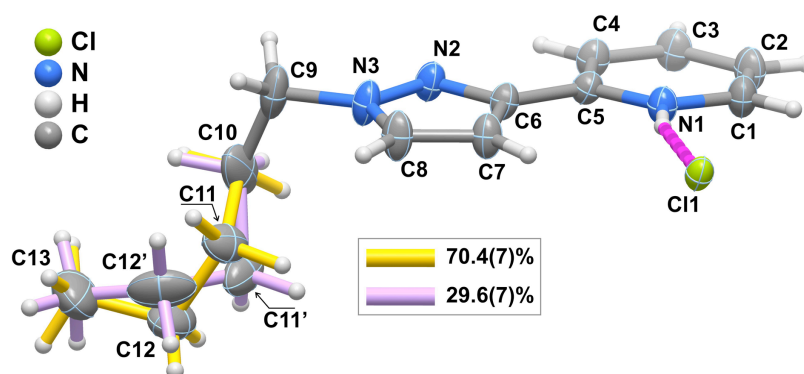


Figure 5.1. Schematic representation of the molecular moieties present in the asymmetric unit of the salt **5.1**·HCl. Non-hydrogen atoms are represented as thermal ellipsoids drawn at the 50% probability level, and identified by their corresponding atomic labels. Hydrogen atoms are represented as small spheres with arbitrary radii. The two crystallographic positions for the disordered pentyl chain are represented in different colour.

The crystal packing of $5.1 \cdot \text{HCl}$ is essentially driven by the need to effectively fill the available space, while optimizing (in terms of internuclear distances and interaction angles) a number of weak $\text{N}-\text{H} \cdots \text{Cl}$ and $\text{C}-\text{H} \cdots \text{Cl}$ hydrogen bonds (see Figure 5.2). The chloride anion arises as a pivotal structure-directing moiety in the crystal structure of $5.1 \cdot \text{HCl}$: on the one hand, it is engaged in a strong and highly directional $\text{N}^+-\text{H} \cdots \text{Cl}^-$ hydrogen bond with the protonated pyridine ring and, on the other, it establishes various weak hydrogen bonds with neighbouring 2-(1-pentyl-3-pyrazolyl)pyridinium molecules. Other contacts are also possible but have been omitted from this discussion due to their long internuclear distances. The orientation of the various 2-(1-pentyl-3-pyrazolyl)pyridinium cations in the crystal structure is such that, while maximizing the various weak hydrogen bonds, the occurrence of $\pi-\pi$ contacts is not possible. Instead, the crystal structure exhibits a rather weak and poorly directional $\text{C}-\text{H} \cdots \pi$ contact between the end part of a pentyl chain and a neighbouring 2-(3-pyrazole) ring.

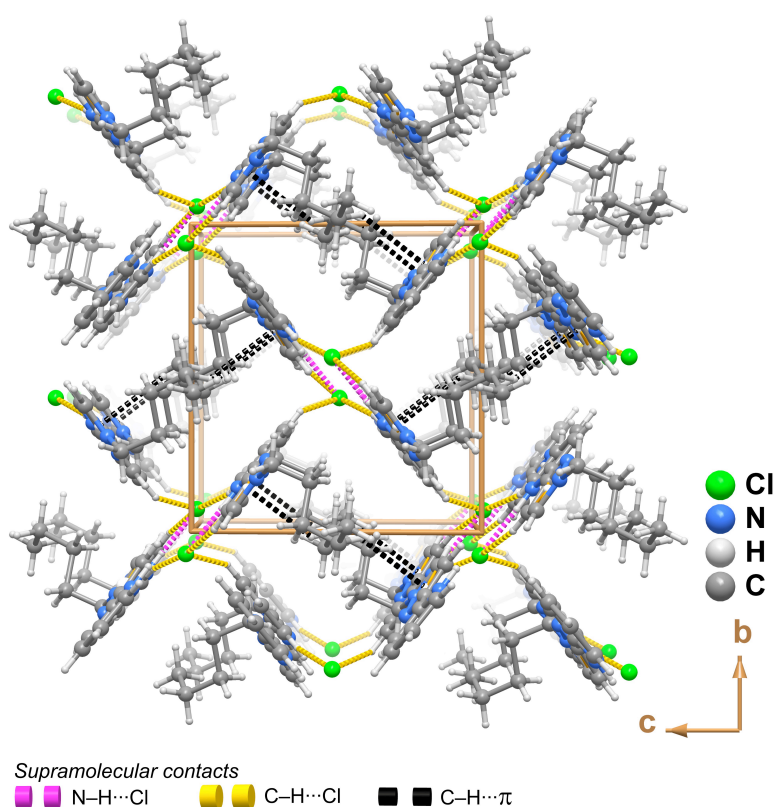
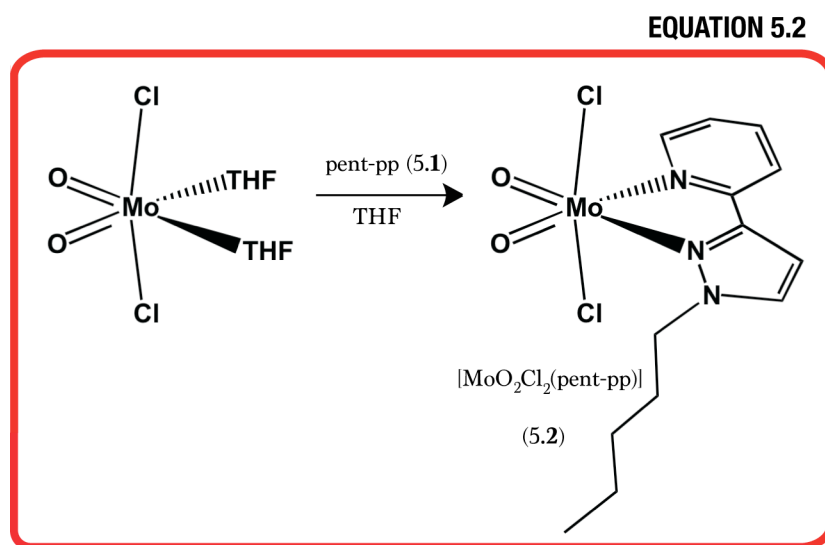


Figure 5.2. Schematic representation of the crystal packing of the salt 2-(1-pentyl-3-pyrazolyl)pyridinium chloride (5.1HCl) viewed in perspective along the $[100]$ direction of the unit cell. For clarity, only the portion of the pentyl substituent group with rate of occupancy of 70.4(7)% is shown.

5.2.2. $[\text{MoO}_2\text{Cl}_2(\text{pent-pp})]$ (5.2)

The synthesis of the dioxomolybdenum(VI) complex $[\text{MoO}_2\text{Cl}_2(\text{pent-pp})]$ (5.2) was performed using standard Schlenk techniques under inert atmosphere (Equation 5.2). The complex 5.2 was prepared in very good yield and at ambient temperature by simple ligand exchange with the solvent adduct $[\text{MoO}_2\text{Cl}_2(\text{THF})_2]$. The complex was fully characterized in the solid- and liquid-states by elemental analysis, FT-IR, ^1H NMR, and single-crystal X-ray diffraction.



5.2.2.1. FT-IR

As depicted in Figure 5.3 unequivocal evidence for the coordination of pent-pp could be derived from the performed FT-IR studies: upon coordination the ligand undergoes structural changes that affect the vibrational modes located in the $1550\text{--}1650\text{ cm}^{-1}$ spectral region. Specifically, the bands of pent-pp centred at *ca.* 1565 cm^{-1} (C-C inter-ring stretching mode) and 1592 cm^{-1} (pyridyl C-N stretching mode) are red-shifted to *ca.* 1568 and 1611 cm^{-1} , respectively, for complex 5.2. This evidence is in good agreement with results for other Mo^{VI} -pyrazolylpyridine complexes.^{[81][80]}

Additionally, the C-H out-of-plane bending mode shifts from *ca.* 761 cm^{-1} in 5.1 to *ca.* 781 cm^{-1} in 5.2. The symmetric and asymmetric $\nu(\text{Mo}=\text{O})$ stretching modes of complex 5.2 are observed as intense bands centred at *ca.* 942 and 908 cm^{-1} , which agree well with typical values reported for dioxomolybdenum(VI) complexes containing the *cis*-dioxo group.^{[73][83][85][80][81][88][205]}

A strong band at *ca.* 336 cm^{-1} (not shown in Figure 5.3) could be assigned to $\nu_{\text{asym}}(\text{Mo}-\text{Cl})$.^[81]

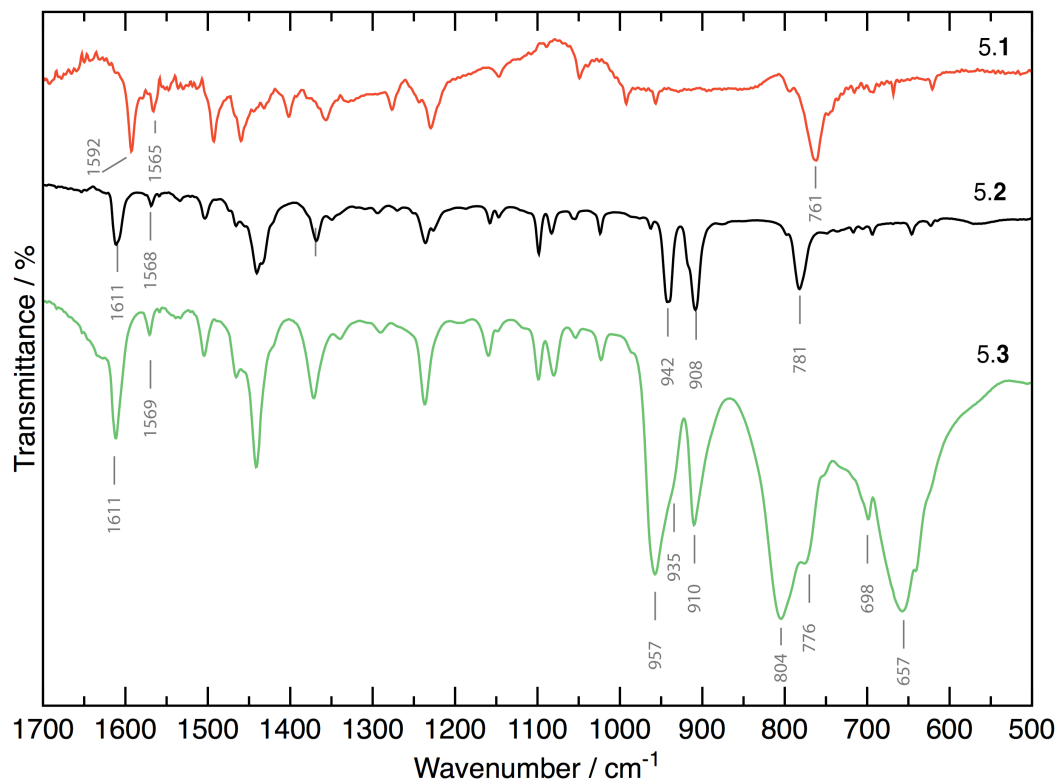


Figure 5.3. Comparison of the FT-IR KBr spectra of the pent-pp (5.1) ligand, the precursor $[\text{MoO}_2\text{Cl}_2(\text{pent-pp})]$ (5.2) complex and the final hybrid material $[\text{Mo}_2\text{O}_6(\text{pent-pp})]$ (5.3).

5.2.2.2. X-RAY DIFFRACTION: CRYSTAL STRUCTURE DESCRIPTION

Single-crystals of complex $[\text{MoO}_2\text{Cl}_2(\text{pent-pp})]$ (5.2) could be sometimes isolated as a minor product from the aqueous mother liquor obtained after its reaction with water to prepare material 5.3. This complex crystallizes in the orthorhombic centrosymmetric space group $Pbca$ with the asymmetric unit being composed of a whole molecular unit as shown in Figure 5.4. In contrast to that observed for the hydrochloride salt of the ligand 5.1, the pendant pentyl chain is not disordered, even though the observed structural differences with 5.1·HCl clearly demonstrate the high conformational flexibility of this chain (compare, for example, the distinct conformations shown in Figures 5.1 and 5.4). Upon coordination to Mo^{6+} the two average planes of the organic ligand (corresponding to the pyridine and the 2-(3-pyrazole) rings) remain, as observed in 5.1·HCl, almost coplanar with the mutual dihedral angle increasing only slightly to $5.41(19)^\circ$.

The crystallographically independent Mo^{6+} metal centre is coordinated to one N,N' -chelated 2-(1-pentyl-3-pyrazolyl)pyridine molecule, two *cis*-oxo groups and two chloride anions, with the overall coordination geometry resembling a highly distorted octahedron, $[\text{MoCl}_2\text{N}_2\text{O}_2]$.

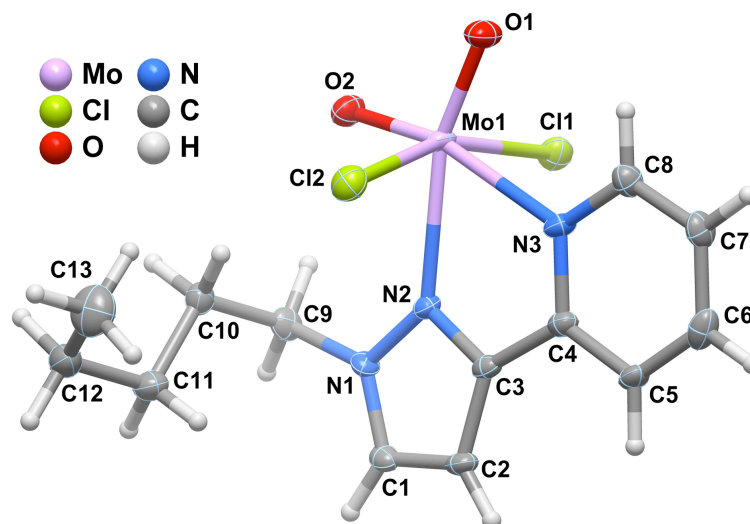


Figure 5.4. Schematic representation of the $[\text{MoO}_2\text{Cl}_2(\text{pent-pp})]$ molecular unit composing the crystal structure of 5.2, showing the labelling scheme for all non-hydrogen atoms, which are represented as thermal ellipsoids drawn at the 50% probability level. Hydrogen atoms are represented as small spheres with arbitrary radii, and the atomic labelling is provided for all non-hydrogen atoms.

While the *cis*-oxido groups are *trans*-coordinated to the organic ligand, forming the equatorial plane of the octahedron and markedly exerting their *trans* effect (as evidenced in Figure 5.4), the chloride anions occupy the apical positions of the octahedron. This multitude of coordinated species leads, simultaneously, to a wide range of bond lengths and angles as evidenced by the refined values summarised in Table 5.1. A search in the literature and in the CSD^{[37][36]} (Version 5.34, November 2012 with 3 updates) shows, nevertheless, that these values fall within the typical ranges found in related compounds.

Table 5.1. Selected bond lengths (Å) and angles (°) for the crystallographically independent Mo^{6+} coordination environment present in complex $[\text{MoO}_2\text{Cl}_2(\text{pent-pp})]$ (5.2).

Mo1–O1	1.700(2)	Mo1–N3	2.344(3)
Mo1–O2	1.685(3)	Mo1–Cl1	2.3769(10)
Mo1–N2	2.326(3)	Mo1–Cl2	2.3694(11)
O1–Mo1–Cl1	95.38(10)	O2–Mo1–N3	164.00(11)
O1–Mo1–Cl2	96.54(10)	N2–Mo1–Cl1	82.24(8)
O1–Mo1–N2	159.71(11)	N2–Mo1–Cl2	80.79(8)
O1–Mo1–N3	90.42(11)	N2–Mo1–N3	69.29(10)
O2–Mo1–O1	105.54(12)	N3–Mo1–Cl1	81.01(8)
O2–Mo1–Cl1	96.08(9)	N3–Mo1–Cl2	82.26(8)
O2–Mo1–Cl2	96.73(10)	Cl2–Mo1–Cl1	159.48(4)
O2–Mo1–N2	94.75(11)		

The crystal packing of individual $[\text{MoO}_2\text{Cl}_2(\text{pent-pp})]$ complexes to form the crystal structure of **5.2** seems to be essentially driven by geometrical factors mostly related to chemical affinity (Figure 5.5). Indeed, in the crystal structure there is a segregation of the hydrophobic part (mainly composed of the pentyl substituent) and the hydrophilic portion of the complexes (the metal coordination sphere). The latter portion is rather rich in a number of weak supramolecular interactions, namely $\text{C-H}\cdots\text{O}$ and $\text{C-H}\cdots\text{Cl}$ hydrogen bonds and π - π contacts between coordinated pent-pp molecules belonging to adjacent complexes.

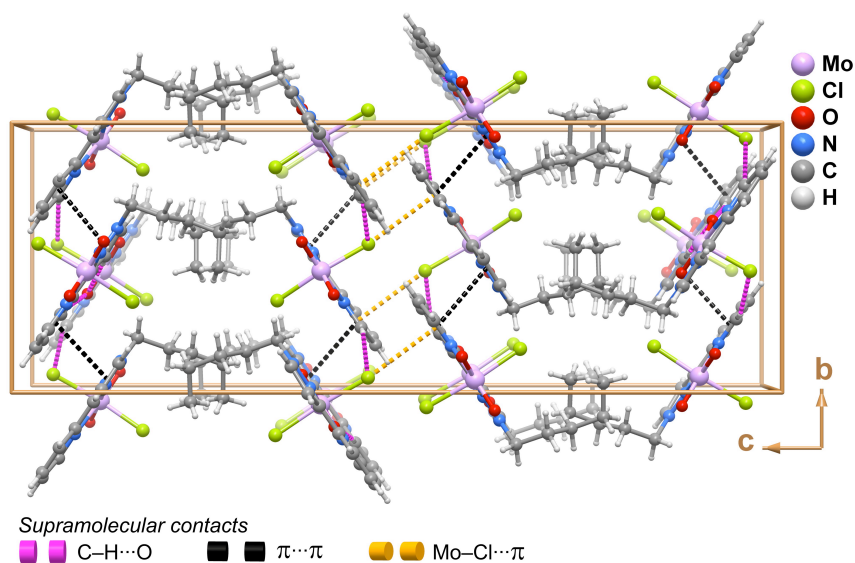


Figure 5.5. Schematic representation of the crystal packing of $[\text{MoO}_2\text{Cl}_2(\text{pent-pp})]$ (**5.2**) viewed in perspective along the $[100]$ direction of the unit cell.

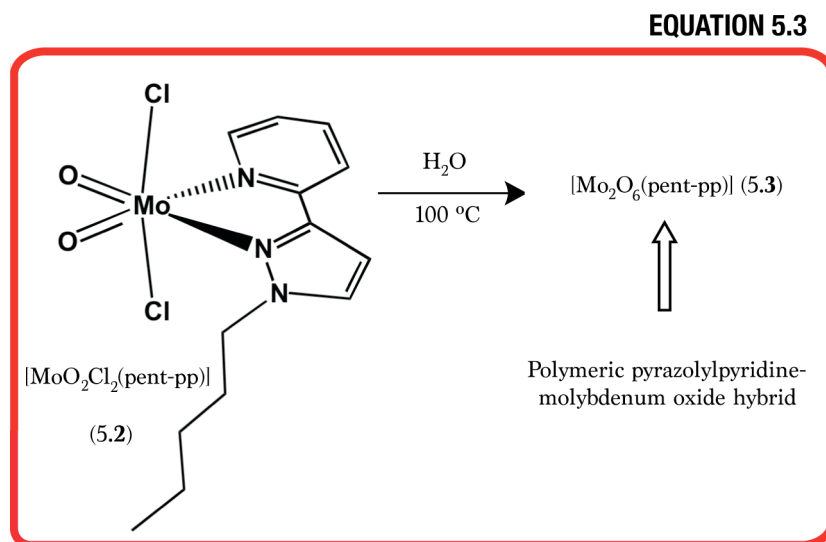
5.2.2.3. ^1H NMR

Complex **5.2** was sufficiently soluble in polar organic solvents to obtain its solution NMR spectrum with very good signal-to-noise ratio. A comparison of the ^1H NMR spectra of the ligand **5.1** and complex **5.2** (recorded in $\text{DMSO-}d_6$) shows that the resonances for the pyrazolylpyridine protons are shifted to lower field after coordination, in a similar fashion to that previously reported for $[\text{MoO}_2\text{Cl}_2(2-(1\text{-butyl-3-pyrazolyl})\text{pyridine})]$ ^[80] and $[\text{MoO}_2\text{Cl}_2(\text{ethyl}[3-(2\text{-pyridyl})\text{-1-pyrazolyl}]\text{acetate})]$ ^[205].

5.2.3. $[\text{Mo}_2\text{O}_6(\text{pent-pp})]$ (**5.3**)

The reaction of $[\text{MoO}_2\text{Cl}_2(\text{pent-pp})]$ (**5.2**) with water in a Teflon-lined stainless steel autoclave at $100\text{ }^\circ\text{C}$ led to the isolation of a new molybdenum oxide/pyrazolylpyridine hybrid material with composition $[\text{Mo}_2\text{O}_6(\text{pent-pp})]$ (**5.3**) (Equation 5.3). This material was fully characterized by FT-IR,

thermogravimetric analysis, variable-temperature powder X-ray diffraction, solid-state NMR and scanning electron microscopy. Elemental analysis of **5.3** (C, H, N and Mo) was consistent with the empirical formula $C_{13}H_{17}Mo_2N_3O_6$, *i.e.*, $[Mo_2O_6(\text{pent-pp})]$.



5.2.3.1. FT-IR

As shown in Figure 5.3 the FT-IR spectrum of material **5.3** in the *ca.* 1000-1650 cm^{-1} spectral range is very similar to that for complex **5.2**. This constitutes further evidence that in **5.3** the ligand pent-pp is structurally intact and coordinated to Mo^{6+} centres via the expected bidentate *N,N*-chelate fashion similar to that found in **5.2**. In the spectral region attributed to the Mo–O stretching vibrations (*ca.* 500-1000 cm^{-1}), compound **5.3** exhibits strong bands centred at *ca.* 657, 804, 910, 935(sh) and 957 cm^{-1} . A shoulder at *ca.* 776 cm^{-1} on the band at *ca.* 804 cm^{-1} is assigned to the C–H out-of-plane bending mode. The bands above *ca.* 900 cm^{-1} may be assigned to $\nu(Mo=O)$ vibrations, while the very intense and broad bands at *ca.* 657 and 804 cm^{-1} may be attributed to Mo–O stretching vibrational modes of bridging Mo–O–Mo units. The former band is typical of molybdenum oxide-based organic-inorganic hybrid materials with polymeric structures.^{[59][142][206]} An example is the polymeric material $[MoO_3(\text{bipy})]_n$ described in the general Introduction as a structure comprising 1D chains of corner-sharing distorted $\{MoO_4N_2\}$ octahedra and for which the FT-IR spectrum exhibits a diagnostic band at *ca.* 622 cm^{-1} attributed to $\nu(Mo-O-Mo)$.^[59] Although at this stage the fine structural details of material **5.3** remain unknown, the characterization data strongly point toward a pyrazolylpyridine-molybdenum oxide hybrid with a polymeric structure.

5.2.3.2. THERMOGRAVIMETRIC ANALYSIS and VARIABLE-TEMPERATURE

POWDER X-RAY DIFFRACTION STUDIES

The thermal decomposition behaviour of compound $[\text{Mo}_2\text{O}_6(\text{pent-pp})]$ (5.3) was studied by a combination of thermogravimetry and variable-temperature powder X-ray diffraction (performed in air; VTPXRD). Both techniques confirm that 5.3 is stable up to *ca.* 200 °C. As shown from the VTPXRD studies within this temperature range the crystalline structure of 5.3 remains unaltered (Figure 5.7). A weight loss of *ca.* 43.1% takes place between *ca.* 200 and 440 °C (Figure 5.6), with this occurrence being attributed to the thermal decomposition of the organic component (theoretical value of 42.8%). Additionally, in this temperature range it is possible to observe a transformation of the powder pattern into that typical of inorganic MoO_3 (Figure 5.7). Thus, the observed final weight of 56.0% (MoO_3 after 5.3 being transformed) is in very good agreement with the theoretical value of 57.2% based on the empirical formula given above. No further weight losses takes place until *ca.* 700 °C. Above this temperature the sublimation of MoO_3 settles in, as clearly indicated by an abrupt mass loss up to 800 °C, an event observed for other materials reported in this thesis.^[140]

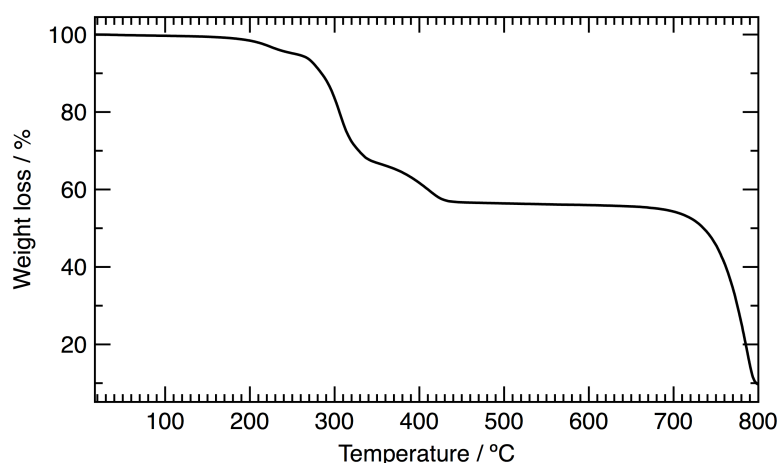


Figure 5.6. Thermogram of $[\text{Mo}_2\text{O}_6(\text{pent-pp})]$ (5.3) between ambient temperature and *ca.* 800 °C.

A full structure solution of compound $[\text{Mo}_2\text{O}_6(\text{pent-pp})]$ (5.3) based on powder X-ray diffraction, in a similar fashion to that described in previous chapters for other materials, could not be achieved due to: i) poor diffraction at high angles and ii) poor angular resolution essentially allied to very wide reflections. Indeed, even with data collected at various synchrotron sources, not even a reliable indexation could be achieved for 5.3 (Figure 5.8).

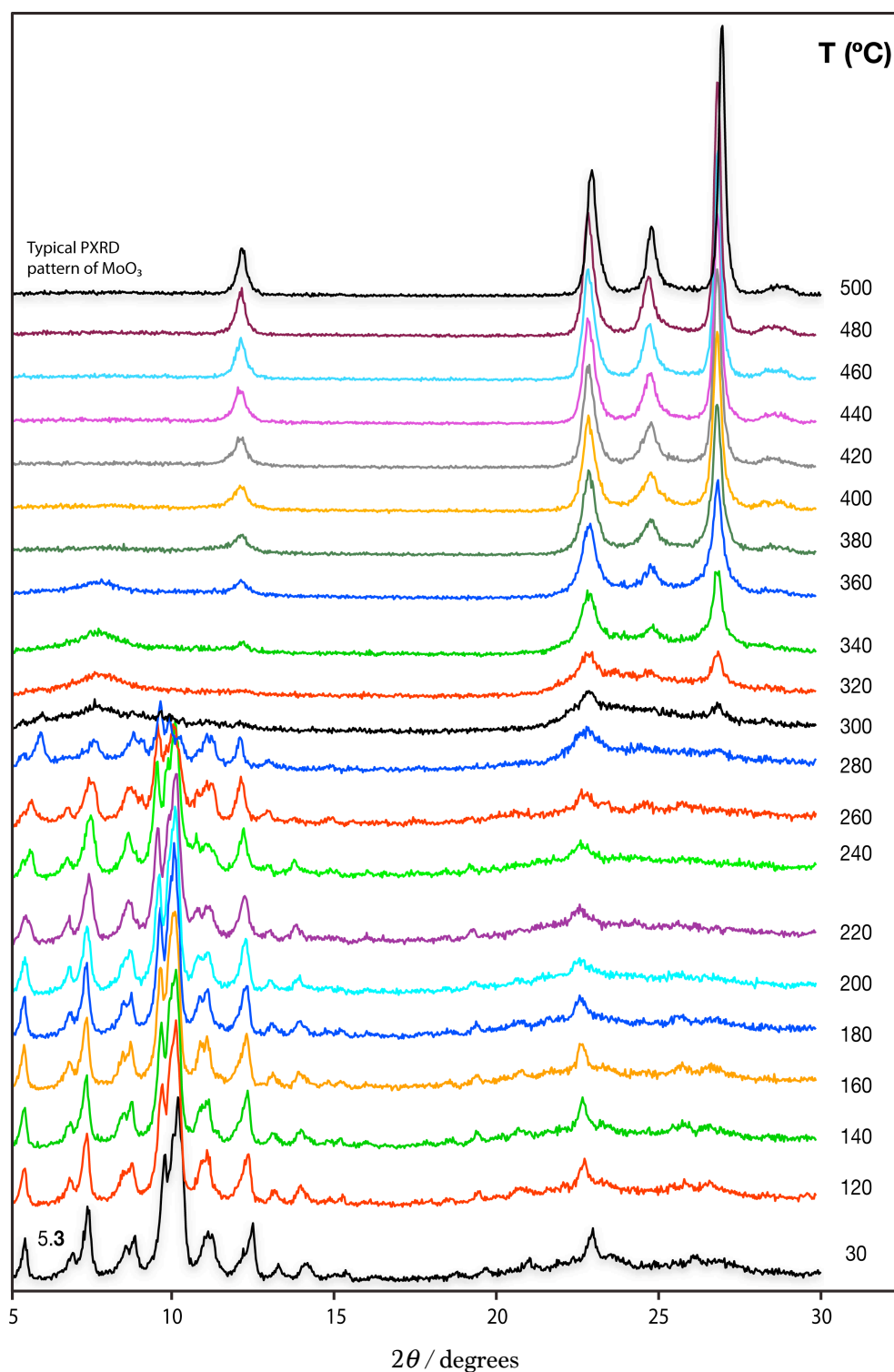


Figure 5.7. Variable-temperature powder X-ray diffraction study (in air atmosphere) on a representative portion of [Mo₂O₆(pent-pp)] (5.3).

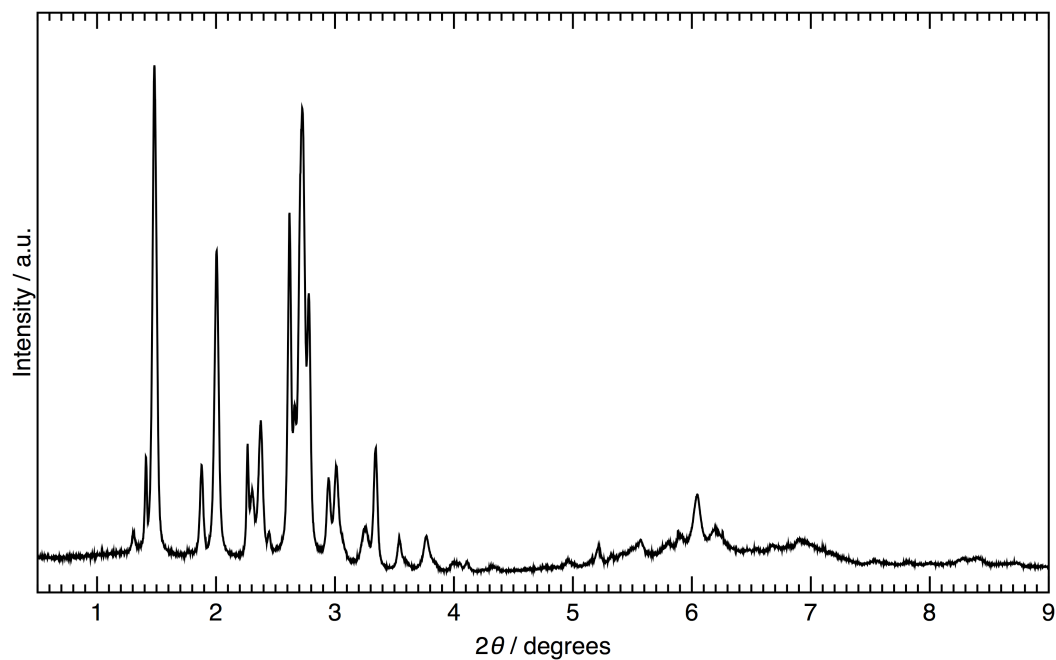


Figure 5.8. High-resolution synchrotron powder X-ray diffraction pattern of $[\text{Mo}_2\text{O}_6(\text{pent-pp})]$ (**5.3**) collected at 100 K using the diffractometer assembled at the beamline ID31 located at the European Synchrotron Radiation Facility (ESRF), Grenoble, France. Radiation wavelength of 0.39981033 \AA .

5.2.3.3. SOLID-STATE NMR

The $^{13}\text{C}\{^1\text{H}\}$ CP MAS NMR spectrum of $[\text{Mo}_2\text{O}_6(\text{pent-pp})]$ (**5.3**) (Figure 5.9) displays two main spectral regions attributed to the aromatic carbons and the alkyl chain, respectively.

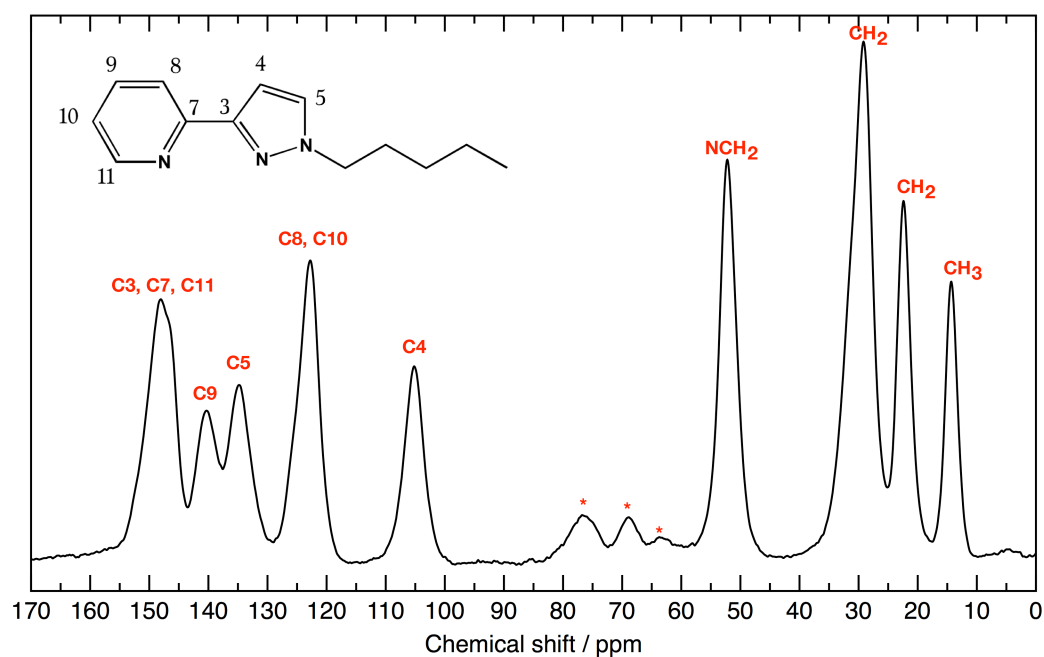


Figure 5.9. $^{13}\text{C}\{^1\text{H}\}$ CP MAS NMR spectrum of $[\text{Mo}_2\text{O}_6(\text{pent-pp})]$ (**5.3**). Spinning sidebands are indicated by asterisks. Spinning rate of 9 kHz using a Bruker Avance 500 spectrometer at 125.76 MHz. Chemical shifts are quoted in parts per million (ppm) with respect to TMS.

In the aromatic portion of the spectrum (*i.e.*, the region between 148.0 and 105.2 ppm) six resonances arise (148.0, 146.5, 140.3, 134.8, 122.8 and 105.2 ppm) being attributed to the eight carbon atoms from the heterocyclic rings. The resonance at 148.0 ppm has a FWHM (Full-Width-at-Half-Maximum) larger than the remaining aromatic signals suggesting there is a superimposition of other possible resonances C3, C7 and C11. The same occurs with the resonance at 122.8 ppm attributed to the C8 and C10 carbon atoms.

The four resonances located in the alkylic portion of the spectrum (52.2, 29.2, 22.4, and 14.3 ppm) are attributed to the five carbon atoms of the alkyl chain. The resonance centred at 29.2 ppm is attributed to two carbon atoms (note the large FWHM of this resonance).

5.2.3.4. SCANNING ELECTRON MICROSCOPY

Scanning Electron Microscopy studies on representative portions of $[\text{Mo}_2\text{O}_6(\text{pent-pp})]$ (**5.3**) reveal irregular grain shapes consisting of sheet-like lamellar structures (Figure 5.10). These morphological characteristics were expected *a priori* because of the overall poor crystallinity of the material. Energy-dispersive X-ray spectroscopy analyses further confirmed the absence of Cl in the chemical composition of compound **5.3**.

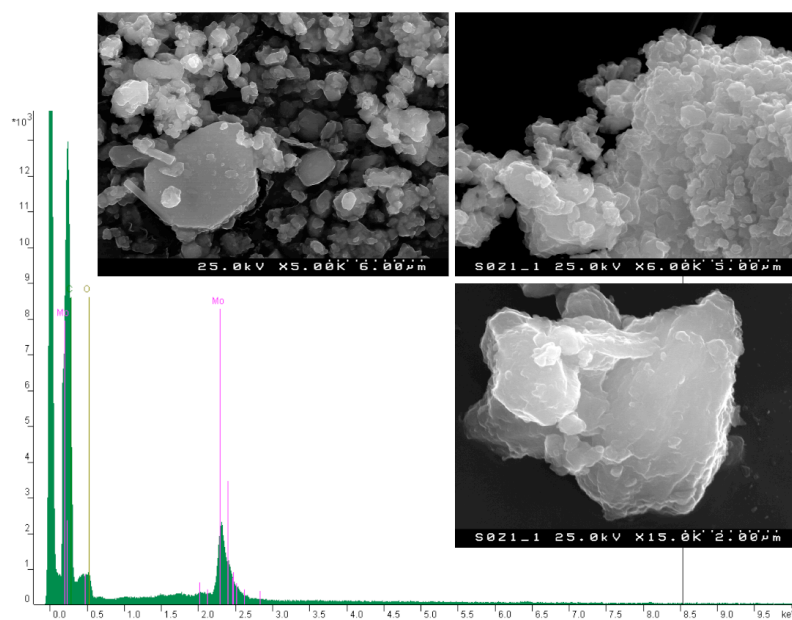


Figure 5.10. Dispersive X-ray spectroscopy (EDS) analysis of $[\text{Mo}_2\text{O}_6(\text{pent-pp})]$ (**5.3**). The insets correspond to electron microscopy (SEM) images collected at an operating energy of 25 kV, magnifications of 3000, 6000 or 15000x.

5.3. CATALYSIS

This section discusses the catalytic performance of both $[\text{MoO}_2\text{Cl}_2(\text{pent-pp})]$ (5.2) and $[\text{Mo}_2\text{O}_6(\text{pent-pp})]$ (5.3) for the conversion of *cis*-cyclooctene (Cy8) into 1,2-epoxycyclooctane (Cy8Ox). Results are analysed in a comparative fashion. Catalytic experiments with 5.3 as pre-catalyst using the bio-derived olefins DL-limonene (Lim) and methyl oleate (Ole) are additionally described (Figure 5.11). It is further shown that the oxodiperoxo complex $[\text{MoO}(\text{O}_2)_2(\text{pent-pp})]$ (5.4) was isolated from solution after a catalytic run, ultimately suggesting that this type of complex is formed *in situ* from 5.3 and also plays an important catalytic role.

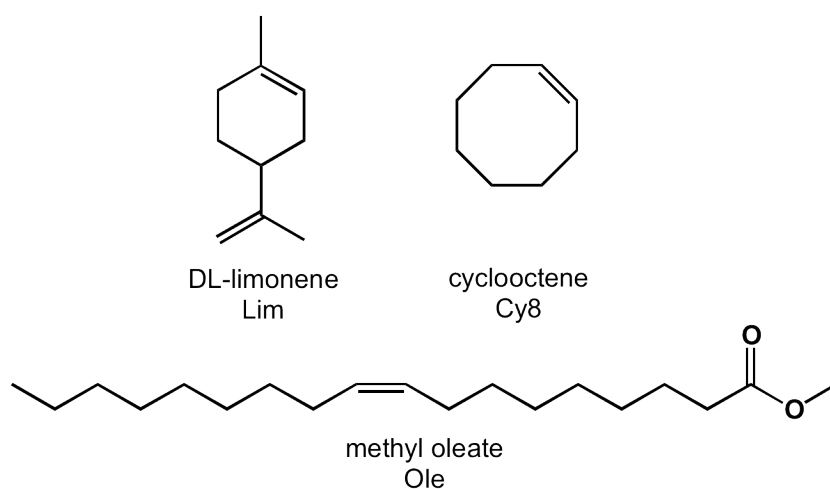


Figure 5.11. Epoxidation substrates used for olefin epoxidation catalyst tests.

5.3.1. Cy8

The catalytic performance of 5.2 and 5.3 was evaluated by using Cy8 as a model substrate, TBHP as the oxidant and 1,2-dichloroethane (DCE) as the co-solvent under the typical reaction conditions (hereafter referred to as TypCs). *Please note:* Typical reaction conditions correspond to the overall procedure for starting the catalytic reaction which involve charging the reactor with catalyst, olefin and co-solvent, and then immersing the reactor into a thermostated oil bath at 55 °C, where it is kept under magnetic stirring (1000 rpm) for 10 min to attain isothermal initial conditions. Subsequently TBHP, also preheated at 55 °C, was added to the reactor. This moment is taken as the initial instant of the reaction.

The two catalysts 5.2 and 5.3 exhibited excellent selectivity (100%) toward the epoxide product (Cy8Ox) until 100% conversion. Without adding a catalyst and/or the oxidant TBHP, the reaction of Cy8 was negligible, which is a clear indication of the crucial roles of the transition metal and the hydroperoxide in the formation of the active oxidizing species.

When compared with other mononuclear complexes of the type $[\text{MoO}_2\text{Cl}_2\text{L}]$, the results obtained for **5.2** (80% Cy8Ox yield at 10 min) are comparable with those reported for $\text{L} = \text{ethyl}[3-(2\text{-pyridyl})-1\text{-pyrazolyl}]\text{acetate}$ (ppEA, 80%) and 2-(1-butyl-3-pyrazolyl)pyridine (92%).^[80] The catalytic results for **5.2** even outperforms that for $\text{L} = 2-[3(5)\text{-pyrazolyl}]\text{pyridine}$ (pzpy, 32%).^[81] The catalytic reaction was faster for **5.2** than for **5.3** (Figure 5.12), which somewhat parallels published data for molybdenum compounds possessing pyrazolylpyridine or bipyridine ligands for which the epoxidation rate of Cy8 tends to be lower for polymeric molybdenum compounds than for the respective mononuclear precursor complexes.^{[80][142][206][172]} The lower activity exhibited by the polymeric compounds may be partly due to poor catalyst solubility and/or inaccessibility of the substrate molecules to some of the active species. Nevertheless, the catalytic activity of **5.3** (based on 60% Cy8Ox yield at 10 min) is higher than that reported for the polymeric compounds $[\text{Mo}_8\text{O}_{24}(\text{ppEA})_4]$ (~18%),^[49] $[\text{Mo}_2\text{O}_4(\mu_2\text{-O})\text{Cl}_2(\text{ppEA})_2]$ (~48%),^[94] $[\text{Mo}_4\text{O}_{12}(\text{pzpy})_4]$ (~4%),^[49] and $[\text{Mo}_2\text{O}_6(\text{[(3-pyridinium-2-yl)-1H-pyrazolyl-1-yl]acetate})_n]$ (74% Cy8Ox yield at 24 h reaction).^[172]

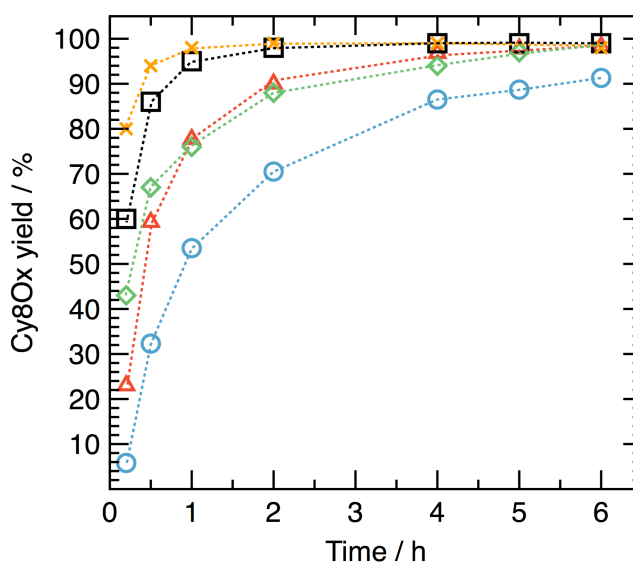


Figure 5.12. Dependence of the *cis*-cyclooctene oxide (Cy8Ox) yield with the reaction time in the epoxidation of *cis*-cyclooctene (Cy8). Catalyst/co-solvent systems: **5.2**/DCE (×), **5.3**/DCE (□), **5.3**/BTF (△), **5.3**/hex (○) and **5.4**/DCE (◇). Reaction conditions as indicated for TypCs in the Experimental section.

The catalytic performance of **5.3** was further investigated using trifluorotoluene (BTF) or *n*-hexane as co-solvent. The non-coordinating nature of these solvent molecules (just like for DCE) should avoid competition between the solvent and the substrate molecules for coordination to the metal centre. The epoxidation rate (conversion at 10 min / 6 h reaction, Figure 5.12) decreased in the order DCE (60 / 99%) > BTF (23 / 98%) > hex (6 / 91%). Product selectivity

was always 100% towards Cy8Ox. Differences in catalyst solubility may be responsible for these different reaction rates. Underlying this hypothesis is the fact that the contact tests (Dissolv_Test – see details in the Experimental section) revealed that the reactions were homogeneous in nature. The conversions at 10 min for the Dissolv_Test decreased in the order DCE (52%) > BTF (40%) > hex (32%), with Cy8Ox selectivity being always 100%. This trend is consistent with both a visual evaluation of the colour of the respective liquid phases (intense yellow for DCE, pale yellow for BTF, and almost colourless for hex) and the amount of undissolved solid that was separated in the procedure for the Dissolv_Test (44 wt.% for DCE, 80 wt.% for BTF and 89 wt.% for hex). These results are consistent with the catalyst being homogeneous, and suggest that its solubility increases in the order hex < BTF < DCE. For each solvent system, the initial amount of active species for the Dissolv_Test is expectedly smaller than, or approximately equal, to that for the TypCs (without filtration). For DCE, the initial reaction rates were similar for the Dissolv_Test and the TypCs, whereas for BTF and *n*-hexane the initial reaction rates were higher for the Dissolv_Test. These results are consistent with the enhanced catalyst solubility in DCE.

5.3.2. BIO-DERIVED OLEFINS: Lim and Ole

Considering the homogeneous nature of the catalytic reaction, there is no practical advantage in using a higher amount of catalyst than that corresponding to its saturation concentration. Hence, a Dissolv_Test-DCE solution was used for the catalytic reactions of the bio-based olefins at 55 °C (the catalytic reaction was initiated with the addition of the olefin to the Dissolv_Test-DCE solution).

The catalytic reaction of Lim gave mainly LimOx and LimDiox in a combined yield of 57 / 93% at 62 / 97% conversion, reached at 10 min / 6 h reaction, respectively. The by-products included *p*-mentha-dienols, which are of interest as fragrances.^[207] Regioselectivity was in favour of the epoxidation of the endocyclic double bond, leading to a LimOx/LimDiox molar ratio of 5.8 at 93% total epoxide yield (6 h). The LimOx yield of *ca.* 79% at 6 h reaction compares favourably with that described in this thesis for polymeric molybdenum compounds (also tested in the same reaction at 55 °C): *ca.* 71-74% yield at 6 h reaction for [Mo₈O₂₂(OH)₄(di-*t*-Bu-bipy)₄] and [Mo₂O₄(μ₂-O)₂(di-*t*-Bu-bipy)₂]^{[151][159]} (chapter 2), and 61% for (DMA)[MoO₃(HbpdC)]·*n*H₂O (chapter 3).^[182]

The catalytic reaction of Ole (chosen as substrate for fatty acid methyl esters) led to 9,10-epoxystearate (OleOx) as the main product in 30 / 78% yield at 30 / 82% conversion, reached at 10 min / 6 h, respectively. In parallel with that observed for the reaction of Lim, the catalytic results for the reaction of Ole in the presence of 5.3 (OleOx yield at 6 h) compare favourably with those reported for polymeric molybdenum compounds tested as catalysts in the same reaction at 55 °C: 39% yield for [Mo₈O₂₂(OH)₄(di-*t*-Bu-bipy)₄] (2.2)^[151], and 43% yield for (DMA)[MoO₃(HbpdC)]·*n*H₂O (3.1)^[182] It is nevertheless important to

stress that the initial Mo : olefin molar ratios used in these studies were greater than that employed in the studies summarized above.

5.3.3. IDENTIFICATION of the ACTIVE SPECIES

For a batch reaction carried out with material **5.3**, under TypCs, DCE as co-solvent and Cy as substrate, a biphasic reaction mixture consisting of a pale green solid and yellow solution was formed. The FT-IR spectrum of the undissolved solid (denoted **5.3-S**, recovered at the end of the reaction as described in the Experimental section) was fairly similar to that for pristine **5.3** (Figure 5.13). Similar results were obtained when using BTF or *n*-hexane as co-solvents. A yellow solid (denoted **5.3-L**) was isolated from the liquid phase of the reaction and found to exhibit an FT-IR spectrum very different from that of **5.3** (Figure 5.13). In a separate experiment, a mixture comprising **5.3**, TBHP and DCE was heated at 55° C for 6 h. Addition of pentane to the resultant reaction solution led to the precipitation of a yellow solid **5.4** (Figure 5.14) that displayed a FT-IR spectrum identical to that for **5.3-L**.

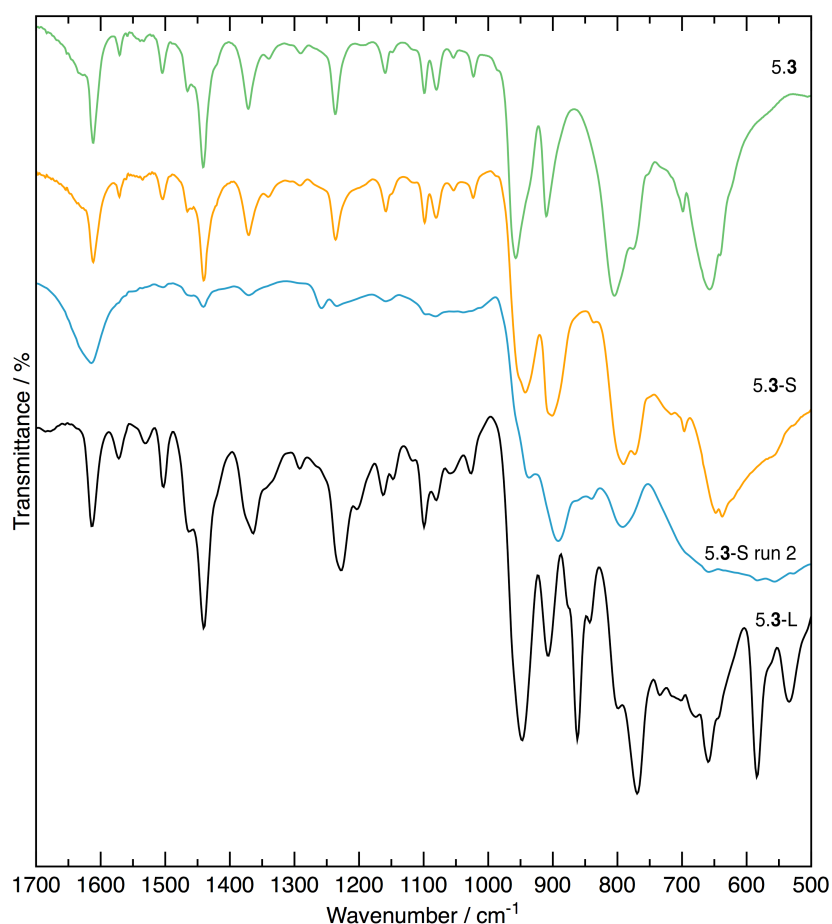


Figure 5.13. FT-IR ATR spectra of the complex **5.3** and the solids **5.3-S**, **5.3-S-run 2** and **5.3-L** recovered from the catalytic reactions.

Further characterization of **5.4** by elemental analysis and ^1H NMR spectroscopy led to its identification as the oxodiperoxido complex $[\text{MoO}(\text{O}_2)_2(\text{pent-pp})]$. The FT-IR spectrum of **5.4** shows diagnostic bands at *ca.* 947 cm^{-1} [$\nu(\text{Mo}=\text{O})$], 861 cm^{-1} [$\nu(\text{O}-\text{O})$], 656 , 582 and 535 cm^{-1} [$\nu(\text{Mo}(\text{O}_2)_2)$], which are all characteristic of $[\text{MoO}(\text{O}_2)_2\text{L}]$ complexes bearing one bidentate ligand (L).^[195] The spectrum of **4.4** in the range $900\text{--}1650\text{ cm}^{-1}$ (comprising the organic ligand modes) is similar to that for **4.2**. Oxodiperoxido complexes like **5.4** are well known as effective homogeneous catalysts for the epoxidation of olefins.^[195] Therefore, the oxodiperoxido complex clearly plays a catalytic role in the system **5.3** / TBHP_{dec} / DCE. The formation of a complex of the type $[\text{MoO}_2(\text{O}_2)_2\text{L}]$ from a polymeric compound during a catalytic epoxidation reaction has only been previously reported for $[\text{Mo}_2\text{O}_4(\mu_2\text{-O})\text{Cl}_2(\text{ppEA})_2]$.^[94] On the other hand, the formation of active monoxobisperoxido species from the reaction of monomeric oxomolybdenum complexes with TBHP has been reported in several cases, e.g. $[\text{Mo}_2\text{Cl}_2(\text{tris}(3,5\text{-dimethyl-1-pyrazolyl})\text{methane})]$ gave $[\text{Mo}_2\text{O}_3(\text{O}_2)_2(\mu_2\text{-O})(\text{H}_2\text{O})(\text{tris}(3,5\text{-dimethyl-1-pyrazolyl})\text{methane})]$,^[160] $[\text{MoO}_2(\text{NCS})_2(\text{di-}t\text{-Bu-bipy})]$ gave $[\text{MoO}(\text{O}_2)_2(\text{di-}t\text{-Bu-bipy})]$,^[114] and $[\text{CpMoO}_2\text{X}]$ (Cp = cyclopentadienyl; X = CF_3 and CH_3) with alkyl hydroperoxides (ROOH) to give $[\text{CpMo}(\text{O}_2)\text{OX}]$ contemplate the formation of ROH as co-product.^{[208][209]} Based on these studies, it may be postulated that the conversion of **5.3** to **5.4** involves the transformation of Mo=O groups by reaction with TBHP_{dec} to give Mo(O₂) groups and *tert*-butanol as co-product.

For comparison with the system **5.3** / TBHP_{dec} / DCE, **5.4** was tested as catalyst, and used in an amount equivalent to the number of moles of organic ligand added with **5.3** under the typical reaction conditions. The reaction was slower for **5.4** than for **5.3**, and the respective kinetic curves after 4 h reaction tended to similar conversions (Figure 5.12). Based on these results it seems that **5.3** is converted to **5.4** plus different active species.

When **5.3-S** was used in a second 6 h batch run (under TypCs), the initial reaction rate decreased (conversion at 10 min was 60% and 17% for runs 1 and 2, respectively), although the Cy8 conversions tended to similar values (99%) after 6 h for both runs. The drop in the initial reaction rate from runs 1 to 2 may be partly due to a lower initial amount of active species in the latter. The FT-IR spectrum of the solid recovered from run 2 (denoted **5.3-S** run 2) was notably different from those of **5.3-S** and **5.3**; the relative intensities of the bands assigned to the organic ligand decreased considerably (Figure 5.13). These results are consistent with the formation of co-product(s) during the conversion of **5.3** to **5.4**, which in this case seem to be poorly soluble.

Synthetic steps that led to the formation of the oxodiperoxido complex 5.4

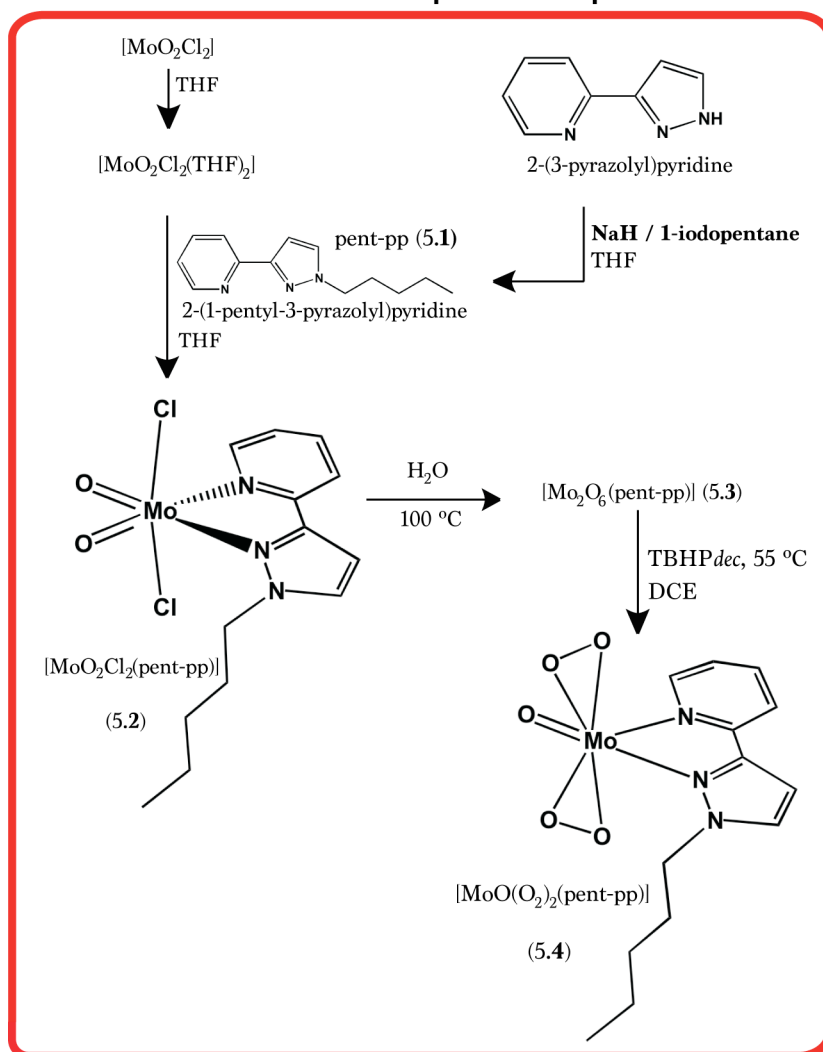


Figure 5.14. Schematic summary of the synthetic steps that led to the formation of 5.4, identified as the oxodiperoxido complex $[\text{MoO}(\text{O}_2)_2(\text{pent-pp})]$.

5.4. CONCLUDING REMARKS

The dioxomolybdenum(VI) complex $[\text{MoO}_2\text{Cl}_2(\text{pent-pp})]$ (5.2) is a highly active and selective catalyst for the epoxidation of the benchmark substrate Cy8. Hydrolysis of 5.2 under hydrothermal conditions reproducibly gives a microcrystalline material with the composition $[\text{Mo}_2\text{O}_6(\text{pent-pp})]$ (5.3). Although the structure of 5.3 is presently unknown, characterization data point toward a polymeric molybdenum oxide hybrid in which the organic ligands are coordinated to oxomolybdenum(VI) centres. When material 5.3 is used in catalytic olefin epoxidation, it acts as a source of soluble active species, which include, but may not be limited to, the oxodiperoxido complex $[\text{MoO}(\text{O}_2)_2(\text{pent-pp})]$. While most of the molybdenum oxide/organic hybrid materials studied in this thesis in catalytic olefin epoxidation behave in a similar way to 5.3, *i.e.*, the materials act as a source of soluble active species, some materials act as true heterogeneous catalysts.

In this thesis, five distinct N,N' -chelate ligands were investigated:

- i) 2,2'-bipyridine (bipy);
- ii) di-*tert*-butyl-2,2'-bipyridine (di-*t*-Bu-bipy);
- iii) 2,2'-bipyridine-5,5'-dicarboxylic acid (H_2 bpdc);
- iv) 2-[3(5)-pyrazolyl]pyridine (pzpy);
- v) 2-(1-pentyl-3-pyrazolyl)pyridine (pent-pp);

These ligands were carefully selected so as to investigate the possible structural diversity that could arise from their use. This small set comprises both symmetrical (bipy, di-*t*-Bu-bipy and H_2 bpdc) and unsymmetrical (pzpy or pent-pp) molecules, some with bulky substituent groups (such as the *tert*-butyl and pentyl moieties), allowing comparison with less sterically hindered molecules (bipy and pzpy). The distinct nature of these molecules promoted the isolation of a series of new materials that clearly reflect their strong structure-directing influence when employed as N,N' -chelating ligands. Thus, this thesis describes the principles behind the design, synthesis, detailed characterization and application in catalysis of new oxomolybdenum organic-inorganic hybrid materials (HMs). The structures of these compounds range from discrete mononuclear, dinuclear and octanuclear complexes, to novel and highly unprecedented polymeric materials. The vast majority of the materials are based, as expected, on the common *cis*-dioxomolybdenum(VI) (*i.e.*, cis - MoO_2^{2+}) moiety.

Isolation of phase-pure materials was found to be highly dependent on the type of the precursor selected for the synthesis and the strategy employed. Discrete $[MoO_2Cl_2L]$ complexes, with L being a bidentate chelating N,N' -donor ligand (bipy, di-*t*-Bu-bipy, pzpy or pent-pp), played a decisive role in the preparation of a handful of the aforementioned materials: the *in situ* hydrolysis and condensation in water of this type of precursor, at 100-120 °C under hydrothermal, reflux or microwave-assisted synthesis, was at the genesis of several compounds. Most likely, the hydrolysis of the Mo-Cl bonds of the precursors yielded reactive Mo-OH species that condensed through oxolation and/or ololation reactions to give the metal-oxido clusters, oligomers and polymers assembled via M-O-M or M-OH-M bridges. In general, the reactions carried out

using these discrete $[\text{MoO}_2\text{Cl}_2\text{L}]$ complexes were highly reproducible with good-to-very good yields of the resulting hybrid materials. Prepared materials presented the same characterization results and yields whenever the synthetic method was hydrothermal, reflux or microwave-assisted synthesis. This was an indication that the heating method had no significant influence on the outcome of the reaction. The most significant difference between these three heating methods was the overall reaction time, which ranged from 4 h in the microwave-assisted synthesis to 19 h (or days) in the hydrothermal approach.

The reaction of the inorganic MoO_3 molybdenum source with some of the free ligands was also investigated under typical hydrothermal conditions, in a manner similar to that commonly reported in the literature for the synthesis of molybdenum oxide-based hybrid materials. It was found that with the selected organic ligands this approach typically led to microcrystalline powder mixtures, most of them difficult to isolate as pure and segregated phases. A fine optimization of the reaction conditions permitted, nevertheless, for some systems the isolation of single-crystals which were pivotal for the structural elucidation using X-ray diffraction. Namely, the structure of the octanuclear discrete complex $[\text{Mo}_8\text{O}_{22}(\text{OH})_4(\text{di-}t\text{-Bu-bipy})_4]$, and of the dinuclear $[\text{Mo}_2\text{O}_6(\text{di-}t\text{-Bu-bipy})_2]$ and tetranuclear $[\text{Mo}_4\text{O}_{12}(\text{pzpy})_4]$ complexes were discovered using this approach.

The use of H_2bpdc as the N,N' -donor ligand necessitated a modification of the precursor and solvent employed for the reaction. Using the analogous $[\text{MoO}_2\text{Cl}_2(\text{H}_2\text{bpdc})]$ precursor in water or reacting H_2bpdc with MoO_3 always led to the isolation of reagent/product mixtures that proved to be very difficult to analyse and even to identify. The polymer $(\text{DMA})[\text{MoO}_3(\text{Hbpdc})] \cdot n\text{H}_2\text{O}$ was prepared as a pure phase solely when the strategy shifted to solvothermal conditions using a solvent mixture of H_2O and DMF to improve the solubility of the organic ligand.

As summarized in the general introduction, only a handful of polymeric oxomolybdenum(VI) materials containing chelating N,N' -donor ligands were known until a few years ago (six in total), most of them arising from the same research group headed by Professor Zubieta.^[59] The research leading to this thesis added novel compounds to this restricted family of polymeric compounds. Even though the fine structural details of compound $[\text{Mo}_2\text{O}_6(\text{pent-pp})]_n$ are presently unknown, characterization data also strongly point toward a polymeric Mo^{6+} oxide hybrid in which the organic ligands are coordinated to oxomolybdenum(VI) centres.

All new polymeric materials were, in general, fully characterized by using solid-state techniques, namely elemental analyses, thermogravimetry, FT-IR, solid-state NMR, electron microscopy and powder X-ray diffraction (both from laboratory and synchrotron sources). This extensive structural characterization contrasts with the previous reports of related materials that were mostly based on single-crystal X-ray diffraction studies complemented, in some cases, with

basic structural data. Another important achievement of the present thesis was the full structural elucidation of three polymeric materials using powder X-ray diffraction data (mostly based on synchrotron). The combination of the aforementioned advanced characterization studies permitted the development of a general strategy to unveil the crystal details of this type of compounds. In short, the present thesis also contributed significantly toward the body of knowledge concerning the structural characterization of oxomolybdenum(VI) hybrid materials.

Polymers $\{[\text{MoO}_3(\text{bipy})][\text{MoO}_3(\text{H}_2\text{O})]\}_n$, $(\text{DMA})[\text{MoO}_3(\text{Hbpd})] \cdot n\text{H}_2\text{O}$ and $[\text{Mo}_3\text{O}_9(\text{pzpy})]_n$ contain the same type of 1D hybrid chain formed by corner-shared distorted $\{\text{MoO}_4\text{N}_2\}$ octahedra (**O**) with a **-O-O-O-O-** distribution. The alignment of the organic ligands along the growth direction of the polymers is different for each material. Whereas in $\{[\text{MoO}_3(\text{bipy})][\text{MoO}_3(\text{H}_2\text{O})]\}_n$, the bipy ligands of the $\infty^1[\text{MoO}_3(\text{bipy})]$ polymer are perfectly aligned so as to minimize steric repulsion with the adjacent inorganic $\infty^1[\text{MoO}_3(\text{H}_2\text{O})]$ polymer, in $(\text{DMA})[\text{MoO}_3(\text{Hbpd})] \cdot n\text{H}_2\text{O}$ the ligands within the anionic $\infty^1[\text{MoO}_3(\text{Hbpd})]_n^{n-}$ polymer alternate and are slightly tilted with respect to the $\text{Mo} \rightarrow \text{O} \rightarrow \text{Mo}$ vector. As observed for $\{[\text{MoO}_3(\text{bipy})][\text{MoO}_3(\text{H}_2\text{O})]\}_n$, the N,N' -chelated ligands in $[\text{Mo}_3\text{O}_9(\text{pzpy})]_n$ are eclipsed along the growth direction of the polymer.

Each new polymer described in this thesis presents a number of truly unique structural features. $\{[\text{MoO}_3(\text{bipy})][\text{MoO}_3(\text{H}_2\text{O})]\}_n$ is the first type of such materials which consists of a crystalline 1:1 adduct of two very distinct 1D polymers (one hybrid and another purely inorganic). $(\text{DMA})[\text{MoO}_3(\text{Hbpd})] \cdot n\text{H}_2\text{O}$, besides being the first negatively-charged polymeric compound of its kind, is also the first 1D polymer based on dioxomolybdenum(VI) units coordinated to a N,N' -chelate ligand which also has other possible coordinative sites. $[\text{Mo}_3\text{O}_9(\text{pzpy})]_n$ is structurally remarkable since the polymer composing the structure can be divided into two very distinct interconnected components, a double ladder-type inorganic core reminiscent of the crystal structure of MoO_3 and a hybrid inorganic 1D polymeric core very much identical to those reported by J. Zubietta.^[59] In addition $[\text{Mo}_3\text{O}_9(\text{pzpy})]_n$ is also the material with the highest metal-to-ligand content reported to date.

Concerning the discrete mononuclear $[\text{MoO}_2\text{Cl}_2(\text{pent-pp})]$, dinuclear $[\text{Mo}_2\text{O}_6(\text{di-}t\text{-Bu-bipy})_2]$ and octanuclear $[\text{Mo}_8\text{O}_{22}(\text{OH})_4(\text{di-}t\text{-Bu-bipy})_4]$ complexes, a considerable level of novelty can be attributed to the two last complexes. As described in the introduction, monomeric hybrid compounds of the $[\text{MoO}_2\text{Cl}_2\text{L}]$ family containing $\text{L} = N,N'$ -chelating ligands started to be investigated many years ago, with most of the research being concentrated in the last 20 years or so. Despite being new, the mononuclear complex $[\text{MoO}_2\text{Cl}_2(\text{pent-pp})]$ represents just another example to be added to the vast list of known $[\text{MoO}_2\text{Cl}_2(N,N)]$ complexes. Its uniqueness is solely focused on the use of the ligand pent-pp that was designed and first prepared under the scope of the present thesis.

Dinuclear structures with the cis-MoO_2^{2+} moiety and the *di-t*-Bu-bipy ligand were already known prior to this work (see Introduction). Nevertheless, the common structural feature among these known complexes was the presence of two cis-MoO_2^{2+} cores interconnected by a monooxidobridge. In this context, complex $[\text{Mo}_2\text{O}_6(\text{di-}t\text{-Bu-bipy})_2]$ stands out in this family being a dinuclear complex assembled by a dioxido bridging moiety. The occurrence of this motif might be related to the use of the alternative synthetic method: hydrothermal reaction of MoO_3 with *di-t*-Bu-bipy, where $[\text{Mo}_2\text{O}_6(\text{di-}t\text{-Bu-bipy})_2]$ was isolated as a trace compound.

The octameric $[\text{Mo}_8\text{O}_{22}(\text{OH})_4(\text{di-}t\text{-Bu-bipy})_4]$ complex stands out as being one of the largest discrete complexes containing N,N' -chelating ligands. In fact, besides the tetranuclear complex $[\text{Mo}_4\text{O}_{12}(\text{pzpy})]$, $[\text{Mo}_8\text{O}_{22}(\text{OH})_4(\text{di-}t\text{-Bu-bipy})_4]$ is the first complex that contains an N,N' -chelating ligand and is not dinuclear. For this complex it is interesting to observe how the change from a non-bulky bipy to the more sterically-hindered *di-t*-Bu-bipy ligand blocked the possibility of having a polymeric structure and forced the complex to adopt a highly distorted form strongly resembling an “S”-shape. This also constitutes the only result where the use of the $[\text{MoO}_2\text{Cl}_2\text{L}]$ precursor under hydrothermal reaction conditions did not produce a 1D polymeric product (compare, for example, with structure $\{[\text{MoO}_3(\text{bipy})][\text{MoO}_3(\text{H}_2\text{O})]\}_n$). This occurrence is attributed to the steric repulsion associated with the large *tert*-butyl substituent groups.

The difficulty in preparing the polymeric materials followed the order $\{[\text{MoO}_3(\text{bipy})][\text{MoO}_3(\text{H}_2\text{O})]\}_n \leq [\text{Mo}_3\text{O}_9(\text{pzpy})]_n < (\text{DMA})[\text{MoO}_3(\text{Hbpd})] \cdot n\text{H}_2\text{O} \ll [\text{Mo}_2\text{O}_6(\text{pent-pp})]_n$, *i.e.*, it increased with the presence of larger (*i.e.*, more sterically impeded) and more complex pendant groups bound to the cores of the bipy or pzpy molecules. For example, polymer $(\text{DMA})[\text{MoO}_3(\text{Hbpd})] \cdot n\text{H}_2\text{O}$ was only formed after a drastic modification of the precursor and solvent of the reaction. Even in this situation, crystallization was only promoted when DMF was converted in situ into DMA^+ cations. The structure of compound $[\text{Mo}_2\text{O}_6(\text{pent-pp})]_n$ is presently unknown, although from the myriad of characterization data gathered to date one can also infer that it is a polymeric structure.

The catalytic behaviour of the discrete $[\text{MoO}_2\text{Cl}_2(\text{pent-pp})]$ (mononuclear), $[\text{Mo}_2\text{O}_6(\text{di-}t\text{-Bu-bipy})_2]$ (dinuclear), $[\text{Mo}_8\text{O}_{22}(\text{OH})_4(\text{di-}t\text{-Bu-bipy})_4]$ (octanuclear) complexes and the polymeric compounds was tested in olefin epoxidation. For the polymeric materials the catalytic tests showed that $\{[\text{MoO}_3(\text{bipy})][\text{MoO}_3(\text{H}_2\text{O})]\}_n$ was a moderately active, highly selective and stable catalyst for the epoxidation of *cis*-cyclooctene at 55 °C using TBHPdec as the oxidant. Catalysis was heterogeneous in nature when *n*-hexane was used as the co-solvent. Furthermore, the selective epoxidation of *cis*-cyclooctene could be performed using $\{[\text{MoO}_3(\text{bipy})][\text{MoO}_3(\text{H}_2\text{O})]\}_n$ and TBHPaq, meaning that this might be a potentially interesting water-tolerant catalyst for the epoxidation of non-functionalized olefins. The $[\text{MoO}_2\text{Cl}_2(\text{bipy})]$ precursor to

$\{[\text{MoO}_3(\text{bipy})][\text{MoO}_3(\text{H}_2\text{O})]\}_n$ was also investigated and, under the employed conditions, transformed into the known polymer $[\text{MoO}_3(\text{bipy})]_n$.

When $(\text{DMA})[\text{MoO}_3(\text{HbpdC})] \cdot n\text{H}_2\text{O}$ was investigated as catalyst in the epoxidation of methyl oleate and DL-limonene the catalytic reaction was homogeneous in nature. This limitation was overcome by using ionic liquids for which the catalyst could be effectively recycled as in typical heterogeneous catalysis.

Under similar conditions for the catalytic tests, polymers $[\text{Mo}_3\text{O}_9(\text{pzpy})]_n$ and $[\text{Mo}_2\text{O}_6(\text{pent-pp})]_n$ acted as sources of soluble active species that were identified as the oxodiperoxido complexes $[\text{MoO}(\text{O}_2)_2(\text{pzpy})]$ and $[\text{MoO}(\text{O}_2)_2(\text{pent-pp})]$, respectively. These $[\text{MoO}(\text{O}_2)_2(\text{L})]$ -type complexes are well known effective homogeneous catalysts for olefin epoxidation. The formation of this type of oxodiperoxido complex from a polymeric compound and during a catalytic epoxidation reaction was only reported once in the past for the dinuclear complex $[\text{Mo}_2\text{O}_4(\mu_2\text{-O})\text{Cl}_2(\text{ethyl}[3\text{-(pyridin-2-yl)-1H-pyrazol-1-yl]acetate)_2]$.^[149] Contrasting with this, the in situ formation of active monobisperoxido species from the reaction of monomeric oxomolybdenum complexes with TBHP has been reported in a handful of cases. Based on those reported studies, it may be postulated that the conversion of the previous two polymers into the oxodiperoxido complexes $[\text{MoO}(\text{O}_2)_2(\text{pzpy})]$ and $[\text{MoO}(\text{O}_2)_2(\text{pent-pp})]$ involved the transformation of $\text{Mo}=\text{O}$ groups by reaction with TBHP to give $\text{Mo}(\text{O}_2)$ groups and *tert*-butanol as co-product.

A pertinent question concerns which material possesses the best catalytic performance when tested in olefin epoxidation at 55 °C. Because at least two of the prepared compounds were used in the same catalytic reaction conditions (*i.e.*, for the same temperature, substrate and oxidant), one can answer the question by making a careful comparison between all collected data described in the previous paragraphs.

For the epoxidation of *cis*-cyclooctene into 1,2-epoxycyclooctane the compound that stands out as the most active when no co-solvent was used is the dinuclear complex $[\text{Mo}_2\text{O}_6(\text{di-}t\text{-Bu-bipy})_2]$. When *n*-hexane or BTF are used as co-solvent the polymeric compound $(\text{DMA})[\text{MoO}_3(\text{HbpdC})] \cdot n\text{H}_2\text{O}$ is more effective than $\{[\text{MoO}_3(\text{bipy})][\text{MoO}_3(\text{H}_2\text{O})]\}_n$. On the other hand, for the epoxidation of DL-limonene into 1,2-epoxy-*p*-menth-8-ene, the octanuclear compound $[\text{Mo}_8\text{O}_{22}(\text{OH})_4(\text{di-}t\text{-Bu-bipy})_4]$ is superior to $(\text{DMA})[\text{MoO}_3(\text{HbpdC})] \cdot n\text{H}_2\text{O}$, at least when using DCE or BFT as the co-solvents. For the epoxidation of methyl oleate good results were achieved by employing $[\text{Mo}_8\text{O}_{22}(\text{OH})_4(\text{di-}t\text{-Bu-bipy})_4]$.

CHAPTER LAYOUT

This chapter compiles all the information about the materials (precursors and solvents) and methods used to prepare the new oxomolybdenum(VI) hybrid materials described in chapters 1 to 6. Technical specifications of all the used instrumentation and detailed technical procedures employed in the characterization steps are also described. Sections from E.1 to E.4 gather all the experimental procedures and characterization data of the final materials. For convenience, this section is properly divided according to each chapter. Section E.5 is solely dedicated to the catalytic studies performed in the present thesis and summarizes all procedures and technical details employed.

E.1. METHODS

Figure E.1 depicts the four heating instrumentation facilities used and mentioned in this present thesis along the various chapters (and also in the introduction).

For the hydrothermal synthetic approach a Teflon-lined stainless steel autoclave (*top left*) was charged with the reactants, then transferred to an oven where static or dynamic conditions (*i.e.*, the Teflon-lined stainless steel autoclave was rotated at a certain rate given in revolutions per minute, rpm) were employed.

Microwave-assisted syntheses were carried out in a Discover S-Class (CEM Corporation, USA) microwave oven (*bottom left*) using a glass vessel with typically a capacity of 35 mL. A dynamic method was used in which the microwave power was automatically controlled on the basis of the temperature feedback measured using a vertically focused IR sensor.

When employing reflux synthesis approaches standard laboratory glass ware was typically used. For some less common reactions a Schlenk tube was immersed in a heated oil bath (see *bottom right* picture).

Hydrothermal Synthesis

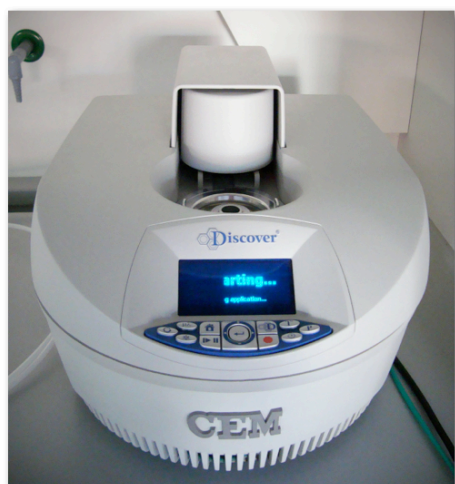
Static Conditions



Dynamic Conditions



Microwave-assisted synthesis



Reflux synthesis



Figure E.1. Pictures of the heating instrumental facilities used to prepare the products described in this thesis.

E.2. MATERIALS

	Compound name or formula	Supplier	Ref.
Mo^{VI} precursors			
Purchased from standard chemical suppliers and used as received without any further purification	MoO ₃ (99.5 %, vacuum dried)	AnalaR	–
	MoO ₂ Cl ₂	Sigma-Aldrich	–
Prepared according to literature procedures	[MoO ₂ Cl ₂ (bipy)] (1.1)	–	[83]
	[MoO ₂ Cl ₂ (di- <i>t</i> -Bu-bipy)] (2.1)	–	[114]
	[MoO ₂ Cl ₂ (pzpy)] (4.1)	–	[81]
	[MoO ₂ Cl ₂ (pent-pp)] (5.1)	–	[81]
Organic ligands			
Purchased from commercial sources and used as received	bipy	Sigma-Aldrich	–
	di- <i>t</i> -Bu-bipy	Sigma-Aldrich	–
	H ₂ bpdc	Sigma-Aldrich	–
Prepared according to literature procedures	pzpy	–	[210]
	pent-pp	–	[204]
Solvents			
Purchased from commercial sources and used as received	Diethyl ether *	Sigma-Aldrich	–
	Acetone *	Fluka	–
	Toluene *	Riedel-de-Haën	–
	Dichloromethane *	Fluka	–
	<i>n</i> -Hexane *	Sigma-Aldrich	–
	<i>n</i> -Hexane (anhydrous 95 %)	Sigma-Aldrich	–
	Dimethylformamide *	Sigma-Aldrich	–
	Tetrahydrofuran *	Scharlau	–
	Pentane (99 %)	Sigma-Aldrich	–
	Ultra-pure deionized water	–	–
Other reagents			
	NaH (60 % oil dispersion)	Sigma-Aldrich	–
	1-Iodopentane (98 %)	Sigma-Aldrich	–

* puris, p.a.

E.3. CHARACTERIZATION TECHNIQUES

In general, all reagents, intermediate and final products were characterized using the instruments described below. In exceptional cases for which the instrumentation was different, a brief description will be an adjunct to the characterization data.

- **ELEMENTAL ANALYSIS** (C, H, N) was performed at the Chemistry Department, University of Aveiro on an LECO CHNS - 932 equipment. Samples were combusted at 1000 °C for 3 min with helium used as the purge gas.
- **ATOMIC ABSORPTION SPECTROSCOPY** (AAS) was performed at Instituto Superior Técnico.
- **FOURIER TRANSFORM – INFRARED** (FT-IR) spectra were recorded as KBr pellets (Sigma-Aldrich 99%, FT-IR grade) using a Unicam Mattson Mod 7000 spectrophotometer equipped with a DTGS CsI detector.
- **ATTENUATED TOTAL REFLECTANCE FT-IR** (ATR) spectra were measured on the same instrument equipped with a Specac Golden Gate Mk II ATR accessory having a diamond top-plate and KRS-5 focusing lenses.
- **FT-RAMAN** spectra were recorded on a RFS-100 Bruker FT-Spectrometer, equipped with a Nd:YAG laser with an excitation wavelength of 1064 nm.
- **THERMOGRAVIMETRIC ANALYSIS** (TGA) were carried out using a Shimadzu TGA 50, from ambient temperature to *ca.* 800 °C, with a heating rate of 5 °C/min under a continuous stream of air at a flow rate of 20 mL/min.
- **¹H and ¹³C SOLUTION NMR** spectra were recorded on a Bruker CXP 300 (UltraShield™ Magnet) spectrometer at 300.13 and 75.47 MHz at ambient temperature. Chemical shifts are quoted in parts per million (ppm) with respect to TMS.
- **SOLID STATE ¹³C CROSS-POLARIZATION MAGIC-ANGLE-SPINNING**, *i.e.*, ¹³C{¹H} CP MAS NMR spectra were recorded using a Bruker Avance 500 (narrow bore) spectrometer with an ultrashielded static magnetic field at 125.76 MHz, and/or using a Bruker Avance 400 spectrometer (9.4 T, wide bore) at 100.62 MHz. Chemical shifts are quoted in parts per million (ppm) with respect to TMS.
- **SCANNING ELECTRON MICROSCOPY** (SEM) images and energy dispersive X-ray spectroscopy (EDS) data were collected using a Hitachi S4100 scanning electron microscope operating at 25 kV. Samples were prepared

scanning electron microscope operating at 25 kV. Samples were prepared by deposition on aluminium sample holders followed by carbon coating using an Emitech K 950 carbon evaporator.

- **POWDER X-RAY DIFFRACTION** (PXRD) Routine data were collected on an X'Pert MPD Phillips diffractometer (Cu $K\alpha$ X-radiation, $\lambda = 1.54060 \text{ \AA}$) fitted with a curved graphite monochromator and a plate sample holder, in a Bragg-Brentano para-focusing optics configuration (40 kV, 50 mA). Samples were step-scanned in the range from 3.5 to $70^\circ 2\theta$ steps with a counting time of 25 s per step.

- **HIGH-RESOLUTION SYNCHROTRON POWDER X-RAY DIFFRACTION** (PXRD) data suitable for crystal solution were collected at 100 K on either the powder diffractometer assembled at the ID31 beam line of the European Synchrotron Radiation Facility (ESRF), Grenoble, France, or at I11 belonging to the Diamond Light Source, Oxford, United Kingdom.

- **SINGLE CRYSTAL X-RAY DIFFRACTION** Suitable single crystals were mounted on Hampton Research CryoLoops using FOMBLIN Y perfluoropolyether vacuum oil (LVAC 140/13). Data were collected on a Bruker X8 Kappa APEX II CCD area-detector diffractometer (Mo $K\alpha$ graphite-monochromated radiation, $\lambda = 0.71073 \text{ \AA}$) controlled by the APEX2 software package,^[211] and equipped with an Oxford Cryosystems Series 700 cryostream monitored remotely using Cryopad.^[212] Images were processed using SAINT+,^[213] and data were corrected for absorption by the multi-scan semi-empirical method implemented in SADABS.^[214]

E.4. EXPERIMENTAL PROCEDURES and CHARACTERIZATION

E.4.1. CHAPTER 1

E.4.1.1. Synthesis of $\{[\text{MoO}_3(\text{bipy})][\text{MoO}_3(\text{H}_2\text{O})]\}_n$ (1.2)

The complex $[\text{MoO}_2\text{Cl}_2(\text{bipy})]$ (1.1) was prepared by following a published procedure.^[83] Three different heating methods were used to prepare the polymeric compound $\{[\text{MoO}_3(\text{bipy})][\text{MoO}_3(\text{H}_2\text{O})]\}_n$ (1.2):

Method A – For the hydrothermal method, a Teflon-lined stainless steel autoclave was charged with $[\text{MoO}_2\text{Cl}_2(\text{bipy})]$ (1.1) (1.67 g, 4.70 mmol) and water (50 mL) and heated for 19 h at 100°C inside an oven.

Method B – For the reflux method, a mixture of 1.1 (0.22 g, 0.62 mmol) and water (30 mL) in a round-bottomed flask was refluxed in air (at atmospheric pressure) for 12 h, using a thermostatted oil bath for heating.

Method C – The microwave-assisted syntheses were carried out using 150 W power and 120 °C during 4 hours. The power was automatically controlled based on the temperature feedback that was measured using a vertical focused IR sensor. For this method, a mixture of [MoO₂Cl₂(bipy)] (**1.1**) (0.85 g, 2.39 mmol) and water (25 mL) was placed inside the sealed glass reactors of the equipment and heated at 120 °C for 4 h.

At the end of each reaction (for all three methods) a white solid suspended in a pale pink solution (pH = 2-3) was always obtained. After cooling to ambient temperature, the solid was recovered by centrifugation, washed with water, acetone, and diethyl ether, and then dried at 100 °C.

Yields (based on Mo):

Method A	Hydrothermal synthesis	(0.78 g) 72%
Method B	Reflux synthesis	(0.13 g) 91%
Method C	Microwave-assisted syntheses	(0.51 g) 92%

Anal. Calcd for C₁₀H₁₀Mo₂N₂O₇ (MW = 462.08 g mol⁻¹) (in %): C, 25.99; H, 2.18; N, 6.06. Found: C, 25.85; H, 2.32; N, 6.04. No Cl was detected by EDS.

Selected FT-IR data (KBr pellets, in cm⁻¹): ν = 3224m (ν (OH)), 3121w, 3086w, 1679m (δ (H₂O)), 1608m, 1600m, 1575w, 1565w, 1496m, 1475m, 1444m, 1315m, 1248w, 1179w, 1159w, 1028m, 1017m, 955s (ν (O=Mo)), 930s (ν (O=Mo)), 916s (ν (O=Mo)), 868s (ν (O=Mo)), 757s, 682s,br (ν (Mo-O-Mo)), 654m, 636sh, 514s,br (ν (OMo₃)), 439w, 415w, 400m, 368w, 317w.

High-resolution synchrotron powder X-ray diffraction data collection: ID31 beam line at the ESRF; wavelength 0.29509(2) Å; temperature 100 K; geometry Debye-Scherrer (capillary); reflections collected in the range 0.519° ≤ 2θ ≤ 20.001°; step size 0.003°.

Unit cell: formula C₁₀H₁₀Mo₂N₂O₇; FW 462.08; crystal system monoclinic; space group *P*2₁/*n*; *a* = 17.32533(14) Å, *b* = 19.80459(16) Å, *c* = 3.75890(3) Å, β = 95.5824(12)°, *V* = 1283.642(18) Å³, *Z* = 4, *D*_c = 2.391 g cm⁻³.

Refinement details: 2257 independent reflections, 1 global refined parameter, 20 profile parameters, 27 intensity-dependent refined parameters.

Reliability factors for data points with Bragg contribution *R*_p = 7.11%, *R*_{wp} = 9.53%, *R*_{exp} = 2.21%, χ^2 = 19.25%. Structure Reliability factors *R*_{Bragg} = 12.0%, *R*_F = 15.8%.

E.4.2. CHAPTER 2

E.4.2.1. Synthesis of $[\text{Mo}_8\text{O}_{22}(\text{OH})_4(\text{di-}t\text{-Bu-bipy})_4]$ (2.2)

Four different heating methods were used to prepare the octanuclear Mo^{6+} complex $[\text{Mo}_8\text{O}_{22}(\text{OH})_4(\text{di-}t\text{-Bu-bipy})_4]$ (2.2):

Method A – A mixture of $[\text{MoO}_2\text{Cl}_2(\text{di-}t\text{-Bu-bipy})]$ (2.1) (0.25 g, 0.53 mmol) and water (25 mL) was stirred and heated to 120 °C inside a microwave oven and maintained at this temperature for 4.5 h. The resultant white solid was separated from the pink aqueous mother liquor ($\text{pH} \cong 2$) by filtration, washed with water, acetone/diethyl ether (1:1), and diethyl ether (10 mL each), and finally vacuum-dried.

Method B – A Schlenk tube was charged with 2.1 (0.97 g, 2.08 mmol) and water (60 mL), and the mixture was refluxed for 18 h under air (at atmospheric pressure) using a thermostatted oil bath as heating source. The resultant white solid was separated from the pink aqueous mother liquor ($\text{pH} \cong 2$) by filtration, washed with water, *n*-hexane, and diethyl ether (10 mL each) and finally vacuum-dried. The compound was identified as $[\text{Mo}_8\text{O}_{22}(\text{OH})_4(\text{di-}t\text{-Bu-bipy})_4]$ (2.2) by elemental analysis, FT-IR spectroscopy and powder X-ray diffraction.

Method C – A Teflon-lined stainless steel autoclave was charged with $[\text{MoO}_2\text{Cl}_2(\text{di-}t\text{-Bu-bipy})]$ (2.1). (0.16 g, 0.34 mmol) and water (10 mL) and heated in an oven at 100 °C for 19 h. The resultant white solid was separated from the pink aqueous mother liquor ($\text{pH} \cong 2$) by filtration, washed with water, *n*-hexane, and diethyl ether (10 mL each) and finally vacuum-dried. The compound was identified as $[\text{Mo}_8\text{O}_{22}(\text{OH})_4(\text{di-}t\text{-Bu-bipy})_4]$ (2.2) by elemental analysis, FT-IR spectroscopy and powder X-ray diffraction.

Method D – A Teflon-lined stainless steel autoclave was charged with MoO_3 (0.34 g, 2.4 mmol), *di-}t\text{-Bu-bipy} (0.64 g, 2.4 mmol), and water (25 mL) and heated in an oven at 160 °C for 3 d with constant rotation at 25 rpm. From this method a light pink solid and small single-crystals were obtained alongside with a colourless solution ($\text{pH} \cong 5$). Crystals were directly harvested from the reaction vessel and immediately immersed in highly viscous FOMBLIN Y perfluoropolyether vacuum oil (LVAC140/13) for the performed X-ray diffraction analysis. The remaining solid material was isolated by filtration, washed with water, *n*-hexane, and diethyl ether (10 mL each) and vacuum-dried. This isolated solid was identified as $[\text{Mo}_8\text{O}_{22}(\text{OH})_4(\text{di-}t\text{-Bu-bipy})_4]$ (2.2) by FT-IR spectroscopy and powder X-ray diffraction.*

Yields (based on Mo):

Method A	Microwave-assisted synthesis	(0.092 g) 61%
Method B	Open reflux synthesis	(0.420 g) 72%
Method C	Hydrothermal synthesis	(0.065 g) 68%
Method D	Dynamic hydrothermal synthesis	(0.470 g) 70%

The formation of complex $[\text{Mo}_8\text{O}_{22}(\text{OH})_4(\text{di-}t\text{-Bu-bipy})_4]$ (**2.2**) was independent of the heating method or the precursor employed. This was confirmed by FT-IR (Figure E.2) and powder X-ray diffraction studies (Figure 2.10, chapter 2). To avoid duplication of information only the characterization data belonging to the product originating from method C is presented.

Anal. Calcd for $\text{C}_{72}\text{H}_{100}\text{Mo}_8\text{N}_8\text{O}_{26}$ (MW = 2261.12 g mol⁻¹) (in %): C, 38.24; H, 4.45; N, 4.95. Found: C, 37.80; H, 4.31; N, 4.94.

Selected FT-IR data (KBr pellets, in cm⁻¹): $\nu = 3262\text{m}$ ($\nu(\text{OH})$), 2967s, 2936sh, 2906m, 2870m, 1732w (aromatic rings), [1615vs, 1548m, 1410vs (bipy C=C and C=N str)], 1369m, 1308w, 1290w, 1254m, 1210w, 1158vw, 1124w, 1080w, 1032m, 1022m, 992w, [935vs, 923s, 914vs, 899vs, 882vs, 865vs $\nu(\text{Mo}=\text{O})$], 850vs (ligand mode), [829vs, 777vs, 751s, 719s, 640vs,br $\nu(\text{Mo}-\text{O}-\text{Mo})$ and $\nu(\text{OMo}_3)$], 608s, 550m, 521m, 447w, 433w, 410w, 377m, 367m, 340m.

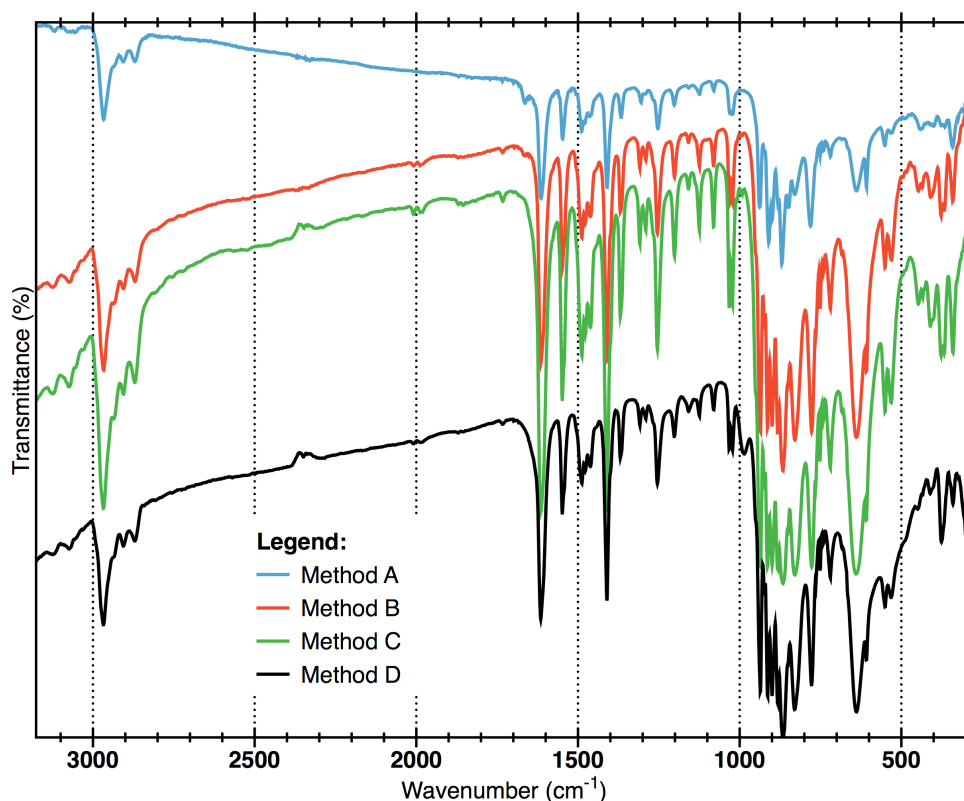


Figure E.2. FT-IR spectra of $[\text{Mo}_8\text{O}_{22}(\text{OH})_4(\text{di-}t\text{-Bu-bipy})_4]$ (**2.2**) prepared using methods A to D.

Selected FT-Raman data (in cm^{-1}): $\nu = 3072\text{m}, 2972\text{s}, 2929\text{m}, 2905\text{m}, 1608\text{s}, 1541\text{vs}, 1415\text{s}, 1318\text{vs}, 957\text{s}, 934\text{vs}, 922\text{vs}, 900\text{s}, 863\text{s}, 827\text{m}, 802\text{m}, 781\text{m}, 718\text{s}$.

^1H NMR (400.13 MHz, CD_3CN , 25 °C, ppm): $\delta = 8.56$ (d, bipy), 8.44 (s, bipy), 7.43 (d, bipy), 1.37 (s, $\text{C}(\text{CH}_3)_3$).

Solid-state $^{13}\text{C}\{^1\text{H}\}$ CP MAS NMR (ppm): $\delta = 31.0, 31.6$ ($(\text{CH}_3)_3\text{C}$, $(\text{CH}_3)_3\text{C}'$), 34.9, 36.0 ($(\text{CH}_3)_3\text{C}$, $(\text{CH}_3)_3\text{C}'$), 117.3–120.0, 126.3, 150.1, 151.1, 151.9, 153.4, 162.7, 163.9, 167.3 (C(2,2')-C(6,6')). Spectra were obtained using a Bruker Avance 400 spectrometer (9.4 T) at 100.62 MHz, with 3.6 μs ^1H 90° pulses, 2 ms contact time, spinning rates of 7 and 11 kHz, and 5 s recycle delays.

Crystal and structure refinement data: formula $\text{C}_{72}\text{H}_{100}\text{Mo}_8\text{N}_8\text{O}_{26}$, fw = 2261.12 g mol^{-1} , crystal system triclinic, space group $P\bar{1}$, $a = 12.90(2)$ Å, $b = 13.111(18)$ Å, $c = 13.46(2)$ Å, $\alpha = 65.98(4)^\circ$, $\beta = 85.61(5)^\circ$, $\gamma = 84.521(5)^\circ$, $V = 2068(5)$ Å³, $Z = 1$, $D_{\text{calcd}} = 1.815$ g cm^{-3} , $\mu(\text{Mo K}\alpha) = 1.252$ mm^{-1} , crystal size 0.01 × 0.01 × 0.01 mm, colourless block, reflections were collected in the range $3.52^\circ \leq \theta \leq 25.35^\circ$, 21721 collected reflections of which 7211 were independent with $R_{\text{int}} = 0.3014$. Completeness to $\theta = 25.35^\circ$ of 95.2%. Final R indices [$I > 2\sigma(I)$]: $R1 = 0.0995$, $wR2 = 0.2051$. Final R indices (all data): $R1 = 0.3317$, $wR2 = 0.3114$.

E.4.2.2. SECONDARY PRODUCT $[\text{Mo}_2\text{O}_6(\text{di-}t\text{-Bu-bipy})_2]$ (2.3)

The filtered off aqueous mother liquor from the synthesis of $[\text{Mo}_8\text{O}_{22}(\text{OH})_4(\text{di-}t\text{-Bu-bipy})_4]$ (2.2) (previous method D) was allowed to slowly evaporate at ambient temperature. Single crystals of $[\text{Mo}_2\text{O}_6(\text{di-}t\text{Bu-bipy})]$ (2.3) were isolated. The complex 2.3 was reproducibly obtained as a microcrystalline powder in approximately 5% yield by evaporating the colourless solution to dryness, and washing the resultant solid with diethyl ether. The powder X-ray diffraction pattern of the solid matches with a simulated pattern calculated from the single-crystal X-ray structural model of 2.3.

Anal. Calcd for $\text{C}_{36}\text{H}_{48}\text{Mo}_2\text{N}_4\text{O}_6$ (MW = 824.67 g mol^{-1}) (in %): C, 52.43; H, 5.87; N, 6.79. Found: C, 52.59; H, 6.0; N, 6.75.

Selected FT-IR (cm^{-1}) $\nu = 3429\text{m}, 3295\text{w}, 3118\text{w}, 3055\text{w}, 2959\text{m}, 2903\text{w}, 2870\text{w}, 1662\text{m}, 1611\text{m}, 1548\text{m}, 1488\text{m}, 1479\text{m}, 1461\text{w}, 1406\text{m}, 1365\text{w}, 1305\text{w}, 1253\text{m}, 1202\text{w}, 1155\text{w}, 1123\text{w}, 1100\text{w}, 1079\text{w}, 1027\text{m}, 1019\text{m}, 934\text{sh}, \text{w}, 907\text{s}, 895\text{s}, 866\text{vs}, 844\text{vs}, 777\text{vs}, 720\text{sh}, 681\text{m}, 609\text{m}, 606\text{s}, 551\text{s}, 487\text{m}, 434\text{vs}, 398\text{s}, 360\text{s}, 351\text{s}, 338\text{s}, 306\text{w}$.

^1H NMR (300.13 MHz, D_2O , 25 °C, TMS): δ = 8.98 (d, 2H, H6/H6'), 8.31 (s, 2H, H3/H3'), 7.77 (d, 2H, H5/H5'), 1.35 (s, $\text{C}(\text{CH}_3)_3$) ppm.

Crystal and structure refinement data: formula $\text{C}_{36}\text{H}_{52}\text{Mo}_2\text{N}_4\text{O}_8$, MW = 860.70 $\text{g}\cdot\text{mol}^{-1}$, crystal system monoclinic, space group $P2_1/n$, $a = 13.0953(15)$ Å, $b = 15.8301(17)$ Å, $c = 18.6972(18)$ Å, $\beta = 100.402(3)^\circ$, $V = 3812.2(7)$ Å³, $Z = 4$, $D_{\text{calcd}} = 1500$ $\text{g}\cdot\text{cm}^{-3}$, $\mu(\text{Mo K}\alpha) = 0.712$ mm^{-1} , crystal size $0.08 \times 0.08 \times 0.06$ mm, colourless block, reflections were collected in the range $3.52^\circ \leq \theta \leq 25.35^\circ$, 37892 collected reflections of which 6708 were independent with $R_{\text{int}} = 0.1282$. Completeness to $\theta = 25.35^\circ$ of 96.1%. Final R indices [$I > 2\sigma(I)$]: $R1 = 0.0700$, $wR2 = 0.1104$. Final R indices (all data): $R1 = 0.1301$, $wR2 = 0.1253$.

E.4.2.3. SECONDARY PRODUCT ($\text{H}_2\text{di-}t\text{-Bu-bipy}$) Cl_2

For methods A to C a crystalline powdered material could be isolated. Its crystal structure (Figure E.3) was determined using single-crystal X-ray diffraction on some sparsely distributed crystals, and formulated as ($\text{H}_2\text{di-}t\text{-Bu-bipy}$) Cl_2 , i.e., $[\text{C}_{18}\text{H}_{26}\text{N}_2]\text{Cl}_2$. The identification of this secondary product^[215] was important during the optimization of the work. A brief characterization is presented in the following paragraphs, which includes FT-IR spectroscopy, solid-state NMR and a detailed structural description based on the performed single-crystal X-ray diffraction studies.

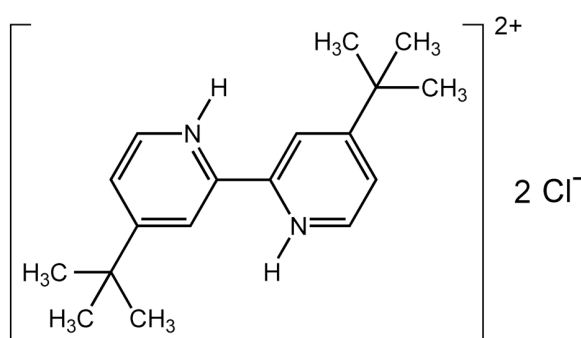


Figure E.3. Chemical diagram of ($\text{H}_2\text{di-}t\text{-Bu-bipy}$) Cl_2 .

E.4.2.3.1. FT-IR and PXRD

FT-IR spectroscopy was used to quickly assess the structural similarities between the isolated crystals and the powdered materials of the ($\text{H}_2\text{di-}t\text{-Bu-bipy}$) Cl_2 salt. As depicted in Figure E.4 there is a complete agreement between the two spectra that indicates that the two batches share the same molecular structure.

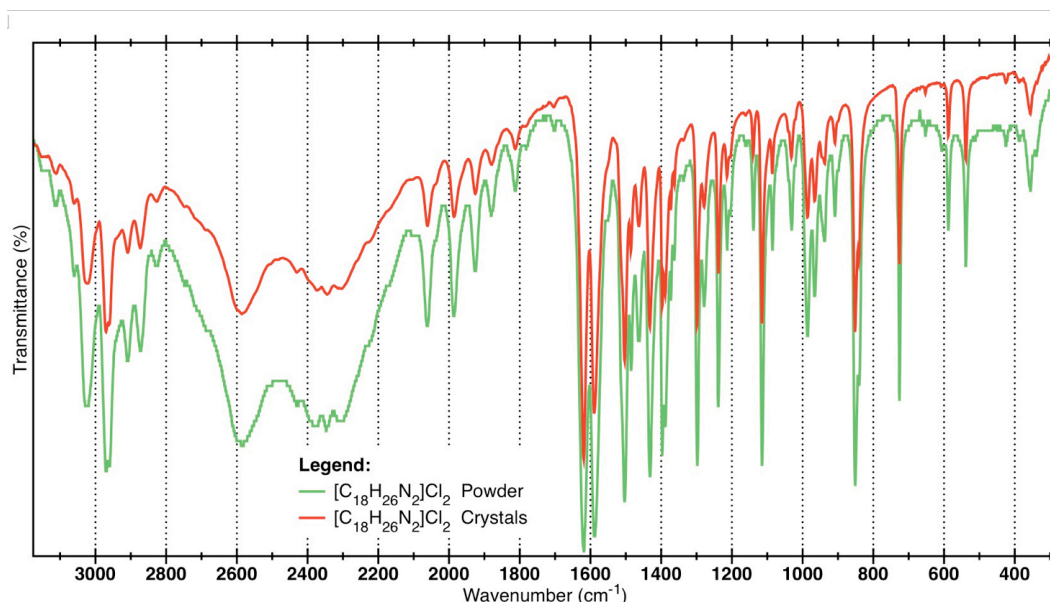


Figure E.4. FT-IR spectra of the isolated powder and of the crystals used to determinate the crystalline structure of the $(\text{H}_2\text{di-}t\text{-Bu-bipy})\text{Cl}_2$ salt.

The experimental powder X-ray diffraction pattern from the isolated microcrystalline powder agrees well with the calculated pattern based on the crystal structure of the $(\text{H}_2\text{di-}t\text{-Bu-bipy})\text{Cl}_2$ salt. (Figure E.5). Small deviations are observed in the range between *ca.* 23 and 27 ° 2 θ which can be explained by the different temperatures at which each acquisition was made (ambient temperatures *vs.* 150 K for the single-crystal X-ray diffraction).

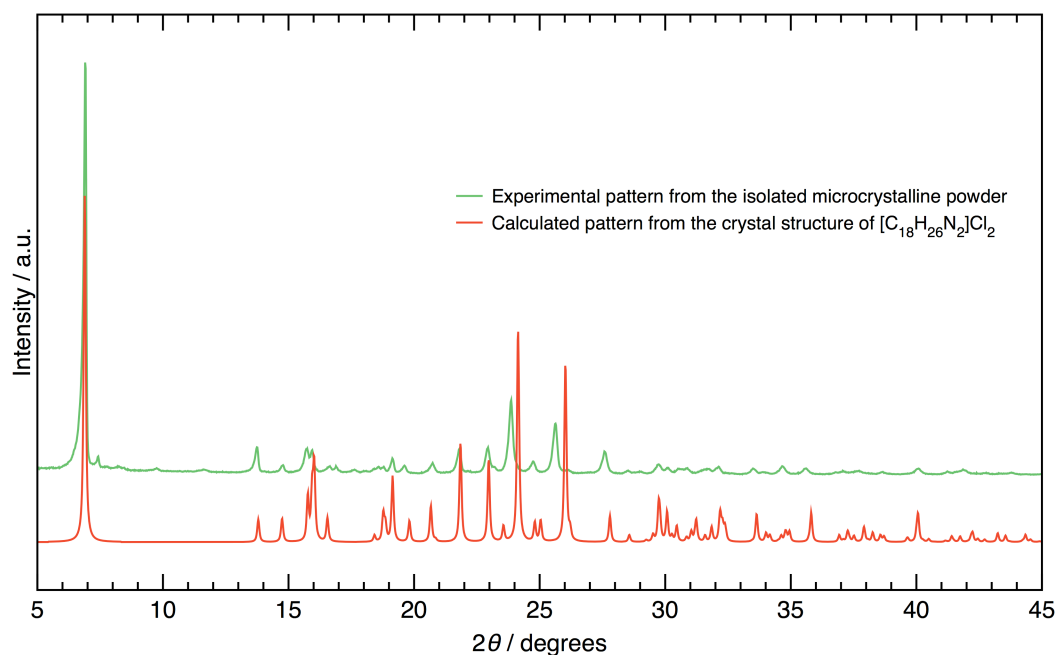


Figure E.5. Comparison between the experimental and simulated (based on single-crystal data) powder X-ray diffraction of $(\text{H}_2\text{di-}t\text{-Bu-bipy})\text{Cl}_2$. The simulation was performed using CCDC Mercury software while using a FWHM of 0.10 2 θ .

E.4.2.3.2. X-RAY STUDIES: STRUCTURAL DESCRIPTION

Unequivocal crystal structure determination of the $(\text{H}_2\text{di-}t\text{-Bu-bipy})\text{Cl}_2$ salt was achieved by using single-crystal X-ray diffraction on the few isolated crystals. A search in the CSD Version 5.32 (November 2010 with three updates)^{[37][36]} reveals that di-*t*-Bu-bipy forms relatively stable complexes with a large range of metallic cations, including lanthanides, actinides and, mainly, *d*-block cations. Surprisingly, not many crystallographic reports are known in which di-*t*-Bu-bipy is chelated to either *s*- or *p*-block cations: there is a single report in the literature of an organometallic complex with Na^+ by Li *et al.*^[81] and another with Sn^{4+} by Momeni *et al.*^{[36][37]} Concerning organic crystals, besides the crystal structure of di-*t*-Bu-bipy which was reported by Gonçalves and co-workers,^[216] there is a single crystallographic determination in which this molecule co-crystallizes with hexafluorobenzene.^[217] As a continuation of the ongoing interest in organic crystals based on pyridine derivatives of the research groups of Gonçalves and co-workers,^{[218][219]} the crystal structure of $(\text{H}_2\text{di-}t\text{-Bu-bipy})\text{Cl}_2$ salt was determined at 150 K, being an organic salt with chloride anions. A search in the literature reveals the existence of only one other salt of protonated di-*t*-Bu-bipy moieties, being reported by Herrman *et al.*^[220] and using perrhenate as the charge-balancing anion.

di-*t*-Bu-bipy is a versatile N,N' -chelating organic ligand by the inclusion of two bulky *t*-butyl substituent groups at the 4 and 4' positions. The asymmetric unit of the title compound is composed of half of a 4,4'-di-*tert*-butyl-2,2'-dipyridinium cation (the molecule has its geometrical centre located over an inversion center) and by a single chloride anion strongly hydrogen bonded to the neighbouring $\text{N}^+\text{-H}$ group as depicted in Figure E.6.

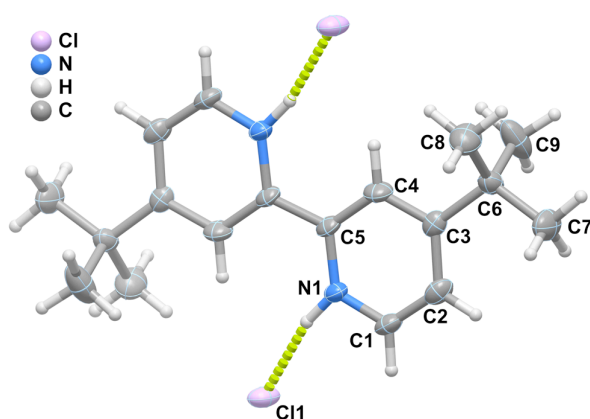


Figure E.6. Schematic representation of the molecular units composing the crystal structure of the $(\text{H}_2\text{di-}t\text{-Bu-bipy})\text{Cl}_2$ salt. Non-hydrogen atoms are represented as thermal ellipsoids drawn at the 70% probability level. Hydrogen atoms are depicted as small spheres with arbitrary radii. The atomic labeling for all non-hydrogen atoms composing the asymmetric unit is provided.

As a consequence, the 4,4'-di-*tert*-butyl-2,2'-dipyridinium cation adopts a typical *trans* conformation around the central C—C bond, very much similar to that observed in the crystal structure of the molecule itself^[221] and also by Batsanov *et al.*^[217] in the co-crystal with hexafluorobenzene. This conformation permits a significant reduction of the overall steric repulsion due to the large *tert*-butyl substituent groups. Additional weak C—H···Cl supramolecular contacts promote the formation of a one-dimensional supramolecular tape (Figure E.7G). The crystal structure can be described by the close packing of these supramolecular tapes (Figure E.8H).

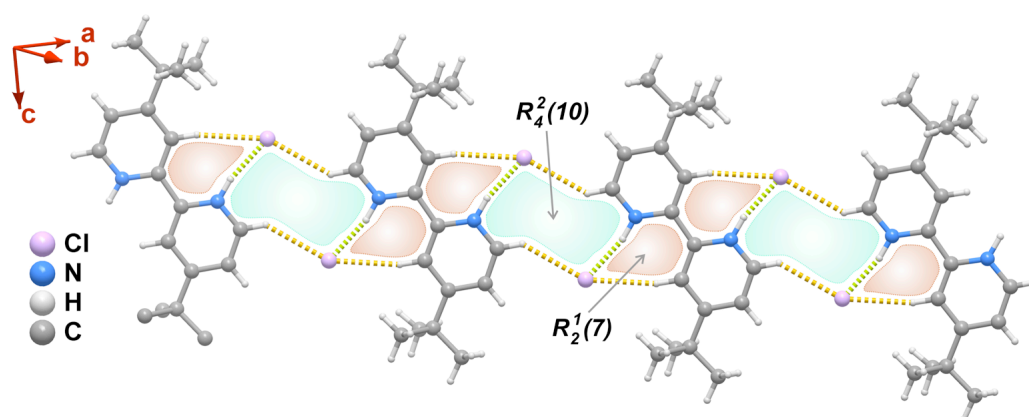


Figure E.7. Interconnection of adjacent chloride anions and protonated organic molecules via $N^+—H\cdots Cl^-$ and $C—H\cdots Cl^-$ contacts (green and brown dashed lines, respectively) leading to the formation of a one-dimensional supramolecular tape.

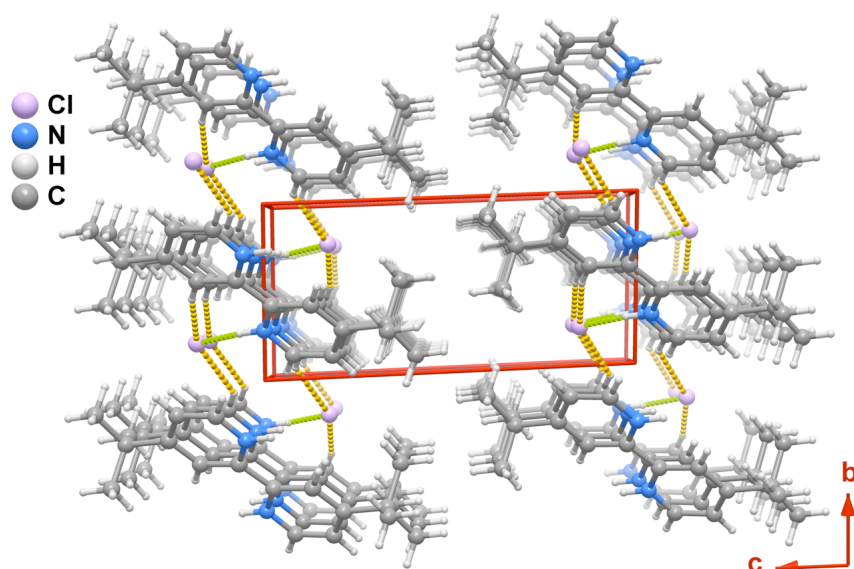


Figure E.8. Crystal packing of the title compound viewed in perspective along the [100] direction of the unit cell. $N^+—H\cdots Cl^-$ and $C—H\cdots Cl^-$ intermolecular interactions are represented as green and brown dashed lines, respectively.

Table E.1. Geometrical details (distances in Å and angles in degrees) of the hydrogen bonds present in (H₂di-*t*-Bu-bipy)Cl₂.

<i>D</i> –H⋯ <i>A</i>	<i>D</i> –H	H⋯ <i>A</i>	<i>D</i> ⋯ <i>A</i>	<i>D</i> –H ⋯ <i>A</i>
N1–H1⋯Cl1	0.95 (1)	2.05 (2)	2.967 (4)	162 (5)
C1–H1A⋯Cl1 ⁱ	0.95	2.70	3.479 (3)	140
C4–H4A⋯Cl1 ⁱⁱ	0.95	2.61	3.543 (9)	166

^a Symmetry transformations used to generate equivalent atoms: (i) $-x-1, -y, -z+2$; (ii) $-x, -y+1, -z+2$.

Crystal and structure refinement data: formula C₃₆H₅₂Mo₂N₄O₈, MW = 341.31 g·mol⁻¹, crystal system triclinic, space group $P\bar{1}$, $a = 5.9017(8)$ Å, temperature 150(2) K, $b = 6.1949(8)$ Å, $c = 13.0758(17)$ Å, $\alpha = 89.633(8)^\circ$, $\beta = 79.049(7)^\circ$, $\gamma = 75.915(7)^\circ$, $V = 454.884(10)$ Å³, $Z = 1$, $D_{\text{calcd}} = 1.246$ g·cm⁻³, $\mu(\text{Mo K}\alpha) = 0.356$ mm⁻¹, crystal size 0.12 × 0.03 × 0.03 mm, colourless block, reflections were collected in the range $3.63^\circ \leq \theta \leq 27.47^\circ$, 14551 collected reflections of which 2054 were independent with $R_{\text{int}} = 0.0742$. Completeness to $\theta = 27.47^\circ$ of 98.5%. Final R indices [$I > 2\sigma(I)$]: $R1 = 0.0827$, $wR2 = 0.1782$. Final R indices (all data): $R1 = 0.1059$, $wR2 = 0.1882$.

E.4.3. CHAPTER 3

E.4.3.1. SYNTHESIS of (DMA)[MoO₃(HbpdC)]·*n*H₂O (3.1)

A Teflon-lined stainless steel autoclave was charged with MoO₃ (88.5 mg, 0.61 mmol), 2,2'-bipyridine-5,5'-dicarboxylic acid (150.8 mg, 0.61 mmol) and the solvent mixture 19 : 6 of H₂O : DMF (25 mL). The autoclave was heated in an oven at 150 °C for 3 d and kept at a constant rotation of about 10 rpm. After cooling, the orange solution of pH = 6 was transfer to a Schlenk and left to rest for 4 d. A white solid gradually precipitated from the solution. The solid was isolated by filtration, washed with water (4 × 10 mL), diethyl ether (4 × 5 mL), and finally vacuum dried.

Yield: 160 mg, 56% (based on Mo).

Anal. Calcd for MoO₃(C₁₂H₇N₂O₄)(H₂N(CH₃)₂)(H₂O)_{1.7} (MW = 464.74 g mol⁻¹) (in %): C, 36.25; H, 4.00; N, 9.06. Found: C, 36.37; H, 3.71; N, 9.02.

Selected FT-IR (KBr pellets, cm⁻¹) ν = 3442s (O–H vibrational stretching of water), 3214m, 3106m, 3086m, 3040m, 2978w, 2787s (ν (N–H)), 2439w (O–H stretching vibrational modes of the carboxylic acid groups involved in hydrogen bonds), 1725s (ν (C=O)), 1648m, 1602s ($[\nu$ (C=C), ν (C=N)]_{py}), 1578m, 1565m, 1497w, 1470m, 1364s, 1293s, 1278s, 1261s, 1144s, 1130s, 1022s, 967s, 922vs ν (Mo–O), 901vs ν (Mo–O), 860s, 819vs, 770vs, 745m, 727s, 692s, 646ssh, 576vs,br, 448s, 411s, 350w, 324w.

Thermogravimetric analysis (TGA) data (weight losses in %): 25-100 °C –3.8%; 100-210 °C –2.8%; 210-470 °C –55.0%.

¹H MAS NMR (400.13 MHz, spinning rate 10 kHz, ppm): δ = 18.4 (–COOH), 8.2 (aromatic protons), 5.0, 3.7, 1.3.

¹³C{¹H} CP MAS NMR (100.62 MHz, ppm): δ = 169.0 and 168.0 (–COOH); 150.0, 148.5, 146.4, 142.4 (*ortho* and *para* carbon atoms of the aromatic rings); 139.4, 130.2, 124.3 (*meta* carbon atoms of the aromatic rings); 36.1 (–CH₃). Acquisition parameters: 3.7 μ s ¹H 90° pulse, 1.5 ms contact time, spinning rate of 11 kHz and 5 s recycle delay.

High-resolution synchrotron powder X-ray diffraction data collection: ID31 beam line at the ESRF; wavelength 0.39981(1) Å; temperature 100 K; geometry Debye-Scherrer (capillary); reflections collected in the range 1.012° ≤ 2 θ ≤ 30.000°; step size 0.001°.

Unit cell: formula C₁₄H₁₇MoN₃O₈; FW 451.25; crystal system monoclinic; space group *Pc*; a = 8.40330(4) Å, b = 13.69246(6) Å, c = 7.24076(2) Å, β = 100.5825(4)°, V = 818.965(6) Å³, Z = 2, D_c = 1.830 g cm⁻³.

Refinement details: 1904 independent reflections, 1 global refined parameter, 13 profile parameters, 123 intensity-dependent refined parameters.

Reliability factors for data points with Bragg contribution: $R_p = 8.86\%$, $R_{wp} = 12.6\%$, $R_{exp} = 4.98\%$, $\chi^2 = 6.42$. Structure Reliability factors $R_{Bragg} = 9.32\%$, $R_F = 11.3\%$.

E.4.4. CHAPTER 4

E.4.4.1. SYNTHESIS of $[\text{Mo}_3\text{O}_9(\text{pzpy})]_n$ (4.2)

The organic ligand 2-[3(5)-pyrazolyl]pyridine (pzpy) and the complex $[\text{MoO}_2\text{Cl}_2(\text{pzpy})]$ (4.1) were prepared following published procedures.^{[81][210]} Three different heating methods were employed to prepare the polymeric compound $[\text{Mo}_3\text{O}_9(\text{pzpy})]_n$ (4.2). A fourth method (typical static hydrothermal synthesis) was also tested but using instead MoO_3 as the Mo^{6+} metallic source to react with pzpy in the presence of H_2O .

Method A – A mixture of $[\text{MoO}_2\text{Cl}_2(\text{pzpy})]$ (4.1) (0.50 g, 1.45 mmol) and distilled water (20 mL) was refluxed in a Schlenk tube for 16 h under nitrogen. The resultant blue precipitate was separated from the colourless solution (pH 1-3) by filtration, washed with water (2×10 mL), acetone (2×10 mL) and diethyl ether (2×10 mL), vacuum-dried, and identified as 4.2.

Method B – A mixture of 4.1 (0.10 g, 0.29 mmol) and water (20 mL) was stirred and heated to 120 °C inside a microwave oven, and maintained at this temperature for 2 h. The resultant blue solid was separated from the colourless mother liquor (pH 1-3) by filtration, washed with water (2×10 mL), acetone (2×10 mL) and diethyl ether (2×10 mL), vacuum-dried, and identified as 4.2.

Method C – A Teflon-lined stainless steel autoclave was charged with 4.1 (0.24 g, 0.70 mmol) and water (15 mL), and heated in an oven at 100 °C for 19 h. The resultant blue solid was separated from the aqueous mother liquor by filtration, washed with acetone (6 mL), vacuum-dried, and identified as 4.2. The secondary product $(\text{pzpyH})_2(\text{MoCl}_4)$ was also isolated from this method (see section 4.2).

Method D – A Teflon-lined stainless steel autoclave with a total capacity of 25 mL was charged with MoO_3 (0.14 g, 0.97 mmol), the ligand pzpy (0.14 g, 0.97 mmol) and water (10 mL), and heated in an oven at 160 °C for 3 d. The resultant pale blue solid was separated from the pale yellow mother liquor by filtration, washed with diethyl ether (4×20 mL), and vacuum-dried.

At the end of each reaction (for all four employed methods) a blue solid was isolated and fully characterized in the solid state by elemental analysis, FT-IR spectroscopy and powder X-ray diffraction.

Yields (based on Mo):

Method A	Reflux synthesis	(0.22 g) 79%
Method B	Microwave-assisted synthesis	(0.04 g) 72%
Method C	Hydrothermal synthesis	(0.10 g) 74%
Method D	Hydrothermal synthesis using MoO_3	(0.054 g) 29%

Anal. Calcd for $C_8H_7Mo_3N_3O_9$ (MW = 576.98 g mol⁻¹) (in %): C, 16.65; H, 1.22; N, 7.28; Mo, 49.9. Found: C, 16.65; H, 1.23; N, 7.10; Mo, 51.8.

Selected FT-IR (KBr pellets, cm⁻¹): ν = 316w, 352m, 399m, 420w, 535vs, 672vs, 698s, 748s, 847vs, 911w, 930s, 935s, 941s, 967vs, 1021m, 1064m, 1096m, 1151m, 1219m, 1261m, 1295m, 1369m, 1385sh, 1433m, 1455m, 1472m, 1519m, 1570m, 1610s, 2827w, 2919sh, 2963w, 3025w, 3050vw, 3081sh, 3115vw, 3128m, 3142m.

Selected FT-Raman (cm⁻¹): ν = 159m, 184m, 193m, 214m, 231m, 245w, 271m, 288w, 298w, 316m, 343m, 384w, 394w, 611w, 667s, 698m, 711sh, 744vw, 848vs, 926m, 946m, 977m, 1021w, 1052w, 1097vw, 1149vw, 1313m, 1369w, 1455w, 1472w, 1518sh, 1539w, 1570w, 1607m, 3067m, 3074sh, 3092m, 3129m, 3142m.

¹H NMR (300.13 MHz, 25 °C, DMSO-*d*₆): δ = 13.05 (br, NH), 8.64 (d, 1H, H11), 8.1–7.8 (series of overlapping broad peaks and multiplets, 3H, H5,8,9), 7.37 (t, 1H, H10), 6.90 (d, 1H, H4) ppm (please see Figure 4.1, chapter 4).

¹³C{¹H} CP MAS NMR (125.76 MHz, ppm) δ = 99.7 (C4), 120.6 (C8), 125.6 (C10), 133.1 (C5/C9), 143.4 (C11), 145.8 (C3), 146.8 (C7) ppm. Acquisition parameters: 3.5 μ s ¹H 90° pulses, 1.5 ms contact time, spinning rate of 9 kHz and 5 s recycle delay.

Routine powder X-ray diffraction (PXRD) of 4.2 products is depicted in Figure E.9:

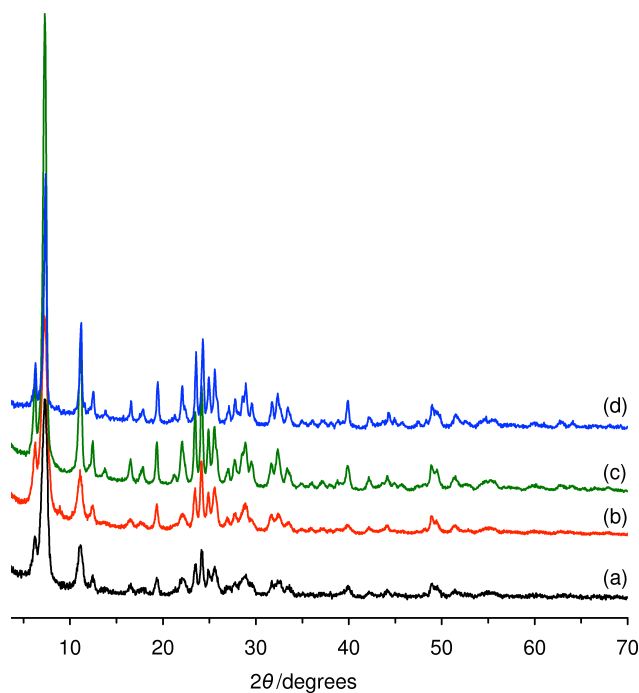


Figure E.9. PXRD patterns of $[Mo_3O_9(pzpy)]_n$ (4.2) prepared using methods: (a) A - reflux synthesis, (b) B - microwave-assisted synthesis, (c) C - hydrothermal synthesis and (d) D - hydrothermal synthesis using MoO_3 .

High-resolution synchrotron powder X-ray diffraction data collection: I11 beam line at the Diamond Light Source (Oxford, United Kingdom); wavelength 0.82661(1) Å; temperature 100 K; geometry Debye-Scherrer (capillary); reflections collected in the range $2.500^\circ \leq 2\theta \leq 50.000^\circ$; step size 0.002° .

Unit cell: formula $C_8H_7Mo_3N_3O_9$; FW 576.99; crystal system monoclinic; space group C2/m; $a = 30.2491(5)$ Å, $b = 3.72717(5)$ Å, $c = 12.8518(3)$ Å, $\beta = 110.1955(16)^\circ$, $V = 1359.88(5)$ Å³, $Z = 4$, $D_c = 2.818$ g cm⁻³.

Reliability factors for data points with Bragg contribution: $R_p = 14.60\%$, $R_{wp} = 16.22\%$, $R_{exp} = 4.01\%$, Goodness-of-fit = 4.05.

E.4.4.2. SECONDARY PRODUCT (pzpyH)₂(MoCl₄)

From method C employed for the synthesis of the polymeric $[Mo_3O_9(pzpy)]_n$ (4.2) material, concentration of the filtrate (autoclave mother liquor) under reduced pressure, followed by slow evaporation in open air led to the isolation of small crystals. This compound was identified by single-crystal X-ray diffraction as the salt $(pzpyH)_2(MoCl_4)$, where pzpyH stands for 2-[3(5)-pyrazolyl]pyridinium.

E.4.4.2.1. Insight into the formation of the salt

$(pzpyH)_2(MoCl_4)$ is a truly unique compound because it is based on a very rare anionic molybdenum-based tetrahedral anion in which the metal center is coordinated to four chloride ions: $MoCl_4^{2-}$. A search in the literature and in the Cambridge Structural Database (CSD, Version 5.34, November 2012 with three updates)^{[37][36]} supports this assumption: besides a very recent report by the groups of Yu and Tsai,^[222] in which this tetrahedral unit composes a large heterometallic complex (with lithium), only one other crystallographic report by Li *et al.* shows $MoCl_4^{2-}$ completely isolated in the crystal structure.^[223] Given the extensive chemistry of molybdenum, the isolation of this rare anion was attributed to the unique set of conditions used in the synthetic steps: i) first, the precursor complex 4.1 is rich in chloride anions which themselves are not included in the final compound 4.2, being solvated in the mother liquor; ii) second, the static hydrothermal synthetic conditions for a period of 19 hours permitted the slow hydrolysis of the precursor, which includes the release of the coordinated *N,N'*-chelated ligand (so as to form the inorganic backbone of polymer 4.2 – see Chapter 4); iii) third, this hydrolysis process was most certainly accompanied by decomposition of part of the pzpy ligand with the concomitant reduction of some Mo^{6+} metallic centers. The combination of these factors seems to be at the genesis of the rare $MoCl_4^{2-}$ species present in solution, which were ultimately precipitated as a salt with protonated pzpy molecules: $(pzpyH)_2(MoCl_4)$. The fact that $(pzpyH)_2(MoCl_4)$ was not isolated in methods A and B suggests that the formation of $MoCl_4^{2-}$ may require either (autogenous) pressure inside the reaction vessel or more time for the reduction of the metal

center from a +6 to +2 oxidation state to occur (*i.e.*, this chemical step is kinetically driven), or even a combination of both.

E.4.4.2.2. Structural description

The asymmetric unit of the salt $(\text{pzpyH})_2(\text{MoCl}_4)$ is composed of three distinct crystallographic units: two protonated 2-[3(5)-pyrazolyl]pyridinium molecules and a single MoCl_4^{2-} anion (Figure E.10). As mentioned above, the unique feature of this salt is the presence of the latter anionic moiety, which was only reported to date as an isolated species in the compound described by Li *et al.*^[223]

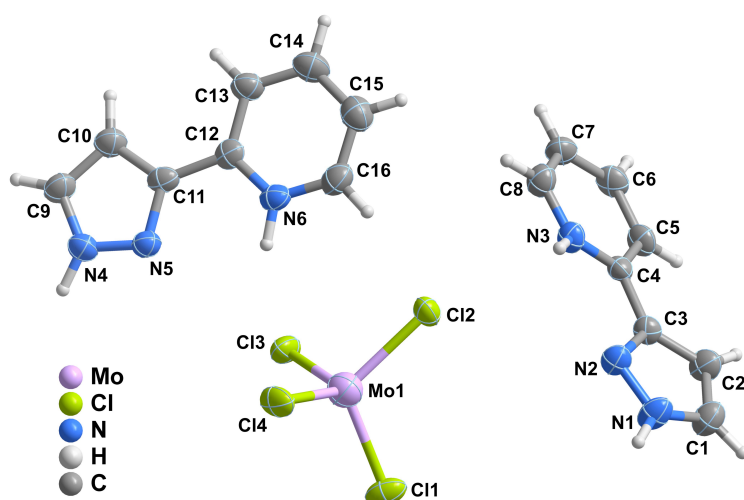


Figure E.10. Schematic representation of the three crystallographically independent molecular units composing the asymmetric unit of the salt $(\text{pzpyH})_2(\text{MoCl}_4)$. Non-hydrogen atoms are represented as thermal ellipsoids drawn at the 80% probability level. Hydrogen atoms are represented as small spheres with arbitrary radii.

The MoCl_4^{2-} anion exhibits a typical tetrahedral geometry with the Mo–Cl bond lengths ranging from 2.2671(13) to 2.3289(13) Å ($\Delta = 0.06$ Å), while the internal tetrahedral angles were found in the 102.45(5)–114.46(5)° ($\Delta = 12.01$ °) interval (see data collection information and Table E.2 for detailed geometrical data). Compared with the only known report of an identical moiety, the MoCl_4^{2-} anion in $(\text{pzpyH})_2(\text{MoCl}_4)$ is significantly more distorted. Indeed, in the compound reported by Li *et al.*^[223] the Mo–Cl bond lengths and the internal Cl–Mo–Cl tetrahedral angles were found in much narrower ranges: *ca.* 2.27–2.30 Å ($\Delta = 0.03$ Å) and 105.8–114.0° ($\Delta = 8.2$ °). The higher distortion of the anion in $(\text{pzpyH})_2(\text{MoCl}_4)$ is attributed to the existence of an extensive hydrogen bonding network (described in more detail below) involving the chloride anions, ultimately driving the Mo–Cl bonds to bend so as to maximize such interactions. Indeed, while in the presently discussed salt the cationic portion permits the

existence of strong hydrogen bonds, in the compound reported by Li *et al.* only weak C–H \cdots Cl interactions could occur, ultimately explaining why in this latter compound the geometrical data for the MoCl₄²⁻ anion approach the ideal values.

Table E.2. Bond distances (in Å) and angles (in degrees) for the crystallographically independent MoCl₄²⁻ anionic complex present in the (pzpyH)₂(MoCl₄) salt.

Mo1–Cl1	2.2671(13)	Cl1–Mo1–Cl2	112.52(5)
Mo1–Cl2	2.2741(13)	Cl1–Mo1–Cl3	107.06(5)
Mo1–Cl3	2.3289(13)	Cl2–Mo1–Cl3	102.45(5)
Mo1–Cl4	2.2632(13)	Cl4–Mo1–Cl1	108.84(5)
		Cl4–Mo1–Cl2	114.46(5)
		Cl4–Mo1–Cl3	111.16(5)

The two crystallographically independent 2-[3(5)-pyrazolyl]pyridinium cations (pzpyH⁺) (Figure E.10) show distinct geometrical features in the crystal structure of the salt. As shown in Figure E.11, the rotation angle between the average pyrazolyl and pyridinium rings is strikingly different: while for one moiety the subtended angle is only 2.8(3)°, which indicates that the rings are almost coplanar, in the other cation this angle increases significantly to 11.5(3)°. This remarkable difference between the two moieties is due to the existence of strong and highly directional hydrogen bonds between the protonated pyridine ring and a neighbouring MoCl₄²⁻ anion. As shown in Figure E.12, the (N3,C4,C5,C6,C7,C8) pyridinium ring is engaged in two supramolecular interactions with the anion, a strong (and charged) N⁺–H \cdots Cl⁻ interaction and a weak C–H \cdots Cl one. In order to maximize these supramolecular interactions the ring has to tilt from the average coplanarity with the corresponding pyrazolyl moiety of the molecule. On the other hand, due to the spatial distribution of the moieties in the crystal structure, the (N6,C12,C13,C14,C15,C16) pyridinium ring does not need to rotate around the C11–C12 bond so as to maximize the N6–H6 \cdots Cl3 hydrogen bond (see Figure E.12).

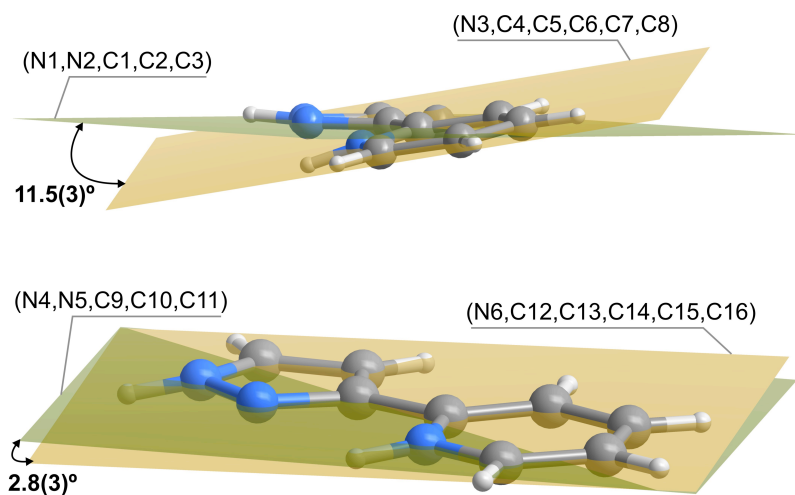


Figure E.11. Schematic representation of the two crystallographically independent 2-[3(5)-pyrazolyl]pyridinium cations (pzpyH^+) composing the crystal structure of the $(\text{pzpyH})_2(\text{MoCl}_4)$ salt. The pictograms emphasize the distinct mutual dihedral angles between the average pyrazolyl and pyridinium rings of each moiety, showing that in one residue there is a significant tilt in order to maximize supramolecular contacts with neighbouring MoCl_4^{2-} anions (see Figure E.12 for a representation of the supramolecular interactions).

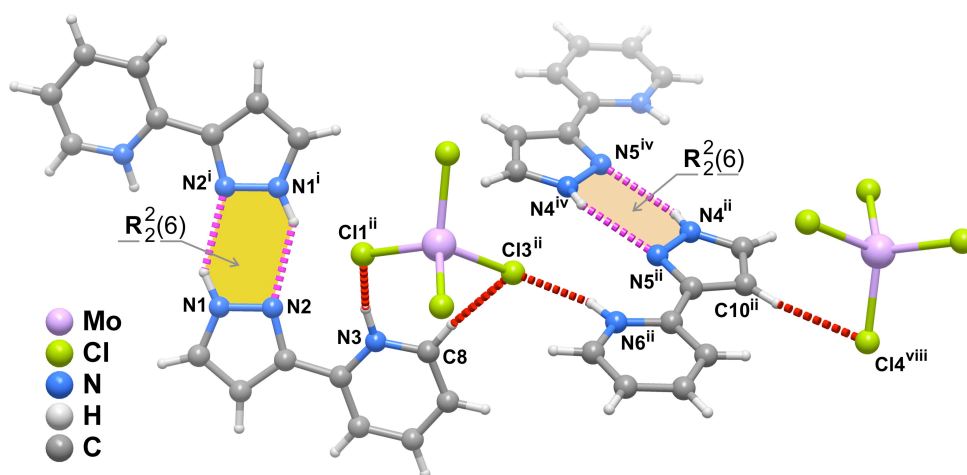


Figure E.12. Schematic representation of the most relevant (*i.e.*, stronger and directional) hydrogen bonds present in the crystal structure of $(\text{pzpyH})_2(\text{MoCl}_4)$: dashed red lines depict the $(\text{N,C})\text{-H}\cdots\text{Cl}$ interactions involving the MoCl_4^{2-} anion, and dashed purple lines depict $\text{N-H}\cdots\text{N}$ interactions connecting adjacent pzpyH^+ cations and forming $\mathbf{R}_2^2(6)$ graph set^[194] motifs. Table E.3 lists geometrical details associated with the represented hydrogen bonds. Symmetry transformations used to generate equivalent atoms: (i) $1-x, 2-y, 1-z$; (ii) $1+x, y, z$; (iv) $1-x, 1-y, -z$; (viii) $2-x, 1-y, -z$.

The most striking supramolecular feature of the pzpyH⁺ cations concerns the formation of centrosymmetric dimers (one per crystallographically independent moiety), by way of $\mathbf{R}^2_2(6)$ graph set motifs^[194] involving two adjacent pyrazolyl rings (Figure E.12). Even though this graph set is commonly found among compounds with this type of pyrazolyl rings (a search in the CSD reveals the existence of 72 compounds with this motif), the internuclear N \cdots N distances observed in (pzpyH)₂(MoCl₄) are longer: 3.013(6) and 3.054(6) Å. These distances contrast with the median value of *ca.* 2.90 Å from the database search (please note: only 7 structures in the CSD exhibit somewhat related internuclear distances longer than 3 Å).

Table E.3. Geometrical details (distances in Å and angles in degrees) of the hydrogen bonds and intermolecular close contacts present in (pzpyH)₂(MoCl₄).^{a,b}

D–H\cdotsA	<i>d</i>(D\cdotsA)	\angle(DHA)
N1–H1 \cdots N2 ⁱ	3.013(6)	142
N3–H3 \cdots Cl1 ⁱⁱ	3.150(4)	149
N4–H4 \cdots N5 ⁱⁱⁱ	3.054(6)	137
N6–H6 \cdots Cl3	3.062(4)	157
C8–H8 \cdots Cl3 ⁱⁱ	3.555(5)	157
C10–H10 \cdots Cl4 ^{iv}	3.589(6)	169

π-π Contacts	<i>Inter-centroid distance</i>
Cg1 \cdots Cg2 ^v	3.612(3)
Cg2 \cdots Cg2 ^{vi}	3.732(3)
Cg3 \cdots Cg4 ^{iv}	3.610(3)

Y–X\cdotsCg	<i>d</i>(X\cdotsCg)	\angle(YXCg)
Mo1–Cl4 \cdots Cg4 ^{vii}	3.893(3)	123

^a Symmetry transformations used to generate equivalent atoms:

- (i) 1-*x*, 2-*y*, 1-*z*; (ii) 1+*x*, *y*, *z*; (iii) -*x*, 1-*y*, -*z*; (iv) 1-*x*, 1-*y*, -*z*;
(v) 1-*x*, 1-*y*, 1-*z*; (vi) 2-*x*, 1-*y*, 1-*z*; (vii) *x*, 1+*y*, *z*.

^b Centres of gravity (Cg):

- Cg1 = N1, N2, C1, C2 and C3;
Cg2 = N3, C4, C5, C6, C7 and C8;
Cg3 = N4, N5, C9, C10 and C11;
Cg4 = N6, C12, C13, C14, C15 and C16.

As shown in Figure E.13, the crystal packing of this supramolecular salt is mostly dictated by the presence of the aforementioned hydrogen bonding interactions. Worth of note are also some weaker supramolecular contacts such as π - π and Y-X \cdots Cg interactions involving mainly the rings of the two crystallographically independent pzpyH⁺ cations. As can be discerned from Figure E.13, the various π - π contacts occur mainly along the [100] and [010] directions of the unit cell.

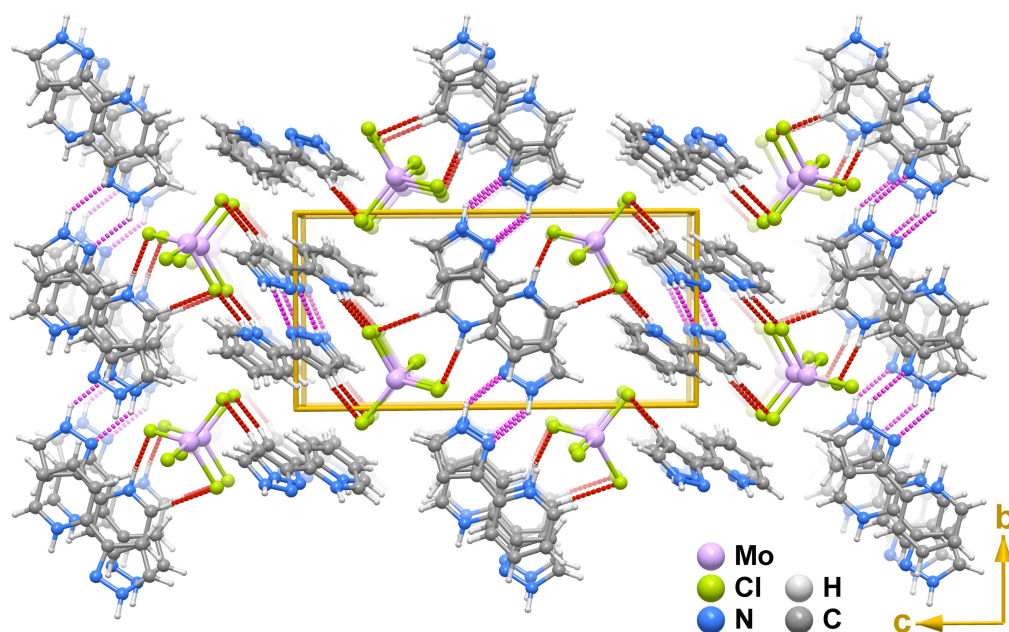


Figure E.11. Crystal packing of the salt (pzpyH)₂(MoCl₄) viewed in perspective along the [100] direction of the unit cell. Hydrogen bonding interactions connecting adjacent molecular units are represented as dashed lines: red for C-H \cdots Cl and N-H \cdots Cl; purple for N-H \cdots N interactions composing the $\mathbf{R}_2^2(6)$ graph set motifs.^[194]

E.4.4.2.3. Data collection information

Crystal and structure refinement data: formula C₁₆H₁₆Cl₄MoN₆, MW = 530.09 g mol⁻¹, crystal system triclinic, space group *Pi*, $a = 7.1856(3)$ Å, $b = 8.2553(3)$ Å, $c = 16.9444(6)$ Å, $\alpha = 89.786(2)^\circ$, $\beta = 83.593(2)^\circ$, $\gamma = 84.279(2)^\circ$, $V = 993.85(7)$ Å³, $Z = 2$, $D_{\text{calcd}} = 1.771$ g cm⁻³, $\mu(\text{Mo K}\alpha) = 1.212$ mm⁻¹, crystal size 0.12 × 0.05 × 0.03 mm, green block, reflections were collected in the range $3.54^\circ \leq \theta \leq 29.13^\circ$, 34574 collected reflections of which 5313 were independent with $R_{\text{int}} = 0.0485$. Completeness to $\theta = 29.13^\circ$ of 99.4%. Final *R* indices [$I > 2\sigma(I)$]: $R_1 = 0.0558$, $wR_2 = 0.1764$. Final *R* indices (all data): $R_1 = 0.0776$, $wR_2 = 0.1914$.

E.4.4.3. SECONDARY PRODUCT [Mo₄O₁₂(pzpy)₄] (4.3)

The secondary product [Mo₄O₁₂(pzpy)₄] (4.3) was only isolated when method D was employed for the preparation of the polymeric hybrid [Mo₃O₉(pzpy)_n] (4.2) material (*i.e.*, hydrothermal synthesis using the metallic precursor MoO₃ and the ligand pzpy). The pale yellow filtrate from method D was evaporated to dryness and the resultant solid washed with diethyl ether (4×20 mL), vacuum-dried, and identified as the tetranuclear compound [Mo₄O₁₂(pzpy)₄] (4.3) (0.05 g, 18%) by a comparison of the experimental powder X-ray diffraction pattern with a simulation based on the structural data reported by Li *et al.*^[48] FT-IR, NMR and elemental analysis data are also in good agreement with published results.^[49]

Selected FT-IR (KBr pellets, cm⁻¹): $\nu = 343\text{m}, 376\text{m}, 402\text{s}, 436\text{m}, 489\text{vw}, 645\text{m}, 692\text{w}, 710\text{w}, 778\text{s}, 798\text{sh}, 818\text{s}, 849\text{s}, 922\text{w}, 936\text{w}, 975\text{w}, 1024\text{w}, 1053\text{sh}, 1064\text{m}, 1093\text{m}, 1152\text{m}, 1230\text{m}, 1255\text{m}, 1296\text{m}, 1314\text{m}, 1372\text{s}, 1383\text{vs}, 1430\text{s}, 1438\text{s}, 1448\text{s}, 1473\text{m}, 1522\text{m}, 1568\text{m}, 1608\text{vs}, 3114\text{m}, 3139\text{m}.$

Selected Raman (cm⁻¹): $\nu = 137\text{vs}, 210\text{m}, 230\text{w}, 245\text{w}, 269\text{m}, 304\text{w}, 342\text{m}, 360\text{w}, 367\text{w}, 376\text{w}, 403\text{m}, 491\text{w}, 508\text{w}, 622\text{vw}, 643\text{m}, 696\text{w}, 709\text{m}, 794\text{sh}, 812\text{m}, 848\text{vs}, 900\text{s}, 908\text{sh}, 943\text{w}, 976\text{m}, 1022\text{m}, 1052\text{m}, 1063\text{sh}, 1088\text{w}, 1114\text{vw}, 1144\text{m}, 1255\text{w}, 1314\text{m}, 1370\text{m}, 1430\text{sh}, 1448\text{w}, 1473\text{m}, 1524\text{s}, 1567\text{s}, 1607\text{vs}, 3044\text{m}, 3060\text{m}, 3088\text{m}, 3114, 3137\text{m}.$

E.4.4.4. SYNTHESIS of [MoO(O₂)₂(pzpy)] (4.4)

A mixture comprising the polymeric [Mo₃O₉(pzpy)_n] (4.2) material (0.10 g, 0.54 mmol Mo), 5-6 M TBHP in decane (82.5 mmol, TBHP_{dec}) and DCE (30 mL) was heated at 55 °C for 24 h. After this time the reaction mixture was centrifuged and pentane/diethyl ether were added to the liquid phase, resulting in the precipitation of a pale yellow solid, which was identified as the oxodiperoxido complex [MoO(O₂)₂(pzpy)] (4.4)^[204] by elemental analysis, powder X-ray diffraction, FT-IR and NMR spectroscopy. Crystals of 4.4 suitable for X-ray diffraction were obtained by slow diffusion of diethyl ether into a concentrated solution of 4.4 in DMF. The powder X-ray diffraction pattern of the bulk product 4.4 was in excellent agreement with a simulated pattern calculated from the single-crystal structural determination.

Anal. Calcd for C₈H₇MoN₃O₅ (MW = 321.10 g mol⁻¹) (in %): C, 29.92; H, 2.20; N, 13.09. Found: C, 29.75; H, 1.96; N 13.08.

Selected FT-IR (KBr, cm⁻¹): $\nu = 288\text{m}, 325\text{m}, 393\text{m}, 437\text{w}, 492\text{m}, 512\text{s}, 539\text{m}, 584\text{s}, 615\text{m}, 643\text{m}, 655\text{s}, 713\text{w}, 778\text{vs}, 864\text{s} (\nu(\text{O}-\text{O})), 875\text{sh}, 924\text{m}, 950\text{vs} (\nu(\text{Mo}=\text{O})), 983\text{m}, 1025\text{m}, 1051\text{m}, 1070\text{m}, 1100\text{m}, 1126\text{m}, 1157\text{m}, 1166\text{sh}, 1216\text{m},$

1227m, 1257m, 1304m, 1315sh, 1364m, 1437s, 1458m, 1479m, 1522m, 1542m, 1570m, 1610vs, 2825w, 2917s, 3010s, 3054m, 3092m, 3124m, 3135m (v(NH)).

Selected FT-Raman (cm^{-1}): $\nu = 155\text{m}, 187\text{w}, 240\text{vw}, 260\text{m}, 295\text{m}, 320\text{w}, 393\text{m}, 492\text{w}, 511\text{m}, 538\text{m}, 585\text{m}, 643\text{m}, 657\text{sh}, 714\text{m}, 862\text{sh}, 873\text{s}, 924\text{m}, 940\text{vs}, 955\text{w}, 982\text{w}, 1023\text{m}, 1052\text{w}, 1075\text{vw}, 1101\text{w}, 1126\text{w}, 1158\text{m}, 1165\text{sh}, 1218\text{vw}, 1230\text{sh}, 1257\text{vw}, 1311\text{s}, 1365\text{m}, 1438\text{sh}, 1458\text{m}, 1480\text{m}, 1522\text{w}, 1541\text{s}, 1570\text{s}, 1610\text{vs}, 3070\text{s}, 3091\text{m}, 3123\text{m}, 3139\text{s}$.

^1H NMR (300.13 MHz, 25 °C, DMSO- d_6): $\delta = 13.05$ (br, NH), 8.58 (d, 1H, H11), 7.95 (d, 1H, H8), 7.84 (t, 1H, H9), 7.76 (br s, 1H, H5), 7.31 (dd, 1H, H10), 6.84 (d, 1H, H4) ppm.

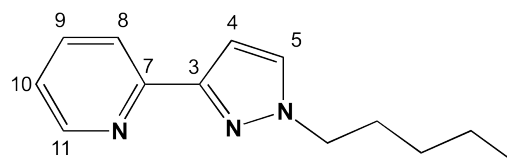
DFT calculations were performed using the G03W program package,^[224] running on a personal computer. Crystallographic data for **4.1**,^[81] **4.3**^[48] and **4.4** were used as a starting point for the B3LYP full geometry optimizations using the standard LanL2DZ basis set and effective core potentials (performed in the gas phase and without symmetry constraints). Harmonic vibrational wavenumbers and infrared/Raman intensities were calculated at the same level for all optimized structures, which were shown to have no negative eigenvalues for the Hessian matrices. In order to provide the best fit with experimental values, the harmonic vibrational wavenumbers were scaled by a factor of 0.961.^[225] Vibrational assignments were based on the atomic displacements and calculated intensities.

Crystal and structure refinement data: formula $\text{C}_8\text{H}_7\text{MoN}_3\text{O}_5$, MW = 321.11 g mol^{-1} , crystal system orthorhombic, space group *Pbca*, $a = 15.1933(14)$ Å, $b = 8.4300(8)$ Å, $c = 15.4515(13)$ Å, $V = 1979.0(3)$ Å³, $Z = 8$, $D_{\text{calcd}} = 2.155$ $\text{g}\cdot\text{cm}^{-3}$, $\mu(\text{Mo K}\alpha) = 1.341$ mm^{-1} , crystal size 0.06 × 0.03 × 0.02 mm, yellow block, reflections were collected in the range $3.61^\circ \leq \theta \leq 29.13^\circ$, 31707 collected reflections of which 2660 were independent with $R_{\text{int}} = 0.0742$. Completeness to $\theta = 29.13^\circ$ of 99.8%. Final *R* indices [$I > 2\sigma(I)$]: $R_1 = 0.0460$, $wR_2 = 0.0697$. Final *R* indices (all data): $R_1 = 0.0700$, $wR_2 = 0.0751$.

E.4.5. CHAPTER 5

E.4.5.1. Synthesis of pent-pp (5.1)

Reactions and experimental manipulations were performed using inert atmosphere standard Schlenk techniques.



2-(1-Pentyl-1H-pyrazol-3-yl)pyridine (pent-pp) was prepared, with minor changes, from the previous ligand pypzH and according to the published procedure.^[204]

A solution of pypzH (1.49 g, 10.26 mmol) in dry THF (20 mL) was added dropwise (because of the release of H₂) to a magnetically stirred suspension of NaH (0.49 g, 20.80 mmol) in THF (15 mL). NaH was previously washed with 15 mL of dry THF. The last procedure ensures that the mineral oil, which was used to safely store the NaH (60% in mineral oil), is removed. Using a syringe, 1-iodopentane (1.6 mL, 12.40 mmol) was added to the previous mixture. The mixture was stirred at 70 °C for 48 h. After this period, the solution was evaporated in the vacuum line and a yellow solid was obtained. The solid was extracted with *n*-hexane (100 mL) and pentane (50 mL). The combined extracts were evaporated to dryness, giving the ligand 5.1 as an oil. Yield: 1.68 g, 76%.

Anal. Calcd for C₁₃H₁₇N₃ (MW = 215.29 g mol⁻¹) (in %): C, 72.52; H, 7.95; N, 19.51. Found: C, 71.28; H, 8.01; N, 18.32.

Selected FT-IR (KBr, cm⁻¹): ν = 2956m, 2930m, 2871m, 2861m, 1592s [ν (C=C), ν (C=N)]py, 1565m, 1492s (δ (C=C)), 1459s, 1431m, 1401m [ν (C=C), ν (C=N)]_{py}, 1356m, 1329w, 1276m, 1229m, 1146m, 1049w, 992w, 956w, 739w, 761s γ (CH=CH) or γ (C-H, py), 715w, 695w, 668w, 620w, 403w.

¹H NMR (300.13 MHz, CDCl₃, r.t., ppm): δ = 0.89 (t, 3H, CH₃), 1.31 (m, 4H, CH₂), 1.92 (t, 2H, CH₂), 4.17 (t, 2H, NCH₂), 6.86 (d, 1H, H₄), 7.18 (m, 1H, H₁₀), 7.43 (d, 1H, H₅), 7.70 (td, 1H, H₉), 7.92 (d, 1H, H₈), 8.62 (dd, 1H, H₁₁).

¹³C NMR (75.47 MHz, CDCl₃, r.t., ppm): δ = 13.19 (CH₃), 22.19 (CH₂), 28.74 (CH₂), 30.15 (CH₂), 52.56 (NCH₂), 103.98 (C₄), 119.95 (C₁₀), 122.13 (C₈), 130.42 (C₅), 136.51 (C₉), 149.31 (C₃), 151.24 (C₁₁), 152.36 (C₇).

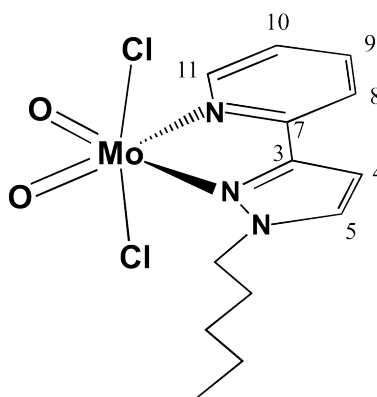
Crystals of the hydrochloride salt (5.1HCl) suitable for XRD studies were isolated from the aqueous mother liquor obtained after reaction of complex [MoO₂Cl₂(pent-pp)] (5.2) with water to prepare the material [Mo₂O₆(pent-pp)]_{*n*} (5.3).

Crystal and structure refinement data for 5.1HCl: formula C₁₃H₁₈ClN₃, MW = 251.75 g mol⁻¹, crystal system monoclinic, space group *P*2₁/*c*,

$a = 11.7600(7) \text{ \AA}$, $b = 11.1632(6) \text{ \AA}$, $c = 10.6280(6) \text{ \AA}$, $\beta = 98.648(3)^\circ$, $V = 1379.37(14) \text{ \AA}^3$, $Z = 4$, $D_{\text{calcd}} = 1.212 \text{ g cm}^{-3}$, crystal size $0.13 \times 0.10 \times 0.10 \text{ mm}$, colourless plate, reflections were collected in the range $3.65^\circ \leq \theta \leq 29.13^\circ$, 33917 collected reflections of which 3697 were independent with $R_{\text{int}} = 0.0507$. Completeness to $\theta = 29.13^\circ$ of 99.6%. Final R indices [$I > 2\sigma(I)$]: $R1 = 0.0415$, $wR2 = 0.1009$. Final R indices (all data): $R1 = 0.0640$, $wR2 = 0.1139$.

E.4.5.2. Synthesis of [MoO₂Cl₂(pent-pp)] (5.2)

The dioxomolybdenum(VI) complex [MoO₂Cl₂(pent-pp)] (5.2) was synthesized according to the procedure described by Kühn and co-workers.^[83] MoO₂Cl₂ (0.51 g, 2.55 mmol) was dissolved in THF (15 mL) and the solution was stirred for 20 min. An orange solution of the ligand 5.1 (0.55 g, 2.55 mmol) in THF (10 mL) was then added, and the mixture stirred for 2 h. The solution was evaporated to dryness and the resultant purple solid washed with *n*-hexane (15 mL), and finally vacuum dried. Yield: 0.99 g, 94% (based on Mo).



Anal. Calcd for C₁₃H₁₇Cl₂MoN₃O₂ (MW = 414.13 g mol⁻¹) (in %): C, 37.70; H, 4.13; N, 10.14. Found: C, 37.60; H, 4.25; N, 9.70.

Selected FT-IR (KBr pellets, cm⁻¹): $\nu = 3155\text{w}$, 3129m , 3094w , 2957m , 2929m , 2871m , 2861m , 1611m , 1568w , 1534w , 1503w , 1440s , 1368m , 1348w , 1294w , 1236m , 1226m , 1158w , 1147w , 1098m , 1082m , 1053w , 1094m , 962w , 942vs , 908vs , 876w , 781vs , 716w , 693w , 646m , 622m , 425w , 403m , 336vs .

¹H NMR (300.13 MHz, DMSO-*d*₆, r.t., ppm): $\delta = 0.86$ (t, 3H, CH₃), 1.18-1.35 (m, 4H, CH₂), 1.78-1.88 (m, 2H, CH₂), 4.21 (t, 2H, NCH₂), 7.04 (d, 1H, H₄), 7.55 (dt, 1H, H₁₀), 7.93 (d, 1H, H₅), 8.14 (overlapping signals, 2H, H₉, H₈), 8.62 (dd, 1H, H₁₁).

Crystal and structure refinement data for 5.2: formula C₁₃H₁₇Cl₂MoN₃O₂, MW = 414.14 g mol⁻¹, crystal system orthorhombic, space group *Pbca*, $a = 8.4532(5) \text{ \AA}$, $b = 11.4651(8) \text{ \AA}$, $c = 32.826(3) \text{ \AA}$, $V = 3181.4(4) \text{ \AA}^3$, $Z = 8$, $D_{\text{calcd}} = 1.729 \text{ g cm}^{-3}$, $\mu(\text{Mo K}\alpha) = 1.167 \text{ mm}^{-1}$, crystal size $0.09 \times 0.04 \times 0.01 \text{ mm}$, colourless plate, reflections were collected in the range $3.53^\circ \leq \theta \leq 29.13^\circ$, 18097 collected reflections of which 4252 were independent with $R_{\text{int}} = 0.0717$.

Completeness to $\theta = 29.13^\circ$ of 99.3%. Final R indices [$I > 2\sigma(I)$]: $R1 = 0.0448$, $wR2 = 0.0800$. Final R indices (all data): $R1 = 0.0898$, $wR2 = 0.0927$.

E.4.5.3. Synthesis of $[\text{Mo}_2\text{O}_6(\text{pent-pp})]_n$ (5.3)

A Teflon-lined stainless steel autoclave was charged with $[\text{MoO}_2\text{Cl}_2(\text{pent-pp})]$ (5.2) (0.25 g, 0.60 mmol) and water (15 mL), and heated in an oven at 100 °C for 19 h. The resultant pale green microcrystalline solid was separated from the aqueous mother liquor ($\text{pH} \approx 2$) by filtration, washed with water (20 mL), acetone (20 mL), and vacuum dried. The compound was characterized by elemental analysis, FT-IR and NMR spectroscopy, and PXRD.

Yield (based on Mo): 0.123 g, 81%.

Anal. Calcd for $\text{C}_{13}\text{H}_{17}\text{Mo}_2\text{N}_3\text{O}_6$ (MW = 503.17 g mol⁻¹) (in %): C, 31.03; H, 3.40; N, 8.35. Found: C, 31.00; H, 3.50; N, 8.18.

Selected FT-IR (KBr, cm⁻¹): $\nu = 3449\text{m}$, 3132w, 2956m, 2930m, 2869m, 1627m, 1611s, 1570m, 1558m, 1533m, 1504m, 1465m, 1441s, 1371m, 1339m, 1290m, 1237m, 1193m, 1159m, 1148m, 1099m, 1079m, 1053m, 1023m, 957vs, 910s, 804vs, 776s, 699s, 657vs, 505m, 427m, 400m, 354m, 323m.

¹³C{¹H} CP MAS NMR: $\delta = 14.3$ (CH₃), 22.4 (CH₂), 29.2 (CH₂), 52.2 (NCH₂), 105.2 (C4), 122.8 (C8, C10), 134.8 (C5), 140.3 (C9), 146.5, 148.0 (C3, C7, C11). Experimental conditions: spectra recorded using a Bruker Avance 500 (narrow bore) spectrometer with an ultrashield static magnetic field. The spectra were recorded at 125.76 MHz with 3.5 μs ¹H 90° pulses, 1.5 ms contact time, spinning rate of 9 kHz and 5 s recycle delays.

E.4.5.4. Synthesis of $[\text{MoO}(\text{O}_2)_2(\text{pent-pp})]$ (5.4)

A mixture comprising 5.3 (9.0 mg, 0.018 mmol), 5-6 M TBHP in decane (2.75 mmol) and 1,2-dichloroethane (1 mL) was heated at 55 °C for 6 h. After this time the reaction mixture was centrifuged and pentane was added to the liquid phase, resulting in the precipitation of a pale yellow solid, which was filtered, washed with pentane, vacuum-dried at 55 °C for 1 h, and identified as the oxodiperoxido complex 5.4 by elemental analysis, FT-IR and NMR spectroscopy. Yield: 2.5 mg, 18% (based on Mo).

Anal. Calcd for $\text{C}_{13}\text{H}_{17}\text{Mo}_2\text{N}_3\text{O}_5$ (MW = 391.23 g mol⁻¹) (in %): C, 39.91; H, 1.38; N, 10.74. Found: C, 40.04; H, 4.35, N, 10.65.

Selected FT-IR (ATR, cm^{-1}): $\nu = 3118\text{br}$, 2956w , 2926m , 2859w , 1613m , 1571w , 1530vw , 1503w , 1463sh , 1440s , 1364m , 1291vw , 1227m , 1203vw , 1099w , 947s , 907m , 861s , 842sh , 769vs , 659s , 583vs , 534m , 426vw , 404w , 356w .

^1H NMR (300 MHz, $\text{DMSO-}d_6$, r.t., ppm): $\delta = 0.86$ (t, 3H, CH_3), 1.31 (m, 4H, CH_2), 1.82 (m, 2H, CH_2), 4.20 (t, 2H, NCH_2), 6.79 (d, 1H, H4), 7.35 (m, 1H, H10), 7.81 (d, 1H, H5), 8.12 (d, 1H, H8), 8.29 (m, 1H, H9), 8.56 (d, 1H, H11).

E.5. CATALYSIS STUDIES: GENERAL CONSIDERATIONS

MATERIALS

	Compound name or formula	Supplier
Substrates		
Purchased from standard chemical suppliers and used as received without any further purification	Methyl oleate (Ole, 99 %)	Sigma-Aldrich
Dried prior to use by using activated 4 Å molecular sieves	DL-limonene (Lim, ≥95 %)	Merck
Co-solvents		
Dried prior to use by stirring over CaH ₂ overnight, followed by distillation, and storage over activated 4 Å molecular sieves	DCE (99 %)	Sigma-Aldrich
	BTF (anhydrous, 99 %)	Sigma-Aldrich
Ionic liquids		
Were pre-dried at 100 °C under vacuum (<0.1 bar) for 2 h	[bmim]BF ₄ (≥98 %)	Merck
	[bmpy]BF ₄ (≥98 %)	Merck
	[bmim]NTf ₂ (99 %)	IoLiTec
Oxidant		
Was acquired from commercial sources and used as received or dried prior to use by using activated 3 Å molecular sieves	5-6 M TBHP in decane	Aldrich

PROCEDURES

The catalytic epoxidations of each substrate with TBHP was performed in 5 mL borosilicate batch reactors (equipped with a PTFE-lined magnetic stirring bar and a valve for sampling), under autogenous pressure.

The evolutions of the catalytic reactions were monitored by using a Varian 3900 GC equipped with a Flame Ionization Detector (FID) and a DB-5 capillary column (30 m × 0.25 mm × 0.25 μm); undecane and methyl decanoate were used as internal standards for the reactions of DL-limonene and methyl oleate, respectively. The reaction products were identified by GC-MS (Trace GC 2000 Series Thermo Quest CE Instruments GC; Thermo Scientific DSQ II) using He as the carrier gas.

BTF and DCE were chosen as co-solvents because they (i) usually dissolve the reagents, (ii) are non-coordinating, thereby avoiding competition between the solvent and the reagent for coordination sites,^{[110][151][185]} and (iii) possess boiling points greater than 80 °C, avoiding high pressure and solvent evaporation during the catalytic reactions. DCE tends to enhance the catalytic epoxidation activity of oligo-/polymeric oxomolybdenum(VI) hybrid compounds with TBHP as oxidant.^[172] The hydrophobic nature of BTF is favourable for avoiding negative effects of moisture, for example, on product selectivity when the target epoxide product is more susceptible to acid-hydrolysis.^[226]

E.5.1. CHAPTER 1

E.5.1.1. INVESTIGATION PROCEDURES

The liquid-phase catalytic epoxidation reactions were carried out with magnetic stirring (800 rpm) at 55 °C under air (atmospheric pressure) in closed borosilicate reaction vessels (5 mL capacity) immersed in a thermostatted oil bath (OB). Typically, the reaction vessel was loaded with [MoO₂Cl₂(bipy)] (1.1) (0.018 mmol) or {[MoO₃(bipy)][MoO₃(H₂O)]_n (1.2) (0.018 mmol), 1.8 mmol of *cis*-cyclooctene (Cy8), and 2.75 mmol of the oxidant TBHP_{dec} (5.5 M in decane). The effect of adding or otherwise a co-solvent such as DCE or *n*-hexane (1 mL), or using 70% aqueous TBHP or 30% aqueous H₂O₂ instead of TBHP/decane, was also investigated.

E.5.1.2. SOLID RECOVERY and REUSABILITY

After each reaction run of 48 h, the solid phase was recovered by centrifugation at 3500 rpm, washed with *n*-hexane, and dried at ambient temperature overnight. Subsequent 48 h runs using these solids were performed using olefin / oxidant / catalyst mass ratios identical to those used in the first runs.

E.5.1.3. SCALED UP REACTION USING COMPOUND 1.1

A round bottomed flask was loaded with 10 times more [MoO₂Cl₂(bipy)] (1.1) than in previous tests, *i.e.*, 0.18 mmol instead of 0.018 mmol, and with the stoichiometric values of Cy8 and TBHP_{dec} (5.5 M in decane). After 24 h, the solid was isolated by filtration, washed with *n*-hexane and diethyl ether. Finally the recovered solid was vacuum dried.

E.5.1.4. CatFilt EXPERIMENTS

The aim of these experiments was to assess the reaction nature (homogeneous or heterogeneous) at a given tested temperature. A commonly used term for similar tests is “leaching test”, which aims to investigate the catalytic contribution of active species which are leached (desorbed) from a

catalyst support into solution at the reaction temperature: hot filtration (with a careful choice of the material/pore size of the filter) of the solid catalyst is performed because physical adsorption is an exothermic process and therefore the cooling of the reaction mixture to ambient temperature may cause adsorption of metal species back onto the surface of the solid catalyst.

The term “leaching”, however, may not be appropriate for the work described in chapter 1 because therein the homogeneous catalytic contribution observed for compound 1.2 while using the co-solvent DCE was most likely due to enhanced catalyst solubility (“oligomers” dissolution), rather than to the “leaching” of metal species.

The reaction courses were monitored using a Varian 3900 GC equipped with a capillary column (DB-5, 30 m × 0.25 mm) and a flame ionization detector. The experiments designated as CatFilt were carried out for *n*-hexane and DCE solvent systems. The first step was to perform the reaction of Cy8 with TBHP_{dec} at 55 °C in the presence (or otherwise) of $\{[\text{MoO}_3(\text{bipy})][\text{MoO}_3(\text{H}_2\text{O})]\}_n$ (1.2). After 1 h of reaction the solution was filtered off (or otherwise) at the reaction temperature through a 0.2 μm PVDF w/GMF Whatman membrane and stirred for a further 23 h at 55 °C. For each procedure the conversion values between 1 and 24 h were taken and denoted as Cat(1h), and Cat(24h), accordingly. The following numbers were calculated:

$$\Delta X_{\text{NoFilt}} = \text{Cat}(24\text{h}) - \text{Cat}(1\text{h})$$

Increase in conversion between 1 and 24 h for the one catalytic reaction in presence of 1.2.

$$\Delta X_{\text{CatFilt}} = \text{CatFilt}(24\text{h}) - \text{CatFilt}(1\text{h})$$

Increase in conversion between 1 and 24 h for the same catalytic reaction although having preformed the filtration at the reaction temperature.

$$\Delta X_{\text{NoCat}} = \text{Blank}(24\text{h}) - \text{Blank}(1\text{h})$$

Increase in conversion between 1 and 24 h in the absence of the solid catalyst.

The contribution of the homogeneous phase is indicated by $\Delta X_{\text{CatFilt}} / \Delta X_{\text{NoCat}}$. The contribution of the homogeneous phase reaction is higher if higher values are obtained. If the result is, e.g., 1, the homogeneous contribution is minimal or inexistent.

E.5.2. CHAPTER 2

E.5.2.1. CATALYTIC STUDIES for 2.2

The catalytic epoxidation reactions were carried out in 5 mL borosilicate reactors immersed in a thermostatted oil bath at 55 °C, under magnetic stirring (800 rpm) and autogenous pressure. The reagents were separately preheated to 55 °C prior to initializing the catalytic reaction by adding the oxidant to the reactor containing the olefin/catalyst. The solvents were distilled, and solvents and reagents were pre-dried using activated 3 or 4 Å molecular sieves. Typically, the initial molar ratio of molybdenum/olefin/oxidant was 1 : 100 : 152 (18 µmol Mo). When 5.5 M *tert*-butylhydroperoxide (TBHP) in decane was the oxidant solution used, the reactions were performed either without additional solvent (TBHP_{dec}) or with 1 mL of DCE, acetonitrile, ethyl acetate (EtOAc), ethanol (EtOH), or BTF as a co-solvent (TBHP_{dec}/co-solvent).

E.5.2.2. PREPARATION of TBHP/DCE and TBHP/EtOH

Mixtures denoted as TBHP/DCE and TBHP/EtOH were prepared by mixing 70% aqueous TBHP and a solvent and subsequently eliminating the excess water using magnesium sulfate. TBHP concentrations of these TBHP/cosolvent mixtures were determined by iodometric titrations. After each 24 h batch run, the solid phase was separated from the liquid phase by centrifugation, thoroughly washed with hexane, dried at ambient temperature overnight, and characterized by ATR FT-IR spectroscopy.

E.5.2.3. FT-IR of RECOVERED MATERIALS in the Lim CATALYST TESTS

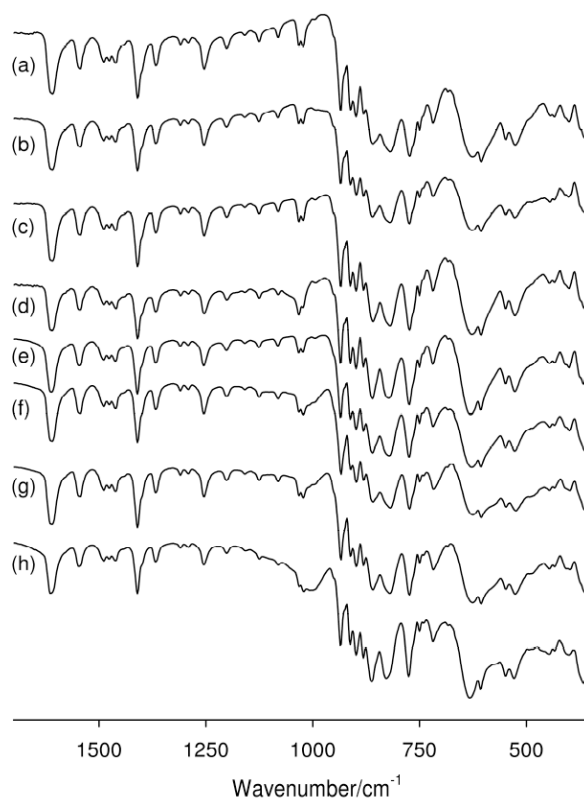


Figure E.14. ATR FT-IR spectra of (a) **2.2**, and of the solids recovered from the reaction of Lim in the presence of **2.2**, using the systems (b) TBHP_{dec}/DCE, (c) TBHP/DCE, (d) TBHP/EtOH and (e) TBHP_{dec}/BTF, and the reaction of methyl oleate in the presence of **2.2**, using the systems (f) TBHP_{dec}/DCE, (g) TBHP_{dec}/EtOAc and (h) TBHP_{dec}/BTF.

E.5.2.4. CATALYTIC STUDIES for **2.3**

[Mo₂O₆(di-*t*-Bu-bipy)₂] (**2.3**) (1 mol% relative to the olefin) was tested as a catalyst in the reactions Cy8, Lim, Cy12, 1-octene and *trans*-2-octene (1.8 mmol) using TBHP_{dec} (ca. 5.5 M in decane, pre-dried using 4 Å molecular sieves) as oxidant, without solvent (other than decane), at 55 °C, under air atmosphere (autogenous pressure) and stirring at 800 rpm. The borosilicate reactor (5 mL capacity, equipped with a magnetic stirring bar and a valve for sampling) was charged with the olefin and **2.3**, and subsequently immersed in the thermostated oil bath (55 °C). After 10 min heating, the catalytic epoxidation reaction was initiated by the addition of the pre-heated (55 °C / 10 min) oxidant (2.75 mmol).

E.6.3. CHAPTER 3

E.6.3.1. CATALYTIC STUDIES for 3.1

The epoxidation reactions were carried out in 5 mL borosilicate microreactors at a stirring rate of 1000 rpm under autogenous pressure. The microreactors containing the olefin / 3.1 / co-solvent were immersed in the thermostated oil bath and preheated to the desired reaction temperature (55 or 75 °C) for 10 min prior to addition of oxidant solution, which was preheated in a similar fashion; the addition of the oxidant was taken as the initial instant of the catalytic reaction. Initial molar ratios of Mo : olefin : TBHP were typically 1 : 103 : 160 (17 μ mol of molybdenum per catalytic test). DCE or BTF (1 mL), or IL (0.3 mL), were added as co-solvents.

To assess the homo/heterogeneous nature of the catalytic reaction for the system 3.1 / olefin / BTF / 75 °C, a catalytic test (denoted CatFilt) was carried out as follows: after 2 h the hot reaction mixture was filtered through a 0.2 μ m PTFE membrane filter, and the filtrate was transferred to a separate microreactor (walls pre-heated at the reaction temperature), and the reaction solution was stirred and monitored for a further 22 h at 75 °C. The catalytic reaction is considered to be homogeneous in nature when $\Delta\text{CatFilt}/\Delta\text{Cat} \cong 1$, where $\Delta\text{CatFilt}$ is the increment in olefin conversion in the time interval 2-24 h for the reaction carried out using the filtered solution, and ΔCat is the increment in olefin conversion during the same time interval for the reaction carried out in the presence of 3.1 (*i.e.*, no filtration step).

In order to recycle the IL-based catalytic systems after a 24 h batch run the reaction products were separated by solvent extraction using *n*-hexane (three extraction cycles using 1.5 mL of solvent). Subsequently the catalyst/IL mixture was heated at 40 °C for 1 h under vacuum in order to remove dissolved volatile organic compounds. The absence of extracting solvent and reaction products in the recovered catalyst/IL mixture was confirmed by GC. A second batch run was initiated by adding the reagents to the recovered catalyst/IL mixture in the same amounts as those used in the first batch run.

E.6.4. CHAPTER 4

E.6.4.1. BATCH CATALYTIC STUDIES OF 4.2

Catalytic experiments were carried out under autogenous pressure in borosilicate reactors (5 mL) equipped with a magnetic stirring bar and a Teflon valve for sampling. The reactors were charged with compound 4.2 (method A) in an amount equivalent to 18 μmol molybdenum, *cis*-cyclooctene (1.8 mmol) and, optionally, co-solvent (1 mL). Subsequently, the reactors were immersed in an oil bath thermostated at the desired reaction temperature (55 or 75 °C) and stirred at 1000 rpm during 10 min. In a similar fashion, the pre-dried TBHP_{dec} (2.75 mmol) was preheated. In a similar fashion to the procedures adopted for chapter 1, the preheating process was carried out in order to obtain isothermal initial conditions since otherwise the initial heating-up period would be *ca.* 7 min.^[142] The initial instant of the catalytic reaction was taken to be the moment that the oxidant solution was added to the reactor. The reactions were carried out under air. Nevertheless, molecular oxygen did not influence the catalytic reaction, ascertained by the fact that no reaction of Cy8 took place in the presence of 4.2 without TBHP_{dec}.

E.6.4.2. CATALYST STABILITY TESTS

Compound 4.2 was not completely soluble in the reaction media for all conditions used. After each 24 h-batch run the solid phase was separated from the liquid phase by centrifugation (3000 rpm), washed with pentane and vacuum-dried at 55 °C for 1 h, giving the recovered solids mentioned throughout the discussion. The recovered solids were characterized and used in a second batch run (initial concentrations of the reagents and mass of catalyst were the same for the two batch runs).

The homogeneous or heterogeneous nature of the catalytic reaction was checked by carrying out catalytic tests denoted CatFilt_Test. The reaction mixture was filtered at 2 h at the reaction temperature (75 °C) using a 0.2 μm PTFE membrane, and then the filtrate was transferred to a separate reactor (with preheated walls) containing a stirring bar, and immersed in an oil bath thermostated at the desired reaction temperature. The evolution of the catalytic reaction was monitored for 6 h counting from the initial instant of the CatFilt_Test. The increment in conversion for the time interval between the instant of the filtration and 6 h reaction is denoted $\Delta\text{CatFilt}$; this value was compared with ΔNoCat for the same time interval, which corresponds to the increment in conversion for the reaction of Cy8 carried out in the absence of catalyst. The catalytic reaction may be considered heterogeneous when $(\Delta\text{CatFilt})/(\Delta\text{NoCat}) = 1$ ($\Delta\text{NoCat} > 0$), and a homogeneous catalytic contribution exists when $(\Delta\text{CatFilt})/(\Delta\text{NoCat}) > 1$.

In some cases the contribution of the dissolved metal species was checked by performing assays denoted Dissolv_Test, which consisted of the

predissolution of **4.2** in the co-solvent/TBHP_{dec} mixture during 24 h at 75 °C, prior to addition of the substrate. This test is particularly important considering that the initial dissolution of the metal species may be rate-limiting to the overall reaction system.^{[182][185]} After 24 h the biphasic solid-liquid mixture was filtered at the reaction temperature using a 0.2 μm PTFE membrane. The filtrate was transferred to a separate reactor that was immersed in an oil bath thermostated at 75 °C. After stirring for 10 min, the olefin (also preheated) was added in an amount equivalent to the molar concentration of substrate used in a typical catalytic test. The evolutions of the homogeneous catalytic reactions were monitored throughout 24 h.

E.6.5. CHAPTER 5

E.6.5.1. CATALYTIC STUDIES for 5.2 and 5.3

Using an initial molybdenum : olefin : oxidant molar ratio of 1 : 113 : 172 (16 $\mu\text{mol Mo}$), and 1 mL of co-solvent DCE, BTF or *n*-hexane. The procedure for starting the catalytic reaction involved charging the reactor with catalyst, olefin and co-solvent, and then immersing the reactor into a thermostated oil bath at 55 °C, where it was kept under stirring (1000 rpm) for 10 min to attain isothermal initial conditions. Subsequently TBHP_{dec}, also preheated at 55 °C, was added to the reactor, and this was taken to be the initial instant of the reaction. These typical reaction conditions are denoted as TypCs.

After a batch run, the reaction mixture was cooled to ambient temperature and the undissolved solid was separated by centrifugation, washed with pentane and vacuum-dried (*ca.* 0.1 bar) at 55 °C for 1 h. In some cases, a solid (corresponding to the dissolved compound) was isolated from the liquid phase after adding pentane to the solution, and storing the resultant mixture at 4 °C overnight. The precipitated solid was separated by centrifugation, washed with pentane and vacuum-dried (*ca.* 0.1 bar) at 55 °C for 1 h.

The Dissolv_Test were carried out as follows: the catalyst, co-solvent and oxidant were charged to a reactor, and heated at 55 °C for 6 h with stirring at 1000 rpm. Afterwards, the mixture was cooled to ambient temperature, centrifuged (3500 rpm), and the liquid phase was separated using a filter containing a 0.2 μm PTFE membrane. The liquid phase (denoted as Dissolv-solv, where solv is the co-solvent used, *i.e.*, BTF, DCE or *n*-hexane) was transferred to a separate reactor, and preheated at 55 °C for 10 min. Finally, the olefin (also preheated) was added in an appropriate amount to obtain a similar initial concentration as that used for the TypCs.

The catalytic studies were extended to Ole and Lim using a Dissolv_Test-DCE solution obtained as described above. The initial concentration of olefin was the same as for the TypCs.

- [1] P. Gómez-Romero, C. Sanchez, Eds., *Functional Hybrid Materials*, Wiley-VCH Verlag GmbH & Co. KGaA, Weinheim, **2004**.
- [2] C. Sanchez, B. Julián, P. Belleville, M. Popall, *J. Mater. Chem.* **2005**, *15*, 3559–3592.
- [3] J. Y. Wen, G. L. Wilkes, *Chem. Mater.* **1996**, *8*, 1667–1681.
- [4] P. Judeinstein, C. Sanchez, *J. Mater. Chem.* **1996**, *6*, 511–525.
- [5] B. P. Gomez-Romero, *Adv. Mater.* **2001**, *13*, 163–174.
- [6] G. Férey, *Chem. Soc. Rev.* **2008**, *37*, 191–214.
- [7] F. Mammeri, E. Le Bourhis, L. Rozes, C. Sanchez, *J. Mater. Chem.* **2005**, *15*, 3787–3811.
- [8] G. Lagaly, K. Beneke, *Colloid. Polym. Sci.* **1991**, *1211*, 1198–1211.
- [9] G. Alberti, M. Casciola, U. Costantino, R. Vivani, *Adv. Mater.* **1996**, *8*, 291–303.
- [10] Q. H. Wang, K. Kalantar-Zadeh, A. Kis, J. N. Coleman, M. S. Strano, *Nature Nanotechnology* **2012**, *7*, 699–712.
- [11] L. Viciu, G. Caruntu, N. Royant, J. Koenig, W. L. Zhou, T. A. Kodenkandath, J. B. Wiley, *Inorg. Chem.* **2002**, *41*, 3385–3388.
- [12] F. Cavani, F. Trifìò, A. Vaccari, *Catal. Today* **1991**, *11*, 173–301.
- [13] R. M. R. Bull, C. Markland, G. R. Williams, D. O'Hare, *J. Mater. Chem.* **2011**, *21*, 1822.
- [14] V. Saxena, A. Diaz, A. Clearfield, J. D. Batteas, M. D. Hussain, *Nanoscale* **2013**, *5*, 2328–2336.
- [15] A. Clearfield, J. A. Stynes, *J. Inorg. Nucl. Chem.* **1964**, *26*, 117–129.
- [16] S. Gago, M. Pillinger, A. A. Valente, T. M. Santos, J. Rocha, I. S. Gonçalves, *Inorg. Chem.* **2004**, *43*, 5422–5431.
- [17] K.-H. Goh, T.-T. Lim, Z. Dong, *Water Res.* **2008**, *42*, 1343–1368.
- [18] K. Mandel, A. Drenkova-Tuhtan, F. Hutter, C. Gellermann, H. Steinmetz, G. Sextl, *J. Mater. Chem. A* **2013**, *1*, 1840–1848.
- [19] K. Katagiri, Y. Goto, M. Nozawa, K. Koumoto, *J. Ceram. Soc. Jpn.* **2009**, *117*, 356–358.
- [20] B. Monteiro, S. Gago, M. S. Balula, A. A. Valente, I. S. Gonçalves, M. Pillinger, *J. Mol. Catal. A: Chem.* **2009**, *312*, 23–30.
- [21] V. Rives, M. A. Ulibarri, *Coord. Chem. Rev.* **1999**, *181*, 61–120.
- [22] C. Sanchez, F. Ribot, *New J. Chem.* **1994**, *18*, 1007–1047.
- [23] S. Gago, M. Pillinger, R. A. S. Ferreira, L. D. Carlos, T. M. Santos, I. S. Gonçalves, *Chem. Mater.* **2005**, *17*, 5803–5809.
- [24] J. A. McCleverty, in *Encyclopedia of Inorganic Chemistry* (Ed.: R.B. King), Wiley, Chichester, **2005**.

- [25] R. Hille, *Chem. Rev.* **1996**, *96*, 2757–2816.
- [26] A. Sigel, H. Sigel, in *Metal Ions in Biological Systems Vol. 39*, Marcel Dekker, New York, **2002**.
- [27] E. I. Stiefel, in *Comprehensive Coordination Chemistry* (Ed.: G. Wilkinson), Pergamon Press, Oxford, **1987**.
- [28] R. A. Sheldon, J. K. Kochi, *Metal-Catalyzed Oxidations of Organic Compounds*, Academic Press, New York, **1981**.
- [29] J. R. R. Frausto da Silva, R. J. P. Williams, *The Biological Chemistry of the Elements*, Clarendon Press, Oxford, **1991**.
- [30] M. R. Pedrosa, J. Escribano, R. Aguado, R. Sanz, V. Díez, F. J. Arnaiz, *Inorg. Chim. Acta* **2010**, *363*, 3158–3164.
- [31] I. S. Gonçalves, A. M. Santos, C. C. Romão, A. D. Lopes, J. E. Rodriguez-Borges, M. Pillinger, P. Ferreira, J. Rocha, F. E. Kühn, *J. Organomet. Chem.* **2001**, *626*, 1–10.
- [32] R. Sanz, M. R. Pedrosa, *Curr. Org. Synth.* **2009**, *6*, 239–263.
- [33] J. H. Enemark, J. J. A. Cooney, *Chem. Rev.* **2004**, *104*, 1175–1200.
- [34] G. Yin, *Coord. Chem. Rev.* **2010**, *254*, 1826–1842.
- [35] R. H. Holm, *Chem. Rev.* **1987**, *87*, 1401–1449.
- [36] F. H. Allen, W. D. S. Motherwell, *Acta Crystallogr., Sect. B: Struct. Sci* **2002**, *58*, 407–422.
- [37] F. H. Allen, *Acta Crystallogr., Sect. B: Struct. Sci* **2002**, *58*, 380–388.
- [38] R. Delmont, C. R. Acad, S. Paris, *Chimie Chemistry* **2000**, *3*, 147–155.
- [39] S. Liu, L. Ma, D. McGowty, J. Zubieta, *Polyhedron* **1990**, *9*, 1541–1553.
- [40] L. Ma, S. Liu, J. Zubieta, *Inorg. Chem.* **1989**, *28*, 175–177.
- [41] V. W. Day, M. F. Fredrich, W. G. Klemperer, W. Shum, *J. Am. Chem. Soc.* **1977**, *99*, 6146.
- [42] E. Gumaer, K. Lettko, L. Ma, D. Macherone, J. Zubieta, *Inorg. Chim. Acta* **1991**, *179*, 47–51.
- [43] W. N. Lipscomb, *Inorg. Chem.* **1965**, *4*, 132–134.
- [44] M. B. Hursthouse, R. L. Short, B. Piggott, Al. Tucker, S. F. Wong, *Polyhedron* **1986**, *5*, 2121–2122.
- [45] A. Proust, P. Gouzerh, F. Robert, *J. Chem. Soc., Dalton Trans.* **1994**, 819–824.
- [46] H. Kang, S. Liu, S. N. Shaikh, T. Nicholson, J. Zubieta, *Inorg. Chem.* **1989**, *28*, 920–933.
- [47] S. Liu, S. N. Shaikh, J. Zubieta, *Inorg. Chem.* **1989**, *28*, 723–732.
- [48] D. Li, Y. Liu, P. Wei, B. Hu, X. Zhang, *Acta Crystallogr., Sect. E: Struct. Rep. Online* **2009**, *E65*, m1074–U576.
- [49] P. Neves, T. R. Amarante, A. C. Gomes, A. C. Coelho, S. Gago, M. Pillinger, I. S. Gonçalves, C. M. Silva, A. A. Valente, *Appl. Catal., A: Gen.* **2011**, *395*, 71–77.
- [50] M. K. Ehlert, S. J. Rettig, A. Storr, R. C. Thompson, J. Trotter, *Inorg. Chem.* **1993**, *32*, 5176–5182.
- [51] B. Q. Chen, S. Liu, J. Zubieta, *Angew. Chem., Int. Ed. Engl.* **1990**, *29*, 70–72.
- [52] A. Goiffon, B. Spinner, *Chim. Minérale* **1975**, *12*, 316.
- [53] C. Kaes, A. Katz, M. W. Hosseini, *Chem. Rev.* **2000**, *100*, 3553–3590.

- [54] S. R. Batten, N. R. Champness, X.-M. Chen, J. Garcia-Martinez, S. Kitagawa, L. Öhrström, M. O’Keeffe, M. Paik Suh, J. Reedijk, *Pure Appl. Chem.* **2013**, *85*, 1715–1724.
- [55] F. Blau, *Ber. Dtsch. Chem. Ges.* **1888**, *21*, 1077–1078.
- [56] G. R. Newkome, A. K. Patri, E. Holder, U. S. Schubert, *Eur. J. Org. Chem.* **2004**, 235–254.
- [57] P. J. Zapf, C. Haushalter, J. Zubieta, *Chem. Commun.* **1997**, 321–322.
- [58] O. Mo, C. Cui, J. Dai, W. Du, Z. Fu, S. Hu, L. Wu, X. Wu, *Polyhedron* **2002**, *21*, 175–179.
- [59] P. J. Zapf, R. C. Haushalter, J. Zubieta, *Chem. Mater.* **1997**, *9*, 2019–2024.
- [60] P. J. Zapf, R. L. LaDuca, R. S. Rarig, K. M. Johnson III, J. Zubieta, *Inorg. Chem.* **1998**, *37*, 3411–3414.
- [61] P. J. Zapf, C. J. Warren, C. Haushalter, J. Zubieta, *Chem. Commun.* **1997**, 1543–1544.
- [62] A. F. Wells, *Structural Inorganic Chemistry*, Clarendon Oxford University Press, New York, **1975**.
- [63] C. E. Housecroft, A. G. Sharpe, *Inorganic Chemistry*, Pearson Education Limited, Harlow, **2005**.
- [64] A. W. Armour, M. G. B. Drew, P. C. H. Mitchell, *J. Chem. Soc., Dalton Trans.* **1975**, 1493–1496.
- [65] F. A. Cotton, G. Wilkinson, C. Murillo, M. Bochmann, *Advanced Inorganic Chemistry*, Wiley-Interscience, New York, **1999**.
- [66] W. G. Klemperer, W. Shum, *J. Am. Chem. Soc.* **1976**, *98*, 8291–8293.
- [67] J. J. Berzelius, *Adv. Phys. Lpz.* **1986**, *46*, 381.
- [68] R. Colton, I. B. Tomkins, *Aust. J. Chem.* **1965**, *18*, 447.
- [69] I. M. Zharskii, E. Z. Zasorin, V. P. Spiridonov, G. I. Novikov, V. N. Kupreev, *Koord. Khim.* **1975**, *1*, 574.
- [70] H. Thomassen, K. Hedberg, *J. Mol. Struct.* **1992**, *273*, 197.
- [71] L. O. Atovmyan, Z. G. Aliev, B. M. Tarakanov, *Zh. Strukt. Khim.* **1968**, *9*, 1097.
- [72] M. L. Larson, F. W. Moore, *Inorg. Chem.* **1966**, *5*, 801.
- [73] A. Günyar, M.-D. Zhou, M. Drees, P. N. W. Baxter, G. Bassioni, E. Herdtweck, F. E. Kühn, *Dalton Trans.* **2009**, 8746–8754.
- [74] R. A. Laudise, *Chemical & Engineering News* **1987**, *65*, 30.
- [75] D. Hagrman, P. J. Hagrman, J. Zubieta, *Angew. Chem., Int. Ed.* **1999**, *38*, 2638–2684.
- [76] C. G. Hull, M. B. H. Stiddard, *J. Chem. Soc. A* **1966**, 1633–1635.
- [77] D. C. Brewer, J. L. Templeton, D. M. P. Mingos, *J. Am. Chem. Soc.* **1987**, *109*, 5203.
- [78] G. Barea, A. Lledos, F. Maseras, Y. Jean, *Inorg. Chem.* **1998**, *37*, 3321.
- [79] Z. Petrovski, M. Pillinger, A. A. Valente, I. S. Gonçalves, A. Hazell, C. C. Romão, *J. Mol. Catal. A: Chem.* **2005**, *227*, 67–73.
- [80] S. M. Bruno, C. C. L. Pereira, M. S. Balula, M. Nolasco, A. A. Valente, A. Hazell, M. Pillinger, P. Ribeiro-Claro, I. S. Gonçalves, *J. Mol. Catal. A: Chem.* **2007**, *261*, 79–87.

- [81] A. C. Coelho, M. M. Nolasco, M. S. Balula, M. M. Antunes, C. C. L. Pereira, F. A. Almeida Paz, A. A. Valente, M. Pillinger, P. Ribeiro-Claro, J. Klinowski, I. S. Gonçalves, *Inorg. Chem.* **2011**, *50*, 525–538.
- [82] S. M. Bruno, B. Monteiro, M. S. Balula, C. Lourenço, A. A. Valente, M. Pillinger, P. Ribeiro-Claro, I. S. Gonçalves, *Molecules* **2006**, *11*, 298–308.
- [83] F. E. Kühn, M. Groarke, E. Bencze, E. Herdtweck, A. Prazeres, A. M. Santos, M. J. Calhorda, C. C. Romão, I. S. Gonçalves, A. D. Lopes, M. Pillinger, *Chem. Eur. J.* **2002**, *8*, 2370–2383.
- [84] F. E. Kühn, E. Herdtweck, J. J. Haider, W. A. Herrmann, I. S. Gonçalves, A. D. Lopes, C. C. Romão, *J. Organomet. Chem.* **1999**, *583*, 3–10.
- [85] M. Groarke, I. S. Gonçalves, W. A. Herrmann, F. E. Kühn, *J. Organomet. Chem.* **2002**, *649*, 108–112.
- [86] F. E. Kühn, A. D. Lopes, A. M. Santos, E. Herdtweck, J. J. Haider, C. C. Romão, A. G. Santos, *J. Mol. Catal. A: Chem.* **2000**, *151*, 147–160.
- [87] A. Günyar, F. E. Kühn, *J. Mol. Catal. A: Chem.* **2010**, *319*, 108–113.
- [88] A. M. Al-Ajlouni, A. Günyar, M.-D. Zhou, P. N. W. Baxter, F. E. Kühn, *Eur. J. Inorg. Chem.* **2009**, 1019–1026.
- [89] H. Arzoumanian, R. Bakhtchadjian, G. Agrifoglio, H. Krentzien, J. C. Daran, *Eur. J. Inorg. Chem.* **1999**, 2255–2259.
- [90] H. Arzoumanian, R. Bakhtchadjian, G. Agrifoglio, R. Atencio, A. Brice O, *Transition Met. Chem.* **2006**, *31*, 681–689.
- [91] J. A. Brito, H. Teruel, G. Muller, S. Massou, M. Gómez, *Inorg. Chim. Acta* **2008**, *361*, 2740–2746.
- [92] P. Deburgomaster, J. Zubieta, *Acta Crystallogr., Sect. E: Struct. Rep. Online* **2010**, *66*, m909.
- [93] Z.-H. Zhou, C.-Y. Chen, Z.-X. Cao, K.-R. Tsai, Y. L. Chow, *Dalton Trans.* **2008**, 2475–9.
- [94] T. R. Amarante, A. C. Gomes, P. Neves, F. A. A. Paz, A. A. Valente, M. Pillinger, I. S. Gonçalves, *Inorg. Chem. Commun.* **2013**, *32*, 59–63.
- [95] D. Xiao, Y. Hou, E. Wang, S. Wang, Y. Li, G. De, L. Xu, C. Hu, *J. Mol. Struct.* **2003**, *659*, 13–21.
- [96] A. C. Gomes, J. A. Fernandes, C. A. Gamelas, I. S. Gonçalves, F. A. Almeida Paz, *Acta Crystallogr., Sect. E: Struct. Rep. Online* **2011**, *67*, m1738–m1739.
- [97] C. A. Gamelas, A. C. Gomes, S. M. Bruno, F. A. Almeida Paz, A. A. Valente, M. Pillinger, C. C. Romão, I. S. Gonçalves, *Dalton Trans.* **2012**, *41*, 3474–3484.
- [98] T. R. Amarante, P. Neves, A. C. Coelho, S. Gago, A. A. Valente, F. A. Almeida Paz, M. Pillinger, I. S. Gonçalves, *Organometallics* **2010**, *29*, 883–892.
- [99] Y. Lu, E. Wang, M. Yuan, Y. Li, C. Hu, *J. Mol. Struct.* **2003**, *649*, 191–195.
- [100] J. Kim, W. T. Lim, B. K. Koo, *Inorg. Chim. Acta* **2007**, *360*, 2187–2191.
- [101] Y. S. Zhou, L. J. Zhang, H. K. Fun, X. Z. You, *Inorg. Chem. Commun.* **2000**, *3*, 114–116.
- [102] B. Zhao, X.-Y. Chen, P. Cheng, B. Ding, D.-Z. Liao, S.-P. Yan, Z.-H. Jiang, *J. Coord. Chem.* **2005**, *58*, 467–472.
- [103] D.-P. Zhou, D.-Q. Bi, *Z. Kristallogr. - New Cryst. Struct.* **2006**, *221*, 503.
- [104] M. I. Khan, Q. Chen, J. Zubieta, *Inorg. Chim. Acta* **1993**, *213*, 325–327.

- [105] Y. Xu, L.-H. An, L.-L. Koh, *Chem. Mater.* **1996**, *8*, 814–818.
- [106] B. M. GateHouse, P. Leverett, *J. Chem. Soc. A* **1968**, 1398–1405.
- [107] I. Lindqvist, *Acta Chem. Scand.* **1950**, *4*, 1066–1074.
- [108] A. B. Lysenko, G. A. Senchyk, J. J. Lincke, D. Lässig, A. A. Fokin, E. D. Butova, P. R. Schreiner, H. Krautscheid, K. V Domasevitch, *Dalton Trans.* **2010**, *39*, 4223–4231.
- [109] G. P. Chisole, M. P. Maitlis, *Metal-catalysis in Industrial Organic Processes*, Royal Society Of Chemistry Publishing, Cambridge, U. K., **2008**.
- [110] S. Gago, P. Neves, B. Monteiro, M. Pessêgo, A. D. Lopes, A. A. Valente, F. A. Almeida Paz, M. Pillinger, J. Moreira, C. M. Silva, I. S. Gonçalves, *Eur. J. Inorg. Chem.* **2009**, 4528–4537.
- [111] J. A. Brito, M. Gómez, G. Muller, H. Teruel, J. C. Clinet, E. Duñach, M. A. Maestro, *Eur. J. Inorg. Chem.* **2004**, 4278–4285.
- [112] A. M. Martins, C. C. Romão, M. Abrantes, M. C. Azevedo, J. L. Cui, A. R. Dias, M. T. Duarte, M. A. Lemos, T. Lourenco, R. Poli, *Organometallics* **2005**, *24*, 2582–2589.
- [113] C. C. L. Pereira, M. S. Balula, F. A. Almeida Paz, A. A. Valente, M. Pillinger, J. Klinowski, I. S. Gonçalves, *Inorg. Chem.* **2007**, *46*, 8508–8510.
- [114] B. Monteiro, S. Gago, P. Neves, A. A. Valente, I. S. Gonçalves, C. C. L. Pereira, C. M. Silva, M. Pillinger, *Catal. Lett.* **2009**, *129*, 350–357.
- [115] P. Chaumette, H. Mimmoun, L. Saussine, J. Fischer, A. Mitschler, *J. Organomet. Chem.* **1983**, *250*, 291–310.
- [116] K. A. Jorgensen, *Chem. Rev.* **1989**, *89*, 431–458.
- [117] J. Kollar, Halcon, **1967**, US 3.350.422, US 3.351.635.
- [118] M. N. Sheng, G. J. Zajaczek, ARCO, **1968**, GB 1.136.923.
- [119] A. Corma, S. Iborra, A. Velty, *Chem. Rev.* **2007**, *107*, 2411–2502.
- [120] U. Neuenschwander, I. Hermans, *J. Org. Chem.* **2011**, *76*, 10236–10240.
- [121] U. Biermann, W. Friedt, S. Lang, W. Lühs, G. Machmüller, J. Metzger, Rüschi Gen Klaas M, H. Schäfer, M. Schneider, *Angew. Chem., Int. Ed.* **2000**, *39*, 2206–2224.
- [122] M. A. R. Meier, J. O. Metzger, U. S. Schubert, *Chem. Soc. Rev.* **2007**, *36*, 1788–1802.
- [123] Y. Xia, R. C. Larock, *Green Chem.* **2010**, *12*, 1893–1909.
- [124] S. G. Tan, W. S. Chow, *Polym. Plast. Technol. Eng.* **2010**, *49*, 1581–1590.
- [125] M. Farias, M. Martinelli, D. P. Bottega, *Appl. Catal., A: Gen.* **2010**, *384*, 213–219.
- [126] S.-F. Cai, L.-S. Wang, C.-L. Fan, *Molecules* **2009**, *14*, 2935–2946.
- [127] B. Monteiro, M. S. Balula, S. Gago, C. Grosso, S. Figueiredo, A. D. Lopes, A. A. Valente, M. Pillinger, J. P. Lourenço, I. S. Gonçalves, *J. Mol. Catal. A: Chem.* **2009**, *297*, 110–117.
- [128] A. Castro, J. C. Alonso, A. A. Valente, P. Neves, P. Brandão, V. Félix, P. Ferreira, *Eur. J. Inorg. Chem.* **2010**, 1405–1412.
- [129] S. M. Bruno, M. S. Balula, A. A. Valente, F. A. Almeida Paz, M. Pillinger, C. Sousa, J. Klinowski, C. Freire, P. Ribeiro-Claro, I. S. Gonçalves, *J. Mol. Catal. A: Chem.* **2007**, *270*, 185–194.
- [130] A. A. Valente, J. Moreira, A. D. Lopes, M. Pillinger, C. D. Nunes, C. C. Romão, F. E. Kühn, I. S. Gonçalves, *New J. Chem.* **2004**, *28*, 308–313.

- [131] P. Neves, S. Gago, C. C. L. Pereira, S. Figueiredo, A. Lemos, A. D. Lopes, I. S. Gonçalves, M. Pillinger, C. M. Silva, A. A. Valente, *Catal. Lett.* **2009**, *132*, 94–103.
- [132] P. Neves, C. C. L. Pereira, F. A. Almeida Paz, S. Gago, M. Pillinger, C. M. Silva, A. A. Valente, C. C. Romão, I. S. Gonçalves, *J. Organomet. Chem.* **2010**, *695*, 2311–2319.
- [133] A. A. Valente, J. D. Seixas, I. S. Gonçalves, M. Abrantes, M. Pillinger, C. C. Romão, *Catal. Lett.* **2005**, *101*, 127–130.
- [134] F. E. Kühn, A. M. Santos, A. D. Lopes, I. S. Gonçalves, E. Herdtweck, C. C. Romão, *J. Mol. Catal. A: Chem.* **2000**, *164*, 25–38.
- [135] J. M. Sobczak, J. J. Ziólkowski, *Appl. Catal., A: Gen.* **2003**, *248*, 261–268.
- [136] P. Wang, B. Y. Tao, *J. Am. Oil Chem. Soc.* **1998**, *75*, 9–14.
- [137] R. Poli, *Coord. Chem. Rev.* **2008**, *252*, 1592.
- [138] B. Soptrajanov, M. Trpkovska, L. Pejov, *Croat. Chem. Acta* **1999**, *72*, 663–672.
- [139] L. Seguin, M. Figlarz, R. Cavagnat, C. Lassègues, *Spectrochim. Acta, Part A* **1995**, *51*, 1323–1344.
- [140] R. Atencio, A. Briceño, P. Silva, J. A. Rodríguez, J. C. Hanson, *New J. Chem.* **2007**, *31*, 33–38.
- [141] T. V Charlu, O. J. Kleppa, *J. Chem. Thermodyn.* **1971**, *3*, 697–700.
- [142] M. Abrantes, T. R. Amarante, M. M. Antunes, S. Gago, F. A. Almeida Paz, I. Margiolaki, A. E. Rodrigues, M. Pillinger, A. A. Valente, I. S. Gonçalves, *Inorg. Chem.* **2010**, *49*, 6865–6873.
- [143] M. Isobe, F. Marumo, T. Yamase, T. Ikawa, *Acta Crystallogr., Sect. B: Struct. Sci* **1978**, *34*, 2728–2731.
- [144] J. Bernstein, R. E. Davis, L. Shimoni, N. L. Chang, *Angew. Chem., Int. Ed.* **1995**, *34*, 1555–1573.
- [145] H. Arzoumanian, G. Agrifoglio, H. Krentzien, M. Capparelli, *J. Chem. Soc., Chem. Commun.* **1995**, 655–656.
- [146] H. Arzoumanian, G. Agrifoglio, H. Krentzien, *New J. Chem.* **1996**, *20*, 699–705.
- [147] H. Arzoumanian, L. Maurino, G. Agrifoglio, *J. Mol. Catal. A: Chem.* **1997**, *117*, 471–478.
- [148] S. Kodama, A. Nomoto, S. Yano, M. Ueshima, A. Ogawa, *Inorg. Chem.* **2011**, *50*, 9942–9947.
- [149] T. R. Amarante, F. A. Almeida Paz, S. Gago, I. S. Gonçalves, M. Pillinger, A. E. A. E. Rodrigues, M. Abrantes, *Molecules* **2009**, *14*, 3610–3620.
- [150] G. Socrates, *Infrared Characteristic Group Frequencies - Tables and Charts*, John Wiley & Sons Ltd, Baffins Lane, Chichester, **1994**.
- [151] T. R. Amarante, P. Neves, C. Tome, M. Abrantes, A. A. Valente, F. A. Almeida Paz, M. Pillinger, I. S. Gonçalves, *Inorg. Chem.* **2012**, *51*, 3666–3676.
- [152] D. Hagrman, C. Zubieta, D. J. Rose, J. Zubieta, R. C. Haushalter, *Angew. Chem., Int. Ed.* **1997**, *36*, 873–876.
- [153] D. G. Allis, R. S. Rarig, E. Burkholder, J. Zubieta, *J. Mol. Struct.* **2004**, *688*, 11–31.
- [154] S. M. O. Quintal, H. I. S. Nogueira, H. M. Carapuça, V. Félix, M. G. B. Drew, *J. Chem. Soc., Dalton Trans.* **2001**, 3196–3201.

- [155] X.-B. Cui, K. Lü, Y. Fan, J.-Q. Xu, L. Ye, Y.-H. Sun, Y. Li, H.-H. Yu, Z.-H. Yi, *Journal of Molecular Structure* **2005**, 743, 151–155.
- [156] L. F. Veiros, A. Prazeres, P. J. Costa, C. C. Romão, F. E. Kühn, M. J. Calhorda, *Dalton Trans.* **2006**, 1383–1389.
- [157] A. M. Al-Ajlouni, A. A. Valente, C. D. Nunes, M. Pillinger, A. M. Santos, J. Zhao, C. C. Romão, I. S. Gonçalves, F. E. Kühn, *Eur. J. Inorg. Chem.* **2005**, 1716–1723.
- [158] L. A. Mukhamedova, M. I. Kudryavtseva, R. R. Shagidullin, Y. Y. Samitov, *Russ. Chem. Bull.* **1973**, 22, 1020–1025.
- [159] T. R. Amarante, P. Neves, F. A. Almeida Paz, M. Pillinger, A. A. Valente, I. S. Gonçalves, *Inorg. Chem.* **2012**, 20, 147–152.
- [160] P. Neves, S. Gago, S. S. Balula, A. D. Lopes, A. A. Valente, L. Cunha-Silva, F. A. Almeida Paz, M. Pillinger, J. Rocha, C. M. Silva, I. S. Gonçalves, *Inorg. Chem.* **2011**, 50, 3490–3500.
- [161] Q. Chen, S. C. Liu, J. Zubieta, *Inorg. Chim. Acta* **1989**, 162, 163–164.
- [162] E. J. Brown, A. C. Whitwood, P. H. Walton, A.-K. Duhme-Klair, *Dalton Trans.* **2004**, 2458–2462.
- [163] J. C. Alonso, P. Neves, M. J. da Silva, S. Quintal, P. D. Vaz, C. Silva, A. A. Valente, P. Ferreira, M. J. Calhorda, V. Félix, M. G. B. Drew, *Organometallics* **2007**, 26, 5548–5556.
- [164] G. D. Dixon, N. W. Carlson, H. E. Saunders, *U.S. Patent* **1983**, 4,412,048.
- [165] B. Schoknecht, R. Kempe, *Z. Anorg. Allg. Chem.* **2004**, 630, 1377–1379.
- [166] M. E. Chapman, P. Ayyappan, B. M. Foxman, G. T. Yee, W. Lin, *Crystal Growth & Design* **2001**, 1, 159–163.
- [167] C. B. Aakeroy, A. M. Beatty, K. R. Lorimer, *J. Chem. Soc., Dalton Trans.* **2000**, 3869–3872.
- [168] R. C. Finn, J. Zubieta, *Inorg. Chem. Commun.* **2000**, 3, 520–524.
- [169] R. C. Finn, J. Zubieta, *Solid State Sci.* **2002**, 4, 83–86.
- [170] A. A. Valente, Ž. Petrovski, L. C. Branco, C. A. M. Afonso, M. Pillinger, A. D. Lopes, C. C. Romão, C. D. Nunes, I. S. Gonçalves, *J. Mol. Catal. A: Chem.* **2004**, 218, 5–11.
- [171] R. Ziessel, *J. Am. Chem. Soc.* **1993**, 115, 118–127.
- [172] S. Figueiredo, A. C. Gomes, P. Neves, T. R. Amarante, F. A. Almeida Paz, R. Soares, A. D. Lopes, A. A. Valente, M. Pillinger, I. S. Gonçalves, *Inorg. Chem.* **2012**, 51, 8629–8635.
- [173] N. F. Drobot, O. A. Noskova, N. A. Ovchinnikova, G. A. Zvereva, G. M. Larin, V. A. Krenev, E. N. Trifonova, D. V Drobot, *Russ. J. Coord. Chem.* **2003**, 29, 474–477.
- [174] G. Bator, J. Baran, R. Jakubas, L. Sobczyk, *J. Mol. Struct.* **1998**, 450, 89–100.
- [175] M. Wojtaś, G. Bator, J. Baran, *Vib. Spectrosc.* **2003**, 33, 143–152.
- [176] F.-N. Shi, L. Cunha-Silva, T. Trindade, F. A. Almeida Paz, J. Rocha, *Cryst. Growth Des.* **2009**, 9, 2098–2109.
- [177] A. D. Burrows, K. Cassar, R. M. W. Friend, M. F. Mahon, S. P. Rigby, J. E. Warren, *CrystEngComm* **2005**, 7, 548–550.
- [178] H. F. Clausen, R. D. Poulsen, A. D. Bond, M.-A. S. Chevallier, B. B. Iversen, *J. Solid State Chem.* **2005**, 178, 3342–3351.
- [179] S. V Ganesan, P. Lightfoot, S. Natarajan, *Solid State Sci.* **2004**, 6, 757–762.

- [180] E. Pretsch, P. Bühlmann, *Structure Determination of Organic Compounds: Tables of Spectral Data*, Springer, **2009**.
- [181] R. K. Harris, P. Jackson, L. H. Merwin, B. J. Say, G. H Gele, G. Hagele, *J. Chem. Soc., Faraday Trans.* **1988**, *84*, 3649.
- [182] T. R. Amarante, P. Neves, A. A. Valente, F. A. Almeida Paz, A. N. Fitch, M. Pillinger, I. S. Gonçalves, *Inorg. Chem.* **2013**, *52*, 4618–4628.
- [183] Y.-G. G. Li, L. M. Dai, Y.-H. H. Wang, X.-L. L. Wang, E.-B. B. Wang, Z.-M. M. Su, L. Xu, *Chem. Commun.* **2007**, 2593–2595.
- [184] L.-M. M. Dai, W. S. You, Y.-G. G. Li, E.-B. B. Wang, L.-J. J. Qi, J. Tang, X.-L. L. Bai, *Inorg. Chem. Commun.* **2010**, *13*, 421–424.
- [185] A. C. Gomes, P. Neves, S. Figueiredo, J. A. Fernandes, A. A. Valente, F. A. Almeida Paz, M. Pillinger, A. D. Lopes, I. S. Gonçalves, *J. Mol. Catal. A: Chem.* **2013**, *370*, 64–74.
- [186] C. A. Gamelas, P. Neves, A. C. Gomes, A. A. Valente, C. C. Romão, I. S. Gonçalves, M. Pillinger, *Catal. Lett.* **2012**, *142*, 1218–1224.
- [187] J. A. Brito, S. Ladeira, E. Teuma, B. Royo, M. Gómez, *Appl. Catal., A: Gen.* **2011**, *398*, 88–95.
- [188] D. Betz, A. Raith, M. Cokoja, F. E. Kühn, *ChemSusChem* **2010**, *3*, 559–62.
- [189] A. Guenyar, D. Betz, M. Drees, E. Herdtweck, F. E. Kühn, A. Günyar, *J. Mol. Catal. A: Chem.* **2010**, *331*, 117–124.
- [190] D. Betz, W. A. Herrmann, F. E. Kühn, *J. Organomet. Chem.* **2009**, *694*, 3320–3324.
- [191] C. Bibal, J.-C. Daran, S. Deroover, R. Poli, *Polyhedron* **2010**, *29*, 639–647.
- [192] F. E. Kühn, J. Zhao, M. Abrantes, W. Sun, C. A. M. Afonso, L. C. Branco, I. S. Gonçalves, M. Pillinger, C. C. Romão, *Tetrahedron Lett.* **2005**, *46*, 47–52.
- [193] W. H. Baur, *Acta Crystallogr., Sect. B: Struct. Sci* **1974**, *30*, 1195–1215.
- [194] J. Grell, J. Bernstein, G. Tinhofer, *Acta Crystallogr., Sect. B: Struct. Sci* **1999**, *55*, 1030–1043.
- [195] S. Figueiredo, A. C. Gomes, J. A. Fernandes, F. A. A. Paz, A. D. Lopes, J. P. Lourenço, M. Pillinger, I. S. Gonçalves, *J. Organomet. Chem.* **2013**, *723*, 56–64.
- [196] E. da Palma Carreiro, G. Yong-En, A. J. Burke, *Inorg. Chim. Acta* **2006**, *359*, 1519–1523.
- [197] M. J. Hinner, M. Groarke, E. Herdtweck, W. R. Thiel, *Z. Anorg. Allg. Chem.* **2003**, *629*, 2251–2257.
- [198] H. Glas, M. Spiegler, W. R. Thiel, *Eur. J. Inorg. Chem.* **1998**, 275–281.
- [199] W. R. Thiel, T. Priermeier, *Angew. Chem., Int. Ed.* **1995**, *34*, 1737–1738.
- [200] W. A. Herrmann, W. R. Thiel, J. G. Kuchler, J. Behm, E. Herdtweck, *Chem. Ber. Recl.* **1990**, *123*, 1963–1970.
- [201] E. O. Schlemper, G. N. Schrauzer, L. A. Hughes, *Polyhedron* **1984**, *3*, 377–380.
- [202] J. Twu, T. H. Fang, C. F. Hsu, Y. Y. Yu, G. J. Wang, C. W. Tang, K. H. Chen, K. H. Lii, *J. Mater. Chem.* **1998**, *8*, 2181–2184.
- [203] W. P. Griffith, *J. Chem. Soc. A - Inorg. Phys. Theor.* **1969**, 211.
- [204] W. R. Thiel, M. Angstl, T. Priermeier, *Chem. Ber.* **1994**, *127*, 2373–2379.
- [205] S. M. Bruno, J. A. Fernandes, L. S. Martins, I. S. Gonçalves, M. Pillinger, P. Ribeiro-Claro, J. Rocha, A. A. Valente, *Catal. Today* **2006**, *114*, 263–271.

- [206] M. Abrantes, I. S. Gonçalves, M. Pillinger, C. Vurchio, F. M. Cordero, A. Brandi, *Tetrahedron Lett.* **2011**, 52, 7079–7082.
- [207] S. P. Bhatia, D. McGinty, C. S. Letizia, A. M. Api, *Food Chem. Toxicol.* **2008**, 46, s197 – s200.
- [208] A. M. Al-Ajlouni, D. Veljanovski, A. Capape, J. Zhao, E. Herdtweck, M. J. Calhorda, F. E. Kühn, **2009**, 28, 639–645.
- [209] P. J. Costa, M. J. Calhorda, F. E. Kühn, *Organometallics* **2010**, 29, 303–311.
- [210] H. Brunner, S. T, *Chem. Ber.* **1992**, 125, 701–709.
- [211] APEX2, Data Collection Software (version 2.1-RC13), Delft, The Netherlands **2006**.
- [212] Cryopad, Remote monitoring and control, Version 1.451, Oxford Cryosystems, Oxford, United Kingdom **2006**.
- [213] SAINT+, Data Integration Engine (Version 7.23a), Bruker AXS, Madison, WI, USA, 2005.
- [214] G. M. Sheldrick, *SADABS version 2.01, Bruker/Siemens Area Detector Absorption Correction Program, Bruker AXS, Madison, Wisconsin, USA* **1998**.
- [215] T. R. Amarante, I. S. Gonçalves, F. A. Almeida Paz, *Acta Crystallogr., Sect. E: Struct. Rep. Online* **2011**, 67, O1903–U1807.
- [216] T. Kottke, D. Stalke, *J. App. Cryst.* **1993**, 26, 615–619.
- [217] A. S. Batsanov, I. A. I. Mkhalid, T. B. Marder, *Acta Crystallogr., Sect. E: Struct. Rep. Online* **2007**, 63, o1196–o1198.
- [218] T. R. Amarante, I. S. Gonçalves, F. A. Almeida Paz, *Acta Crystallogr., Sect. E: Struct. Rep. Online* **2009**, 65, o1962–u3860.
- [219] A. C. Coelho, I. S. Gonçalves, F. A. Almeida Paz, *Acta Crystallogr., Sect. E: Struct. Rep. Online* **2007**, 63, o1380–o1382.
- [220] W. A. Herrmann, J. G. Kuchler, P. Kiprof, J. Riede, *J. Organomet. Chem.* **1990**, 395, 55–67.
- [221] T. R. Amarante, S. Figueiredo, A. D. Lopes, I. S. Gonçalves, F. A. Almeida Paz, *Acta Crystallogr., Sect. E: Struct. Rep. Online* **2009**, 65, O2047–U4597.
- [222] S.-C. Liu, W.-L. Ke, J.-S. K. Yu, T.-S. Kuo, Y.-C. Tsai, *Angew. Chem., Int. Ed.* **2012**, 51, 6394–6397.
- [223] L. Li, G. D. Yang, G. R. Zhang, Z. K. Tang, G. Q. He, X. B. Qu, C. T. Sun, Q. J. Huang, *Chin. Sci. Bull.* **1991**, 36, 464–469.
- [224] M. J. Frisch, G. W. Trucks, H. B. Schlegel, G. E. Scuseria, M. A. Robb, J. R. Cheeseman, J. A. Montgomery, Jr., T. Vreven, K. N. Kudin, J. C. Burant, *et al.*, *Gaussian, Inc., Wallingford CT* **2003**.
- [225] R. D. Johnson III, *NIST Computational Chemistry Comparison and Benchmark Database, NIST Standard Reference Database Number 101, Release 12, Aug 2005*, <http://srdata.nist.gov/cccbdb>.
- [226] J. J. Maul, P. J. Ostrowski, G. A. Ublacker, B. Linclau, D. P. Curran, *Top Curr. Chem.* **1999**, 206, 79–105.

